UNIVERSITY OF SOUTHAMPTON

Faculty of Natural and Environmental Sciences

School of Chemistry

Group 13 and 14 Coordination Complexes and Reagents for the Electrodeposition of Tin and Lead from Supercritical Fluids

by

Jennifer Burt

Thesis for the degree of Doctor of Philosophy

March 2016

UNIVERSITY OF SOUTHAMPTON

ABSTRACT

FACULTY OF NATURAL AND ENVIRONMENTAL SCIENCES

Chemistry

Thesis for the degree of Doctor of Philosophy

GROUP 13 AND 14 COORDINATION COMPLEXES AND REAGENTS FOR THE ELECTRODEPOSITION OF TIN AND LEAD NANOMATERIALS FROM SUPERCRITICAL FLUIDS

by Jennifer Burt

Supercritical fluid electrodeposition is a new technique being developed that aims to deposit technologically important p-block materials at the nanoscale. This requires significant synthetic effort in precursor development, and investigations into fundamental p-block coordination chemistries, primarily through the use of neutral phosphine and arsine ligands, have been undertaken to aid the design process. The compounds synthesised have been characterised by microanalysis, IR spectroscopy and multinuclear NMR spectroscopy (^{1}H, ^{11}B, ^{19}F, ^{31}P{^{1}H}, ^{27}Al and ^{119}Sn, where appropriate), while single crystal X-ray structure determinations have been performed for representative examples.

AlX_3 (X = Cl, Br, I) form both $[AlX_3(PMe_3)]$ and $[AlX_3(PMe_3)_2]$ depending on the reagent stoichiometry employed. While all reported arsine complexes are four-coordinate, neutral diphosphine ligands show a preference for six-coordinate Al; the crystal structures of $[AlCl_2\{o\text{-}C_6H_4(PR_2)_2\}_2][AlCl_4]$ (R = Me, Ph) and $[AlCl_2\{Me_2P(CH_2)_2PMe_2\}_2][AlCl_4]$ are reported, along with $[(AlCl_3)_2\{\mu\text{-}R_2P(CH_2)_2PR_2\}]$ (R = Me, Cy). The importance of solvent choice and hydrolysis in these systems is discussed. Steric and electronic effects are considered in comparing the behaviour of MX_3 (M = Al, Ga, In) towards phosphines.

A number of new phosphine complexes of BX_3 (X = F, Cl, Br, I) have been synthesised, and $[BF_3(PMe_3)]$ is crystallographically authenticated. Flexible diphosphine ligands yield bridging $[(BX_3)_2\{\mu\text{-}R_2P(CH_2)_2PR_2\}]$ (R = Me, Et), while rigid chelating ligands produce the unusual ionic $[BX_2\{o\text{-}C_6H_4(PMe_2)_2\}]^+$ and $[BCl_2\{o\text{-}C_6H_4(AsMe_2)_2\}]^+$. The *d*(B–P) are consistent with the order of Lewis acidity being $BI_3 > BBr_3 > BCl_3 > BF_3$. The rare $[B_2F_7]^-$ ion is thought to drive the unexpected formation of $[BF_2\{Ph_2P(O)CH_2P(O)Ph_2\}][B_2F_7]$.

The effect of the weakly coordinating fluoroanions $[BF_4]^-$ and $[SiF_6]^{2-}$ on the coordination environments around Pb(II) in di- and tri-imine complexes is investigated, with several different coordination modes observed. A method is devised to synthesise some Pb(II) diphosphine complexes; the crystal structures of $[Pb\{o\text{-}C_6H_4(PMe_2)_2\}(H_2O)(SiF_6)]\cdot H_2O$ and $[Pb(L\text{–}L)(NO_3)_2]$ (L–L = $Me_2P(CH_2)_2PMe_2$, $o\text{-}C_6H_4(PMe_2)_2$) are reported, which reveal chelating diphosphines and intermolecular anion interactions, giving extended structures. Adventitious O_2 forms the bridging ligand complex $[Pb\{Et_2(O)P(CH_2)_2P(O)Et_2\}_2(NO_3)_2]$.

The well-defined and stable $[N^nBu_4][SnX_3]$ and $[PPh_4][PbX_3]$ (X = Cl, Br, I) precursors are shown by cyclic voltammetry to give reproducible metal deposition and stripping peak features in CH_2Cl_2, with the reduction potential becoming more accessible Cl → Br → I. Good quality thin films of Sn and Pb can be electrodeposited from CH_2Cl_2 using these precursors, which are analysed by SEM, EDX and XRD. Subsequent work in the group has shown that $[N^nBu_4][SnCl_3]$ can be used to deposit 13 nm Sn nanowires from supercritical CH_2F_2, highlighting the potential of this versatile electrolyte system for future applications in p-block materials deposition at the extreme nanoscale, and device fabrication.

Table of Contents

List of Tables

List of Figures

List of Accompanying Materials

- One CD containing the Crystallographic Information Files (cifs) for the X-ray diffraction studies reported throughout this thesis.

DECLARATION OF AUTHORSHIP

I, Jennifer Burt, declare that this thesis and the work presented in it are my own and has been generated by me as the result of my own original research.

Group 13 and 14 Coordination Complexes and Reagents for the Electrodeposition of Tin and Lead from Supercritical Fluids

I confirm that:

1. This work was done wholly or mainly while in candidature for a research degree at this University;
2. Where any part of this thesis has previously been submitted for a degree or any other qualification at this University or any other institution, this has been clearly stated;
3. Where I have consulted the published work of others, this is always clearly attributed;
4. Where I have quoted from the work of others, the source is always given. With the exception of such quotations, this thesis is entirely my own work;
5. I have acknowledged all main sources of help;
6. Where the thesis is based on work done by myself jointly with others, I have made clear exactly what was done by others and what I have contributed myself;
7. Parts of this work have been published as:

   'Phosphine complexes of aluminium(III) halides – preparation and structural and spectroscopic systematics' J. Burt, W. Levason, M. E. Light and G. Reid, *Dalton Trans.*, 2014, **43**, 14600-14611.

   'Hexafluorosilicate and tetrafluoroborate coordination to lead(II) di- and tri-imine complexes – unusual fluoroanion coordination modes' J. Burt, W. Grantham, W. Levason, M. E. Light and G. Reid, *Polyhedron*, 2015, **85**, 530-536.

   'Lead(II) nitrate and hexafluorosilicate complexes with neutral diphosphine coordination' J. Burt, W. Grantham, W. Levason and G. Reid, *Dalton Trans.*, 2015, **44**, 11533-11541.

'Complexes of aluminium, gallium and indium trifluorides with neutral oxygen donor ligands: synthesis, properties and reactions' R. Bhalla, J. Burt, A. L. Hector, W. Levason, S. K. Luthra, G. McRobbie, F. M. Monzittu and G. Reid, *Polyhedron*, 2016, **106**, 65-74.

'A versatile precursor system for supercritical fluid electrodeposition of main-group metals' P. N. Bartlett, J. Burt, D. A. Cook, C. Y. Cummings, M. W. George, A. L. Hector, M. M. Hasan, J. Ke, W. Levason, D. Pugh, G. Reid, P. W. Richardson, D. C. Smith, J. Spencer, N. Suleiman and W. Zhang, *Chem. Eur. J.*, 2016, **22**, 302-309.

Figures have been reproduced with copyright permission.

Signed: .....

Date: .....

Acknowledgements

I have many people to thank for helping me throughout my PhD studies. Most importantly I would like to thank my supervisors Prof. Gill Reid and Prof. Bill Levason for their time, support and inexhaustible knowledge. Special thanks go to Dr. Mark Light and Dr. Michael Webster for their X-ray crystallography advice and for their help in solving any crystallographic problems. Thanks also go to Dr. David Pugh and Dr. Wenjian Zhang for their patient assistance with crystallography, and to Dr. Neil Wells for multinuclear NMR spectroscopy training and support. Also to Prof. James Emsley and Dr. Ilya Kuprov for the NMR spectrum simulation. Thank you to all the members of the Reid/Levason group, past and present, for help and advice in the laboratory and for moral support. I have been fortunate in having two excellent undergraduate students, William Grantham and Iain Tinkler, both of whom have contributed to parts of the work discussed.

I would like to thank the EPSRC for funding through a Programme Grant (EP/1033394/1). Thanks go to Prof. Philip Bartlett and his group, in particular Dr. Peter Richardson, for all their help with electrochemistry, for the use of their equipment and for performing the supercritical fluid work included in this thesis. I must also thank Dr. Richardson and Dr. Jay Naik for collecting the SEM and EDX data reported. Thanks to Mahboba Hasan for collecting the XRD patterns presented and to Karl Kaye for modelling the data.

Finally I would like to thank Karl and my family and friends at home for their continued encouragement and support through what has been a very enjoyable and rewarding three years.

Definitions and Abbreviations

Bu	Butyl group
Cy	Cyclohexyl group
Et	Ethyl group
L	General ligand group
L–L	bidentate ligand
M	Any metal or Lewis acid centre
Me	Methyl group
Ph	Phenyl group
R	General alkyl or aryl group
X	Halide ion
15-crown-5	1,4,7,10,13-Pentaoxacyclopentadecane
18-crown-6	1,4,7,10,13,16-Hexaoxacyclooctadecane
AAO	Anodic Aluminium Oxide
acac	acetylacetonate
bipy	2,2’-bipyridyl
$BzMe_2$-tacn	1,4-dimethyl-7-benzyl-1,4,7-triazacyclononane
CVD	Chemical Vapour Deposition
δ/Δ	chemical shift/chemical shift difference
DFT	Density Functional Theory
DMF	Dimethylformamide
DMSO	Dimethyl Sulfoxide
EDX	Electron Dispersive X-ray spectroscopy

ESI	Electrospray Ionisation
GC	Glassy Carbon
IR	Infrared
(w = weak; m = medium; s = strong; vs = very strong; br = broad)	
J	coupling constant
Me_3-tacn	1,4,7-trimethyl-1,4,7-triaazacyclononane
ν	vibrational frequency
N.A.	Natural Abundance
NMR	Nuclear Magnetic Resonance
(s = singlet; d = doublet; t = triplet; q = quartet; m = multiplet)	
$\{^1H\}$	Proton decoupled NMR spectroscopy
o-	ortho-
PEEK	Polyether Ether Ketone
phen	1,10-phananthroline
ppm	parts per million
PTFE	Polytetrafluoroethylene
PVD	Physical Vapour Deposition
py	pyridine
sc	supercritical
SCFED	Supercritical Fluid Electrodeposition
SEM	Scanning Electron Microscopy
terpy	2,2':6',2''-terpyridyl
THF	Tetrahydrofuran
XRD	X-Ray Diffraction

Chapter 1: Introduction

Supercritical fluid electrodeposition (SCFED) is a transformative materials deposition technique that is being developed at the University of Southampton as part of a large Programme Grant. A major area of focus is on the SCFED of p-block elements and materials, and the work described in this thesis builds on and contributes to an already significant body of active research,[1] specifically through the synthesis and characterisation of compatible reagents suitable for use in low polarity supercritical fluids. The studies have been focused on new compound development and have involved an exploration of the fundamental coordination chemistries of boron, aluminium, tin and lead. For tin and lead this has enabled informed choices to be made about reagent design, and the suitability of some reagents for the SCFED of tin and lead materials has been evaluated electrochemically.

1.1 p-Block Materials at the Nanoscale

Nanomaterials, that is, materials with at least one dimension in the 1-100 nm range, are of vast technological importance because their properties can be tuned by adjusting their size and shape.[2] The use of p-block elemental and compound semiconductors (e.g. Si, GaN) in optical and electronic devices is long established and these fields remain highly active, with an ever-growing demand to further miniaturise components and devices.[3,4] Nanostructuring materials at the extreme nanoscale may also lead them to exhibit hitherto undetermined properties and phenomena. For instance, it has been predicted that Si nanowires with diameters less than 2 nm will have a direct band gap, with strong optical emission.[5] Indeed, ultra-small diameter p-block nanowires have particularly attracted a lot of interest due to their unique properties and their ability to be incorporated as the functional components and interconnects in useful devices.[4] As well as having the potential to make existing electronic components even smaller, concepts for new nanowire based devices are constantly being envisioned and developed.[1,3,4] Nanowires show promise in improving the performance of thermoelectric materials,[4,6] while functionalised semiconductor nanowires can be used as highly sensitive real-time biochemical sensors.[7] Nanowires are also less susceptible to defects, and thus can exhibit ultra-strength behaviour.[8] Nanowire synthetic methodologies, properties and applications have been extensively reviewed in the literature.[4,9,10]

The fabrication of nanowires and other nanostructures can be achieved through either top-down or bottom-up strategies. The top-down approach includes several lithographic techniques such as photolithography and electron beam lithography, which are being continually developed and optimised for applications in the semiconductor industry.[11,12] However as the scaling of these current device fabrication methods reach their fundamental limits, continued progress demands new techniques to be developed. Vapour deposition techniques (e.g. CVD or PVD) are elaborate and expensive top-down methods[13] that are prone to causing pore blockage at the top of high aspect ratio pores.[11] More recently, bottom-up approaches to nanowire synthesis have attracted a lot of attention,[3,4] and electrodeposition is one such key technique.[14] Since the early 1990s it has been used in the copper Damascene process pioneered by IBM for the large scale production of electrical interconnects within integrated circuits.[15] For this and many other electrodeposition processes however the medium used is water, which has significant limitations in p-block element deposition due to its narrow electrochemical window and boiling point.[16] Electrodeposition from ionic liquids has recently been widely studied due to their tuneable solvent properties, good ionic conductivities and wide electrochemical windows, which enables a range of reactive materials to be deposited.[17] Industrial scale use of ionic liquids is not common though because of their high costs and expensive disposal/recovery,[16] and their high viscosities and surface tensions mean that ionic liquids are poorly suited to filling sub-20 nm nanostructures.[18]

1.2 Supercritical Fluid Electrodeposition

To provide the broader context for the work described in the main body of this thesis, it is appropriate to begin with an overview of the aims of the SCFED project. A supercritical fluid is a substance above its critical temperature (T_c) and critical pressure (p_c); it possesses properties that are intermediate between those of the liquid and gaseous states (supercritical fluids can dissolve materials like a liquid but like a gas occupy the entire volume of the system), which are tuneable by temperature and pressure.[1,19] Supercritical fluids have been used as green alternatives to conventional organic solvents in chemical reactions; for example, various hydrogenation and oxidation reactions have been performed in $scCO_2$ as gases are totally miscible with supercritical fluids, potentially increasing reaction rates, while it has been used as the reaction medium for several polymerisation processes as $scCO_2$ is effectively inert to free radical chemistry and is good at polymer swelling.[19] Supercritical fluids have also been used in a variety of separation

(e.g. decaffeination) and mechanical (e.g. extrusion) processes, and in the supercritical drying of nanomaterials,[1] including the preparation of free-standing CdS nanowire arrays.[20]

Importantly, the lack of surface tension and the very low viscosities (and hence fast mass transport rates) of supercritical fluids enable them to penetrate high aspect ratio, small diameter nanopores. This property is being exploited by supercritical fluid electrodeposition, a new bottom-up technique being developed at the University of Southampton that aims to enable the template-assisted[21] deposition of a wide range of reactive materials to produce nanowires, and ultimately complex nanomaterials, on the sub-10 nm scale.[1,16] SCFED is well suited for this as it combines the unique properties of supercritical fluids with the advantages of electrodeposition, which include efficient reagent usage, conformal deposition for which growth is spatially defined and occurs directionally away from the electrode, and having direct control over the driving force for deposition through the applied potential.[1] Sub-10 nm diameter nanowires are currently an emerging field of great interest to many sectors of the scientific community,[13] and SCFED has already been successfully used to fabricate 3 nm diameter Cu nanowires.[16]

Judiciously chosen supercritical fluids, such as hydrofluorocarbon solvents,[22] have the advantage of being chemically stable and resistant to oxidation and reduction, resulting in wide electrochemical windows. This opens up the prospects for the deposition of very reactive materials such as germanium,[1] of which amorphous films have been successfully deposited using SCFED.[18,23] There is also the opportunity to deposit at significantly elevated temperatures, which could improve the crystallinity of deposits due to greater surface mobility.[1]

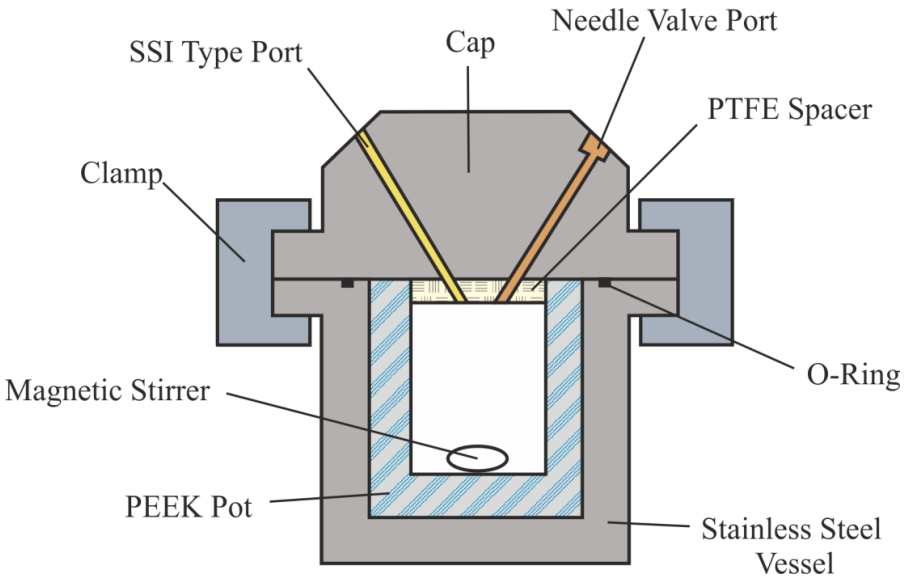

Figure 1.1 Schematic of a high-pressure electrochemistry cell used for SCFED.[1]

To safely work at the high pressures required for SCFED a specialised electrochemistry cell (Figure 1.1) needs to be used. This consists of a two-part stainless steel vessel assembled using a failsafe clamp system, with a PEEK pot and PTFE spacer inside to reduce contamination from the stainless steel, and a magnetic stirrer. The cap has a needle valve and six ports for electrodes, thermocouples and a fluid inlet/outlet.[1] The reagents and supporting electrolyte are transferred into the cell inside a N_2-filled glove box. Once fully assembled and sealed the cell is removed from the glove box, connected to a high-pressure rig and heated to the desired temperature using a band heater. The supercritical fluid is then pumped in until the desired pressure is achieved, while the system is stirred to ensure that the solution is homogenous. The stirring is stopped prior to performing the electrochemical measurements.[24]

To be able to deposit a wide range of p-block elements by SCFED, with the potential for co-deposition (e.g. to form compound semiconductors), a complete system needs to be developed with mutually compatible reagents and supporting electrolyte. While metallic Cu[16] and Ag[25] nanowires have been electrodeposited from $scCO_2/CH_3CN$ using the precursor $[Cu(CH_3CN)_4][B\{3,5\text{-}(CF_3)_2C_6H_3\}_4]$ or $[Ag(CH_3CN)_4][BF_4]$ respectively, translation of the technique to deposit p-block materials is very challenging, highlighted by the difficulties encountered in trying to deposit Ge.[1,18,23]

The choice of supercritical fluid is very important; it is desirable that the supercritical fluid used is non-corrosive, and has an accessible critical temperature and pressure. Supercritical difluoromethane ($scCH_2F_2$) is a good choice for the SCFED of p-block materials it has accessible critical conditions (T_c = 351.26 K; p_c = 5.78 MPa) and a very wide electrochemical window.[22] Supercritical fluids normally have low dielectric constants (generally $\varepsilon < 8$,[24] compared to ε = 36.6 for CH_3CN,[1] a solvent frequently used for non-aqueous electrodeposition), which makes dissolving and dissociating into ions sufficient supporting electrolyte (required to achieve a high conductivity) difficult. This can be partly overcome by using a polar co-solvent (CH_3CN co-solvent was used with $scCO_2$ to deposit Cu)[16,24] or by using a more polar supercritical fluid such as $scCH_2F_2$.[1,26] It is necessary to be able to work under conditions where the density of the supercritical fluid is sufficient for it to be a good solvent for ionic species.[1] Supporting electrolyte design is also important in order to increase its solubility in the low dielectric constant fluids as much as possible. A good supporting electrolyte for SCFED should be both thermally and chemically stable in the supercritical fluid used and with respect to the reagents added, dissociate easily to form discrete cations and anions, and have a wide potential window.[1]

A good precursor (i.e. the chemical compound used to deliver the p-block element to be electrodeposited) for SCFED must be thermally and chemically stable, particularly to trace oxygen and water, as well as be soluble in the supercritical fluid. For these reasons it has been established that coordinative saturation is an important characteristic of a good precursor. A careful choice of ligand set and/or counterion is vital to ensure that these properties are achieved, while avoiding fouling of the electrode or of the deposited material upon release during deposition.[1] Work in the group has focused on designing reagents where the p-block element is in a lower oxidation state as the reduction potentials are likely to be more accessible and within the available electrochemical window. As an example of precursor optimisation for the SCFED of germanium, well-defined salts containing the Ge(II) anion $[GeCl_3]^-$ were found to be much less moisture sensitive and easier to handle than $GeCl_4$, a volatile liquid that generates HCl upon reaction with trace water. Furthermore, cyclic voltammetry studies showed that the $[GeCl_3]^-$ anion had the most accessible reduction potential of the chloride based precursors.[27] The synthetic procedure has to be reproducible and provide practically useful amounts of suitably pure product, while exposure to oxygen and water should be minimised throughout both the synthesis and subsequent handling of the precursor to maintain purity.[1]

1.3 Aims

The aim of this project was to develop, synthesise and fully characterise a range of compounds that could potentially be used as (or aid in the design of) precursors for the SCFED of selected p-block elements, primarily tin and lead. As SCFED is a relatively new technique, significant synthetic effort in precursor development is required, and investigating the coordination chemistry (such as the favoured coordination number and geometry around the central atom and its sensitivity and solubility under the conditions employed) of the element in question beforehand is key to being able to rationalise what compound is most likely to be successful under SCFED conditions, allowing the technique to be developed faster and applied much more broadly. In order to develop the underlying coordination chemistry focus has been on using phosphine (PR_3) ligands for these studies as by changing the denticity and/or R groups it allows the electronics and sterics of the ligand, and hence the complex formed, to be tuned. It is hoped that the fundamentals gained from these studies may be applied to the design and synthesis of precursors from across the p-block, thus expanding the capabilities of SCFED as a technique.

This work also provided a unique opportunity to expand the known coordination chemistry of Groups 13 and 14. While neutral phosphine and arsine ligands are ubiquitous in transition metal coordination and organometallic chemistry,[28,29] much less research effort has been devoted to the main group, particularly with aluminium and lead.[30] By systematically studying the behaviour of B(III), Al(III) and Pb(II) towards neutral bidentate phosphine and arsine ligands the aim was to further elucidate and rationalise the rich and diverse coordination chemistry that the p-block exhibits.

This thesis is divided into five experimental chapters, which are briefly outlined below:

Chapter 2

A series of novel aluminium(III) halide coordination complexes with neutral mono- and bi-dentate phosphine and arsine ligands are synthesised and fully characterised, with investigations centred around exploring the effect of the halide and the ligand on the coordination environment around the aluminium centre. Comparisons are made with gallium(III) halide and indium(III) halide – phosphine coordination chemistry.

Chapter 3

The coordination chemistry of the boron(III) halides with neutral bidentate phosphine and arsine ligands is systematically studied for the first time, and the effect of the ligand and the Lewis acidity of BX_3 (X = F, Cl, Br, I) on complex formation is discussed in detail.

Chapter 4

The coordination numbers and environments around new lead(II) di- and tri-imine complexes with the weakly coordinating fluoroanions $[BF_4]^-$ and the little studied $[SiF_6]^{2-}$ is investigated, with an emphasis on single crystal X-ray crystallographic characterisation.

Chapter 5

A new synthetic strategy is devised and employed to overcome the challenges associated with the poor solubility of Pb(II) salts and complexes in organic solvents in order to synthesise and characterise some novel bidentate phosphine complexes of $Pb(NO_3)_2$ and $Pb(SiF_6)$. The behaviour and structures adopted by the complexes are discussed as a function of the phosphine ligand and the anion present.

Chapter 6

The final chapter reports the synthesis and characterisation of, and initial voltammetric and deposition studies on, specially designed tin and lead reagents that aimed to achieve the electrodeposition of these metals from CH_2Cl_2, and ultimately $scCH_2F_2$.

1.4 Neutral Phosphine and Arsine Ligands

Like their lighter congeners amines (NR_3), neutral phosphines (PR_3) and arsines (AsR_3) are versatile ligands that can be carefully tuned sterically and electronically by the choice of substituents (R groups), allowing the properties of the donor-acceptor complex to be adjusted.[31] The ready availability of multidentate ligands provides a further opportunity to fine tune the properties of the Lewis base, while the chelate effect can aid in complex formation. For complexes involving phosphine ligands, ^{31}P NMR spectroscopy provides a highly convenient opportunity to probe the site of coordination from the atom bonded directly to the Lewis acid. While amines are classed as hard Lewis bases, due to their greater polarizability phosphines and arsines are soft Lewis bases and so will favour coordination to soft (typically large and polarisable) Lewis acids.[32]

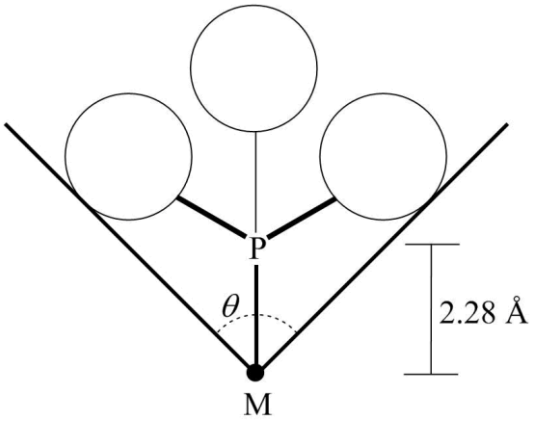

Figure 1.2 Tolman cone angle (θ) model.[33]

The standard method of quantifying the steric properties of a neutral phosphine ligand are by its cone angle θ, defined as the apex angle of a cone formed by a point 2.28 Å (representing an idealised M–P bond length) from the phosphorus atom and just touching the Van der Waals radii of the outermost atoms of the R group when folded up (Figure 1.2). Wider cone angles indicate a greater steric bulk (e.g. for PMe_3 θ = 118°, while for PPh_3 θ = 145°).[33,34] For bidentate ligands the cone angle is derived from the outer non-bridging substituents and the bisector of the P–M–P angle (e.g. θ = 107° for $Me_2P(CH_2)_2PMe_2$).[35] The model has been extended to include arsines and stibines, with the cone angle decreasing by a few degrees as Group 15 is descended.[36] The Tolman cone angle model has its limitations and has been found to generally underestimate the steric demands of phosphine ligands. This is highlighted by the recent computation of exact cone angles (θ°), which are typically larger than θ by 15 to 25°, the differences for bidentate ligands being even greater.[37]

For chelating diphosphines and diarsines the bite angle is also important. Generally the most stable complexes are obtained when a five-membered ring is formed upon chelation (i.e. the bridge between the P/As donor atoms is two carbons long).[38] Upon complex formation the P–M–P angle observed is a balance between the preferred bite angle of the ligand (which is largely dictated by constraints imposed by the backbone of the ligand and by steric repulsion between substituents) and the steric and electronic requirements of the Lewis acid, including any other ligands that might be coordinated. The *d*(M–P) strongly influences the bite angle observed.[39]

The handling of phosphine ligands is often challenging, as alkyl phosphines in particular are readily oxidised by O_2, are malodorous and can be pyrophoric.[40] Similarly, low molecular weight alkyl arsines are toxic, malodorous and air sensitive.[41] While alkyl phosphines must be handled under an inert atmosphere, aryl phosphines typically show greater stability in air and are easier to synthesise and subsequently handle;[40] on the other hand these are poorer ligands.

The oxidation of phosphines yields another important class of neutral ligand, phosphine oxides (OPR_3), which are generally easy to handle and coordinate through oxygen, meaning they have their own distinct coordination chemistry. Phosphine oxides are easily identifiable by ^{31}P NMR spectroscopy (their resonances are observed at higher frequencies to the parent phosphine ligands), while an IR spectrum of a complex can quickly show if the phosphine oxide has coordinated as if successful the ν(PO) moves to lower wavenumbers. The nature of the P–O bond has long been contentious, but computer modelling studies[42,43] indicate that the P–O bond is best described as comprising of a highly polarised σ-bond, plus a π component from the back-donation of the oxygen π orbitals. The back-bonding can be viewed as two π back-bonds formed between lone pairs on oxygen and acceptor antibonding orbitals on the PR_3 moiety.[44]

1.4.1 Bonding in p-block complexes

For p-block – phosphine complexes, the traditional σ-donor π-acceptor model used to explain bonding in transition metal complexes (σ-donation from the phosphorus lone pair into an empty metal orbital with the correct symmetry, supplemented by π back-donation from filled metal d orbitals into vacant P–R σ* orbitals)[34] cannot be applied, due to the inaccessibility of the d orbitals on the p-block Lewis acid. The filled (n–1)d orbitals are too low in energy to be available for π-donation, while the nd orbitals are empty and too high

in energy to significantly contribute to bonding.[30,45] Therefore the p-block Lewis acid – phosphine bond is largely based on σ-donation (the same is true for arsine ligands).[30,31] The increase in energy separation between the valence s and p orbitals as Group 15 is descended results in the lone pair on arsenic having greater s character than on phosphorus, making it less available due to it being less directional. This, and the increased diffusivity of the orbitals, means that arsine ligands are weaker σ-donors than phosphines.[36] Electron donating substituents improve the σ-donor power of PR_3 and AsR_3, meaning alkyl phosphines and arsines are much better σ-donors than aryl phosphines and arsines.[40]

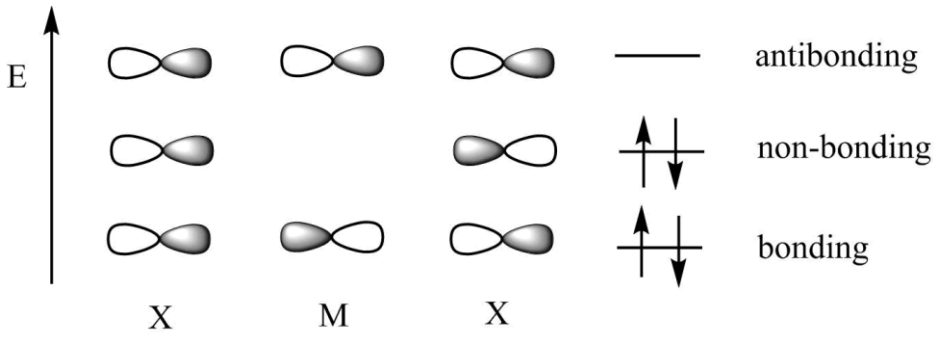

Figure 1.3 3-centre-4-electron bonding model.[46]

It is easy to rationalise the formation of a four-coordinate species such as $[AlCl_3(L)]$, formed when aluminium(III) chloride reacts with e.g. one equivalent of a neutral monodentate phosphine ligand, as the Lewis acid centre accepting a pair of electrons from the Lewis base to achieve a stable electronic configuration (octet). Higher coordination numbers yield hypervalent molecules, and invoke the use of the 3-centre-4-electron (3c-4e$^-$) bonding model. For a linear X–M–X unit an empty np orbital on M is combined with a filled donor p orbital on each X to form three molecular orbitals (Figure 1.3), with the bonding and non-bonding orbitals occupied.[46] In an octahedron the three orthogonal p orbitals on M are used to form three 3c-4e$^-$ bonds.

When the groups around the Lewis acid centre are different (i.e. X–M–Y) the M–X bond is modelled so that the lower energy bonding σ orbital is polarised towards the more electronegative X, while the empty antibonding σ^* orbital is polarised more towards M (Figure 1.4) and can thus act as the acceptor orbital for an electron pair from Y. The energy of the σ^* antibonding orbital depends on the electronegativities and match in the orbital sizes of M and X. The resulting X–M–Y geometry should be close to linear.[47]

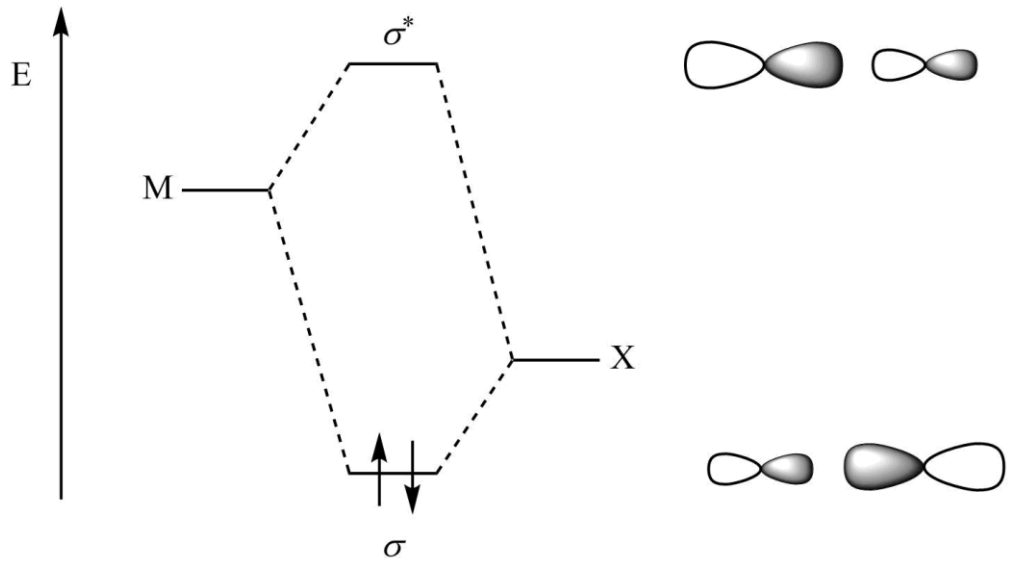

Figure 1.4 Orbital interaction diagram representing the M–X σ-bonding model.[47]

There remains no satisfactorily detailed models to explain bonding when the coordination number around the p-block Lewis acid centre exceeds six however,[30] as is the case in many complexes of Pb(II), for example.[48]

1.5 Group 13 Halide Coordination Chemistry

Group 13 has a rich and varied chemistry, with boron having very distinct properties on account of its very small atomic radius, meaning it is often discussed separately to the heavier, metallic elements. With the ground state electron configuration ns^2np^1 the preferred oxidation state is +3 for M = B, Al, Ga and In, though the +1 state becomes more stable as the group is descended.[49] Though the Group 13 monohalides MX (M = B, Al, Ga; X = F, Cl, Br, I) have all been identified, they are usually only accessible when high energy conditions are used; only InX (X = Cl, Br, I) are stable in the solid state.[50,51] The monohalides are characteristically relatively weak Lewis acids, but the lone pair of electrons (originating in the ns^2 valence shell of M) means the MX are good Lewis bases that have been shown to act as both bridging and terminal ligands towards transition metals. They are valence isoelectronic with CO and N_2, with σ-donor π-acceptor properties.[49,50] The coordination chemistry of the Group 13 monohalides has recently been reviewed.[50] In contrast, the Group 13 trihalides (MX_3) are readily available and are inherently good Lewis acids (a property exploited in applications such as catalysis) as the electron-withdrawing halides enhance the natural Lewis acidity of M(III), which stems from their innate electrophilicity and formally empty p orbital.[49] Thus the Group 13 trihalides have been the focus of this work.

1.5.1 Boron

While hypervalent compounds (see Section 1.4.1) are widely known for the heavier p-block elements, they are very rare for the small second row elements, including boron, which preferentially forms four-coordinate complexes.[52,53] Through the careful choice of ligands (both steric and electronic effects are important)[52,54] however, the first examples of five- and six-coordinate hypervalent boron compounds were synthesised in 1984.[55] Since then several five-coordinate complexes have been crystallographically authenticated,[52-54,56] including the compound shown in Figure 1.5, which has a 3-centre-4-electron N–B–N bond that was also studied by computational methods.[52] The synthesis and isolation of hypervalent boron compounds is extremely challenging;[52] the complexes formed between BX_3 and neutral mono- and bi-dentate ligands (of the type which are being studied in this project) are all expected to be four-coordinate.

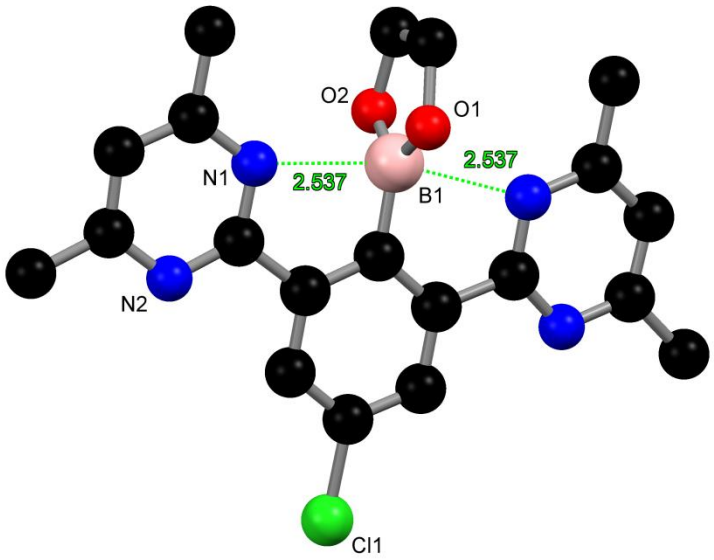

Figure 1.5 View of a five-coordinate hypervalent boron compound.[52] The sum of the Van der Waals radii for B and N is 3.47 Å.[57]

The BX_3 (X = F, Cl, Br, I) form four-coordinate complexes with a range of neutral and charged donor atom ligands from Groups 15 and 16. As hard Lewis acids, they typically form stronger complexes (and thus more complexes are known) with harder O and N donor ligands,[58] but complexes with the softer donor atoms P, As, Sb[30] and S, Se and Te[59] are also known. A literature survey of the known phosphine and arsine complexes of BX_3 can be found in Section 3.1.2. If the ligand has a hydrogen atom directly bonded to the donor atom (as in e.g. H_2O, alcohols and Me_2NH) then the resulting complex with BX_3 (X = Cl,

Br, I) is vulnerable to protonolysis of the B–X bond, ultimately leading to the formation of 3HX and e.g. $B(OH)_3$. The B–F bond in BF_3 however is too strong and so forms stable complexes with these ligands.[58] Boron trihalides will also coordinate to X^- to form $[BX_4]^-$, particularly with the hard fluoride ion. The tetrafluoroborate anion $[BF_4]^-$ has a long history of being used as a weakly coordinating anion.[60]

During complex formation with a Lewis base energy is required to reorganise the trigonal planar BX_3 molecule into a pyramidal fragment (this is known as the deformation energy), then bond formation (an exothermic process) occurs. Based on experimental studies, the Lewis acidity of the boron trihalides is generally reported to increase $BF_3 < BCl_3 < BBr_3 < BI_3$, but the origin of the differences in Lewis acidity has long remained controversial.[61] The trend is the opposite of that expected on electronegativity grounds (as fluorine, the most electronegative halogen, yields the most electron poor boron centre), and so the traditional explanation given is that of hyperconjugation, that is, pπ–pπ bonding between the filled p orbitals on the halogen and the formally empty 2p orbital on boron, making the orbital less available for lone pair donation from a Lewis base, and resonance stabilising the trigonal planar state. The orbital overlap is greatest for fluorine (making BF_3 the weakest Lewis acid), and decreases as the halogen gets heavier, as its orbitals become more diffuse.[62-64] However it has been calculated that the pπ orbital overlap between B and X is greater in BCl_3 and BBr_3 than in BF_3.[64] Furthermore a theoretical (*ab initio*) study has reported that the π-donor strength of the halogens in MX_3 (M = B, Al, Ga, In, Tl) increases F < Cl < Br < I.[65]

Numerous different experimental and theoretical studies have tried to establish and explain the relative Lewis acid strengths of BX_3, and over time several other theories have been proposed. Recently, detailed computational studies have concluded that the intrinsic Lewis acidity of BX_3 originates from a balance between the electronegativity of X and the overlap between the orbitals on B and X that form the σ-bond (the greater the overlap, the weaker the Lewis acidity), independent of π-overlap.[61] Most papers discuss the Lewis acidity of BX_3 in terms of their interactions with specific Lewis bases, and one key point that has emerged is that the apparent order of Lewis acidity depends on the particular pair involved; for example, BCl_3 is reportedly a stronger Lewis acid than BF_3 towards the strong Lewis bases PMe_3 and PCl_3, but for PF_3 and $P(CN)_3$ BF_3 is a stronger Lewis acid.[66] It has also been found that computational studies on coordinate covalent bonding in boron trihalide complexes are highly sensitive to the level of theory applied, sometimes giving conflicting results, and so must be treated critically.[61] Studies have shown that the bond

dissociation energy (bond strength) is not always a good measure of Lewis acidity,[61] and does not always correlate with the intrinsic interaction energy (the donor-acceptor strength, which can be separated into three main components: electrostatic attraction, Pauli repulsion and covalent bonding) as the deformation energy of both the Lewis acid and Lewis base can (but does not always) significantly change the trend observed.[31,66]

1.5.2 Aluminium, gallium and indium

As textbook Lewis acids the MX_3 (M = Al, Ga, In) readily coordinate to a range of neutral and anionic ligands, and are susceptible to aggregation by M–X–M bridges in the solid state.[49] The MF_3 are polymeric inert solids that are insoluble and unreactive with water. Their limited coordination chemistry with neutral donors has been recently reviewed,[67] and consists of complexes with hard O and N donor ligands only. For instance, the X-ray crystal structures of $[MF_3(bipy)(H_2O)]\cdot 2H_2O$ (M = Al, Ga, In) are all known.[68,69] Recently, the strength and stability in aqueous solution of the M–F bonds in $[MF_3(L)]$ (M = Al, Ga, In; L = Me_3-tacn, $BzMe_2$-tacn) has been a driving force in the development of new potential ^{18}F-labelled positron emission tomography (PET) imaging agents.[70]

Much more diverse coordination chemistry is found with MX_3 (X = Cl, Br, I), and a lot of the literature in this area has been dedicated to revealing and rationalising the composition of complexes in both the solution and solid states, though systematic studies are rare and the chemistry with some types of ligand (such as that of AlX_3 with neutral phosphine ligands)[30] has been underexplored. A review of the literature published on phosphine and arsine complexes of AlX_3 can be found in Section 2.1.2. The outcome of a reaction between MX_3 and a donor L is governed by an often subtle interplay of a number of factors, including the nature of M, L, X, and the solvent, reagent stoichiometries and reaction conditions employed.[49] For example, the donor solvent THF dissolves $AlCl_3$ with complexation to form trigonal bipyramidal[71] $[AlCl_3(THF)_2]$ (Figure 1.6(b)) as the major species (which undergoes *cis-trans* isomerisation in solution), with the ionic $[AlCl_2(THF)_4][AlCl_4]$ also present as a minor (~ 10%) species.[72] Crystals were later grown using a 1:2 $AlCl_3$: THF ratio in toluene showing the geometry of the cation to be *trans*-$[AlCl_2(THF)_4]^+$ (Figure 1.6(c)).[73] Distorted tetrahedral[74] $[AlCl_3(THF)]$ (Figure 1.6(a)) can be obtained by pumping on the 1:2 complex *in vacuo*.[75]

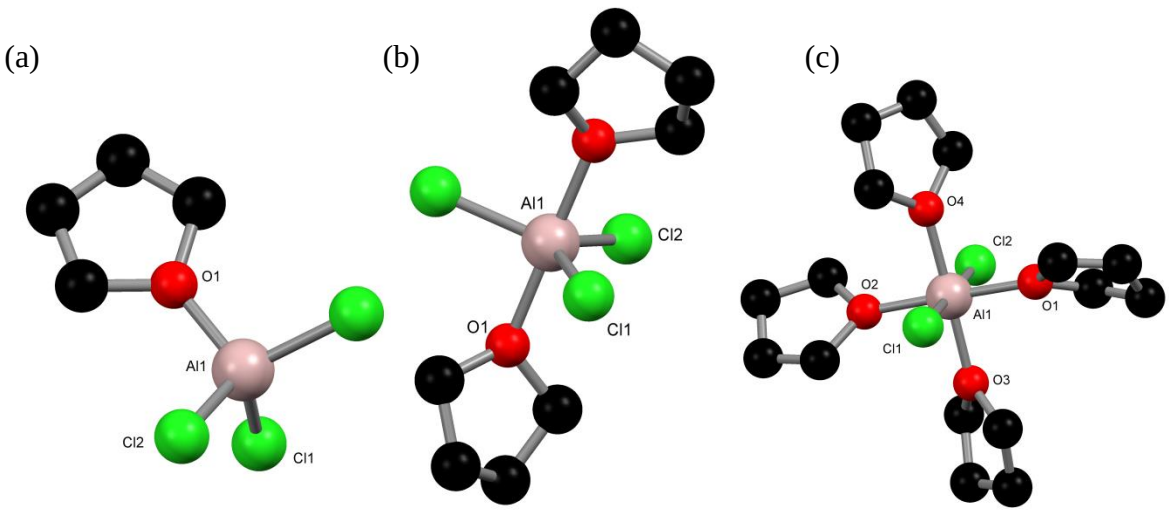

Figure 1.6 Views of (a) $[AlCl_3(THF)]$, (b) $[AlCl_3(THF)_2]$ and (c) $[AlCl_2(THF)_4]^+$.[71,73,74]

Steric effects can be important; for instance with pyridine 1:1, 1:2 and 1:3 complexes have all been isolated as $[AlCl_3(py)]$,[76] ionic *trans*-$[AlCl_2(py)_4][AlCl_4]$[77] and neutral *mer*-$[AlCl_3(py)_3]$[77] respectively, while the reaction of $AlCl_3$ with an excess of 2-methylpyridine (mpy) yielded crystals of *pseudo*-tetrahedral $[AlCl_3(mpy)]$ only.[74] While AlX_3 readily forms four-, and hypervalent five- and six-, coordinate complexes, the majority of GaX_3 coordination chemistry is four-coordinate. Due to the larger size of indium, InX_3 often forms complexes with higher coordination numbers,[49] including seven-coordinate complexes such as $[InCl_3(L)(MeOH)]$ (Figure 1.7), $[InCl_3(L)(H_2O)]$ and $[InCl_4(L)]^-$ (where L = 2,6-$C_5H_3N(C_2H_3NOH)_2$), which all have a pentagonal bipyramidal structure.[78]

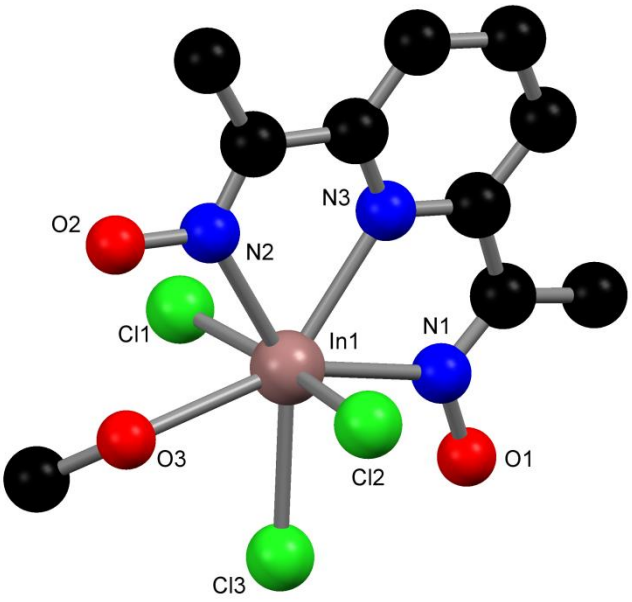

Figure 1.7 View of $[InCl_3\{2,6\text{-}C_5H_3N(C_2H_3NOH)_2\}(MeOH)]$.[78]

The factors that govern the intrinsic Lewis acidity (i.e. valence deficiency) of BX_3 can be extended to AlX_3 also, with the theoretical study suggesting that the aluminium(III) halides are better Lewis acids than the corresponding boron(III) halides due to a greater electronegativity difference between M and X.[61] When the Lewis acidities of AlX_3 are discussed in terms of their donor-acceptor interactions with specific Lewis bases, the intrinsic interaction energies are typically lower than for the corresponding BX_3 complexes, but because the deformation energies of AlX_3 are much smaller the resulting bond strengths are often higher.[31] Recently a joint theoretical (DFT) and experimental (X-ray crystallography) study has established that the order of Lewis acidity decreases $AlCl_3$ > $AlBr_3$ >> AlI_3, though the calculations are made on gas phase molecules and effects such as intermolecular packing were found to sometimes cause anomalous results in the solid state. The study also establishes the orders of Lewis acidity as $AlCl_3$ > $AlBr_3$ > $GaCl_3$ > $GaBr_3$ and $GaCl_3$ > $GaBr_3$ > GaI_3.[79] The lower Lewis acidity of GaI_3 is used to explain why it forms only the monomeric adduct [GaI_3(pyz)] with the non-chelating rigid bidentate ligand pyrazine, while infinite polymeric chains of [MX_3(μ-pyz)] are obtained from the 1:1 reactions with $AlBr_3$ and $GaCl_3$.[80]

1.6 Heavy Group 14 Coordination Chemistry

The Group 14 elements have the ground state electron configuration ns^2np^2, meaning the common oxidation states are +2 and +4. As the group is descended the +2 oxidation state becomes more favourable due to the "inert pair effect"; tin has extensive chemistries of both Sn(II) and Sn(IV) and can readily switch between oxidation states, while for lead, Pb(II) dominates in inorganic complexes.[58,81] Inorganic Pb(IV) species are typically unknown or are highly reactive (known compounds such as PbO_2 are strong oxidising agents), whereas organolead(IV) compounds (PbR_4) are relatively stable, but are very poor Lewis acids. This division has been attributed to the more electronegative substituents in the inorganic compounds increasing the positive charge on the lead centre, which in turn causes the 6s orbital to contract more than the 6p orbitals, making sp^n hybridisation less favourable. Therefore the stability of the electronegatively substituted Pb(IV) compounds is decreased.[82]

The large size of both tin and lead (see Table 1.1) and the intermediate Lewis acidity of Sn(II) and Pb(II)[32] means that the divalent metals form complexes with a range of neutral and anionic donor atom ligands and coordination numbers. While there are a greater number of complexes reported with harder O and N donor ligands,[48,81] complexes

containing the softer donor atoms S, Se and P also exist,[30,83,84] and the known chemistry with neutral Group 15 donor ligands is detailed in Section 5.1.1. In many cases the range of distances between M(II) and the donor atoms of the ligands are widely spread, which makes establishing the exact coordination number of the metal problematic, and so the upper length limit for a bond is usually set as the sum of the Van der Waals radii for the two atoms in question.[85] Ten-coordinate complexes (such as $[Sn(15\text{-crown-}5)_2][BF_4]_2$) have been reported for Sn(II),[84] while for Pb(II) coordination numbers up to twelve are known,[48] including the crystallographically authenticated $[Pb(NO_3)_6]^{4-}$ anion.[86]

Table 1.1 Selected radii (Å) of Sn and Pb

	Ionic radius of M(II)[58]	Covalent Radius[87]	Van der Waals Radius[57]
Sn	1.18	1.39	2.17
Pb	1.19	1.46	2.02

The geometry of the coordination complexes of Sn(II) and Pb(II) are significantly influenced by whether the ns^2 electron pair is stereochemically active or not. If stereochemically active the lone pair is presumed to occupy one of the bonding orbitals of the metal, and is normally identified by a void in the coordination sphere. In the 3-centre-4-electron bonding model (see Section 1.4.1) the stereochemically active lone pair occupies the non-bonding orbital. If stereochemically inactive the lone pair is assumed to occupy the spherically symmetric ns orbital, which makes the orbital unavailable for bonding to ligands and weakens the M–L bonding due to its screening effect.[30,85]

Shimoni-Livny *et al.*[88] have investigated the influence of the lone pair on the coordination geometry of Pb(II) complexes. They assigned the complexes as being either "holodirected", where bonds to the ligand donor atoms are distributed around the entirety of the metal, and "hemidirected," (Figure 1.8) where there is an identifiable void in the distribution of bonds (presumed to be occupied by a stereochemically active lone pair). Which geometry was observed was found to strongly depend on the coordination number around the Pb(II) centre and the steric repulsion of the ligands (multidentate ligands favour a hemidirected geometry). Complexes with low coordination numbers (two to five) were typically found to be hemidirected and those with high coordination numbers (nine to ten) holodirected, while for intermediate coordination numbers (six to eight) both geometries were found.[88] Through a joint crystal structure and DFT study Davidovich *et al.*[89] reviewed the stereochemistry of Pb(II) complexes with oxygen donor ligands and a stereochemically

active lone pair and found that there were commonly two ranges of Pb–O bond lengths, with the shorter bonds being primarily covalent in nature, while the longer bonds were to a great extent ionic, often bridging between molecules to give extended structures in the solid state. The work was later extended to include complexes with sulfur and selenium donor ligands, which were found to nearly all contain a stereochemically active lone pair, though they exhibit fewer preferred geometries.[83]

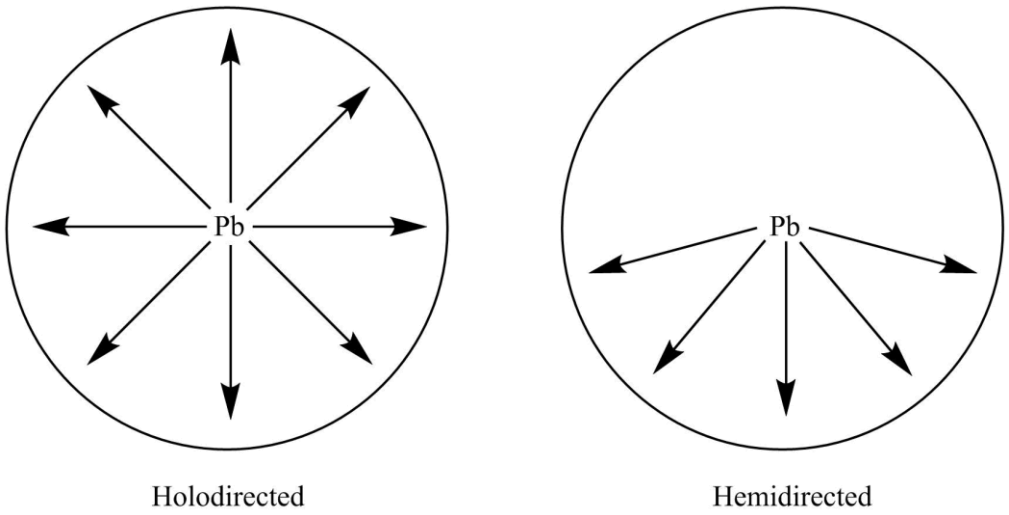

Figure 1.8 Stereochemical influence of the lone pair on Pb(II) coordination complexes.[88]

Though there are various studies that attempt to classify the stereochemistry of Pb(II) coordination complexes, the often irregular coordination geometries exhibited by Sn(II) and particularly Pb(II) complexes means that they generally do not lend themselves to simple descriptions. The combination of the unusual geometries and high coordination numbers that are frequently observed ultimately makes it difficult to rationalise the bonding in these complexes and to evaluate the influence of the lone pair.[30,90]

1.7 Analytical Techniques

The compounds discussed in this work have typically been characterised using solid- and solution-state techniques that are widely used in synthetic coordination chemistry. It is important to note that solution NMR spectroscopic data may not be representative of the compound in the solid state (e.g. due to poor solubility or dissociation of the compound in solution owing to the high lability of these donor-acceptor interactions), making solid state characterisation essential. Infrared spectroscopy (performed as a Nujol mull over the range 4000-200 cm^{-1}) has been used to identify the bonds present in the species, with an emphasis on M–X bands (where present) due to their characteristic stretching frequencies.

Group theory can be used to determine the molecular symmetry from the number of stretches corresponding to a bond type observed;[91] this has proved to be especially useful for the M–X bonds in this work. Single crystal X-ray diffraction is a powerful technique that allows the solid state structure of the complex to be asserted unambiguously (though the structure may not be reflective of the bulk solid), and shows the presence of any solid state intramolecular and intermolecular interactions. Microanalyses (C, H and N elemental analysis) have also been obtained to confirm the molecular formulae and check the purity of the compounds synthesised. The NMR nuclei pertinent to this project and cyclic voltammetry and chronoamperometry, used in Chapter 6 to investigate the electrochemical behaviour of Sn(II) and Pb(II) compounds, will be discussed further in the following sections.

1.7.1 Multinuclear NMR spectroscopy

NMR spectroscopy is valuable tool for obtaining solution state data on the complexes synthesised. Where possible, chemical shifts, coupling constants and coordination shifts are reported, and variable temperature NMR spectroscopy is utilised for dynamic systems. Table 1.2 gives the nuclear properties of the principle nuclei studied. Complimentary data can be obtained on a compound by studying several NMR nuclei in parallel, often leading to further elucidation of its behaviour in solution, so that more conclusions can be drawn.

Table 1.2 Selected properties of the NMR nuclei studied[92]

Nucleus	Spin	Natural Abundance (%)	Receptivity Relative to ^{13}C	Quadrupole Moment (10^{-28} m^2)
^{1}H	1/2	99.9	5.67×10^{3}	–
^{13}C	1/2	1.1	1.00	–
^{11}B	3/2	80.4	7.54×10^{2}	0.04
^{19}F	1/2	100	4.73×10^{3}	–
^{27}Al	5/2	100	1.17×10^{3}	0.14
^{31}P	1/2	100	3.77×10^{2}	–
^{119}Sn	1/2	8.6	25.7	–
^{207}Pb	1/2	22.6	11.9	–

As part of this work, NMR spectroscopy has been performed with the quadrupolar nuclei ^{11}B and ^{27}Al. Quadrupolar nuclei ($I > ½$) possess an ellipsoidal distribution of charge which reflects the presence of an electric quadrupole moment. In a molecule there is an electric field gradient at the nucleus due to asymmetry in the local charge distribution (caused by the electrons and other nearby nuclei), which constantly fluctuates due to molecular motions. The electric field gradient couples with the quadrupole moment to provide an efficient relaxation pathway that is termed quadrupolar relaxation; it normally dominates over other relaxation mechanisms and causes line broadening (sometimes to the extent that a resonance cannot be observed). Resonances for nearby nuclei are also expected to be broadened as a result of interactions with the quadrupolar nucleus. The electric field gradient of a molecule depends on the arrangement of ligands and the electron imbalance in the bonds; more symmetrical molecules have a slower relaxation rate, and hence they generally give sharper resonances and sometimes allow coupling to other nuclei to be observed, though usually only over one bond.[92]

As previously mentioned, the favourable nuclear properties of the ^{31}P NMR nucleus (I = ½) make it a key tool for monitoring reactions and characterising complexes involving phosphine or phosphine oxide ligands. In contrast, the large quadrupole moment (Q = 0.29 x 10^{-28} m^2) of ^{75}As (I = 3/2, N.A. = 100%) leads to severe broadening of the NMR lines, meaning only highly symmetrical molecules can be observed,[92] and so it has not been studied.

Boron NMR Spectroscopy

Boron has two naturally occurring isotopes, ^{10}B and ^{11}B, both of which are quadrupolar nuclei (see Table 1.3), though ^{11}B is normally studied because of its greater abundance, better sensitivity and lower nuclear spin.[93]

Table 1.3 Selected properties of the boron nuclei[92]

Nucleus	Spin	Natural Abundance (%)	Receptivity Relative to ^{13}C	Quadrupole Moment (10^{-28} m^2)
^{10}B	3	19.58	22.1	0.082
^{11}B	3/2	80.42	7.54 x 10^2	0.041

The known chemical shift range of ^{11}B for non-paramagnetic species spans about 200 ppm with δ^{11}B for $[BF_3(OEt_2)]$ at zero;[92] the $[BX_4]^-$ anions alone span around 130 ppm, with δ =

–1.7 (X = F), +6.5 (X = Cl), –23.0 (X = Br) and –127.7 (X = I) reported.[94] Chemical shifts can vary with solvent and temperature by up to ~ 2 ppm.[92] The observation of J^{11}_{BX} coupling constants in the spectra of both ^{11}B and the other nucleus X can be hindered or prevented by line broadening, particularly when the couplings are small. In particular, the $^{1}J_{BF}$ coupling constant for $[BF_4]^-$ is very small (1-5 Hz, depending on solution conditions)[92] and so is not always observed.

Aluminium NMR Spectroscopy

Selected properties of the quadrupolar NMR nucleus, ^{27}Al, can be found in Table 1.2. The chemical shift range of ^{27}Al spans about 300 ppm (~ +270 to –30) with $\delta^{27}Al$ for aqueous $[Al(H_2O)_6]^{3+}$ at zero, though only alkyl aluminium species typically resonate above 120 ppm. Chemical shifts are chiefly determined by the coordination number and nature of the ligands bonded to the aluminium, with shifts generally moving to lower frequencies going from four- to five- to six-coordinate aluminium (the obvious exception to this is $[AlI_4]^-$ which has an anomalously low frequency chemical shift at δ = –26.5), and also with increasing halogen atomic number. Highly symmetric molecules give narrow lines that can have linewidths of just a few hertz, while distorted environments typically give much broader lines.[92]

Tin NMR Spectroscopy

There are three naturally occurring tin isotopes whose I = ½, ^{115}Sn, ^{117}Sn and ^{119}Sn, though in practise only the latter two are studied as NMR nuclei as ^{115}Sn is more than twenty times less abundant and receptive than the other isotopes (see Table 1.4). Usually it is ^{119}Sn NMR spectroscopy that is used due to its slightly greater abundance and receptivity. The chemical shift range for ^{119}Sn is approximately 6500 ppm (~ 4000 to –2500, with $\delta^{119}Sn$ for Me_4Sn at zero).[92,95] In the NMR spectra of nuclei bonded to tin, satellites corresponding to both ^{119}Sn and ^{117}Sn are usually readily recognisable.

Table 1.4 Selected properties of tin nuclei with I = ½[92]

Nucleus	Natural Abundance (%)	Receptivity Relative to ^{13}C	Magnetogyric Ratio (γ / 10^7 rad s^{-1} T^{-1})
^{115}Sn	0.35	0.707	–8.801
^{117}Sn	7.61	19.9	–9.589
^{119}Sn	8.58	25.7	–10.032

Different coordinating solvents can produce sometimes large changes in the chemical shifts observed for a tin species, which varies with concentration.[96,97] For $^{119}Sn\{^{1}H\}$ NMR spectroscopy the large negative magnetogyric ratio of ^{119}Sn often results in the NOE (nuclear Overhauser effect, which arises from cross-relaxation processes) diminishing the signal. In order to overcome the NOE a relaxation agent (a non-reactive paramagnetic species) such as $[Cr(acac)_3]$ can be used, which provides a dominating relaxation mechanism.[92]

Lead NMR Spectroscopy

There is only one NMR active (I = ½) nucleus for lead, ^{207}Pb, selected properties of which can be found in Table 1.2. The chemical shift range for ^{207}Pb is over 16000 ppm, with $\delta^{207}Pb$ for Me_4Pb at zero.[98] Due to the poor solubility of many of the compounds synthesised, and the labile nature of Pb(II) in solution,[99] lead NMR spectroscopy was found to be of very limited use in this project.

1.7.2 Cyclic voltammetry and electrodeposition

One of the aims of the project has been to design suitable reagents for the supercritical fluid electrodeposition of tin and lead, and once synthesised their electrochemical behaviour was preliminarily studied in liquid CH_2Cl_2 (see Chapter 6). Cyclic voltammetry was chosen as it provides a fast, efficient and straightforward assessment of the redox behaviour of a compound, providing key information such as the metal deposition potential (E_{pc}) and the available electrochemical window of the system.

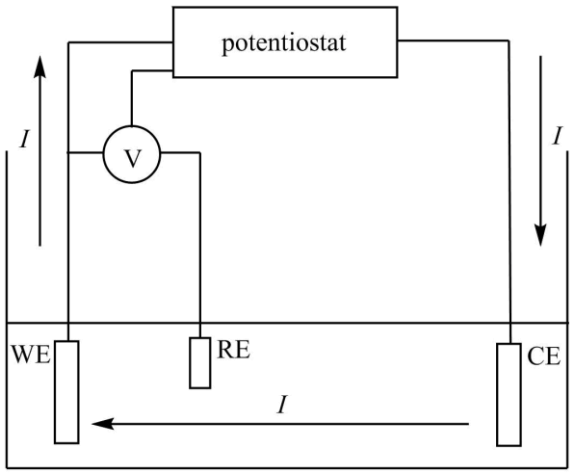

Figure 1.9 Schematic representation of a standard three electrode electrochemical cell where the working electrode (WE), counter electrode (CE) and reference electrode (RE) are immersed in an electrolyte solution.

To study electrochemical reactions a three (working, reference and counter) electrode system (Figure 1.9) is immersed in the electrolyte solution containing the electroactive species to be studied. The potential of the working electrode is controlled against a reference electrode while the current (*I*) flows between the counter and working electrodes. The working electrode is typically composed of a highly conducting material, such as platinum, gold or glassy carbon, that is ideally inert under the conditions and potential range employed. If a reduction process is occurring at the working electrode then an oxidation reaction will occur at the counter electrode (and *vice versa*) to balance the system. Platinum gauze is often chosen to be the counter electrode to provide an electrochemically inert material with a large surface area. The reference electrode should maintain a constant potential throughout the experiment(s). For the experiments in CH_2Cl_2 a Ag/AgCl reference electrode submersed in 0.1 M $[N^nBu_4]Cl$ in CH_2Cl_2 (i.e. the same concentration of supporting electrolyte), kept separate from the main electrolyte bath by a porous glass frit to minimise contamination, was used. A judicious choice of a compatible supporting electrolyte is required to maintain sufficient conductivity in the solution and thereby lower the resistance of the solution.[100]

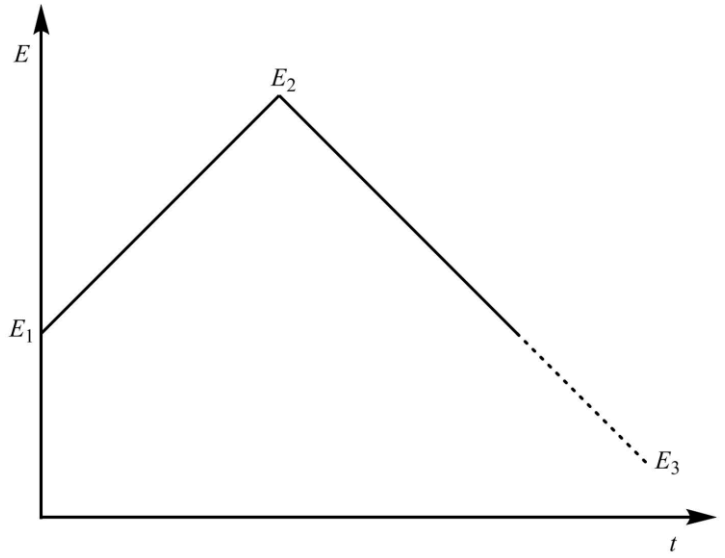

Figure 1.10 The potential-time profile employed in cyclic voltammetry.[100]

In cyclic voltammetry the potential of the working electrode is varied linearly with time from the initial potential (E_1) by a fixed value known as the scan rate. After reaching a chosen potential value (E_2) the potential is then scanned back to either E_1 or a new potential E_3 before returning to E_1 to complete the cycle (Figure 1.10). During the experiment the current (*I*) is measured as a function of the potential and the response is typically plotted as current (or current density) *vs*. potential, known as a cyclic

voltammogram. Generally the open circuit potential (i.e. the potential where the current density is zero) is chosen to be E_1 and the potential can either be scanned positive to study oxidation processes or negative to probe reductions first.[100]

The information gained from cyclic voltammetry studies of a precursor can be then used to help choose the parameters (e.g. the deposition potential) to use for electrodeposition from that precursor. In electrodeposition, metal ions in solution are reduced to neutral species, whereby they form a new solid phase on the electrode surface. For tin and lead, cathodic deposition of the metals from precursors containing Sn and Pb in the +2 oxidation state proceeds via the equation $M^{2+} + 2e^- \rightarrow M$. Potentiostatic electrodeposition involves applying and holding a constant potential. It can be performed using chronoamperometry, where the potential of the working electrode is stepped from a potential where no reaction is occurring to the desired deposition potential. The resulting current is monitored as a function of time, which can be plotted as a chronoamperogram.[100] The deposition potentials and times can be tailored in order to obtain films of a desired thickness (typically a 1 to 2 μm thickness is sufficient for EDX and XRD analysis).[101]

1.8 References

1. P. N. Bartlett, D. A. Cook, M. W. George, A. L. Hector, J. Ke, W. Levason, G. Reid, D. C. Smith and W. Zhang, *Phys. Chem. Chem. Phys.*, 2014, **16**, 9202-9219.

2. T. Chivers and J. Konu, *Comments Inorg. Chem.*, 2009, **30**, 131-176.

3. W. Lu and C. M. Lieber, *Nat. Mater.*, 2007, **6**, 841-850.

4. N. P. Dasgupta, J. Sun, C. Liu, S. Brittman, S. C. Andrews, J. Lim, H. Gao, R. Yan and P. Yang, *Adv. Mater.*, 2014, **26**, 2137-2184.

5. M. Palummo, F. Iori, R. Del Sole and S. Ossicini, *Phys. Rev. B*, 2010, **81**, 121303(R).

6. C. J. Vineis, A. Shakouri, A. Majumdar and M. G. Kanatzidis, *Adv. Mater.*, 2010, **22**, 3970-3980.

7. J. Wang, *Biosens. Bioelectron.*, 2006, **21**, 1887-1892.

8. T. Zhu and J. Li, *Prog. Mater. Sci.*, 2010, **55**, 710-757.

9. Y. Xia, P. Yang, Y. Sun, Y. Wu, B. Mayers, B. Gates, Y. Yin, F. Kim and H. Yan, *Adv. Mater.*, 2003, **15**, 353-389.

10. C. N. R. Rao, F. L. Deepak, G. Gundiah and A. Govindaraj, *Prog. Solid State Chem.*, 2003, **31**, 5-147.

11. T. Djenizian, I. Hanzu, M. Eyraud and L. Santinacci, *C. R. Chim.*, 2008, **11**, 995-1003.

12. M.-C. Sun, G. Kim, J. H. Lee, H. Kim, S. W. Kim, H. W. Kim, J.-H. Lee, H. Shin and B.-G. Park, *Microelectron. Eng.*, 2013, **110**, 141-146.

13. L. Cademartiri and G. A. Ozin, *Adv. Mater.*, 2009, **21**, 1013-1020.

14. R. Schuster, *ChemPhysChem*, 2001, **2**, 411-412.

15. P. C. Andricacos, C. Uzoh, J. O. Dukovic, J. Horkans and H. Deligianni, *IBM J. Res. Dev.*, 1998, **42**, 567-574.

16. J. Ke, W. Su, S. M. Howdle, M. W. George, D. Cook, M. Perdjon-Abel, P. N. Bartlett, W. Zhang, F. Cheng, W. Levason, G. Reid, J. Hyde, J. Wilson, D. C. Smith, K. Mallik and P. Sazio, *Proc. Natl. Acad. Sci. U. S. A.*, 2009, **106**, 14768-14772.

17. H. Liu, Y. Liu and J. Li, *Phys. Chem. Chem. Phys.*, 2010, **12**, 1685-1697.

18. J. Ke, P. N. Bartlett, D. Cook, T. L. Easun, M. W. George, W. Levason, G. Reid, D. Smith, W. Su and W. Zhang, *Phys. Chem. Chem. Phys.*, 2012, **14**, 1517-1528.

19. R. S. Oakes, A. A. Clifford and C. M. Rayner, *J. Chem. Soc., Perkin Trans. 1*, 2001, 917-941.

20. Y. Liang, C. Zhen, D. Zou and D. Xu, *J. Am. Chem. Soc.*, 2004, **126**, 16338-16339.

21. D. Bera, S. C. Kuiry and S. Seal, *JOM*, 2004, **56**, 49-53.

22. A. P. Abbott, C. A. Eardley, J. C. Harper and E. G. Hope, *J. Electroanal. Chem.*, 1998, **457**, 1-4.

23. C. Y. Cummings, P. N. Bartlett, D. Pugh, G. Reid, W. Levason, M. M. Hasan, A. L. Hector, J. Spencer and D. C. Smith, *J. Electrochem. Soc.*, 2015, **162**, D619-D624.

24. D. Cook, P. N. Bartlett, W. Zhang, W. Levason, G. Reid, J. Ke, W. Su, M. W. George, J. Wilson, D. Smith, K. Mallik, E. Barrett and P. Sazio, *Phys. Chem. Chem. Phys.*, 2010, **12**, 11744-11752.

25. P. N. Bartlett, M. Perdjon-Abel, D. Cook, G. Reid, W. Levason, F. Cheng, W. Zhang, M. W. George, J. Ke, R. Beanland and J. Sloan, *ChemElectroChem*, 2014, **1**, 187-194.

26. A. P. Abbott and C. A. Eardley, *J. Phys. Chem. B*, 2000, **104**, 9351-9355.

27. P. N. Bartlett, C. Y. Cummings, W. Levason, D. Pugh and G. Reid, *Chem. Eur. J.*, 2014, **20**, 5019-5027.

28. J. A. McCleverty and T. J. Meyer, eds., *Comprehensive Coordination Chemistry II*, Elsevier, Oxford, 2004.

29. C. A. McAuliffe and W. Levason, *Phosphine, Arsine and Stibine Complexes of the Transition Elements*, Elsevier, Amsterdam, 1979.

30. J. Burt, W. Levason and G. Reid, *Coord. Chem. Rev.*, 2014, **260**, 65-115.

31. F. Bessac and G. Frenking, *Inorg. Chem.*, 2006, **45**, 6956-6964.

32. R. G. Pearson, *J. Chem. Educ.*, 1968, **45**, 581.

33. C. A. Tolman, *Chem. Rev.*, 1977, **77**, 313-348.

34. P. B. Dias, M. E. M. de Piedade and J. A. M. Simões, *Coord. Chem. Rev.*, 1994, **135**, 737-807.

35. C. A. Tolman, W. C. Seidel and L. W. Gosser, *J. Am. Chem. Soc.*, 1974, **96**, 53-60.

36. W. Levason and G. Reid, *Coord. Chem. Rev.*, 2006, **250**, 2565-2594.

37. J. A. Bilbrey, A. H. Kazez, J. Locklin and W. D. Allen, *J. Comput. Chem.*, 2013, **34**, 1189-1197.

38. P. W. N. M. van Leeuwen, P. C. J. Kamer, J. N. H. Reek and P. Dierkes, *Chem. Rev.*, 2000, **100**, 2741-2770.

39. P. Dierkes and P. W. N. M. van Leeuwen, *J. Chem. Soc., Dalton Trans.*, 1999, 1519-1530.

40. A. J. Kendall and D. R. Tyler, *Dalton Trans.*, 2015, **44**, 12473-12483.

41. W. I. Cross, S. M. Godfrey, C. A. McAuliffe, A. G. Mackie and R. B. Pritchard, in *Chemistry of Arsenic, Antimony and Bismuth*, ed. N. C. Norman, Blackie Academic & Professional, London, 1998, pp. 207-282.

42. D. B. Chesnut, *J. Am. Chem. Soc.*, 1998, **120**, 10504-10510.

43. D. B. Chesnut and A. Savin, *J. Am. Chem. Soc.*, 1999, **121**, 2335-2336.

44. F. R. Hartley, ed., *The Chemistry of Organophosphorus Compounds*, John Wiley and Sons, Chichester, 1992, vol. 2.

45. A. E. Reed and P. v. R. Schleyer, *J. Am. Chem. Soc.*, 1990, **112**, 1434-1445.

46. G. A. Landrum, N. Goldberg and R. Hoffmann, *J. Chem. Soc., Dalton Trans.*, 1997, 3605-3613.

47. N. C. Norman, *Phosphorus, Sulfur Silicon Relat. Elem.*, 1994, **87**, 167-176.

48. E. S. Claudio, H. A. Godwin and J. S. Magyar, *Prog. Inorg. Chem.*, 2003, **51**, 1-144.

49. S. Aldridge and A. J. Downs, eds., *The Group 13 Metals Aluminium, Gallium, Indium and Thallium: Chemical Patterns and Peculiarities*, John Wiley and Sons, UK, 2011.

50. D. Vidovic and S. Aldridge, *Chem. Sci.*, 2011, **2**, 601-608.

51. J. A. J. Pardoe and A. J. Downs, *Chem. Rev.*, 2007, **107**, 2-45.

52. Y. Hirano, S. Kojima and Y. Yamamoto, *J. Org. Chem.*, 2011, **76**, 2123-2131.

53. C. Dou, S. Saito and S. Yamaguchi, *J. Am. Chem. Soc.*, 2013, **135**, 9346-9349.

54. G. P. McGovern, D. Zhu, A. J. A. Aquino, D. Vidović and M. Findlater, *Inorg. Chem.*, 2013, **52**, 13865-13868.

55. D. Y. Lee and J. C. Martin, *J. Am. Chem. Soc.*, 1984, **106**, 5745-5746.

56. T. Yano, T. Yamaguchi and Y. Yamamoto, *Chem. Lett.*, 2009, **38**, 794-795.

57. M. Mantina, A. C. Chamberlin, R. Valero, C. J. Cramer and D. G. Truhlar, *J. Phys. Chem. A*, 2009, **113**, 5806-5812.

58. N. N. Greenwood and A. Earnshaw, *Chemistry of the Elements*, Butterworth-Heinemann, Oxford, 2 edn., 1997.

59. M. Schmidt and H. D. Block, *Chem. Ber.*, 1970, **103**, 3705-3710.

60. S. H. Strauss, *Chem. Rev.*, 1993, **93**, 927-942.

61. J. A. Plumley and J. D. Evanseck, *J. Phys. Chem. A*, 2009, **113**, 5985-5992.

62. B. D. Rowsell, R. J. Gillespie and G. L. Heard, *Inorg. Chem.*, 1999, **38**, 4659-4662.

63. F. Bessac and G. Frenking, *Inorg. Chem.*, 2003, **42**, 7990-7994.

64. T. Brinck, J. S. Murray and P. Politzer, *Inorg. Chem.*, 1993, **32**, 2622-2625.

65. G. Frenking, S. Fau, C. M. Marchand and H. Grützmacher, *J. Am. Chem. Soc.*, 1997, **119**, 6648-6655.

66. C. Loschen, K. Voigt, J. Frunzke, A. Diefenbach, M. Diedenhofen and G. Frenking, *Z. Anorg. Allg. Chem.*, 2002, **628**, 1294-1304.

67. S. L. Benjamin, W. Levason and G. Reid, *Chem. Soc. Rev.*, 2013, **42**, 1460-1499.

68. R. Bhalla, W. Levason, S. K. Luthra, G. McRobbie, F. M. Monzittu, J. Palmer, G. Reid, G. Sanderson and W. Zhang, *Dalton Trans.*, 2015, **44**, 9569-9580.

69. A. B. Ilyukhin and M. A. Malyarik, *Zh. Neorg. Khim.*, 1999, **44**, 1511-1513.

70. R. Bhalla, C. Darby, W. Levason, S. K. Luthra, G. McRobbie, G. Reid, G. Sanderson and W. Zhang, *Chem. Sci.*, 2014, **5**, 381-391.

71. A. H. Cowley, M. C. Cushner, R. E. Davis and P. E. Riley, *Inorg. Chem.*, 1981, **20**, 1179-1181.

72. J. Derouault, P. Granger and M. T. Forel, *Inorg. Chem.*, 1977, **16**, 3214-3218.

73. N. C. Means, C. M. Means, S. G. Bott and J. L. Atwood, *Inorg. Chem.*, 1987, **26**, 1466-1468.

74. L. M. Engelhardt, P. C. Junk, C. L. Raston, B. W. Skelton and A. H. White, *J. Chem. Soc., Dalton Trans.*, 1996, 3297-3301.

75. J. Derouault and M. T. Forel, *Inorg. Chem.*, 1977, **16**, 3207-3213.

76. A. Dimitrov, D. Heidemann and E. Kemnitz, *Inorg. Chem.*, 2006, **45**, 10807-10814.

77. P. Pullmann, K. Hensen and J. W. Bats, *Z. Naturforsch., B: Anorg. Chem., Org. Chem.*, 1982, **37**, 1312-1315.

78. S. Abram, C. Maichle-Mössmer and U. Abram, *Polyhedron*, 1997, **16**, 2183-2191.

79. A. Y. Timoshkin, M. Bodensteiner, T. N. Sevastianova, A. S. Lisovenko, E. I. Davydova, M. Scheer, C. Graßl and A. V. Butlak, *Inorg. Chem.*, 2012, **51**, 11602-11611.

80. T. N. Sevastianova, M. Bodensteiner, A. S. Lisovenko, E. I. Davydova, M. Scheer, T. V. Susliakova, I. S. Krasnova and A. Y. Timoshkin, *Dalton Trans.*, 2013, **42**, 11589-11599.

81. J. Parr, in *Comprehensive Coordination Chemistry II*, eds. J. A. McCleverty and T. J. Meyer, Elsevier, Oxford, 2004, vol. 3, pp. 545-608.

82. M. Kaupp and P. v. R. Schleyer, *J. Am. Chem. Soc.*, 1993, **115**, 1061-1073.

83. R. L. Davidovich, V. Stavila and K. H. Whitmire, *Coord. Chem. Rev.*, 2010, **254**, 2193-2226.

84. C. Beattie, P. Farina, W. Levason and G. Reid, *Dalton Trans.*, 2013, **42**, 15183-15190.

85. J. S. Casas and J. Sordo, eds., *Lead: Chemistry, Analytical Aspects, Environmental Impact and Health Effects*, Elsevier B.V., Amsterdam, 2006.

86. R. E. Cramer, K. A. Mitchell, A. Y. Hirazumi and S. L. Smith, *J. Chem. Soc., Dalton Trans.*, 1994, 563-569.

87. B. Cordero, V. Gomez, A. E. Platero-Prats, M. Reves, J. Echeverria, E. Cremades, F. Barragan and S. Alvarez, *Dalton Trans.*, 2008, 2832-2838.

88. L. Shimoni-Livny, J. P. Glusker and C. W. Bock, *Inorg. Chem.*, 1998, **37**, 1853-1867.

89. R. L. Davidovich, V. Stavila, D. V. Marinin, E. I. Voit and K. H. Whitmire, *Coord. Chem. Rev.*, 2009, **253**, 1316-1352.

90. P. Farina, T. Latter, W. Levason and G. Reid, *Dalton Trans.*, 2013, **42**, 4714-4724.

91. K. Nakamoto, *Infrared and Raman Spectra of Inorganic and Coordination Compounds*, Wiley-Interscience, NY, 4 edn., 1986.

92. J. Mason, ed., *Multinuclear NMR*, Plenum Press, NY, 1987.

93. H. Nöth and B. Wrackmeyer, *NMR 14, Nuclear Magnetic Resonance Spectroscopy of Boron Compounds*, Springer-Verlag, Berlin, 1978.

94. J. S. Hartman and G. J. Schrobilgen, *Inorg. Chem.*, 1972, **11**, 940-951.

95. B. Wrackmeyer, *Annu. Rep. NMR Spectrosc.*, 1999, **38**, 203-264.

96. P. J. Smith and L. Smith, *Inorg. Chim. Acta, Rev.*, 1973, **7**, 11-33.

97. J. M. Coddington and M. J. Taylor, *J. Chem. Soc., Dalton Trans.*, 1989, 2223-2227.

98. B. Wrackmeyer and K. Horchler, *Annu. Rep. NMR Spectrosc.*, 1990, **22**, 249-306.

99. A. J. Rossini, A. W. Macgregor, A. S. Smith, G. Schatte, R. W. Schurko and G. G. Briand, *Dalton Trans.*, 2013, **42**, 9533-9546.

100. D. Pletcher, *A First Course in Electrode Processes*, RSC Publishing, Cambridge, 2 edn., 2009.

101. P. N. Bartlett, D. Cook, C. H. de Groot, A. L. Hector, R. Huang, A. Jolleys, G. P. Kissling, W. Levason, S. J. Pearce and G. Reid, *RSC Adv.*, 2013, **3**, 15645-15654.

Chapter 2: Coordination Complexes of Aluminium(III) Halides with Phosphine and Arsine Ligands

2.1 Introduction

In contrast with the heavier Group 13 halides, GaX_3 and InX_3, there has been very limited study of coordination complexes of AlX_3 with neutral phosphine and arsine ligands, with known complexes limited to monodentate examples.[1] The aim of this chapter was to take a systematic approach to the synthesis and characterisation of novel phosphine and arsine complexes, in order to draw comparisons with the analogous GaX_3 and InX_3 systems, whilst rationalising the influence of the halide and (the architecture, steric- and electronic requirements of) the ligand on the coordination environment around the Al(III) centre.

2.1.1 Properties and uses of the aluminium(III) halides

As a light Group 13 element with the ground state electron configuration $3s^2 3p^1$ the most common oxidation state for aluminium is +3, and the aluminium(III) halides (AlX_3) are readily available. The aluminium(I) halides (AlX) are not thermodynamically stable under standard conditions, and disproportionate into metallic aluminium and AlX_3.[2] Crystalline $AlCl_3$ forms a layer lattice with six-coordinate Al(III) centres, while $AlBr_3$ is dimeric (Al_2Br_6) in the solid state. Solid AlI_3 has a chain structure with the repeating unit [$I_2Al(\mu$-I)], so that the Al(III) centre is four-coordinate. The solid state structure of aluminium(III) fluoride (AlF_3) is based on a distorted six-coordinate layer lattice, and unlike the heavier halides it is predominantly ionic in character and is insoluble even in water.[3]

A discussion of the Lewis acidity and bonding trends of Group 13 is given in Section 1.5.2. The aluminium(III) halides are good Lewis acids; a detailed joint experimental (X-ray) and theoretical (DFT) study[4] has recently concluded that Lewis acidity decreases in the order $AlCl_3 > AlBr_3 >> AlI_3$, although in the solid state effects such as hydrogen bonding and intermolecular packing can mask this trend. Unlike the inert AlF_3, the AlX_3 (X = Cl, Br or I) are all very moisture sensitive and readily form complexes with coordinating solvents such as THF and CH_3CN. In weakly coordinating solvents (such as CH_2Cl_2 and toluene) AlX_3 have the dimeric structure $X_2Al(\mu\text{-}X)_2AlX_2$;[3] during complex formation one can view the ligand as cleaving the dimer either symmetrically (Figure 2.1(a)) to give neutral $[AlX_3(L)_n]$ species, or asymmetrically (Figure 2.1(b)) to form a $[AlX_2(L)_n]^+$ cation and an

$[AlX_4]^-$ anion. Four-coordinate Al(III) is the most common geometry observed for complexes with neutral ligands, but five- and six-coordinate geometries occur as well.[2,3] With such a rich structural diversity (exemplified in Section 1.5.2) it is difficult to predict which structure(s) will form for a given ligand without actually performing the relevant experiment(s), and altering the experimental conditions (such as the solvent or reagent stoichiometry employed) can change the composition of the complex obtained.

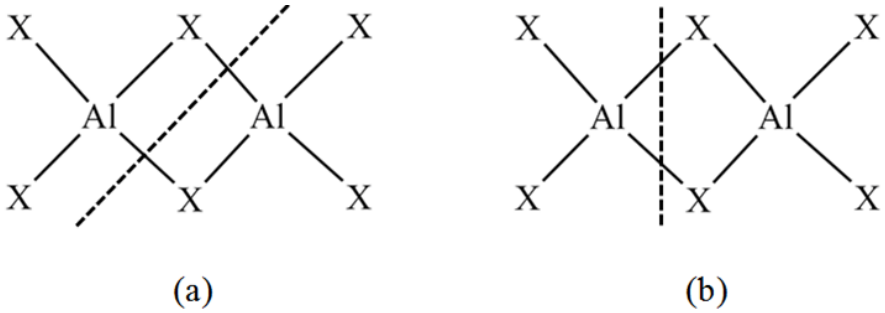

Figure 2.1 The structure of Al_2X_6, showing (a) symmetric cleavage and (b) asymmetric cleavage during complex formation.

AlX_3 molecules have a propensity to halide abstract (forming $[AlX_4]^-$, which can then act as weakly coordinating anions), which has found use both in the laboratory and commercially. Traditionally $AlCl_3$ is used as a catalyst in processes such as Friedel-Crafts acylation and alkylation which proceed via complexation;[5] however more environmentally benign and tolerant alternatives such as $Bi(OTf)_3$ ($OTf = CF_3SO_3$) are now often used.[2,6] Chloroaluminate melts, regarded as the first generation of ionic liquids, have historically been used as effective media for many organic and inorganic reactions and syntheses, but have been largely superseded due to their susceptibility to hydrolysis.[2] More recently, macrocyclic aluminium(III) halide complexes suitable for medical imaging applications have been obtained by ^{18}F radiolabelling.[7,8] Complexes with neutral ligands can also be used as single source precursors for III–V semiconductor materials, for example $[AlCl_3(^tBuNH_2)]$ has been used to prepare AlN thin films via metal organic chemical vapour deposition (MOCVD).[9]

2.1.2 Coordination complexes with phosphine and arsine ligands

Structurally authenticated adducts of AlX_3 (X = Cl, Br, I; there are no reported complexes with AlF_3) with neutral phosphine and arsine ligands are limited to examples with monodentate ligands. The crystal structures of *pseudo*-tetrahedral $[AlCl_3(PPh_3)]$[4] and $[AlX_3(AsPh_3)]$[10] (X = Cl, I) are known. Burford *et al.*[10] also report the synthesis and

spectroscopic data for all $[AlX_3(AsR_3)]$ (X = Cl, Br, I; R = Me, Et, Ph). The reaction of AlX_3 (X = Cl, Br) with $P(SiMe_3)_3$ yielded the adducts $[AlX_3\{P(SiMe_3)_3\}]$[11] which did not undergo dehalosilylation (-Me_3SiX) to form AlP, whereas in the analogous reaction $[AlCl_3\{As(SiMe_3)_3\}]$[12] was isolated as an intermediate in the formation of AlAs. Other known four-coordinate complexes include the weakly bound $[AlX_3\{P(Mes)_3\}]$[13] (X = Cl, Br; Mes = 2,4,6-$C_6H_2Me_3$) which act as a frustrated Lewis pair to activate CO_2 towards reduction to MeOH (using ammonia borane as the hydrogen source) and $[AlX_3(HP^tBu_2)]$[14] (X = Cl, Br) which readily oxidise into the equivalent phosphine oxide species in the air. The complexes are normally synthesised by combining the constituents in an inert solvent such as toluene, but other methods are sometimes used, such as by direct combination under vacuum. Schnöckel *et al.* have reported trigonal bipyramidal *trans*-$[AlI_3(PEt_3)_2]$,[15] as well as the low valent aluminium cyclic species $[Al_4I_4(PEt_3)_4]$[15] (formally Al(I)) and dimeric $[Al_2I_4(PEt_3)_2]$[16] (formally Al(II)), both of which have Al–Al bonds. While higher coordination numbers can be obtained with the aluminium(III) halides only four-coordinate complexes with aluminium(III) alkyls are known,[1] which reflects the greater Lewis acidity of AlX_3 over AlR_3.

2.2 Results and Discussion

The aluminium(III) halides are increasingly moisture sensitive (owing to weaker Al–X bonds due to a mismatch in orbital size) moving down the group, prompting the need for rigorous inert atmosphere conditions and dry solvents to be employed throughout all the syntheses, manipulations and spectroscopic measurements. As avoiding the use of donor solvents (see Section 2.1.1) was necessary, CH_2Cl_2 or toluene were the chosen reaction solvents. While chlorinated solvents are fine for reactions involving $AlCl_3$, it was found that $AlBr_3$ and AlI_3 undergo halide exchange with CH_2Cl_2 (see Section 2.2.1), and so toluene was used in these systems. Solid $AlCl_3$ is only sparingly soluble in hydrocarbons or chlorinated solvents[3] and so a suspension is formed upon addition of either CH_2Cl_2 or toluene; complexation reactions therefore rely on the ligand forcing the $AlCl_3$ into solution. Owing to their more simple solid state structures (see Section 2.1.1) both $AlBr_3$ and AlI_3 dissolve to form yellow solutions in toluene.

The aluminium(III) halide phosphine and arsine complexes synthesised were found to be moisture- and, to a lesser extent, oxygen-sensitive, particularly in solution. Solutions of the complexes used to obtain NMR spectra were found to partially hydrolyse in varying amounts, which resulted (for the phosphine complexes) in resonances attributable to phosphonium cations $[R_3PH]^+$ in the spectra which grew in intensity over time. Therefore NMR spectra were run immediately on freshly prepared samples where possible. NMR spectra were run in CD_2Cl_2 (or a combination of CH_2Cl_2 and CD_2Cl_2) as halide exchange with the solvent was found to be negligible for all the complexes once they had been isolated.

During spectroscopic analysis of the complexes peaks corresponding to the tetrahalide anions $[AlX_4]^-$ were often observed (either as the anion in an ionic complex or due to some hydrolysis of the complexes having occurred). In ^{27}Al NMR spectroscopy the $[AlX_4]^-$ give a sharp peak at δ = 103.3 (X = Cl), 80.4 (X = Br) and –26.5 (X = I). In their IR spectra $[AlX_4]^-$ have strong diagnostic bands at 489 ν(AlCl), 398 ν(AlBr) and 336 ν(AlI) cm^{-1} (only the t_2 vibrational mode is IR active with a frequency above 200 cm^{-1}).[17] The Al–X bands for the complexes synthesised were sometimes difficult to assign, often giving quite broad features, which is probably a result of solid state effects such as cation-anion interactions or lower site symmetry.

2.2.1 Complexes with phosphine oxide and arsine oxide ligands

Initially the coordination chemistry of phosphine oxide and arsine oxide ligands with AlX_3 (X = Cl, Br) were investigated in order to obtain reference spectra to aid the later identification of any such products formed via unwanted oxidation of the phosphine ligands. Furthermore, there are very few reported phosphine oxide complexes with AlX_3, while no arsine oxide complexes have been isolated, and so the synthesis and characterisation of new complexes gives further insight into the nature and trends of this little-studied class of compounds. The crystal structures of $[AlX_3(OPPh_3)]$[18] (X = Cl, Br) and $[(AlCl_3)_2\{\mu\text{-}Ph_2P(O)CH_2P(O)Ph_2\}]$[19] (formed from the reaction of methylaluminium sesquichloride with $Ph_2P(O)CH_2P(O)Ph_2$) have been reported; in each case a distorted tetrahedral geometry is observed around the aluminium centre. Reaction of $[Mn(OP^nBu_3)_2Cl_2]$ with two molar equivalents of $AlCl_3$ yields $[AlCl_3(OP^nBu_3)]$, thought to have a similar structure to $[AlCl_3(OPPh_3)]$ based on its ^{31}P and ^{27}Al NMR spectra.[20]

The novel complex $[AlCl_3(OPMe_3)]$ was synthesised by reacting $AlCl_3$ and $OPMe_3$ in a 1:1 molar ratio in CH_2Cl_2. Although no suitable crystals were grown to allow for structure determination using single crystal X-ray diffraction, spectroscopic analysis of the white powder isolated supports the assignment of the 1:1 adduct. The ^1H NMR spectrum shows a sharp doublet for the Me groups, while the chemical shift (δ = 70.0) of the single resonance in the $^{31}P\{^1H\}$ NMR spectrum is at a much higher frequency with respect to free $OPMe_3$ (δ = 36.9), showing that the $OPMe_3$ has strongly coordinated. In the ^{27}Al NMR spectrum a single, sharp peak is observed at δ = 91.4, which is close to that of $[AlCl_3(OPPh_3)]$ (δ = 90)[18] and is thus indicative that the aluminium centre is in a similar, *pseudo*-tetrahedral environment. The ν(PO) stretch is at 1149 cm^{-1} in the IR spectrum, lowered from 1165 cm^{-1} in $OPMe_3$, while the bands at 495 and 392 cm^{-1} are assignable as the ν(AlCl) a_1 and e modes (as the complex has C_{3v} symmetry).

The attempted synthesis of $[AlBr_3(OPR_3)]$ (R = Me, Ph) from $AlBr_3$ and OPR_3 at room temperature using CH_2Cl_2 as the solvent yielded solids whose room temperature ^{27}Al NMR spectra in CH_2Cl_2/CD_2Cl_2 showed up to four singlets of varying intensities (see Figure 2.2), with chemical shifts that can be assigned to the neutral complexes $[AlBr_nCl_{(3-n)}(OPR_3)]$ (n = 0-3). These resonances were also observed when CH_3CN/CD_3CN was used as the solvent for NMR spectroscopic analysis, showing that the halide exchange occurred during the synthesis. It has been proposed that $AlCl_3$ in CH_2Cl_2 forms the intermediate carbenium ion $[CH_2Cl][AlCl_4]$.[21] Therefore it is assumed that when

$AlBr_3$ is dissolved in CH_2Cl_2 initially $[CH_2Cl][AlBr_3Cl]$ is formed, with the Al–Br bonds being susceptible to cleavage and exchange with chloride from the solvent. Interestingly, Burford *et al.*[18] reported that Br/Cl exchange occurred for $[AlBr_3(OPPh_3)]$ in CH_2Cl_2 upon heating the NMR sample at 80 °C for 15 hours, reasoning that it was due to the strong thermodynamic preference for the Al-Cl bond, but they did not observe the exchange process during their reaction at room temperature. Only one singlet is observed in the $^{31}P\{^1H\}$ NMR spectra; cooling the NMR solution of $[AlBr_nCl_{(3-n)}(OPPh_3)]$ down to 193 K served only to broaden the peak slightly.

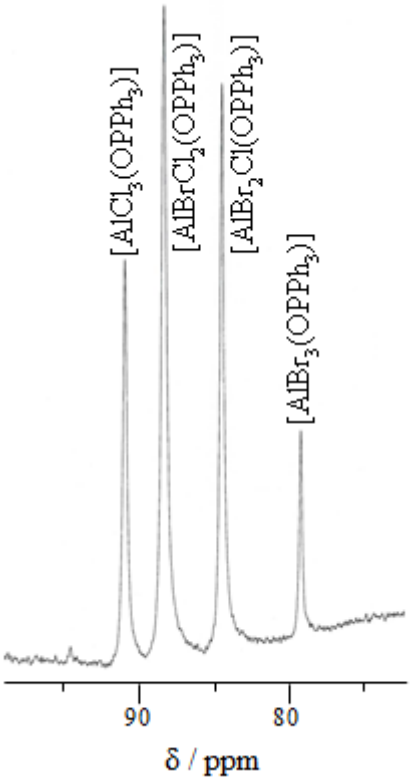

Figure 2.2 ^{27}Al NMR spectrum of the mixed species $[AlBr_nCl_{(3-n)}(OPPh_3)]$ (n = 0-3) in CH_2Cl_2/CD_2Cl_2 at 295 K.

The white powder isolated from the 1:1 reaction of $AlBr_3$ with $OPMe_3$ in toluene was shown spectroscopically and by microanalysis to be the desired complex $[AlBr_3(OPMe_3)]$. The ^{27}Al NMR spectrum shows a singlet at $\delta = 78.1$ (which is similar to $[AlBr_3(OPPh_3)]$, $\delta = 79$),[18] a low frequency shift with respect to $[AlCl_3(OPMe_3)]$ ($\delta = 91.4$) that reflects the weaker electron-withdrawing power of bromide with respect to chloride. The chemical shift of the resonance in the $^{31}P\{^1H\}$ NMR spectrum is very similar (taking into account solvent effects) to the one observed for $[AlCl_3(OPMe_3)]$. In the IR spectrum the bands corresponding to ν(AlBr) are roughly 100 cm^{-1} lower than for ν(AlCl) at 411 and 291 cm^{-1}.

The [$AlBr_3(OPPh_3)$] complex isolated from a similar reaction was dissolved in CH_2Cl_2 and the solution left under an inert atmosphere for a month before a ^{27}Al NMR spectrum was obtained in CH_2Cl_2/CD_2Cl_2. The spectrum showed that the major species was still [$AlBr_3(OPPh_3)$]; there was a small amount of [$AlBr_2Cl(OPPh_3)$] evident but no significant amounts of the [$AlBr_nCl_{(3-n)}(OPPh_3)$] (n = 0-1) species. This suggests that once formed the complexes only react extremely slowly with CH_2Cl_2; it is 'free' AlX_3 which initiates the rapid halide exchange with the chlorocarbon solvent during synthesis.

Reaction of $AlCl_3$ with $OAsPh_3$ in a 1:1 molar ratio in CH_2Cl_2 afforded [$AlCl_3(OAsPh_3)$], which is the first example of an aluminium(III) halide – arsine oxide complex. Single crystal X-ray structure determination of the colourless crystals grown identified two similar but independent [$AlCl_3(OAsPh_3)$] molecules in the asymmetric unit, as well as a disordered CH_2Cl_2 solvate molecule. The complex is *pseudo*-tetrahedral (Figure 2.3) around the aluminium centre with a bent Al–O–As linkage (146.7(3)°). This is in contrast to the linear Al–O–P linkage of [$AlCl_3(OPPh_3)$], whose linearity is attributed by Burford *et al.*[18] to the electronic environment of the oxygen centre, influenced by the acceptor capabilities of the aluminium; steric effects are not involved. The *d*(Al–O) (1.735(5) *vs*. 1.733(4) Å in [$AlCl_3(OPPh_3)$][18]) and *d*(Al–Cl) (2.118(3)–2.144(3) *vs*. 2.099(2) Å) are very similar in both complexes, while the *d*(As–O) (1.687(5) Å) is lengthened from the value in $OAsPh_3$ itself (1.645 Å).[22] Crystals of Ph_3AsCl_2 (identified by a unit cell comparison with literature data)[23] were found one week later in the same solution which had been kept at a constant –18 °C. The conversion of $OAsR_3$ to R_3AsCl_2 under mild conditions has been reported before when $GeCl_4$ was stirred with $OAsR_3$ (R = Me or Ph) in CH_2Cl_2 or CH_3CN,[24] although evidently this process does not dominate with $AlCl_3$ as the desired adduct was obtained first.

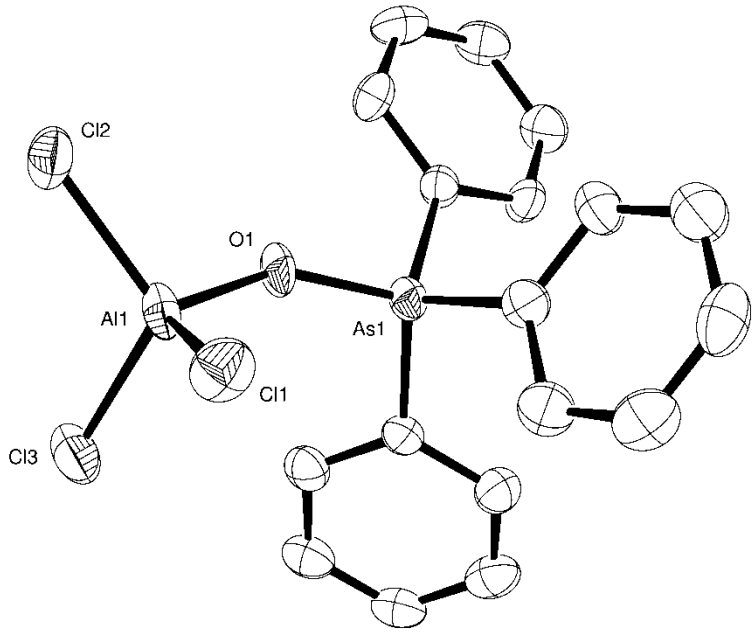

Figure 2.3 The structure of the Al1 centred molecule of $[AlCl_3(OAsPh_3)]\cdot 0.5CH_2Cl_2$ showing the atom labelling scheme. Ellipsoids are drawn at the 50% probability level. H atoms and solvate molecules are omitted for clarity. The other molecule is similar.

Table 2.1 Selected bond lengths (Å) and angles (°) for $[AlCl_3(OAsPh_3)]\cdot 0.5CH_2Cl_2$

Al1–O1	1.735(5)	O1–Al1–Cl1	110.7(2)
Al1–Cl1	2.124(3)	O1–Al1–Cl2	105.5(2)
Al1–Cl2	2.118(3)	O1–Al1–Cl3	109.5(2)
Al1–Cl3	2.144(3)	Cl1–Al1–Cl2	110.44(13)
As1–O1	1.687(5)	Cl1–Al1–Cl3	108.21(13)
		Cl2–Al1–Cl3	112.47(13)
		Al1–O1–As1	146.7(3)

The spectroscopic data and microanalysis results are consistent with the bulk solid being the solvent-free 1:1 adduct $[AlCl_3(OAsPh_3)]$. The ^{27}Al NMR spectrum shows a singlet at $\delta = 93.1$, which has shifted to a slightly higher frequency compared to $[AlCl_3(OPPh_3)]$ ($\delta = 90$).[18] In the IR spectrum the ν(AsO) stretch appears at 929 cm^{-1} (free $OAsPh_3$ is at 881 cm^{-1}), while the ν(AlCl) bands are evident at 491 and 392 cm^{-1}.

2.2.2 Complexes with monodentate phosphines

The reaction of AlX_3 with PMe_3 in either CH_2Cl_2 (X = Cl) or toluene (X = Br, I) in a 1:1 or 1: ≥2 molar ratio afforded $[AlX_3(PMe_3)]$ or $[AlX_3(PMe_3)_2]$ respectively, as white powders. The $[AlX_3(PMe_3)_2]$ appear to be less stable than the corresponding $[AlX_3(PMe_3)]$; $[AlCl_3(PMe_3)_2]$ was found (by microanalysis) to convert into $[AlCl_3(PMe_3)]$ upon prolonged times *in vacuo*. Both $[AlX_3(PMe_3)]$ and $[AlX_3(PMe_3)_2]$ were found to be very moisture sensitive, particularly when X = Br or I.

Selected NMR spectroscopic data are given in Table 2.2. A combined $^{31}P\{^1H\}$ and ^{27}Al NMR spectroscopic study showed that addition of one molar equivalent of PMe_3 to a solution of $[AlCl_3(PMe_3)]$ in CH_2Cl_2/CD_2Cl_2 led to the disappearance of the $[AlCl_3(PMe_3)]$ resonance and the appearance of a resonance attributable to $[AlCl_3(PMe_3)_2]$, but the spectra remained unchanged upon the addition of another molar equivalent of PMe_3 (to give a 1:3 $AlCl_3$:PMe_3 ratio), suggesting that the octahedral $[AlCl_3(PMe_3)_3]$ species does not exist. In solutions containing excess PMe_3 a singlet is observed at room temperature in the $^{31}P\{^1H\}$ NMR spectra due to fast exchange between the free and coordinated phosphine; separate resonances can be seen by cooling the solution, which slows the exchange.

Table 2.2 Selected NMR spectroscopic data for $[AlX_3(PMe_3)_n]$ (X = Cl, Br, I; n = 1 or 2)

Complex	$\delta(^1H)$ / 295 K[a]	$\delta(^{31}P\{^1H\})$ / 295 K[b]	$\delta(^{27}Al)$ / 295 K[b]
$[AlCl_3(PMe_3)]$	1.50 (d)	–42.6 (br s)	108.8 (s)
$[AlBr_3(PMe_3)]$	1.39 (d)	–40.9 (sextet)[c]	101.5 (d)[c]
$[AlI_3(PMe_3)]$	1.45 (d)	–42.8 (br s)	50.2 (br s)
$[AlCl_3(PMe_3)_2]$	1.28 (d)	–37.9 (s)	66.0 (s)
$[AlBr_3(PMe_3)_2]$	1.25 (d)	–37.4 (br s)	44.5 (br s)
$[AlI_3(PMe_3)_2]$	1.33 (d)	–31.6 (br s)	4.4 (br s)

[a] CD_2Cl_2; [b] CH_2Cl_2/CD_2Cl_2 except c; [c] toluene/d^8 toluene

The spectroscopic properties of the $[AlX_3(PMe_3)]$ (X = Cl, Br, I) are as expected for *pseudo*-tetrahedral complexes having C_{3v} symmetry, with significant ($\Delta = \sim +0.5$) high frequency shifts from free PMe_3 in the ^1H NMR spectra. The resonances in the $^{31}P\{^1H\}$ NMR spectra have shifted to a higher frequency from PMe_3 ($\delta = -62$) and differ very little with X. For X = Cl and Br, the chemical shift of the resonances in the ^{27}Al NMR spectra are in good agreement with Vriezen *et al.*[25] who performed ^{27}Al and ^{31}P NMR studies on toluene solutions of $[AlX_3(PR_3)]$ (X = Cl, Br; R = Me, Et, Ph); as expected for the heavier halide the resonance for X = I is at a much lower frequency. At room temperature (295 K) in CH_2Cl_2/CD_2Cl_2 the $^{31}P\{^1H\}$ and ^{27}Al NMR spectra show broad singlets for all three complexes but on cooling the solutions $^1J_{PAl}$ coupling (a six line pattern due to coupling to the quadrupolar ^{27}Al nucleus in the $^{31}P\{^1H\}$ NMR spectra and a doublet in the ^{27}Al NMR spectra) is observed, with separate resonances for $[AlX_3(PMe_3)]$ and $[AlX_3(PMe_3)_2]$ being resolved at 193 K for X = Br and I in the $^{31}P\{^1H\}$ NMR spectra. Rapid ligand exchange between the four- and five-coordinate complexes must therefore occur if there is any excess PMe_3 in solution, which can be slowed on cooling. By adding AlX_3 to the NMR solution (tested by adding $AlBr_3$ to a solution of $[AlBr_3(PMe_3)]$ in toluene, to avoid halide scrambling) $^1J_{PAl}$ coupling is observed at room temperature, suggesting that formation and ligand exchange with the five-coordinate complex is suppressed. The decrease in the coupling constant values ($^1J_{PAl}$ (CH_2Cl_2/CD_2Cl_2) = 275 (Cl), 258 (Br), 209 (I) Hz) indicates that there is the expected reduction in the Al–P bond strength as the halide gets heavier. The values are comparable to those reported by Vriezen *et al.*[25] and are similar to those observed for other four-coordinate phosphine complexes (e.g. for $[AlCl_3\{P(Mes)_3\}]$ $^1J_{PAl}$ = 258 Hz).[13]

Highly thermally sensitive crystals of $[AlCl_3(PMe_3)]$ were obtained by storing the reaction solution at –18 °C; only by holding the crystals at 223 K during sample preparation could a single crystal suitable for X-ray crystallography be selected and mounted successfully. The structure (Figure 2.4) reveals the expected C_{3v} geometry; it is isomorphous with $[GaCl_3(PMe_3)]$,[26] and like its gallium analogue it adopts an eclipsed conformation in the solid state, which is thought to allow for closer packing of the molecules. As expected for a stronger σ-donating ligand, the d(Al–P) is ~0.04 Å shorter than in $[AlCl_3(PPh_3)]$[4] (2.4296(15) Å), which adopts a staggered arrangement.

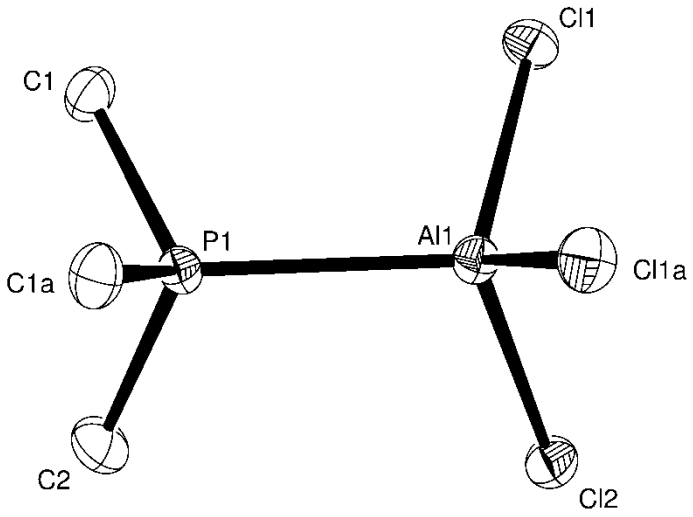

Figure 2.4 The structure of $[AlCl_3(PMe_3)]$ showing the atom labelling scheme. The molecule lies on a mirror plane going through C2, P1, Al1 and Cl2. Ellipsoids are drawn at the 50% probability level and H atoms are omitted for clarity. Symmetry operation: a = x, 1/2 – y, z.

Table 2.3 Selected bond lengths (Å) and angles (°) for $[AlCl_3(PMe_3)]$

Al1–Cl1	2.1291(15)	Cl1–Al1–Cl1a	111.15(10)
Al1–Cl2	2.130(2)	Cl1–Al1–Cl2	111.06(6)
Al1–P1	2.392(2)	Cl1–Al1–P1	107.22(6)
		Cl2–Al1–P1	108.94(9)

The X-ray crystal structure of *trans*-$[AlCl_3(PMe_3)_2]$ reveals a near-ideal trigonal bipyramidal geometry (Figure 2.5), with the methyl groups staggered with respect to the chlorine atoms. The structure is very similar to that of *trans*-$[AlI_3(PEt_3)_2]$,[15] which has longer *d*(Al–P) bonds (2.520(4) and 2.528(4) Å), consistent with the weaker Lewis acidity of AlI_3. The *d*(Al–P) and *d*(Al–Cl) are ~0.07 Å longer than in $[AlCl_3(PMe_3)]$, attributable to the increase in coordination number. While there are no known five-coordinate complexes of GaX_3 with monodentate phosphine ligands,[1] the crystal structure of *trans*-$[InCl_3(PMe_3)_2]$ is known and is isomorphous with $[AlCl_3(PMe_3)_2]$ with *d*(In–P) = 2.576(3) Å.[27]

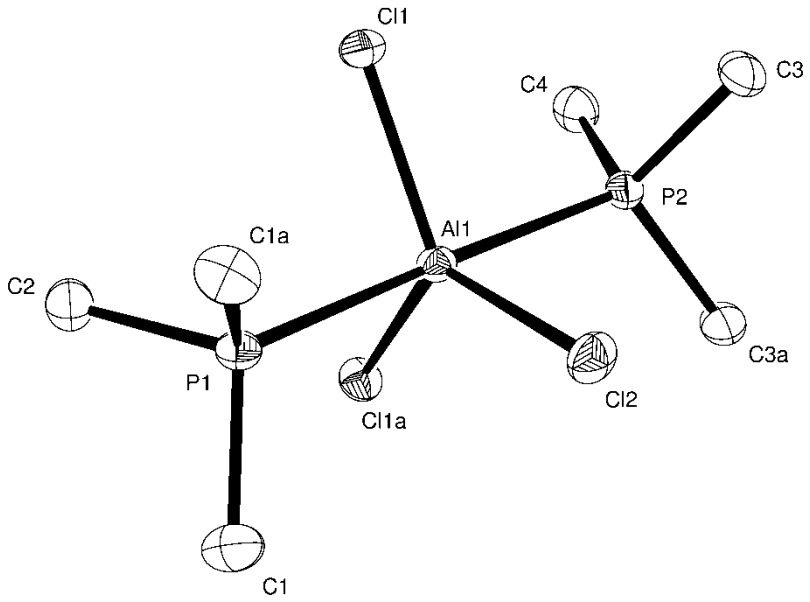

Figure 2.5 The structure of $[AlCl_3(PMe_3)_2]$ showing the atom labelling scheme. The molecule lies on a mirror plane going through C4, P2, Al1, Cl2, P1 and C1. Ellipsoids are drawn at the 50% probability level and H atoms are omitted for clarity. Symmetry operation: a = x, 1/2 – y, z.

Table 2.4 Selected bond lengths (Å) and angles (°) for $[AlCl_3(PMe_3)_2]$

Al1–Cl1	2.2029(14)	Cl1–Al1–Cl1a	117.56(9)
Al1–Cl2	2.203(2)	Cl1–Al1–Cl2	121.22(5)
Al1–P1	2.452(2)	Cl1–Al1–P1	90.44(6)
Al1–P2	2.459(2)	Cl2–Al1–P1	88.79(8)
		Cl1–Al1–P2	90.96(6)
		Cl2–Al1–P2	88.52(8)
		P1–Al1–P2	177.31(9)

The NMR and IR spectroscopic data support the assignment of the geometry of $[AlX_3(PMe_3)_2]$ (X = Br, I) as *trans* (D_{3h} symmetry) also. The ν(AlX) e' mode is evident in the IR spectra of all the $[AlX_3(PMe_3)_2]$, with the position of the features observed in the 500-300 cm^{-1} region agreeing well with the IR data reported by Beattie *et al.*[28] for $[AlCl_3(PMe_3)_2]$. The resonances in the ^1H and $^{31}P\{^1H\}$ NMR spectra of $[AlX_3(PMe_3)_2]$ are at a lower frequency compared with $[AlX_3(PMe_3)]$ (see Table 2.2), consistent with the increase in aluminium coordination number to five, which has also resulted in the ^{27}Al

NMR resonance shifting systematically (with the halogen present) to lower frequencies (Δ = ~ –50). Owing to their lower symmetry (see Section 1.7.1) no well-defined $^{1}J_{PAl}$ coupling is observed for any of the complexes, even at low temperatures. As mentioned earlier, the $^{31}P\{^{1}H\}$ NMR spectra are often complicated by the presence of traces of 'free' PMe_3, which undergoes fast ligand exchange with the complexes at room temperature.

2.2.3 Complexes with bidentate phosphines

2.2.3.1 Complexes with *o*-$C_6H_4(PR_2)_2$ (R = Me, Ph)

The bidentate phosphine *o*-$C_6H_4(PMe_2)_2$, which is preorganised for chelation, has small steric demands and is an excellent *σ*-donor, was reacted with $AlCl_3$ in CH_2Cl_2 in both a 1:1 and 1:2 molar ratio, yielding the ionic 1:1 complex $[AlCl_2\{o\text{-}C_6H_4(PMe_2)_2\}_2][AlCl_4]$ in both cases. X-ray analysis identified the structure as *trans*-$[AlCl_2\{o\text{-}C_6H_4(PMe_2)_2\}_2][AlCl_4]$ with a *pseudo*-octahedral cation (Figure 2.6) and a tetrahedral anion. The *d*(Al–P) and *d*(Al–Cl) for the cation are longer than for the $[AlCl_3(PMe_3)_n]$ (n = 1 or 2) complexes, again attributable to the increase in coordination number to six around the aluminium centre. The small chelate bite of *o*-$C_6H_4(PMe_2)_2$ means that ∠P1–Al1–P2 is 81.415(13)°, giving a very distorted octahedral environment around Al(III). The crystals are isomorphous with *trans*-$[GaCl_2\{o\text{-}C_6H_4(PMe_2)_2\}_2][GaCl_4]$,[29] with very similar *d*(M–P) (M = Al or Ga), ∠Cl–M–P and ∠P–M–P, while *d*(M–Cl) is ~0.09 Å shorter for M = Al. While the reaction of $GaCl_3$ with *o*-$C_6H_4(PMe_2)_2$ in a 2:1 molar ratio yielded an insoluble complex thought to be $[GaCl_2\{o\text{-}C_6H_4(PMe_2)_2\}][GaCl_4]$,[29] for $AlCl_3$ there was no evidence for the formation of the *pseudo*-tetrahedral cation $[AlCl_2\{o\text{-}C_6H_4(PMe_2)_2\}]^+$ in the reactions, or from *in situ* $^{31}P\{^{1}H\}$ and ^{27}Al NMR spectra with a four-fold excess of $AlCl_3$.

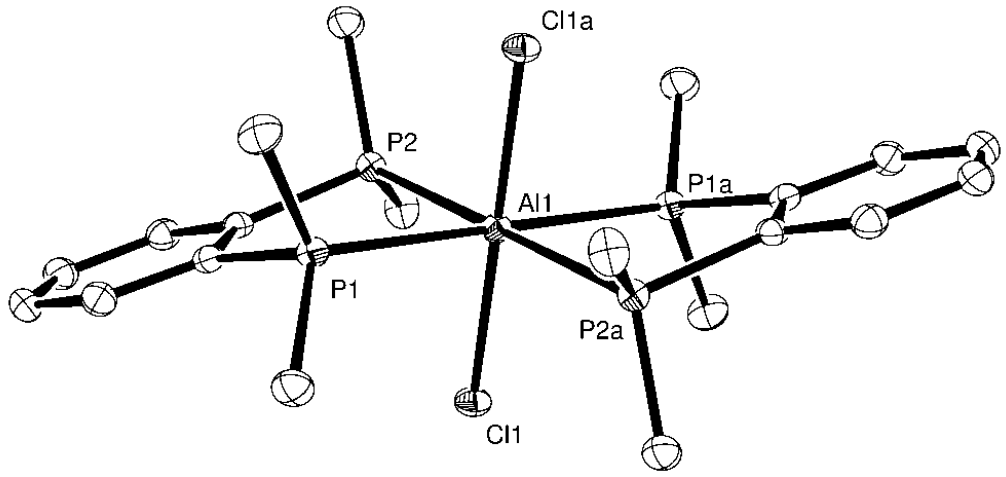

Figure 2.6 The structure of the centrosymmetric cation in *trans*-$[AlCl_2\{o\text{-}C_6H_4(PMe_2)_2\}_2][AlCl_4]$ showing the atom labelling scheme. Ellipsoids are drawn at the 50% probability level and H atoms are omitted for clarity. Symmetry operation: a = – x, – y, 1 – z.

Table 2.5 Selected bond lengths (Å) and angles (°) for $[AlCl_2\{o\text{-}C_6H_4(PMe_2)_2\}_2]^+$

Al1–Cl1	2.2692(7)	Cl1–Al1–P1	87.703(14)
Al1–P1	2.4745(8)	Cl1–Al1–P2	87.46(3)
Al1–P2	2.4832(7)	P1–Al1–P2	81.415(13)

The corresponding reactions with $AlBr_3$ and AlI_3, using toluene as the solvent, formed $[AlX_2\{o\text{-}C_6H_4(PMe_2)_2\}_2][AlX_4]$ as the only products; they immediately precipitate out of solution as white powders, which has prevented the growth of crystals for single crystal X-ray structure determination. While solution state spectroscopic data could be collected on the complexes in CH_2Cl_2, its use as a crystallisation solvent was not possible due to halide exchange issues (see Section 2.2.1). The complexes are decomposed by CH_3CN with partial displacement of the phosphine. Attempts to grow single crystals of $[AlBr_2\{o\text{-}C_6H_4(PMe_2)_2\}_2][AlBr_4]$ from the pre-formed complex in CH_2Br_2 failed due to the poor solubility of the complex, while performing the reaction using CH_2Br_2 as the solvent also failed to give crystals of the complex. Nevertheless the spectroscopy of the three complexes show that all contain six-coordinate *trans* isomers, which are the first examples of aluminium(III) phosphine complexes with a six-coordinate aluminium centre.[1]

Table 2.6 Selected NMR spectroscopic data for $[AlX_2\{o\text{-}C_6H_4(PMe_2)_2\}_2]^+$ (X = Cl, Br, I)

Complex Cation	$\delta(^1H)$ CH_3 / 295 K[a]	$\delta(^{31}P\{^1H\})$ / 295 K[b]	$\delta(^{27}Al)$ / 295 K[b]
$[AlCl_2\{o\text{-}C_6H_4(PMe_2)_2\}_2]^+$	1.74 (s)	–42.8 (sextet)	+0.7 (quintet)
$[AlBr_2\{o\text{-}C_6H_4(PMe_2)_2\}_2]^+$	1.80 (s)	–42.6 (br s)	–12.0 (br s)
$[AlI_2\{o\text{-}C_6H_4(PMe_2)_2\}_2]^+$	1.90 (s)	–42.3 (br s)	Not observed

[a] CD_2Cl_2; [b] CH_2Cl_2/CD_2Cl_2

Very strong bands corresponding to the $[AlX_4]^-$ anions are evident in the IR spectra, alongside weaker ν(AlX) features at lower frequencies assigned to the a_{2u} mode of the $[AlX_2\{o\text{-}C_6H_4(PMe_2)_2\}_2]^+$ cations (which have local D_{4h} symmetry). Selected NMR spectroscopic data for the cations are given in Table 2.6; the expected resonances for the $[AlX_4]^-$ anions are evident in the ^{27}Al NMR spectra also. Only one methyl resonance (without resolved $^2J_{HP}$ coupling) is observed in the ^1H NMR spectra, consistent with only the *trans* forms being present. The coordination shifts in both the ^1H and $^{31}P\{^1H\}$ NMR spectra vary little with X, and are modest high frequency shifts from free $o\text{-}C_6H_4(PMe_2)_2$ ($\delta(^{31}P\{^1H\}) = –55$). For X = Cl, $^1J_{PAl}$ coupling is observed at room temperature (Figure 2.7) with a coupling constant (155 Hz) that, consistent with the larger aluminium coordination number, is much smaller than for $[AlCl_3(PMe_3)]$ (275 Hz). The binomial quintet at δ = 0.7 in the ^{27}Al NMR spectrum, from coupling to four equivalent P atoms in the cation, is further confirmation that the complex is exclusively *trans* in the solution state as well; as expected for the increased coordination number (six) its chemical shift is at a lower frequency compared to four- and five-coordinate aluminium(III) complexes.[30] The peaks are broad and coupling is not clearly resolved for X = Br or I in the $^{31}P\{^1H\}$ NMR spectra; a broad resonance at δ = –12.0 is observed for X = Br in the ^{27}Al NMR spectrum, while no resonance for the cation is seen for X = I over the temperature range 295-223 K. This loss of coupling, followed by the loss of the cation resonance going from X = Cl to Br to I is attributable to the increase in quadrupolar relaxation rates due to increasing electric field gradients around the aluminium nucleus with the change in halide. Below 273 K the resonances in the $^{31}P\{^1H\}$ NMR spectra of all three complexes begin to coalesce and then sharpen upon further cooling. Wasylishen *et al.*[31] report that the $^1J_{GaP}$ coupling patterns for $[GaX_3\{P(p\text{-anis})_3\}]$ (X = Br, I; P(*p*-anis)$_3$ = tris-*para*-methoxyphenylphosphine) in $CDCl_3$ collapse below 300 K in solution phase $^{31}P\{^1H\}$ NMR spectra due to the rapid relaxation of $^{69/71}Ga$ (^{71}Ga: $I = 3/2$, Q = 0.11 x 10^{-28} m^2), with the $^{69/71}Ga$ and ^{31}P nuclei being essentially self-decoupled at 213 K; a similar process between the ^{27}Al and ^{31}P nuclei is

presumably occurring for $[AlX_2\{o\text{-}C_6H_4(PMe_2)_2\}_2]^+$ below 273 K. There is no evidence of rapid ligand exchange at any of the temperatures studied.

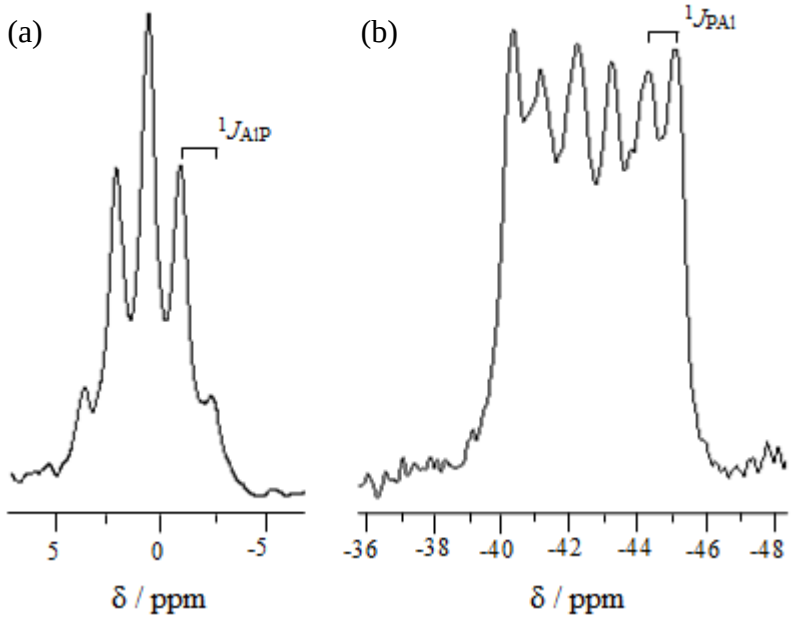

Figure 2.7 (a) ^{27}Al NMR and (b) $^{31}P\{^1H\}$ NMR spectra of $[AlCl_2\{o\text{-}C_6H_4(PMe_2)_2\}_2]^+$ in CH_2Cl_2/CD_2Cl_2 at 295 K.

The reaction of $AlCl_3$ with the much more sterically bulky $o\text{-}C_6H_4(PPh_2)_2$ in either a 1:1 or 2:1 molar ratio in CH_2Cl_2 or toluene invariably yielded white powders with an $AlCl_3$ to $o\text{-}C_6H_4(PPh_2)_2$ ratio of 2:1. The IR spectra contain a strong band at 483 cm^{-1}, assignable as $[AlCl_4]^-$, suggesting that the complex isolated is $[AlCl_2\{o\text{-}C_6H_4(PPh_2)_2\}][AlCl_4]$, with a *pseudo*-tetrahedral cation. Similarly, only $[GaX_2\{o\text{-}C_6H_4(PPh_2)_2\}][GaX_4]$ has ever been isolated from the reactions of GaX_3 (X = Cl, Br, I) with $o\text{-}C_6H_4(PPh_2)_2$, irrespective of the reagent ratios and conditions used.[29,32] Though $[AlCl_4]^-$ is evident, no resonance is observable for the cation in the ^{27}Al NMR spectrum of $[AlCl_2\{o\text{-}C_6H_4(PPh_2)_2\}][AlCl_4]$, even at 183 K. The $^{31}P\{^1H\}$ NMR spectrum shows a broad resonance at δ = –8.3 at 295 K, which shifts on cooling to δ = –12.4 at 183 K, but remains broad. Upon addition of excess $o\text{-}C_6H_4(PPh_2)_2$ a peak for free ligand appears at δ = –13.3 that does not change with temperature, suggesting that fast ligand exchange is not occurring. A possible explanation for the NMR spectroscopic behaviour observed is that the $o\text{-}C_6H_4(PPh_2)_2$ is (or is close to being) lower symmetry κ^1-coordinated. The X-ray crystal structures of both $[GeCl_2\{o\text{-}C_6H_4(PPh_2)_2\}]$[33] and $[SnCl_2\{o\text{-}C_6H_4(PPh_2)_2\}]$[34] show the ligand to be very asymmetrically coordinated, while their $^{31}P\{^1H\}$ NMR spectra exhibit broad resonances down to 200/190 K, ascribed to fast equilibration between the 'free' and bound phosphine groups of the

diphosphine in solution. Unfortunately, despite several attempts, single crystals of $[AlCl_2\{o\text{-}C_6H_4(PPh_2)_2\}][AlCl_4]$ could not be obtained to determine the *d*(Al–P).

A few crystals of the 1:1 species *trans*-$[AlCl_2\{o\text{-}C_6H_4(PPh_2)_2\}_2][AlCl_4]$ were grown from a CH_2Cl_2 solution of $AlCl_3$ and $o\text{-}C_6H_4(PPh_2)_2$ in a 2:1 molar ratio. There are two independent but similar *trans*-$[AlCl_2\{o\text{-}C_6H_4(PPh_2)_2\}_2][AlCl_4]$ moieties in the asymmetric unit, both with centrosymmetric six-coordinate cations. The cation (Figure 2.8) has a very sterically crowded, distorted (∠P1–Al1–P2 = 78.69(4)°) octahedral environment around Al(III). The *d*(Al–P) are ~0.1 Å longer than in *trans*-$[AlCl_2\{o\text{-}C_6H_4(PMe_2)_2\}_2][AlCl_4]$ while the *d*(Al–Cl) are ~0.05 Å shorter; this is presumably a combination of the weaker *σ*-donating ability of $o\text{-}C_6H_4(PPh_2)_2$ as well as the increased steric bulk from the phenyl rings preventing the diphosphine from approaching the aluminium so closely. The X-ray crystal structure of the similarly distorted *pseudo*-octahedral cation in $[InCl_2\{o\text{-}C_6H_4(PPh_2)_2\}_2][InCl_4]$ has been reported.[32] All attempts to isolate the six-coordinate complex as a bulk product have failed, with the products obtained analysing (by microanalysis and spectroscopic data) as the four-coordinate $[AlCl_2\{o\text{-}C_6H_4(PPh_2)_2\}][AlCl_4]$ instead, suggesting that although it must only be a minor constituent *trans*-$[AlCl_2\{o\text{-}C_6H_4(PPh_2)_2\}_2][AlCl_4]$ preferentially crystallises out.

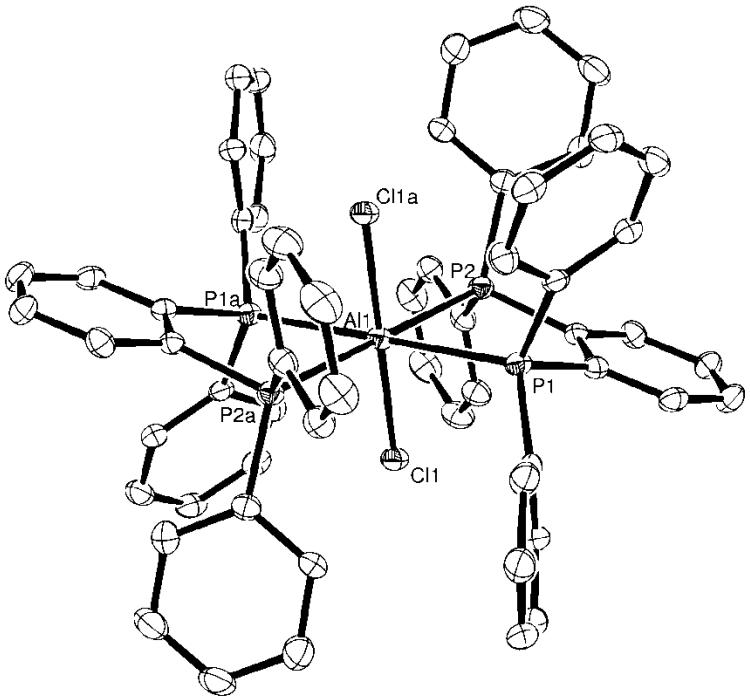

Figure 2.8 The structure of the centrosymmetric Al1 centred cation in *trans*-$[AlCl_2\{o\text{-}C_6H_4(PPh_2)_2\}_2][AlCl_4]$ showing the atom labelling scheme. Ellipsoids are drawn at the 50% probability level and H atoms are omitted for clarity. The other cation is similar. Symmetry operation: a = 2 – x, 1 – y, 1 – z.

Table 2.7 Selected bond lengths (Å) and angles (°) for $[AlCl_2\{o\text{-}C_6H_4(PPh_2)_2\}_2]^+$

Al1–Cl1	2.2222(13)	Cl1–Al1–P1	87.80(5)
Al1–P1	2.5574(15)	Cl1–Al1–P2	87.13(5)
Al1–P2	2.5843(15)	P1–Al1–P2	78.69(4)

2.2.3.2 Complexes with $R_2P(CH_2)_2PR_2$ (R = Me, Cy)

It was of interest to also investigate the behaviour of AlX_3 towards the more flexible bidentate phosphines which have an aliphatic, saturated backbone, as these behave exclusively as bridging ligands towards GaX_3 and InX_3.[1] The reaction of AlX_3 (X = Cl, Br, I) with $Me_2P(CH_2)_2PMe_2$ (a strong *σ*-donor with small steric requirements) in a 1:1 molar ratio yields *trans*-$[AlX_2\{Me_2P(CH_2)_2PMe_2\}_2][AlX_4]$, with the now-familiar six-coordinate cation containing chelating diphosphine ligands. The IR and NMR spectroscopic data show that the only species present are the *trans*-$[AlX_2\{Me_2P(CH_2)_2PMe_2\}_2][AlX_4]$, and that they behave similarly to *trans*-$[AlX_2\{o\text{-}C_6H_4(PMe_2)_2\}_2][AlX_4]$ in CH_2Cl_2 solution, with comparable chemical shifts (free $Me_2P(CH_2)_2PMe_2$: $\delta(^{31}P\{^1H\}) = -49$), coupling patterns and behaviour with temperature in the $^{31}P\{^1H\}$ and ^{27}Al NMR spectra (Table 2.8). Notably, a broad singlet can be observed for $[AlI_2\{Me_2P(CH_2)_2PMe_2\}_2]^+$ in the ^{27}Al NMR spectrum at 295 K, illustrating how very small changes in the coordination environment can affect the quadrupolar relaxation rate, which determines whether a resonance is seen or not. There was no evidence for the formation of the *cis*-isomer (or of any *cis*-*trans* isomerisation occurring) in any of the spectra collected on $[AlX_2\{Me_2P(CH_2)_2PMe_2\}_2][AlX_4]$; this is in contrast to the analogous thioether complexes $[AlX_2\{MeS(CH_2)_2SMe\}_2][AlX_4]$ which show mixtures of both the *cis* and *trans* isomers at low temperatures, with the X-ray crystal structures of both *trans*-$[AlCl_2\{MeS(CH_2)_2SMe\}_2][AlCl_4]$ and *cis*-$[AlI_2\{MeS(CH_2)_2SMe\}_2][AlI_4]$ having been determined.[35]

Table 2.8 Selected NMR spectroscopic data for $[AlX_2\{Me_2P(CH_2)_2PMe_2\}_2]^+$ (X = Cl, Br, I)

Complex Cation	$\delta(^1H)$ CH_3 / 295 K[a]	$\delta(^{31}P\{^1H\})$ / 295 K[b]	$\delta(^{27}Al)$ / 295 K[b]
$[AlCl_2\{Me_2P(CH_2)_2PMe_2\}_2]^+$	1.44 (s)	–40.6 (sextet)	+1.2 (quintet)
$[AlBr_2\{Me_2P(CH_2)_2PMe_2\}_2]^+$	1.52 (s)	–38.0 (br s)	–12.3 (br s)
$[AlI_2\{Me_2P(CH_2)_2PMe_2\}_2]^+$	1.63 (s)	–39.1 (br s)	–33.9 (br s)

[a] CD_2Cl_2; [b] CH_2Cl_2/CD_2Cl_2

The near-identical $^1J_{PAl}$ coupling constants for $[AlCl_2\{Me_2P(CH_2)_2PMe_2\}_2][AlCl_4]$ (164 Hz) and $[AlCl_2\{o\text{-}C_6H_4(PMe_2)_2\}_2][AlCl_4]$ (155 Hz) suggest a similar phosphine donor power. This is supported by the X-ray crystal structure of *trans*-$[AlCl_2\{Me_2P(CH_2)_2PMe_2\}_2][AlCl_4]$ (Figure 2.9), which has very similar *d*(Al–P) and *d*(Al–Cl), though the geometry overall is less distorted (∠P–Al1–P = 83.51(5)–83.56(5)°) around the *pseudo*-octahedral Al(III), presumably reflecting the greater flexibility of the ligand. Interestingly, Z = 16 in the unit cell, which is in part explained by the diphosphine chelate rings (–P–C–C–P–) having different conformations in the two chemically identical but independent cations.

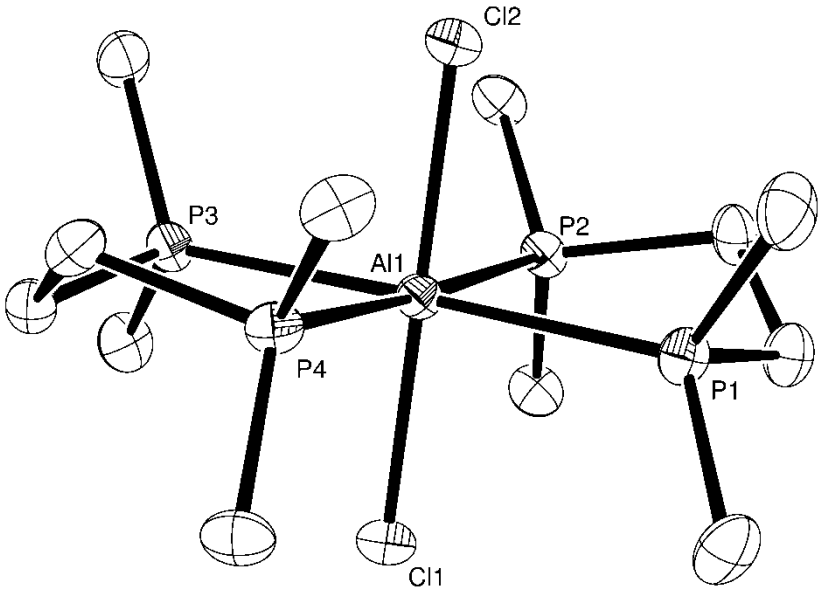

Figure 2.9 The structure of the Al1 centred cation in *trans*-$[AlCl_2\{Me_2P(CH_2)_2PMe_2\}_2][AlCl_4]$ showing the atom labelling scheme. Ellipsoids are drawn at the 50% probability level and H atoms are omitted for clarity. The other cation is similar.

Table 2.9 Selected bond lengths (Å) and angles (°) for $[AlCl_2\{Me_2P(CH_2)_2PMe_2\}_2]^+$

Al1–Cl1	2.2911(16)	Cl1–Al1–Cl2	179.83(8)
Al1–Cl2	2.2959(16)	P1–Al1–P2	83.51(5)
Al1–P1	2.4929(16)	P3–Al1–P4	83.56(5)
Al1–P2	2.4773(16)	Cl1–Al1–P1	89.50(5)
Al1–P3	2.4863(16)	Cl2–Al1–P1	90.44(5)
Al1–P4	2.4899(16)	Cl1–Al1–P2	91.96(6)
		Cl2–Al1–P2	87.88(5)
		Cl1–Al1–P3	89.03(5)
		Cl2–Al1–P3	91.02(5)
		Cl1–Al1–P4	91.35(5)
		Cl2–Al1–P4	88.81(5)

The reaction of $AlCl_3$ with <1 equivalent of $Me_2P(CH_2)_2PMe_2$ in either CH_2Cl_2 or toluene gives a mixture containing varying amounts of *trans*-$[AlCl_2\{Me_2P(CH_2)_2PMe_2\}_2][AlCl_4]$ and $[(AlCl_3)_2\{\mu\text{-}Me_2P(CH_2)_2PMe_2\}]$. The bridged complex can be clearly identified in the ^1H, $^{31}P\{^1H\}$ and ^{27}Al NMR spectra of the mixed species. In the $^{31}P\{^1H\}$ NMR spectrum $[(AlCl_3)_2\{\mu\text{-}Me_2P(CH_2)_2PMe_2\}]$ appears as a broad singlet at $\delta = -31.6$, which is at a higher frequency than $[AlCl_2\{Me_2P(CH_2)_2PMe_2\}_2][AlCl_4]$ ($\delta = -40.6$) reflecting the smaller aluminium coordination number. The bridged complex gives a broad singlet at $\delta = 109.3$ in the ^{27}Al NMR spectrum, which is in the expected region for four-coordinate aluminium.[30] Interestingly the $^1J_{PAl}$ coupling is observed for *trans*-$[AlCl_2\{Me_2P(CH_2)_2Me_2\}_2][AlCl_4]$ at 295 K in the ^{27}Al and $^{31}P\{^1H\}$ NMR spectra of the mixed species as well, while the resonances for the diphosphine-bridged complex are broad singlets. Despite several attempts, $[(AlCl_3)_2\{\mu\text{-}Me_2P(CH_2)_2PMe_2\}]$ could not be isolated as a pure bulk solid. Analogous reactions using $AlBr_3$ and AlI_3 in toluene yielded only the six-coordinate *trans*-$[AlX_2\{Me_2P(CH_2)_2PMe_2\}_2][AlX_4]$, indicating that steric factors from the increased halide radius does not drive what geometry is observed around the aluminium centre.

The X-ray crystal structure of $[(AlCl_3)_2\{\mu\text{-}Me_2P(CH_2)_2PMe_2\}]$ was obtained when a few crystals grew from a CH_2Cl_2 solution containing $AlCl_3$ and $Me_2P(CH_2)_2PMe_2$ in a 1.5:1

molar ratio kept at –18 °C. The complex is centrosymmetric, with *pseudo*-tetrahedral aluminium centres (Figure 2.10). As expected for a lower aluminium coordination number the *d*(Al–P) and *d*(Al–Cl) are much shorter (~0.08 and ~0.17 Å shorter respectively). Though more distorted from an ideal tetrahedral geometry, the *d*(Al–P) and *d*(Al–Cl) are similar to those of $[AlCl_3(PMe_3)]$, suggesting a similar ligand coordination strength as neither complex is sterically crowded.

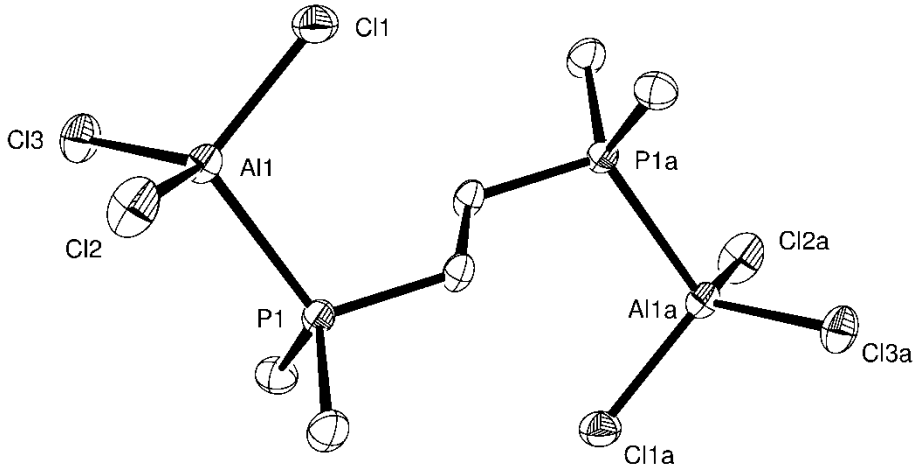

Figure 2.10 The structure of centrosymmetric $[(AlCl_3)_2\{\mu\text{-}Me_2P(CH_2)_2PMe_2\}]$ showing the atom labelling scheme. Ellipsoids are drawn at the 50% probability level and H atoms are omitted for clarity. Symmetry operation: a = – x, 1 – y, – z.

Table 2.10 Selected bond lengths (Å) and angles (°) for $[(AlCl_3)_2\{\mu\text{-}Me_2P(CH_2)_2PMe_2\}]$

Al1–Cl1	2.1284(15)	Cl1–Al1–Cl2	112.54(6)
Al1–Cl2	2.1166(14)	Cl1–Al1–Cl3	110.78(5)
Al1–Cl3	2.1203(15)	Cl2–Al1–Cl3	112.15(6)
Al1–P1	2.4059(14)	Cl1–Al1–P1	104.68(5)
		Cl2–Al1–P1	106.34(5)
		Cl3–Al1–P1	109.97(6)

As control to favour the bridging coordination mode could not be achieved by changing the halide bound to aluminium, it was decided to see if changing the steric requirements of the bidentate phosphine used would lead to the four-coordinate complex being preferred. The flexible but much more sterically bulky cyclohexyl-substituted diphosphine $Cy_2P(CH_2)_2PCy_2$ was found to only give the bridged complex

$[(AlCl_3)_2\{\mu\text{-}Cy_2P(CH_2)_2PCy_2\}]$ irrespective of the ratio of reagents used. The complex is extremely sensitive and is readily hydrolysed by trace moisture (see Section 2.2.4), presumably because $Cy_2P(CH_2)_2PCy_2$ is such a good proton base.[36] It also decomposes fairly rapidly on standing in CH_2Cl_2 solution at room temperature.

The IR spectrum of $[(AlCl_3)_2\{\mu\text{-}Cy_2P(CH_2)_2PCy_2\}]$ has two ν(AlCl) bands at 478 and 375 cm^{-1}, consistent with a C_{3v} geometry at aluminium, while the singlet in the ^{27}Al NMR spectrum is in the expected four-coordinate region at $\delta = 110.6$ at 295 K, and varies little with temperature. The $^{31}P\{^1H\}$ NMR spectrum shows a singlet at $\delta = -0.5$ at 295 K (in CH_2Cl_2/CD_2Cl_2), which (unlike the other phosphine complexes) is at a lower frequency ($\Delta = -2.7$) compared to free $Cy_2P(CH_2)_2PCy_2$. This trend is also observed with phosphine complexes of $AlMe_3$, where small phosphines exhibit small positive (high frequency) shifts, but as the steric bulk of the phosphine increases the shifts become negative; this is attributed to increased steric repulsion between the $AlMe_3$ and the phosphine (PR_3) substituents which decreases the ∠R–P–R.[37]

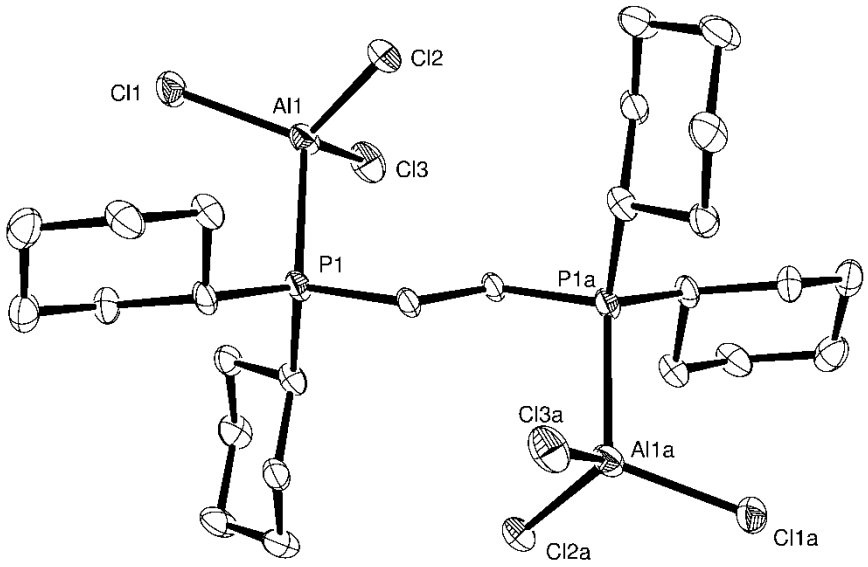

Figure 2.11 The structure of centrosymmetric $[(AlCl_3)_2\{\mu\text{-}Cy_2P(CH_2)_2PCy_2\}]$ showing the atom labelling scheme. Ellipsoids are drawn at the 50% probability level and H atoms are omitted for clarity. Symmetry operation: a = 2 – x, 1 – y, 1 – z.

Table 2.11 Selected bond lengths (Å) and angles (°) for $[(AlCl_3)_2\{\mu\text{-}Cy_2P(CH_2)_2PCy_2\}]$

Al1–Cl1	2.123(3)	Cl1–Al1–Cl2	112.00(12)
Al1–Cl2	2.129(3)	Cl1–Al1–Cl3	112.98(12)
Al1–Cl3	2.114(3)	Cl2–Al1–Cl3	113.23(12)
Al1–P1	2.407(3)	Cl1–Al1–P1	108.76(11)
		Cl2–Al1–P1	102.90(10)
		Cl3–Al1–P1	106.20(11)

The X-ray crystal structure of $[(AlCl_3)_2\{\mu\text{-}Cy_2P(CH_2)_2PCy_2\}]$ was obtained from a very small crystal grown from a CH_2Cl_2 solution kept at –18 °C. The complex is centrosymmetric (Figure 2.11), with similar *d*(Al–P), *d*(Al–Cl), ∠Cl–Al–Cl and ∠Cl–Al–P to $[(AlCl_3)_2\{\mu\text{-}Me_2P(CH_2)_2PMe_2\}]$, showing that the bulkier cyclohexyl groups have little effect sterically on the geometry around the four-coordinate aluminium centre (though the increased steric bulk prevents two $Cy_2P(CH_2)_2PCy_2$ ligands from chelating to Al(III) to give a six-coordinate complex) and that the two diphosphine ligands are of similar donor strength.

2.2.4 Hydrolysis of aluminium(III) halide – phosphine complexes

Although some phosphine oxidation was occasionally observed (due to the appearance of minor peaks corresponding to the relevant phosphine oxide complex in the $^{31}P\{^1H\}$ and ^{27}Al NMR spectra) oxidation was generally not an issue when trying to obtain pure samples. However, as mentioned previously, partial hydrolysis of the complexes (leading to the formation of phosphonium salts $[R_3PH][AlX_4]$) was observed by varying degrees in the ^1H, $^{31}P\{^1H\}$ and ^{27}Al NMR spectra of most of the systems studied, for all of the AlX_3 (X = Cl, Br, I). Similar behaviour was observed for GaX_3,[38] while InX_3 does not form phosphonium cations, but instead water simply displaces the phosphine ligand.[39]

Hydrolysis was found to occur when the NMR solutions (in CD_2Cl_2 or a mixture of CH_2Cl_2 and CD_2Cl_2) were made up using the pre-formed complex, as the bulk powders otherwise analysed as the pure complex. The longer the NMR solutions were left standing before the spectra were run, the more intense the peaks corresponding to $[R_3PH]^+$ became, possibly due to the slow ingress of water into the NMR tube over time. The amount of protonation observed (if any) was therefore a subtle interplay of the dryness of the NMR

solvent, the time taken to run the NMR spectra and the basicity of the phosphine involved (for example, no resonances of significant intensity corresponding to a phosphonium salt of the aryl diphosphine *o*-$C_6H_4(PPh_2)_2$ were ever observed, whereas intense resonances for $[Cy_2HP(CH_2)_2PCy_2]^+$ or $[Cy_2HP(CH_2)_2PHCy_2]^{2+}$ were frequently seen). Alkyl phosphines are stronger proton bases than aryl phosphines, with the basicity of representative examples decreasing in the order $PCy_3 > PMe_3 > PPh_3$.[36]

Resonances corresponding to the phosphonium cations in the $^{31}P\{^1H\}$ NMR spectra (see Table 2.12) were observed at a higher frequency than the aluminium complexes and were typically sharp, with doublets ($^3J_{PP}$ = ~ 40-60 Hz) seen in favourable cases for the mono-protonated diphosphines. This is in contrast to the broad, ill-defined $[R_3PH]^+$ resonances observed in gallium(III) halide – phosphine complex systems.[38] The phosphonium cations could be easily identified by running the equivalent ^{31}P NMR spectra, as the resonances became doublets ($^1J_{PH}$ = ~ 500 Hz). In most cases the diphosphine was only mono-protonated, and the resonance ascribed to the unprotonated phosphorus atom had a chemical shift close to that of the free ligand. Though the ^{31}P NMR chemical shifts of the $[R_3PH]^+$ were found to be susceptible to solvent shifts, they do not change significantly with the halide in $[AlX_4]^-$. Variable temperature $^{31}P\{^1H\}$ NMR studies reveal that the phosphonium salts do not appear to interact with the complexes where both are observed in the spectra; rather the $[R_3PH]^+$ resonances simply drift slightly on cooling.

Table 2.12 Observed ^{31}P NMR spectroscopic data for phosphonium cations in CD_2Cl_2[a]

Phosphonium cation	$\delta(^{31}P)$ PH^+ / 295 K	$^1J_{PH}$ / Hz	$\delta(^{31}P)$ P / 295 K
$[Me_3PH]^+$	–4.0[b]	497[b]	–
$[o\text{-}C_6H_4(PMe_2)(PHMe_2)]^+$	–4.2	540	–51.9
$[Me_2HP(CH_2)_2PMe_2]^+$	+3.2	500	–43.9
$[Cy_2HP(CH_2)_2PCy_2]^+$	+26.6	462	+0.6

[a] values taken from spectra of the aluminium complexes where (partial) hydrolysis has occurred; [b] literature value in HSO_3F: δ = –3.2 ($^1J_{PH}$ = 497 Hz)[40]

Confirmation of the identity of the hydrolysis products comes from the X-ray crystal structures of $[Cy_2HP(CH_2)_2PHCy_2][AlCl_4]_2$ and $[o\text{-}C_6H_4(PMe_2)(PHMe_2)]_2[AlX_4][X]$ (X = Cl, Br). The structure of $[Cy_2HP(CH_2)_2PHCy_2][AlCl_4]_2$ was obtained from a few crystals that grew from a CH_2Cl_2 solution of $AlCl_3$ and $Cy_2P(CH_2)_2PCy_2$ in a 2:1 molar ratio that

had been layered with hexane. The centrosymmetric cation can be seen in Figure 2.12. The X-ray crystal structure of $Cy_2P(CH_2)_2PCy_2$ is not known and so structural comparisons between the unprotonated and protonated forms are not possible.

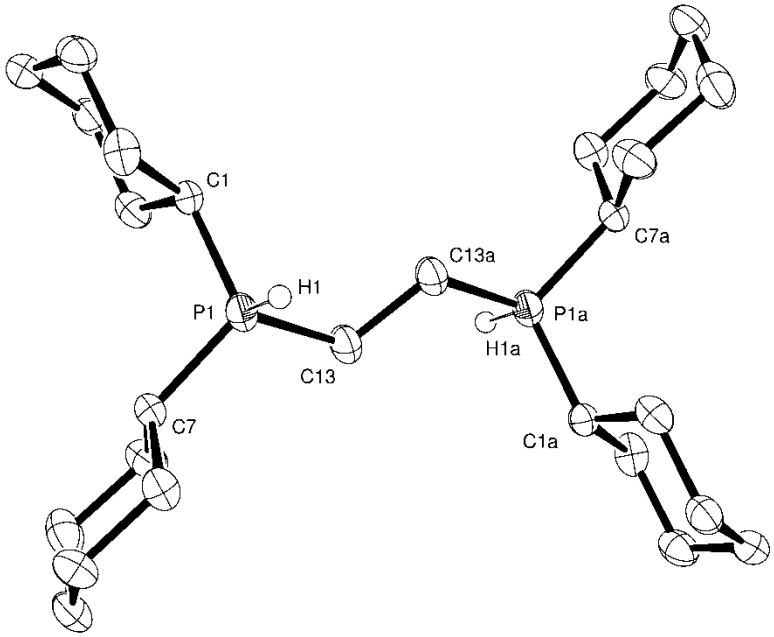

Figure 2.12 The structure of the centrosymmetric cation in $[Cy_2HP(CH_2)_2PHCy_2][AlCl_4]_2$ showing the atom labelling scheme. Ellipsoids are drawn at the 50% probability level and H atoms bonded to C are omitted for clarity. Symmetry operation: a = 1 – x, 1 – y, 2 – z.

Table 2.13 Selected bond lengths (Å) and angles (°) for $[Cy_2HP(CH_2)_2PHCy_2]^{2+}$

P1–C1	1.812(6)	C1–P1–C7	111.0(3)
P1–C7	1.822(6)	C1–P1–C13	113.0(3)
P1–C13	1.811(6)	C7–P1–C13	114.4(3)
P1–H1	1.36(6)		

Crystals of $[o\text{-}C_6H_4(PMe_2)(PHMe_2)]_2[AlCl_4][Cl]$ were obtained by storing a CH_2Cl_2/hexane solution of $[AlCl_2\{o\text{-}C_6H_4(PMe_2)_2\}_2][AlCl_4]$ at –18 °C for several weeks. The X-ray crystal structure (Figure 2.13) reveals the $[o\text{-}C_6H_4(PMe_2)(PHMe_2)]^+$ cation with *d*(P–C) that are ~0.06 Å shorter and ∠C–P–C that are widened by ~ 10 ° for the protonated phosphine as compared to the unprotonated phosphine group. The structure of the cation is very similar to the reported $[o\text{-}C_6H_4(PPh_2)(PHPh_2)][GaBr_4]$,[41] which shows similar but less pronounced changes in the *d*(P–C) and ∠C–P–C between the protonated and unprotonated

phosphine groups. The X-ray crystal structure of the isomorphous $[o\text{-}C_6H_4(PMe_2)(PHMe_2)]_2[AlBr_4][Br]$ was obtained from small crystals that grew when a toluene solution of $o\text{-}C_6H_4(PMe_2)_2$ was carefully layered onto a toluene solution of $AlBr_3$.

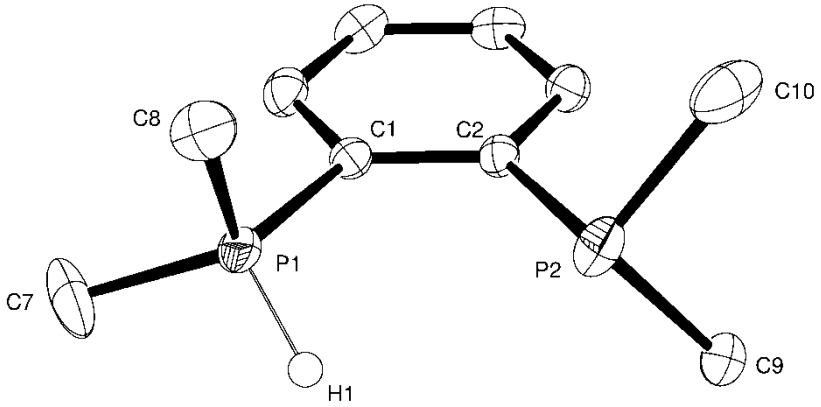

Figure 2.13 The structure of the cation in $[o\text{-}C_6H_4(PMe_2)(PHMe_2)]_2[AlCl_4][Cl]$ showing the atom labelling scheme. Ellipsoids are drawn at the 50% probability level and H atoms bonded to C are omitted for clarity. The cation in the isomorphous $[o\text{-}C_6H_4(PMe_2)(PHMe_2)]_2[AlBr_4][Br]$ has effectively identical dimensions.

Table 2.14 Selected bond lengths (Å) and angles (°) for $[o\text{-}C_6H_4(PMe_2)(PHMe_2)]^+$

P1–C1	1.799(3)	C1–P1–C7	111.31(17)
P1–C7	1.777(4)	C1–P1–C8	110.64(15)
P1–C8	1.783(3)	C7–P1–C8	108.79(18)
P1–H1	1.29(3)	C2–P2–C9	100.94(15)
P2–C2	1.845(3)	C2–P2–C10	100.15(15)
P2–C9	1.838(3)	C9–P2–C10	101.31(17)
P2–C10	1.836(4)		

2.2.5 Complexes with arsine ligands

While Burford *et al.*[10] have reported the *pseudo*-tetrahedral $[AlX_3(AsR_3)]$ (X = Cl, Br, I; R = Me, Et, Ph), supported by the X-ray crystal structures of $[AlX_3(AsPh_3)]$ (X = Cl, I), the singlet resonances reported in the ^{27}Al NMR spectra (δ = 104-113) for all the complexes are in the typical region for four-coordinate chloro-aluminium species. Their spectra were obtained *in situ* from reaction mixtures in CH_2Cl_2, which suggests that halide exchange had

most probably occurred. To confirm this *in situ* ^{27}Al NMR spectra were recorded for $[AlI_3(AsEt_3)]$ ($\delta = 31.9$) and $[AlI_3(AsPh_3)]$ ($\delta = 33.1$) in toluene/d^8 toluene solution, which, when taking into account the different solvents used, have similar chemical shifts to $[AlI_3(PMe_3)]$ ($\delta = 50.2$) and are in the expected region for four-coordinate AlI_3 complexes. The ^{27}Al NMR spectrum of $[AlI_3(AsEt_3)]$ remained unchanged upon addition of excess $AsEt_3$ to the solution, showing that the five-coordinate $[AlI_3(AsEt_3)_2]$ does not form under these conditions, which is in contrast to the phosphine systems studied.

The reaction of $AlCl_3$ with the diarsine *o*-$C_6H_4(AsMe_2)_2$ in a 2:1 molar ratio in CH_2Cl_2 initially gave a white powder which slowly redissolved while, over the period a week, small colourless crystals grew. Single crystal X-ray structure determination identified these as $[o\text{-}C_6H_4(AsMe_2)_2(CH_2)][AlCl_4]_2$, in which the diarsine has been diquaternized by the solvent to give a near-symmetrical CH_2-bridged dication (Figure 2.14). Similar CH_2Cl_2 solvent activation has been reported before from the reactions of SnF_2 with *o*-$C_6H_4(PMe_2)_2$ which yielded crystals of the diphosphine analogue $[o\text{-}C_6H_4(PMe_2)_2(CH_2)]^{2+}$ (this could also be synthesised directly from *o*-$C_6H_4(PMe_2)_2$ and CH_2I_2 in toluene). This reactivity was ascribed to the SnF_2 polarising the CH_2Cl_2 towards nucleophilic attack by the phosphine.[34] $AlCl_3$ presumably behaves similarly towards CH_2Cl_2, but reaction with the solvent was not significant in the phosphine systems as fast ligand complexation is the dominant process.

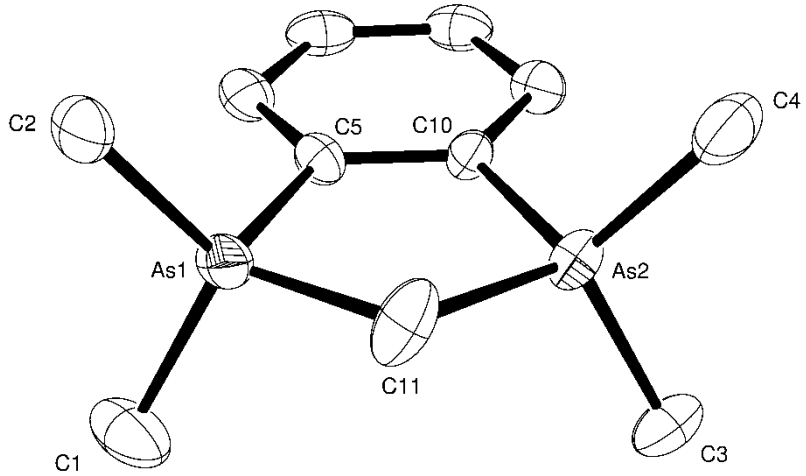

Figure 2.14 The structure of the cation in $[o\text{-}C_6H_4(AsMe_2)_2(CH_2)][AlCl_4]_2$ showing the atom numbering scheme. Ellipsoids are drawn at the 50% probability level and H atoms are omitted for clarity.

Table 2.15 Selected bond lengths (Å) and angles (°) for $[o\text{-}C_6H_4(AsMe_2)_2(CH_2)]^{2+}$

As1–C1	1.910(7)	C1–As1–C2	112.7(3)
As1–C2	1.907(6)	C5–As1–C11	101.0(3)
As1–C5	1.910(5)	C3–As2–C4	110.8(3)
As1–C11	1.968(7)	C10–As2–C11	100.7(2)
As2–C3	1.906(6)	As1–C11–As2	104.2(3)
As2–C4	1.910(7)		
As2–C10	1.907(5)		
As2–C11	1.969(7)		

IR and ^{27}Al NMR spectroscopy of the isolated crystals of $[o\text{-}C_6H_4(AsMe_2)_2(CH_2)][AlCl_4]_2$ confirm the presence of the $[AlCl_4]^-$ anions. There are three distinct resonances in the ^{1}H NMR spectrum, with the δ(Me) and δ(o-C_6H_4) resonances having shifted to a higher frequency compared to free o-$C_6H_4(AsMe_2)_2$, while there is a new singlet at δ = 3.43 corresponding to the bridging CH_2 group. The $[o\text{-}C_6H_4(AsMe_2)_2(CH_2) + CH_3CN]^{2+}$ ion could also be identified in the ESI+ mass spectrum of the crystals dissolved in CH_3CN.

The reaction of $AlCl_3$ with o-$C_6H_4(AsMe_2)_2$ in a 2:1 molar ratio in toluene yielded a slightly sticky white solid shown by microanalysis to have an $AlCl_3$ to o-$C_6H_4(AsMe_2)_2$ composition of 2:1. The $[AlCl_4]^-$ ion is evident in the IR and ^{27}Al NMR spectrum of the solid, leading to the identity of the complex being proposed as the four-coordinate $[AlCl_2\{o\text{-}C_6H_4(AsMe_2)_2\}][AlCl_4]$. Though no resonance for the cation (or any other species) was observed in the ^{27}Al NMR spectrum (even when cooled to 203 K), resonances for the cation with chemical shifts that are at a higher frequency relative to free o-$C_6H_4(AsMe_2)_2$ are evident in the ^{1}H NMR spectrum.

The reaction of $AlCl_3$ with o-$C_6H_4(AsMe_2)_2$ in a 1:1 molar ratio in toluene and all the reactions performed with AlX_3 (X = Br, I) yielded solids that were difficult to manipulate and appeared by ^{1}H NMR spectroscopy to be a mixture of species which could not be easily identified, even upon cooling the NMR solutions. In the analogous gallium systems $GaCl_3$ was found to form the four-coordinate $[GaCl_2\{o\text{-}C_6H_4(AsMe_2)_2\}][GaCl_4]$ irrespective of the ratio of reagents used, while $GaBr_3$ and GaI_3 formed $[GaX_2\{o\text{-}C_6H_4(AsMe_2)_2\}][GaX_4]$ only when a 2:1 molar ratio of reagents was employed. It

was postulated that with a 1:1 reagent ratio, mixtures of $[GaX_2\{o\text{-}C_6H_4(AsMe_2)_2\}][GaX_4]$ and $[GaX_2\{o\text{-}C_6H_4(AsMe_2)_2\}][X]$ (X = Br, I) were formed.[29] The InX_3 were observed to form $[InX_2\{o\text{-}C_6H_4(AsMe_2)_2\}][InX_4]$ when a 2:1 molar ratio of reagents was used; with other reagent ratios a variety of six-coordinate complexes with different structural motifs were obtained that depended on the halide present.[39] This apparent reduction in the affinity of AlX_3 (X = Cl, Br, I) for arsines when compared to analogous phosphine systems is also seen in complexes of other light p-block elements. For example, SiX_4 (X = Cl, Br) will readily form complexes with both mono- and bi-dentate phosphines, but does not react with $AsMe_3$ or $o\text{-}C_6H_4(AsMe_2)_2$.[42]

2.2.6 Comparisons with gallium and indium systems

The gallium(III) halides show a clear preference in forming four-coordinate *pseudo*-tetrahedral complexes with both mono- and bi-dentate phosphines and arsines,[1] with six-coordinate (distorted octahedral) cations only being achieved with $o\text{-}C_6H_4(PMe_2)_2$ in $[GaX_2\{o\text{-}C_6H_4(PMe_2)_2\}_2][GaX_4]$ (X = Cl, Br, I).[29] In contrast, the indium(III) halides readily form four-, five- and six-coordinate complexes with phosphine and arsine ligands, and for a particular InX_3/ligand system changing the reagent stoichiometry allows more than one complex to be isolated.[1] For example, a 2:1 ratio of $InCl_3$ and $o\text{-}C_6H_4(PMe_2)_2$ yields $[InCl_2\{o\text{-}C_6H_4(PMe_2)_2\}][InCl_4]$, while a 1:1 (or 1:2) ratio gives the centrosymmetric halide-bridged dimer $[In_2Cl_6\{o\text{-}C_6H_4(PMe_2)_2\}_2]$, which appears to partially rearrange in solution to $[InCl_2\{o\text{-}C_6H_4(PMe_2)_2\}_2][InCl_4]$ and perhaps $[InCl_3\{o\text{-}C_6H_4(PMe_2)_2\}]$.[39] The present work shows that the aluminium(III) halides will also readily form four-, five- and six-coordinate complexes with mono- and bi-dentate phosphines, often preferring higher coordination numbers (except with very sterically bulky diphosphines). While flexible diphosphines act exclusively as bridging ligands with GaX_3 e.g. $[(GaX_3)_2\{\mu\text{-}Et_2P(CH_2)_2PEt_2\}]$ (X = Cl, Br),[29] both bridging and chelating coordination modes were observed for $AlCl_3$ with $Me_2P(CH_2)_2PMe_2$. In contrast to InX_3 the structural variety in a particular AlX_3/PR_3 system tends to be limited; for example only $[AlX_2\{o\text{-}C_6H_4(PMe_2)_2\}_2][AlX_4]$ was ever isolated with $o\text{-}C_6H_4(PMe_2)_2$. Only four-coordinate aluminium(III) halide complexes have been isolated with the softer arsine ligands. As noted for the gallium-[29] and indium-[39] halide – phosphine and arsine complexes the structural data for the aluminium complexes show that the primary interactions are the Al–X bonds, with weaker bonds formed to the neutral phosphine and arsine ligands.

In p-block chemistry both steric (covalent radius) and electronic (Lewis acidity) effects control the coordination numbers and geometries seen around the Lewis acid centre. The single bond covalent radii are quoted as being 1.25 Å for both Al and Ga, while the value is 1.50 Å for In.[3] In a study of comparable complexes with Group 16 donor ligands, the *d*(M–X) and *d*(M–E) (M = Al, Ga, In; E = S, Se, Te) were found to be very similar for Al and Ga, and typically ~0.2 Å longer for In.[35] In order to further investigate whether Al and Ga are the same size the *d*(M–X) of the tetrahalide ions $[MX_4]^-$ (X = Cl, Br, I) were compared for Al, Ga and In using data taken from the Cambridge Structural Database[43] (see Section 2.6 – Appendix 2), the results of which are summarised in Table 2.16. The results show that the *d*(M–X) are essentially the same for Al and Ga (and again ~0.2 Å longer for In). The similarity in size of Al and Ga results from d-block contraction, where the increased nuclear charge due to the insertion of the 3d transition metals is not fully screened by the valence 3d electrons.

Table 2.16 Summary of the mean M−X bond lengths (*d*(M−X) in Å), with associated errors, in $[MX_4]^-$. Data taken from the Cambridge Structural Database[43]

$[MX_4]^-$	X = Cl	X = Br	X = I
M = Al	2.126 ± 0.018	2.289 ± 0.015	2.527 ± 0.012
M = Ga	2.166 ± 0.018	2.321 ± 0.016	2.544 ± 0.018
M = In	2.337 ± 0.022	2.484 ± 0.018	2.702 ± 0.014

Steric effects are therefore not the reason for AlX_3 to prefer to go to higher coordination numbers while GaX_3 largely remain four-coordinate upon phosphine coordination, and so it must be attributable to electronic effects. Based on computed dissociation enthalpies the order of Lewis acidity has been established as decreasing in the order $AlCl_3 > AlBr_3 > GaCl_3 > GaBr_3$.[4] The differences must therefore originate in the match (or mismatch) in the donor and acceptor orbital energies upon bond formation with the ligand.[35] The wide range of structures obtainable with InX_3 is ascribed to the larger size of In, making five- and six-coordinate complexes more favourable, as well as fact that the ligands are less strongly bound due to the weaker Lewis acidity of InX_3.[39]

2.2.7 Towards aluminium(III) fluoride complexes with phosphines

As an inert fluorine-bridged polymer there is very little known concerning the coordination chemistry of AlF_3. Its relatively open structure allows it to form a range of hydrates, most

notably $AlF_3.nH_2O$ (n = 1, 3 or 9), which have an enhanced solubility in water.[2] The exchange of Cl for F in $[AlCl_3(py)_3]$ using Me_3SiF as a fluorinating agent yields *trans*-$[AlF_2(py)_4]Cl$,[44] while the analogous *trans*-$[AlF_2(THF)_4]^+$ cation is found in $[AlF_2(THF)_4][\{(SiMe_3)_3C\}_2Al_2F_5]$, formed by the reaction of $[\{(SiMe_3)_3C\}AlF_2]_3$ with THF and the fluorinating agent AgF_2.[45] More recently a hydrothermal synthesis approach has enabled a number of AlF_3 complexes with neutral nitrogen donor ligands to be synthesised. The complexes $[AlF_3(bipy)(H_2O)].2H_2O$, $[AlF_3(phen)(H_2O)]$ and $[AlF_3(terpy)].3H_2O$ have been synthesised by mixing $AlF_3.3H_2O$ with the ligand in distilled water and heating it in a high pressure vessel at 180 °C for 15 hours.[46] Hydrothermal synthesis has also been successfully used with the macrocycle Me_3-tacn to form $[AlF_3(Me_3\text{-tacn})].xH_2O$, which, along with $[AlF_3(BzMe_2\text{-tacn})]$, can also be formed from the analogous chloride complexes in CH_3CN using aqueous KF as the fluorinating agent.[47]

As complexes of AlF_3 can be synthesised with neutral hard N donor ligands it was of interest to see if an aluminium(III) fluoride – phosphine oxide complex could also be made via a hydrothermal synthesis route. $AlF_3.3H_2O$ was mixed with both 1 and 3 molar equivalents of $OPPh_3$ (as it is not known what coordination number AlF_3 might prefer) in distilled water and heated to 180 °C for 20 hours in high pressure vessels. After filtering the resulting mixtures to remove a white solid (which was shown by IR spectroscopy to be free $OPPh_3$) in both cases the solvent was removed *in vacuo* to yield a small amount of white powder, which was shown by IR spectroscopy to be mainly $AlF_3.nH_2O$ (ν(AlF) = 664 and 345 cm^{-1}). The unit cell of the colourless crystals that grew from the slow evaporation of a portion of the 1:3 reaction filtrate was found to match $Ph_3PO{\cdot}0.5H_2O$.[48] It is thought that the phosphine oxide cannot compete for the Al(III) centre with the large excess of water present. As attempts to form a phosphine oxide complex of AlF_3 were unsuccessful, and given that the AlX_3 appear to promote the hydrolysis of phosphines, no hydrothermal experiments were attempted with phosphine ligands.

Although no aluminium(III) fluoride – phosphine complexes have been synthesised theoretical studies of $[AlX_3(PMe_3)]$ (X = F, Cl) and related PY_3 (Y = F, Cl, CN) complexes predict that $[AlF_3(PMe_3)]$ will have a *d*(Al–P) of 2.420 Å (*ab initio*) and that the Lewis acidity follows $AlCl_3 \geq AlF_3$.[49] In order to try and synthesise $[AlF_3(PMe_3)]$, halide metathesis was attempted with $[AlCl_3(PMe_3)]$ using two easy to handle and versatile[50] fluorinating agents, $[NMe_4]F$ and Me_3SnF. The reactions were performed in CD_2Cl_2 to enable a detailed multinuclear NMR study to be conducted, using variable temperature ^1H,

^{19}F, ^{27}Al and $^{31}P\{^{1}H\}$ NMR spectroscopy. While it is known that the fluoride anion will react slowly with CH_2Cl_2 to form CH_2ClF[51] there was no evidence for this in any of the ^{1}H or ^{19}F NMR spectra recorded. The reaction of $[AlCl_3(PMe_3)]$ with three molar equivalents of Me_3SnF generated Me_3SnCl ($\delta(^{1}H) = 0.66$ (s, $^{2}J_{HSn} = 60.8$ Hz)) but only $[Me_3PH]^+$ was evident in the $^{31}P\{^{1}H\}$ NMR spectrum of the reaction solution. Upon the addition of three molar equivalents of $[NMe_4]F$ to a solution of $[AlCl_3(PMe_3)]$ a white solid immediately precipitated out, which showed IR spectroscopic features corresponding to the insoluble $[NMe_4]Cl$ at 1491, 1405 and 950 cm^{-1}, as well as a band at 667 cm^{-1} which is assigned as ν(AlF). The only resonance observed in the $^{31}P\{^{1}H\}$ NMR spectrum of the filtrate was free PMe_3, with no resonances seen in the ^{19}F and ^{27}Al NMR spectra. Similar results were obtained when the coordinatively saturated $[AlCl_2\{o\text{-}C_6H_4(PMe_2)_2\}_2][AlCl_4]$ was made *in situ* in CH_2Cl_2/CD_2Cl_2 and then six molar equivalents of $[NMe_4]F$ added, as only free $o\text{-}C_6H_4(PMe_2)_2$ was evident in the $^{31}P\{^{1}H\}$ NMR spectrum.

It therefore appears that in these compounds fast Cl/F exchange does occur, but this is accompanied by dissociation of the phosphine from the aluminium centre (which is then susceptible to protonation), while the "AlF_3" produced polymerises and precipitates out of solution. Similar behaviour has been observed with zirconium(IV) diphosphine complexes, whereby polymeric ZrF_4 and free diphosphine ligand were obtained when diphosphine complexes of ZrI_4 were reacted with Me_3SnF.[52] The use of fluorinating agents to exchange Cl for F in pre-formed aluminium(III) halide – phosphine complexes has therefore so far been unsuccessful; it appears that the hard Lewis acidic Al(III) centre prefers to form Al–F–Al bridges, rather than coordinate to soft phosphine ligands.[53]

2.3 Conclusions

A number of novel aluminium(III) halide – phosphine complexes have been successfully synthesised and characterised both structurally and spectroscopically, including several examples with bidentate phosphine ligands, an area which has not been previously studied. $AlCl_3$ has been shown to form both 1:1 and 1:2 complexes with the monodentate ligand PMe_3 (there was no evidence that a 1:3 complex could be formed), the structure of *trans*-$[AlCl_3(PMe_3)_2]$ being a rare example of a *pseudo*-trigonal bipyramidal complex. With bidentate phosphines there is a clear preference for aluminium to go six-coordinate, with *trans*-$[AlCl_2\{o\text{-}C_6H_4(PR_2)_2\}_2][AlCl_4]$ (R = Me, Ph) and *trans*-$[AlCl_2\{Me_2P(CH_2)_2PMe_2\}_2][AlCl_4]$ being the first reported *pseudo*-octahedral aluminium(III) halide – phosphine complexes.[1] This is in contrast to the gallium(III) halide – phosphine systems, where a four-coordinate geometry is almost always adopted, and is ascribed to the greater Lewis acidity of AlX_3, consistent with theoretical studies.[4] While sterically the halide present at the aluminium centre does not affect the coordination geometry observed, the use of a more sterically bulky diphosphine (such as $Cy_2P(CH_2)_2PCy_2$) results in a four-coordinate geometry around aluminium being favoured. The affinity of AlX_3 for arsine ligands is significantly less than for phosphines, with only a small number of four-coordinate complexes being identified. The first example of an aluminium(III) halide – arsine oxide complex, $[AlCl_3(OAsPh_3)]$, has been crystallographically identified, while the $[AlX_3(OPMe_3)]$ (X = Cl, Br) have also been synthesised, all supported by spectroscopic characterisation. Attempts to form phosphine complexes of AlF_3 from the analogous chloride complexes via a halide metathesis route were unsuccessful and this class of aluminium(III) complex remains unknown.

This area remains synthetically challenging due to the high reactivity of AlX_3, which makes chlorocarbon solvents unsuitable for reactions with $AlBr_3$ or AlI_3 due to halide exchange with the solvent, while the activation of CH_2Cl_2 to form the CH_2-bridged dication in $[o\text{-}C_6H_4(AsMe_2)_2(CH_2)][AlCl_4]_2$ was also observed. The systems are also very sensitive to trace moisture, with the complexes often partially hydrolysing in solution.

2.4 Experimental

The general experimental techniques used in this chapter can be found in Appendix 1 at the end of the thesis.

$[AlCl_3(OPMe_3)]$

A solution of $OPMe_3$ (0.060 g, 0.65 mmol) in CH_2Cl_2 (5 mL) was added to a suspension of $AlCl_3$ (0.088 g, 0.66 mmol) in CH_2Cl_2 (5 mL). The resulting solution was stirred for 1 h, then concentrated to about 2 mL *in vacuo*. The resulting white precipitate was isolated, washed with hexane (5 mL) and dried *in vacuo* to yield a white powder. Yield: 0.070 g (48%). Anal. Calc. for $C_3H_9AlCl_3OP$: C, 16.0; H, 4.0. Found: C, 15.2; H, 4.5%. ^{1}H NMR (CD_2Cl_2, 295 K): δ = 1.92 (d, $^2J_{HP}$ = 13.5 Hz, CH_3). $^{31}P\{^1H\}$ NMR (CH_2Cl_2/CD_2Cl_2, 295 K): δ = 70.0 (s). ^{27}Al NMR (CH_2Cl_2/CD_2Cl_2, 295 K): δ = 91.4 (s). IR (Nujol): ν = 1149 (s) (PO), 495 (vs), 392 (m, br) (AlCl) cm^{-1}.

$[AlCl_nBr_{(3-n)}(OPPh_3)]$ (n = 0-3)

A solution of $OPPh_3$ (0.066 g, 0.24 mmol) in CH_2Cl_2 (5 mL) was added to a pale yellow solution of $AlBr_3$ (0.065 g, 0.24 mmol) in CH_2Cl_2 (5 mL). The resulting pale yellow solution was stirred for 2 h and then the solvent volume was reduced to about 3 mL *in vacuo* onto which hexane (6 mL) was layered. Reduction of the solvent volume *in vacuo* caused the precipitation of a yellow-white powder which was isolated by filtration and dried *in vacuo*. Yield: 0.059 g. ^{1}H NMR (CD_2Cl_2, 295 K): δ = 7.60-7.82 (m, C_6H_5). $^{31}P\{^1H\}$ NMR (CH_2Cl_2/CD_2Cl_2, 295 K): δ = 47.5 (s); (193 K): 48.2 (br s). ^{27}Al NMR (CH_2Cl_2/CD_2Cl_2, 295 K): δ = 90.9 (s, n = 3), 88.3 (s, n = 2), 84.4 (s, n = 1), 79.1 (s, n = 0); (193 K): 90.2 (s), 87.8 (s), 84.0 (s), 78.9 (s). IR (Nujol): ν = 1155 (vs) (PO), 515 (s) (AlCl), 426 (s) (AlBr) cm^{-1}.

$[AlBr_3(OPMe_3)]$

To a yellow solution of $AlBr_3$ (0.292 g, 1.09 mmol) in toluene (4 mL) was added $OPMe_3$ (0.101 g, 1.09 mmol) in toluene (4 mL). The reaction gradually became colourless, and a precipitate formed after 10 min. stirring. The reaction was stirred for 1 h, filtered and the white powder isolated dried *in vacuo*. Yield: 0.252 g (64%). Anal. Calc. for $C_3H_9AlBr_3OP$:

C, 10.0; H, 2.5. Found: C, 10.2; H, 2.6%. ^{1}H NMR (CD_3CN, 295 K): δ = 1.90 (d, $^{2}J_{HP}$ = 12.0 Hz, CH_3). $^{31}P\{^{1}H\}$ NMR (CD_3CN, 295 K): δ = 73.5 (s). ^{27}Al NMR (CH_3CN/CD_3CN, 295 K): δ = 78.1 (s). IR (Nujol): ν = 1144 (vs) (PO), 411 (vs), 291 (m) (AlBr) cm^{-1}.

[$AlCl_3(OAsPh_3)$]

A solution of $OAsPh_3$ (0.301 g, 0.93 mmol) in CH_2Cl_2 (5 mL) was added to a suspension of $AlCl_3$ (0.128 g, 0.95 mmol) in CH_2Cl_2 (5 mL). The reaction was stirred for 2 h, then the colourless solution was decanted off to isolate a white solid. The solid was washed with hexane (5 mL) and dried *in vacuo* to give a white powder. A second crop was obtained by layering the supernatant with hexane (5 mL) and later concentrating it to about 4 mL *in vacuo*, whereupon a white powder precipitated out which was isolated by filtration and dried *in vacuo*. Block colourless crystals suitable for single crystal X-ray diffraction study were grown from the filtrate upon cooling to –18 °C. The overall yield was 0.135 g (32%). Anal. Calc. for $C_{18}H_{15}AlAsCl_3O$: C, 47.4; H, 3.3. Found: C, 47.3; H, 3.4%. ^{1}H NMR (CD_2Cl_2, 295 K): δ = 7.59-8.06 (m, C_6H_5). ^{27}Al NMR (CH_2Cl_2/CD_2Cl_2, 295 K): δ = 93.1 (s). IR (Nujol): ν = 929 (s) (AsO), 491 (s), 392 (m) (AlCl) cm^{-1}.

[$AlCl_3(PMe_3)$]

To a suspension of $AlCl_3$ (0.177 g, 1.33 mmol) in CH_2Cl_2 (5 mL) was added PMe_3 (0.100 g, 1.31 mmol) in CH_2Cl_2 (5 mL). The resulting colourless solution was stored at –18 °C and over a few days large, colourless, temperature-sensitive crystals suitable for single crystal X-ray diffraction study formed. These were separated and dried. The solvent was then removed *in vacuo* and the resulting white solid was washed with hexane (5 mL), and dried *in vacuo*. Yield: 0.174 g (63%). Anal. Calc. for $C_3H_9AlCl_3P$: C, 17.2; H, 4.3. Found: C, 17.2; H, 4.4%. ^{1}H NMR (CD_2Cl_2, 295 K): δ = 1.50 (d, $^{2}J_{HP}$ = 10.0 Hz, CH_3). $^{31}P\{^{1}H\}$ NMR (CH_2Cl_2/CD_2Cl_2, 295 K): δ = –42.6 (br s); (248 K): –42.3 (sextet); (223 K): –42.3 (sextet, $^{1}J_{PAl}$ = 275 Hz). ^{27}Al NMR (CH_2Cl_2/CD_2Cl_2, 295 K): δ = 108.8 (s); (223 K): 111.4 (d, $^{1}J_{AlP}$ = 275 Hz). IR (Nujol): ν = 482 (vs, br) (AlCl) cm^{-1}.

[$AlBr_3(PMe_3)$]

To a yellow solution of $AlBr_3$ (0.175 g, 0.66 mmol) in toluene (3 mL) was added PMe_3 (0.050 g, 0.66 mmol) in toluene (3 mL). The resulting colourless solution was stirred for 1.5 h, then the solvent was removed *in vacuo* to yield a white powder, which was dried *in vacuo*. Yield: 0.186 g (83%). Anal. Calc. for $C_3H_9AlBr_3P$: C, 10.5; H, 2.6. Found: C, 10.6; H, 2.6%. ^{1}H NMR (CD_2Cl_2, 295 K): δ = 1.39 (d, $^2J_{HP}$ = 9.6 Hz, CH_3). $^{31}P\{^1H\}$ NMR (toluene/d^8 toluene, 295 K): δ = –40.9 (sextet $^1J_{AlP}$ = 242 Hz); (CH_2Cl_2/CD_2Cl_2, 193 K): δ = –37.1 (sextet, $^1J_{PAl}$ = 259 Hz). ^{27}Al NMR (toluene/d^8 toluene, 295 K): δ = 101.5 (d $^1J_{AlP}$ = 242 Hz); (CH_2Cl_2/CD_2Cl_2, 193 K): δ = 102.7 (d, $^1J_{AlP}$ = 258 Hz). IR (Nujol): ν = 414 (m), 393 (s) (AlBr) cm^{-1}.

[$AlI_3(PMe_3)$]

To a solution of AlI_3 (0.282 g, 0.69 mmol) in toluene (5 mL) was added PMe_3 (0.053 g, 0.69 mmol) in toluene (3 mL). The resulting colourless solution was stirred for 1 h, then the solvent was removed *in vacuo* to yield a white powder, which was dried *in vacuo*. Yield: 0.264 g (78%). Anal. Calc. for $C_3H_9AlI_3P$: C, 7.4; H, 1.9. Found: C, 7.5; H, 2.0%. ^{1}H NMR (CD_2Cl_2, 295 K): δ = 1.45 (d, $^2J_{HP}$ = 10.0 Hz, CH_3). $^{31}P\{^1H\}$ NMR (CH_2Cl_2/CD_2Cl_2, 295 K): δ = –42.8 (br s); (193 K): –40.8 (sextet, $^1J_{PAl}$ = 205 Hz). ^{27}Al NMR (CH_2Cl_2/CD_2Cl_2, 295 K): δ = 50.2 (br s); (193 K): 52.6 (d, $^1J_{AlP}$ = 209 Hz). IR (Nujol): ν = 367 (s), 340 (s) (AlI) cm^{-1}.

***Trans*-[$AlCl_3(PMe_3)_2$]**

To a suspension of $AlCl_3$ (0.133 g, 1.00 mmol) in CH_2Cl_2 (5 mL) was added PMe_3 (0.154 g, 2.02 mmol) in CH_2Cl_2 (5 mL). The resulting solution was stirred for 1.5 h, then the solvent was removed *in vacuo* and the resulting white solid was washed with hexane (6 mL). The hexane was decanted off and the white powder was dried *in vacuo*. Yield: 0.191 g (67%). Small colourless crystals suitable for single crystal X-ray diffraction study were grown from a concentrated CH_2Cl_2 reaction solution kept at –18°C. ^{1}H NMR (CD_2Cl_2, 295 K): δ = 1.28 (d, $^2J_{HP}$ = 8.0 Hz, CH_3). $^{31}P\{^1H\}$ NMR (CH_2Cl_2/CD_2Cl_2, 295 K): δ = –37.9 (s); (253 K): –38.6 (br s); (183 K): –39.7 (broad, ill-defined coupling). ^{27}Al NMR (CH_2Cl_2/CD_2Cl_2, 295 K): δ = 66.0 (s); (253 K): 61.3 (s). IR (Nujol): ν = 488 (vs, br) (AlCl) cm^{-1}.

***Trans*-[$AlBr_3(PMe_3)_2$]**

To a yellow solution of $AlBr_3$ (0.173 g, 0.65 mmol) in toluene (2 mL) was added PMe_3 (0.100 g, 1.31 mmol) in toluene (3 mL) which immediately led to the solution turning colourless, with formation of a large amount of white precipitate. The reaction was stirred for 45 min., then the solvent volume was reduced to about 1 mL *in vacuo*. A white powder was isolated by filtration and dried *in vacuo* for 15 min. Yield: 0.182 g (66%). Anal. Calc. for $C_6H_{18}AlBr_3P_2$: C, 17.2; H, 4.3. Found: C, 17.1; H, 4.4%. ^{1}H NMR (CD_2Cl_2, 295 K): δ = 1.25 (d, $^2J_{HP}$ = 7.0 Hz, CH_3). $^{31}P\{^1H\}$ NMR (CH_2Cl_2/CD_2Cl_2, 295 K): δ = –37.4 (br s); (223 K): –32.6 (br s); (193 K): –30.3 (s). ^{27}Al NMR (CH_2Cl_2/CD_2Cl_2, 295 K): δ = 44.5 (br s); (193 K): no resonance. IR (Nujol): ν = 373 (s) (AlBr) cm^{-1}.

***Trans*-[$AlI_3(PMe_3)_2$]**

To a solution of AlI_3 (0.135 g, 0.33 mmol) in toluene (5 mL) was added PMe_3 (0.050 g, 0.66 mmol) in toluene (5 mL), which immediately caused the precipitation of a white solid. The reaction was stirred for 1 h, then the solvent volume was reduced to about 1 mL *in vacuo*. A white powder was isolated by filtration and dried *in vacuo* for 15 min. Yield: 0.090 g (49%). Anal. Calc. for $C_6H_{18}AlI_3P_2$: C, 12.9; H, 3.2. Found: C, 12.8; H, 3.3%. ^{1}H NMR (CD_2Cl_2, 295 K): δ = 1.33 (d, $^2J_{HP}$ = 9.2 Hz, CH_3). $^{31}P\{^1H\}$ NMR (CH_2Cl_2/CD_2Cl_2, 295 K): δ = –31.6 (br s); (223 K): –28.1 (br s); (193 K): –27.2 (s). ^{27}Al NMR (CH_2Cl_2/CD_2Cl_2, 295 K): δ = 4.4 (br s); (193 K): no resonance. IR (Nujol): ν = 324 (s) (AlI) cm^{-1}.

***Trans*-[$AlCl_2\{o\text{-}C_6H_4(PMe_2)_2\}_2$][$AlCl_4$]**

To a suspension of $AlCl_3$ (0.067 g, 0.51 mmol) in CH_2Cl_2 (5 mL) was added *o*-$C_6H_4(PMe_2)_2$ (0.100 g, 0.51 mmol) in CH_2Cl_2 (5 mL) to form a colourless solution, which was allowed to stir for 1.5 h. The solvent volume was reduced to about 3 mL *in vacuo*. The resulting white precipitate was isolated by filtration and dried *in vacuo* to give a white powder. Yield: 0.071 g (43%). Small colourless blocks suitable for single crystal X-ray diffraction study were grown from a CH_2Cl_2 solution containing $AlCl_3$ and *o*-$C_6H_4(PMe_2)_2$ in a 2:1 mol. ratio kept at –18 °C. Anal. Calc. for $C_{20}H_{32}Al_2Cl_6P_4$: C, 36.2; H, 4.9. Found: C, 36.0; H, 4.8%. ^{1}H NMR (CD_2Cl_2, 295 K): δ = 1.74 (s, [24H], CH_3), 7.67-

7.77 (m, [8H], C_6H_4). $^{31}P\{^1H\}$ NMR (CH_2Cl_2/CD_2Cl_2, 295 K): δ = –42.8 (sextet, $^1J_{PAl}$ = 155 Hz); (253 K): –42.6 (sextet). ^{27}Al NMR (CH_2Cl_2/CD_2Cl_2, 295 K): δ = 103.3 (s, $[AlCl_4]^-$), 0.7 (quintet, $^1J_{AlP}$ = 164 Hz); (253 K): 103.4 (s), 0.4 (quintet). IR (Nujol): ν = 488 (vs) ($[AlCl_4]^-$), 410 (s) (AlCl) cm^{-1}.

***Trans*-[$AlBr_2${*o*-$C_6H_4(PMe_2)_2$}$_2$][$AlBr_4$]**

$AlBr_3$ (0.135 g, 0.51 mmol) was dissolved in toluene (5 mL) to form a yellow solution. To this was added *o*-$C_6H_4(PMe_2)_2$ (0.100 g, 0.51 mmol) in toluene (5 mL) which immediately led to the solution turning colourless, with evidence of a large amount of white precipitate. The reaction was stirred for 2 h, then the white powder was isolated by filtration and dried *in vacuo*. Yield: 0.213 g (91%). Anal. Calc. for $C_{20}H_{32}Al_2Br_6P_4$: C, 25.8; H, 3.5. Found: C, 26.0; H, 3.3%. ^1H NMR (CD_2Cl_2, 295 K): δ = 1.80 (s, [24H], CH_3), 7.71-7.78 (m, [8H], C_6H_4). $^{31}P\{^1H\}$ NMR (CH_2Cl_2/CD_2Cl_2, 295 K): δ = –42.6 (br s); (223 K): –42.6 (br s). ^{27}Al NMR (CH_2Cl_2/CD_2Cl_2, 295 K): δ = 80.5 (s, $[AlBr_4]^-$), –12.0 (br s); (253 K): 80.5 (s), –11.4 (br s). IR (Nujol): ν = 398 (vs) ($[AlBr_4]^-$), 326 (m) (AlBr) cm^{-1}.

***Trans*-[AlI_2{*o*-$C_6H_4(PMe_2)_2$}$_2$][AlI_4]**

AlI_3 (0.166 g, 0.41 mmol) was dissolved in toluene (5 mL) to form a pale yellow solution. To this was added *o*-$C_6H_4(PMe_2)_2$ (0.080 g, 0.41 mmol) in toluene (5 mL) which caused the immediate precipitation of a white solid. The reaction was stirred for 2 h, then the white powder was isolated by filtration and dried *in vacuo*. Yield: 0.231 g (94%). Anal. Calc. for $C_{20}H_{32}Al_2I_6P_4$: C, 19.8; H, 2.7. Found: C, 20.0; H, 2.8%. ^1H NMR (CD_2Cl_2, 295 K): δ = 1.90 (s, [24H], CH_3), 7.79-7.89 (m, [8H], C_6H_4). $^{31}P\{^1H\}$ NMR (CH_2Cl_2/CD_2Cl_2, 295 K): δ = –42.3 (br s); (223 K): –42.2 (br s). ^{27}Al NMR (CH_2Cl_2/CD_2Cl_2, 295 K): δ = –26.5 (s, $[AlI_4]^-$); (223 K): –23.9 (s). IR (Nujol): ν = 334 (vs) ($[AlI_4]^-$), 281 (m) (AlI) cm^{-1}.

[$AlCl_2${*o*-$C_6H_4(PPh_2)_2$}][$AlCl_4$]

To a solution of *o*-$C_6H_4(PPh_2)_2$ (0.075 g, 0.17 mmol) in CH_2Cl_2 (10 mL) was added $AlCl_3$ (0.045 g, 0.34 mmol). The resulting solution was stirred for 1.5 h, then the solvent volume was reduced to about 3 mL *in vacuo* and hexane (3 mL) was added. The resulting white precipitate was isolated by filtration and dried *in vacuo*. Yield = 0.035 g (29%). Anal. Calc.

for $C_{30}H_{24}Al_2Cl_6P_2$: C, 50.5; H, 3.4. Found: C, 50.5; H, 3.7%. ^{1}H NMR (CD_2Cl_2, 295 K): δ = 7.22-7.53 (aromatics). $^{31}P\{^1H\}$ NMR (CH_2Cl_2/CD_2Cl_2, 295 K): δ = –8.3 (br s); (183 K): –12.4 (br s). ^{27}Al NMR (CH_2Cl_2/CD_2Cl_2, 295 K): δ = 103.3 (s, $[AlCl_4]^-$); (183 K): 103.5 (s). IR (Nujol): ν = 483 (s, br) ($[AlCl_4]^-$) cm^{-1}. Some small crystals of $[AlCl_2\{o\text{-}C_6H_4(PPh_2)_2\}_2][AlCl_4]$ were obtained from a similar preparation by careful hexane layering.

***Trans*-[AlCl$_2${Me$_2$P(CH$_2$)$_2$Me$_2$}$_2$][AlCl$_4$]**

To a suspension of $AlCl_3$ (0.090 g, 0.67 mmol) in CH_2Cl_2 (5 mL) was added $Me_2P(CH_2)_2PMe_2$ (0.100 g, 0.67 mmol) in CH_2Cl_2 (5 mL). The resulting solution was stirred for 2 h, then the solvent volume was reduced to about 2 mL *in vacuo* and layered with hexane (2.5 mL), whereupon small colourless blocks suitable for single crystal X-ray diffraction study grew. The crystalline material was then isolated by filtration and dried *in vacuo* to give a white solid. Yield: 0.145 g (77%). Anal. Calc. for $C_{12}H_{32}Al_2Cl_6P_4$: C, 25.4; H, 5.7. Found: C, 25.2; H, 5.9%. ^{1}H NMR (CD_2Cl_2, 295 K): δ = 1.44 (br s, [24H], CH_3), 2.00 (br s, [8H], CH_2). $^{31}P\{^1H\}$ NMR (CD_2Cl_2, 295 K): δ = –40.6 (sextet, $^1J_{PAl}$ = 164 Hz). ^{27}Al NMR (CH_2Cl_2/CD_2Cl_2, 295 K): δ = 103.3 (s, $[AlCl_4]^-$), 1.2 (quintet, $^1J_{AlP}$ = 164 Hz). IR (Nujol): ν = 478 (vs, br) ($[AlCl_4]^-$), 377 (s) (AlCl) cm^{-1}.

***Trans*-[AlBr$_2${Me$_2$P(CH$_2$)$_2$Me$_2$}$_2$][AlBr$_4$]**

$AlBr_3$ (0.133 g, 0.50 mmol) was dissolved in toluene (5 mL) to form a yellow solution. To this was added $Me_2P(CH_2)_2PMe_2$ (0.075 g, 0.50 mmol) in toluene (5 mL) which caused the immediate precipitation of a white solid. The reaction was stirred for 1 h, then the white powder was isolated by filtration and dried *in vacuo*. Yield: 0.176 g (85%). Anal. Calc. for $C_{12}H_{32}Al_2Br_6P_4$: C, 17.3; H, 3.9. Found: C, 17.2; H, 3.9%. ^{1}H NMR (CD_2Cl_2, 295 K): δ = 1.52 (br s, [24H], CH_3), 2.04 (br s, [8H], CH_2). $^{31}P\{^1H\}$ NMR (CH_2Cl_2/CD_2Cl_2, 295 K): δ = –38.0 (br s); (193 K): –37.2 (s). ^{27}Al NMR (CH_2Cl_2/CD_2Cl_2, 295 K): δ = 80.4 (s, $[AlBr_4]^-$), –12.3 (br s); (193 K): 81.2 (s). IR (Nujol): ν = 394 (vs) ($[AlBr_4]^-$), 326 (m) (AlBr) cm^{-1}.

***Trans*-[AlI_2{$Me_2P(CH_2)_2Me_2$}$_2$][AlI_4]**

AlI_3 (0.204 g, 0.50 mmol) was dissolved in toluene (5 mL) to form a yellow solution. To this was added $Me_2P(CH_2)_2PMe_2$ (0.078 g, 0.51 mmol) in toluene (5 mL) which caused the immediate precipitation of a white solid. The reaction was stirred for 2 h, then the white powder was isolated by filtration and dried *in vacuo*. Yield: 0.270 g (97%). Anal. Calc. for $C_{12}H_{32}Al_2I_6P_4$: C, 12.9; H, 2.9. Found: C, 13.0; H, 3.0%. ^{1}H NMR (CD_2Cl_2, 295 K): δ = 1.63 (br s, [24H], CH_3), 2.09 (br s, [8H], CH_2). ^{31}P{^{1}H} NMR (CH_2Cl_2/CD_2Cl_2, 295 K): δ = –39.1 (br s); (203 K): –37.7 (br s). ^{27}Al NMR (CH_2Cl_2/CD_2Cl_2, 295 K): δ = –27.1 (s, $[AlI_4]^-$), –33.9 (br s); (203 K): –26.1 (s). IR (Nujol): ν = 337 (vs) ($[AlI_4]^-$), 285 (s) (AlI) cm^{-1}.

[$(AlCl_3)_2${*μ*-$Me_2P(CH_2)_2PMe_2$}]

To a suspension of $AlCl_3$ (0.178 g, 1.33 mmol) in CH_2Cl_2 (5 mL) was added $Me_2P(CH_2)_2PMe_2$ (0.099 g, 0.66 mmol) in CH_2Cl_2 (5 mL). The resulting solution was stirred for 1 h, then the solvent volume was reduced to about 4 mL *in vacuo* whereupon a white solid precipitated out. The solid was isolated by filtration and dried *in* vacuo. Yield: 0.055 g. The solid is a mixture of t*rans*-[$AlCl_2${$Me_2P(CH_2)_2Me_2$}$_2$][$AlCl_4$] and [$(AlCl_3)_2${*μ*-$Me_2P(CH_2)_2PMe_2$}]. Small colourless blocks suitable for single crystal X-ray diffraction study were grown from a CH_2Cl_2 solution containing $AlCl_3$ and $Me_2P(CH_2)_2PMe_2$ in a 1.5:1 mol. ratio kept at –18 °C. *Spectroscopic data obtained from the mixture*: ^{1}H NMR (CD_2Cl_2, 295 K): δ = 1.90 (m, [12H], CH_3), 2.17 (d, [4H], CH_2). ^{31}P{^{1}H} NMR (CH_2Cl_2/CD_2Cl_2, 295 K): δ = –31.6 (br s). ^{27}Al NMR (CH_2Cl_2/CD_2Cl_2, 295 K): δ = 109.3 (br s); (253 K): 108.9 (s).

[$(AlCl_3)_2${*μ*-$Cy_2P(CH_2)_2PCy_2$}]

To a suspension of $AlCl_3$ (0.063 g, 0.47 mmol) in CH_2Cl_2 (5 mL) was added a solution of $Cy_2P(CH_2)_2PCy_2$ (0.101 g, 0.24 mmol) in CH_2Cl_2 (5 mL). The resulting solution was stirred for 1 h, then the solvent volume was reduced to about 3 mL *in vacuo*. Small colourless blocks suitable for single crystal X-ray diffraction study grew upon cooling the solution to –18 °C. Anal. Calc. for $C_{26}H_{48}Al_2Cl_6P_2$: C, 45.3; H, 7.0. Found: C, 45.1; H, 7.0%. ^{1}H NMR (CD_2Cl_2, 295 K): δ = 1.32-1.89 (m, [44H], C_6H_{11}), 2.53 (m, [4H], CH_2). ^{31}P{^{1}H} NMR (CH_2Cl_2/CD_2Cl_2, 295 K): δ = –0.5 (s); (213 K): –1.4 (br s). ^{27}Al NMR (CH_2Cl_2/CD_2Cl_2,

295 K): δ = 110.6 (s); (213 K): 111.3 (s). IR (Nujol): ν = 478 (vs, br), 375 (w, br) (AlCl) cm^{-1}.

$[AlI_3(AsR_3)]$ (R = Et or Ph)

The two $[AlI_3(AsR_3)]$ (R = Et or Ph)[10] were made by reaction of a 1:1 mol. ratio of AlI_3 and AsR_3 in toluene. **$[AlI_3(AsPh_3)]$**: ^{27}Al NMR (toluene/d^8 toluene, 295 K): δ = 33.1 (br s); (203 K): no resonance; **$[AlI_3(AsEt_3)]$:** ^{27}Al NMR (toluene/d^8 toluene, 295 K): δ = 31.9 (s); (243 K): 32.4 (s); (203 K): 31.4 (br s).

$[AlCl_2\{o\text{-}C_6H_4(AsMe_2)_2\}][AlCl_4]$

To a suspension of $AlCl_3$ (0.093 g, 0.70 mmol) in toluene (5 mL) was added *o*-$C_6H_4(AsMe_2)_2$ (0.101 g, 0.35 mmol) in toluene (5 mL), resulting in a colourless solution with a white solid suspended in it. After the reaction was stirred for 1.5 h the solid was isolated by filtration, washed with hexane and dried *in vacuo* to give a sticky white solid. Anal. Calc. for $C_{10}H_{16}Al_2As_2Cl_6$: C, 21.7; H, 2.9. Found: C, 21.6; H, 3.1%. ^{1}H NMR (CD_2Cl_2, 295 K): δ = 1.76 (s, [12H], CH_3), 7.62-7.70 (m, [4H], C_6H_4). ^{27}Al NMR (CH_2Cl_2/CD_2Cl_2, 295 K): δ = 103.2 (s, $[AlCl_4]^-$); (203 K): 103.2 (s). IR (Nujol): ν = 490 (s, br) ($[AlCl_4]^-$) cm^{-1}.

[*o*-$C_6H_4(AsMe_2)_2(CH_2)][AlCl_4]_2$

To a suspension of $AlCl_3$ (0.094 g, 0.70 mmol) in CH_2Cl_2 (5 mL) was added *o*-$C_6H_4(AsMe_2)_2$ (0.100 g, 0.35 mmol) in CH_2Cl_2 (5 mL). Initially a colourless solution formed, with a white solid precipitating out after 15 min. stirring. The reaction was stirred for 2.5 h and then allowed to sit overnight, whereupon small colourless crystals suitable for single crystal X-ray diffraction study grew. Over the period of a week the white precipitate slowly redissolved and more colourless crystals grew, which were isolated and dried *in vacuo* to give a white powder. Yield: 0.052 g (23%). Anal. Calc. for $C_{11}H_{18}Al_2As_2Cl_8$: C, 20.7; H, 2.8. Found: C, 20.6; H, 2.7%. ESI+ (CH_3CN): *m/z* 191.2 $[M + CH_3CN]^{2+}$. ^{1}H NMR (CD_3CN, 295 K): δ = 2.43 (s, [12H], CH_3), 3.43 (s, [2H], CH_2), 8.02−8.15 (m, [4H], C_6H_4). ^{27}Al NMR (CH_3CN/CD_3CN, 295 K): δ = 103.5 (s, $[AlCl_4]^-$). IR (Nujol): ν = 478 (vs, br, $[AlCl_4]^-$) cm^{-1}.

Reaction of $AlF_3.3H_2O$ with $OPPh_3$

$AlF_3.3H_2O$ (0.061 g, 0.44 mmol) was suspended in distilled water (7 mL) and $OPPh_3$ (0.362 g, 1.30 mmol) was added. The suspension was transferred into a Teflon container and loaded into a stainless steel high pressure vessel and heated to 180 °C for 20 h. The vessel was then allowed to cool. The colourless solution was filtered to remove a white solid. IR (Nujol): ν = 1185 (s) (PO), 664 (m), 353 (s, br) (AlF) cm^{-1}. After an aliquot was separated and retained to grow crystals the solvent was then removed *in vacuo* to yield a small amount of white solid. IR (Nujol): ν = 1188 (m) (PO), 664 (vs, br), 345 (s, br) (AlF) cm^{-1}. Slow evaporation of the reaction solvent gave small colourless block crystals suitable for X-ray diffraction; the unit cell was found to match that of $Ph_3PO{\cdot}0.5H_2O$.[48]

Reaction of $[AlCl_3(PMe_3)]$ with $[NMe_4]F$

To a solution of $[AlCl_3(PMe_3)]$ (0.020 g, 0.10 mmol) in CD_2Cl_2 (5 mL) was added dried $[NMe_4]F$ (0.027 g, 0.29 mmol) which immediately led to the precipitation of a white solid. After the reaction was stirred overnight the solid was isolated by filtration and dried *in vacuo*. IR (Nujol): ν = 1491 (vs), 1405 (m), 950 (vs) ($[NMe_4]Cl$), 667 (m) (AlF) cm^{-1}. *Spectroscopic data obtained from the colourless filtrate*: $^{31}P\{^1H\}$ NMR (CD_2Cl_2, 295 K): δ = –58.6 (s); (203 K): –58.2 (s). ^{19}F NMR (CD_2Cl_2, 295 K): no resonance. ^{27}Al NMR (CD_2Cl_2, 295 K): no resonance.

Reaction of $[AlCl_3(PMe_3)]$ with Me_3SnF

To a solution of $[AlCl_3(PMe_3)]$ (0.020 g, 0.10 mmol) in CD_2Cl_2 (5 mL) was added dried Me_3SnF (0.052 g, 0.29 mmol). Initially the Me_3SnF was suspended in the solution but it appeared to react over time, with a purple-coloured solid forming. After the reaction was stirred overnight the solid was removed by filtration. *Spectroscopic data obtained from the colourless filtrate*: ^1H NMR (CD_2Cl_2, 295 K): 0.66 (s, $^2J_{HSn}$ = 60.8 Hz, CH_3). $^{31}P\{^1H\}$ NMR (CD_2Cl_2, 295 K): δ = –1.3 (s); (203 K): –0.1 (s). ^{19}F NMR (CD_2Cl_2, 295 K): no resonance. ^{27}Al NMR (CD_2Cl_2, 295 K): no resonance.

2.5 Appendix 1 – X-Ray Crystallographic Data

Compound	$[AlCl_3(OAsPh_3)]\cdot 0.5\,CH_2Cl_2$	$[AlCl_3(PMe_3)]$	$[AlCl_3(PMe_3)_2]$
Formula	$C_{18.5}H_{16}AlAsCl_4O$	$C_3H_9AlCl_3P$	$C_6H_{18}AlCl_3P_2$
M	498.01	209.40	285.47
Crystal system	triclinic	monoclinic	orthorhombic
Space group (no.)	*P*-1 (2)	$P2_1/m$ (11)	*Pnma* (62)
a /Å	9.3430(18)	6.414(3)	9.970(3)
b /Å	13.727(3)	10.292(4)	10.599(4)
c /Å	16.894(3)	7.649(4)	13.562(4)
α /°	99.220(3)	90	90
β /°	90.170(4)	113.698(12)	90
γ /°	97.248(4)	90	90
U /Å^3	2121.1(7)	462.4(4)	1433.1(8)
Z	4	2	4
μ(Mo-K$_\alpha$) /mm^{-1}	2.153	1.174	0.883
F(000)	996	212	592
Total no. reflns	19433	4220	14433
R_{int}	0.050	0.056	0.140
Unique reflns	9548	1113	1486
No. of params, restraints	469, 0	44, 9	66, 0
R_1, wR_2 [$I > 2\sigma(I)$][a]	0.084, 0.217	0.052, 0.124	0.065, 0.087
R_1, wR_2 (all data)	0.112, 0.235	0.055, 0.125	0.088, 0.091

Common items: T = 100 K; wavelength (Mo-Kα) = 0.71073 Å; θ(max) = 27.5°.

[a] $R_1 = \Sigma||F_o| - |F_c|| / \Sigma|F_o|$; $wR_2 = [\Sigma w(F_o^2 - F_c^2)^2 / \Sigma w F_o^4]^{1/2}$.

Compound	$[AlCl_2\{o\text{-}C_6H_4(PMe_2)_2\}_2][AlCl_4]$	$[AlCl_2\{o\text{-}C_6H_4(PPh_2)_2\}_2][AlCl_4]$	$[AlCl_2\{Me_2P(CH_2)_2\text{-}PMe_2\}_2][AlCl_4]$
Formula	$C_{20}H_{32}Al_2Cl_6P_4$	$C_{60}H_{48}Al_2Cl_6P_4$	$C_{12}H_{32}Al_2Cl_6P_4$
M	663.00	1159.52	566.92
Crystal system	monoclinic	triclinic	orthorhombic
Space group (no.)	*C*2/*c* (15)	*P*-1 (2)	*Pbca* (61)
a /Å	13.278(4)	10.024(3)	19.631(5)
b /Å	14.545(4)	11.752(4)	16.157(4)
c /Å	16.554(5)	24.434(8)	34.831(8)
α /°	90	81.926(14)	90
β /°	104.126(6)	85.52(2)	90
γ /°	90	82.25(2)	90
U /Å^3	3100.2(16)	2818.9(16)	11048(5)
Z	4	2	16
μ(Mo-K$_\alpha$) /mm^{-1}	0.828	0.489	0.916
F(000)	1360	1192	4672
Total no. reflns	14366	24430	92232
R_{int}	0.032	0.076	0.117
Unique reflns	3544	12194	10858
No. of params, restraints	151, 0	652, 0	449, 0
R_1, wR_2 [$I > 2\sigma(I)$][a]	0.030, 0.065	0.079, 0.159	0.050, 0.099
R_1, wR_2 (all data)	0.035, 0.067	0.135, 0.193	0.087, 0.115

Common items: T = 100 K; wavelength (Mo-Kα) = 0.71073 Å; θ(max) = 27.5°.

[a] $R_1 = \Sigma||F_o| - |F_c|| / \Sigma|F_o|$; $wR_2 = [\Sigma w(F_o^2 - F_c^2)^2 / \Sigma wF_o^4]^{1/2}$.

Compound	$[(AlCl_3)_2\{\mu\text{-}Me_2P(CH_2)_2PMe_2\}]$	$[(AlCl_3)_2\{\mu\text{-}Cy_2P(CH_2)_2PCy_2\}]$	$[Cy_2HP(CH_2)_2PHCy_2][AlCl_4]_2$
Formula	$C_6H_{16}Al_2Cl_6P_2$	$C_{26}H_{48}Al_2Cl_6P_2$	$C_{26}H_{50}Al_2Cl_8P_2$
M	416.79	689.24	762.16
Crystal system	monoclinic	triclinic	monoclinic
Space group (no.)	$P2_1/c$ (14)	P-1 (2)	$P2_1/c$ (14)
a /Å	10.738(6)	8.251(2)	7.073(6)
b /Å	7.948(4)	9.830(2)	17.551(13)
c /Å	11.772(6)	11.921(3)	14.924(13)
α /°	90	113.905(8)	90
β /°	113.938(9)	91.329(6)	101.682(15)
γ /°	90	103.390(7)	90
U /Å^3	918.2(8)	852.4(4)	1814(3)
Z	2	1	2
μ(Mo-K$_\alpha$) /mm^{-1}	1.182	0.666	0.775
F(000)	420	362	796
Total no. reflns	10169	8428	10205
R_{int}	0.062	0.114	0.074
Unique reflns	2093	3884	3545
No. of params, restraints	73, 0	163, 0	175, 0
R_1, wR_2 [$I > 2\sigma(I)$][a]	0.051, 0.076	0.086, 0.175	0.088, 0.166
R_1, wR_2 (all data)	0.065, 0.081	0.174, 0.228	0.115, 0.179

Common items: T = 100 K; wavelength (Mo-Kα) = 0.71073 Å; θ(max) = 27.5°.

[a] $R_1 = \Sigma||F_o| - |F_c|| / \Sigma|F_o|$; $wR_2 = [\Sigma w(F_o^2 - F_c^2)^2 / \Sigma wF_o^4]^{1/2}$.

Compound	[*o*-$C_6H_4(PMe_2)$-$(PHMe_2)]_2[AlCl_4]$[Cl]	[*o*-$C_6H_4(PMe_2)$-$(PHMe_2)]_2[AlBr_4]$[Br]	[*o*-$C_6H_4(AsMe_2)_2$-$(CH_2)][AlCl_4]_2$
Formula	$C_{20}H_{34}AlCl_5P_4$	$C_{20}H_{34}AlBr_5P_4$	$C_{11}H_{18}Al_2As_2Cl_8$
M	602.58	824.88	637.65
Crystal system	monoclinic	monoclinic	orthorhombic
Space group (no.)	*C*2/*c* (15)	*C*2/*c* (15)	*Pna*21 (33)
a /Å	14.599(5)	14.834(7)	14.7537(10)
b /Å	20.672(7)	21.144(8)	14.9361(10)
c /Å	11.006(5)	11.274(5)	10.9633(8)
α /°	90	90	90
β /°	115.061(5)	115.646(6)	90
γ /°	90	90	90
U /Å^3	3009(2)	3188(2)	2415.9(3)
Z	4	4	4
μ(Mo-K$_\alpha$) /mm^{-1}	0.733	6.540	3.719
F(000)	1248	1608	1248
Total no. reflns	18200	13640	19941
R_{int}	0.093	0.031	0.049
Unique reflns	3461	3631	4813
No. of params, restraints	146, 0	146, 0	213, 1
R_1, wR_2 [$I > 2\sigma(I)$][b]	0.064, 0.104	0.032, 0.053	0.041, 0.095
R_1, wR_2 (all data)	0.086, 0.111	0.038, 0.055	0.050, 0.100

[a] Common items: T = 100 K; wavelength (Mo-Kα) = 0.71073 Å; θ(max) = 27.5°.

[b] $R_1 = \Sigma||F_o| - |F_c|| / \Sigma|F_o|$; $wR_2 = [\Sigma w(F_o^2 - F_c^2)^2 / \Sigma wF_o^4]^{1/2}$.

2.6 Appendix 2 – Analysis of M–X Bond Lengths in $[MX_4]^-$ (M = Al, Ga, In)

Data were taken from the Cambridge Structural Database (CSD version 5.34; latest update = May 2013) on the 21st January 2014.[43] The data were analysed in Legacy Vista (version 2.1).[54] The REFcodes used all contained discrete $[MX_4]^-$ molecules; those containing bonds to other atoms and structures containing any disorder were omitted.

The purpose of this study was to establish whether steric effects (i.e. the size of M) could account for the differences in preferred coordination geometries observed for MX_3 (M = Al, Ga, In; X = Cl, Br, I). The study is topical and follows on from recently published work[4] that compares the solid state structures of simple MX_3 complexes (M = Al, Ga) with the Lewis acidity trends of MX_3. Like Timoshkin *et al.*[4] who found that the donor-acceptor bond length can be affected by solid state effects such as intermolecular hydrogen bonding, the M–X bond lengths for a given $[MX_4]^-$ in the present study vary by up to 0.22 Å, which is presumably caused by some combination of solid state effects, anion-cation interactions and experimental error. This highlights that there is no simple, single effect that explains the trends observed.

It is important to note that there are limitations to this study; there are considerably fewer X-ray crystal structures for $[InCl_4]^-$ and $[InBr_4]^-$ than for the corresponding lighter Group 13 trihalides, and also fewer structures containing $[MI_4]^-$ compared to $[MBr_4]^-$, while there are over one hundred more structures containing $[MCl_4]^-$ (M = Al, Ga).

Table A1 Summary of the Al–X bond length distribution in $[AlX_4]^-$ (X = Cl, Br, I)

$[AlX_4]^-$	Data Points (REFcodes)	Al–X Length Range / Å	Mean Al–X Length / Å
X = Cl	915 (184)	2.055-2.216	2.126 ± 0.018
X = Br	64 (13)	2.244-2.320	2.289 ± 0.015
X = I	12 (3)	2.506-2.555	2.527 ± 0.012

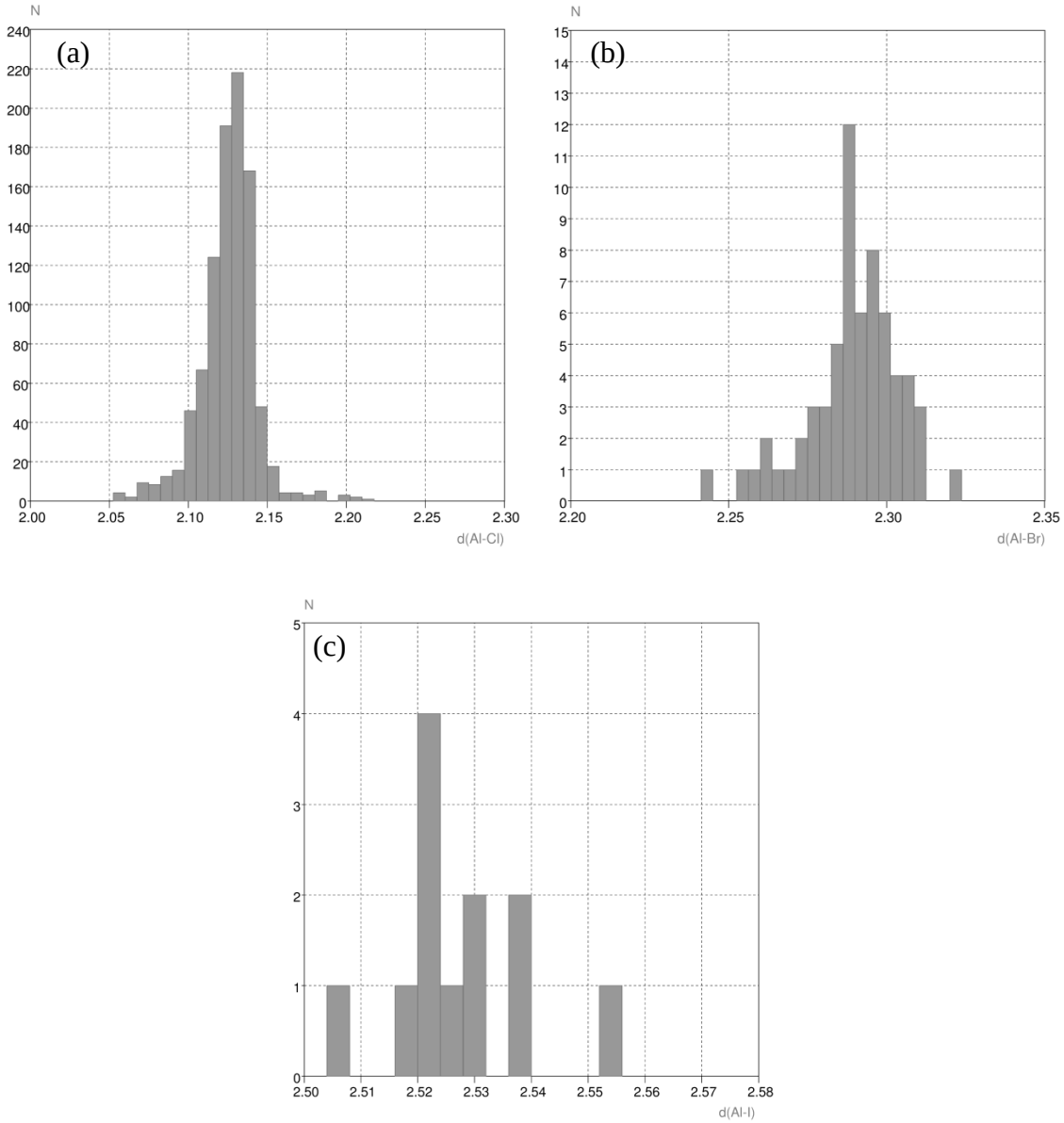

Figure A1 The Al–X bond distribution in (a) $[AlCl_4]^-$, (b) $[AlBr_4]^-$ and (c) $[AlI_4]^-$.

Table A2 Summary of the Ga–X bond length distribution in $[GaX_4]^-$ (X = Cl, Br, I)

$[GaX_4]^-$	Data Points (REFcodes)	Ga–X Length Range / Å	Mean Ga–X Length / Å
X = Cl	705 (157)	2.036-2.258	2.166 ± 0.018
X = Br	91 (27)	2.277-2.361	2.321 ± 0.016
X = I	31 (8)	2.506-2.586	2.544 ± 0.018

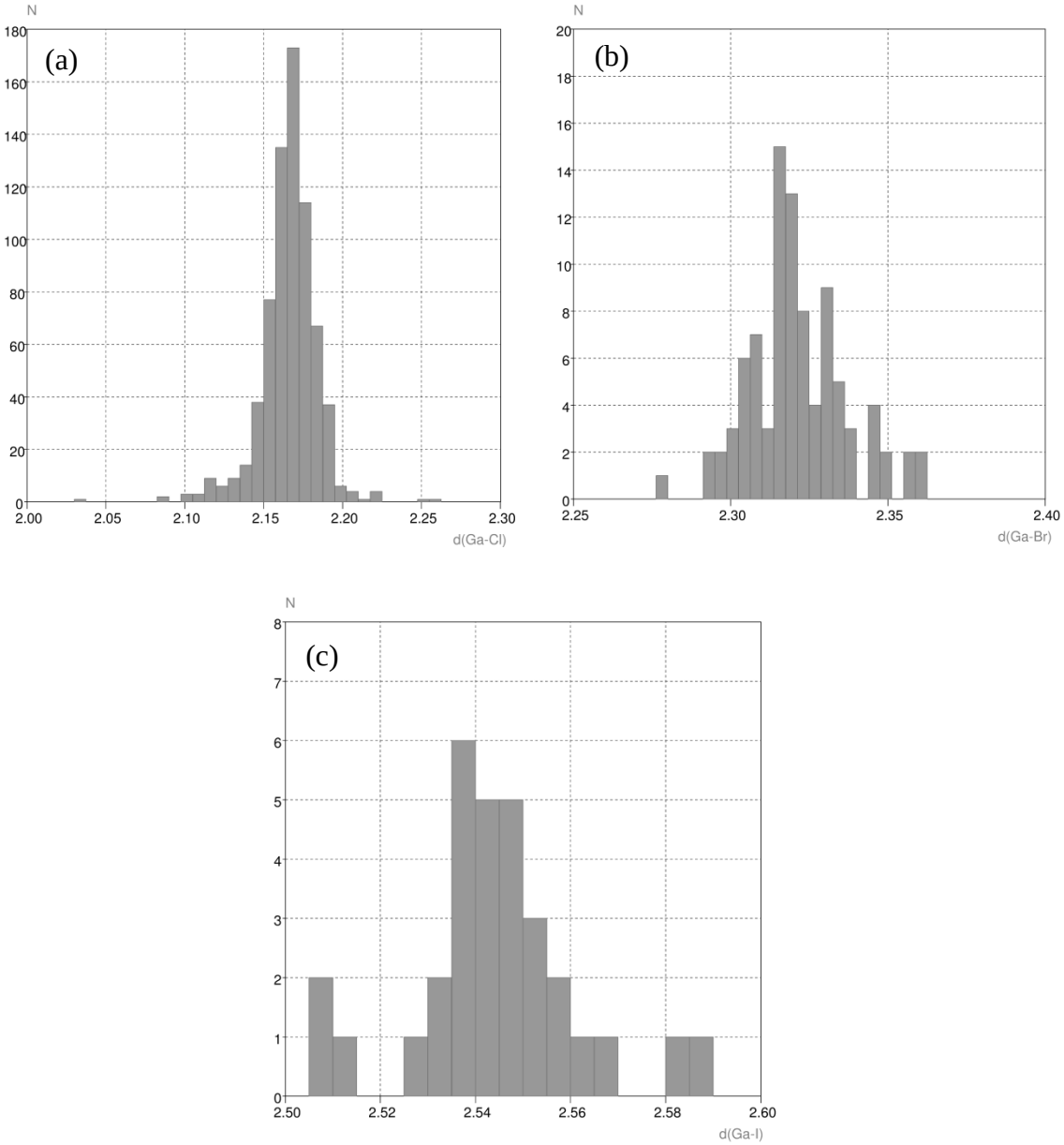

Figure A2 The Ga–X bond distribution in (a) $[GaCl_4]^-$, (b) $[GaBr_4]^-$ and (c) $[GaI_4]^-$.

Table A3 Summary of the In–X bond length distribution in $[InX_4]^-$ (X = Cl, Br, I)

$[InX_4]^-$	Data Points (REFcodes)	In–X Length Range / Å	Mean In–X Length / Å
X = Cl	26 (7)	2.295-2.368	2.337 ± 0.022
X = Br	50 (11)	2.438-2.510	2.484 ± 0.018
X = I	35 (8)	2.663-2.731	2.702 ± 0.014

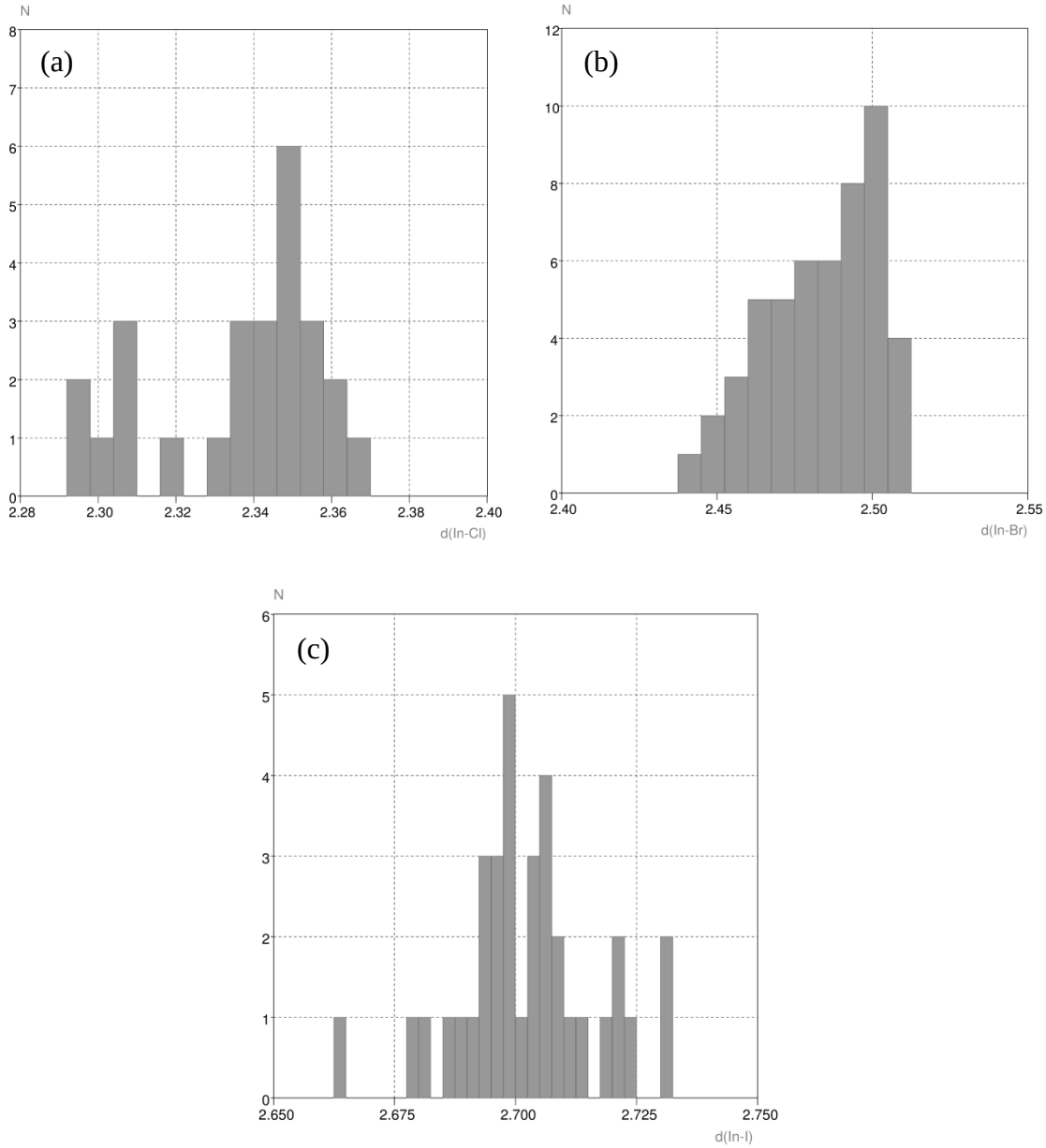

Figure A3 The In–X bond distribution in (a) $[InCl_4]^-$, (b) $[InBr_4]^-$ and (c) $[InI_4]^-$.

2.7 References

1. J. Burt, W. Levason and G. Reid, *Coord. Chem. Rev.*, 2014, **260**, 65-115.
2. S. Aldridge and A. J. Downs, eds., *The Group 13 Metals Aluminium, Gallium, Indium and Thallium: Chemical Patterns and Peculiarities*, John Wiley and Sons, UK, 2011.
3. A. J. Downs, ed., *Chemistry of Aluminium, Gallium, Indium and Thallium*, Blackie, London, 1993.
4. A. Y. Timoshkin, M. Bodensteiner, T. N. Sevastianova, A. S. Lisovenko, E. I. Davydova, M. Scheer, C. Graßl and A. V. Butlak, *Inorg. Chem.*, 2012, **51**, 11602-11611.
5. S. E. Rasmussen and N. C. Broch, *Chem. Commun. (London)*, 1965, 289b-290.
6. M. Rueping and B. J. Nachtsheim, *Beilstein J. Org. Chem.*, 2010, **6**, 1-24.
7. P. Laverman, W. J. McBride, R. M. Sharkey, A. Eek, L. Joosten, W. J. G. Oyen, D. M. Goldenberg and O. C. Boerman, *J. Nucl. Med.*, 2010, **51**, 454-461.
8. W. J. McBride, C. A. D'Souza, R. M. Sharkey, H. Karacay, E. A. Rossi, C.-H. Chang and D. M. Goldenberg, *Bioconjugate Chem.*, 2010, **21**, 1331-1340.
9. O. S. Joo, K. D. Jung, S. H. Cho, J. H. Kyoung, C. K. Ahn, S. C. Choi, Y. Dong, H. Yun and S. H. Han, *Chem. Vap. Deposition*, 2002, **8**, 273-276.
10. E. Conrad, J. Pickup, N. Burford, R. McDonald and M. J. Ferguson, *Can. J. Chem.*, 2010, **88**, 797-803.
11. R. L. Wells, A. T. McPhail, J. A. Laske and P. S. White, *Polyhedron*, 1994, **13**, 2737-2744.
12. R. L. Wells, C. G. Pitt, A. T. McPhail, A. P. Purdy, S. Shafieezad and R. B. Hallock., *Mater. Res. Soc. Symp. Proc.*, 1988, **131**, 45-50.
13. G. Ménard and D. W. Stephan, *J. Am. Chem. Soc.*, 2010, **132**, 1796-1797.
14. F. Dornhaus, S. Scholz, I. Sänger, M. Bolte, M. Wagner and H.-W. Lerner, *Z. Anorg. Allg. Chem.*, 2009, **635**, 2263-2272.
15. A. Ecker and H. Schnöckel, *Z. Anorg. Allg. Chem.*, 1998, **624**, 813-816.
16. A. Ecker, E. Baum, M. A. Friesen, M. A. Junker, C. Üffing, R. Köppe and H. Schnöckel, *Z. Anorg. Allg. Chem.*, 1998, **624**, 513-516.
17. K. Nakamoto, *Infrared and Raman Spectra of Inorganic and Coordination Compounds*, Wiley-Interscience, NY, 4 edn., 1986.
18. N. Burford, B. W. Royan, R. E. v. H. Spence, T. S. Cameron, A. Linden and R. D. Rogers, *J. Chem. Soc., Dalton Trans.*, 1990, 1521-1528.
19. S. A. Sangokoya, B. Lee, M. F. Self, W. T. Pennington and G. H. Robinson, *Polyhedron*, 1989, **8**, 1497-1502.

20. S. M. Godfrey, D. G. Kelly and C. A. McAuliffe, *J. Chem. Soc., Dalton Trans.*, 1992, 1305-1310.

21. R. T. Tjahjanto, M. F. Peintinger, T. Bredow and J. Beck, *Eur. J. Inorg. Chem.*, 2012, **2012**, 3625-3635.

22. M. Shao, X. Jin, Y. Tang, Q. Huang and Y. Huang, *Tetrahedron Lett.*, 1982, **23**, 5343-5346.

23. M. Nieger, G. Trommeschlager and B. Ross, *CCDC 233886: Private Communication to the Cambridge Structural Database*, 2004.

24. F. Cheng, M. F. Davis, A. L. Hector, W. Levason, G. Reid, M. Webster and W. Zhang, *Eur. J. Inorg. Chem.*, 2007, **2007**, 2488-2495.

25. W. H. N. Vriezen and F. Jellinek, *Chem. Phys. Lett.*, 1967, **1**, 284.

26. J. C. Carter, G. Jugie, R. Enjalbert and J. Galy, *Inorg. Chem.*, 1978, **17**, 1248-1254.

27. I. A. Degnan, N. W. Alcock, S. M. Roe and M. G. H. Wallbridge, *Acta Crystallogr. Sect. C: Cryst. Struct. Commun.*, 1992, **48**, 995-999.

28. I. R. Beattie and G. A. Ozin, *J. Chem. Soc. A*, 1968, 2373-2377.

29. F. Cheng, A. L. Hector, W. Levason, G. Reid, M. Webster and W. Zhang, *Inorg. Chem.*, 2007, **46**, 7215-7223.

30. J. Mason, ed., *Multinuclear NMR*, Plenum Press, NY, 1987.

31. F. Chen, G. Ma, G. M. Bernard, R. E. Wasylishen, R. G. Cavell, R. McDonald and M. J. Ferguson, *Chem. Eur. J.*, 2013, **19**, 2826-2838.

32. M. Sigl, A. Schier and H. Schmidbaur, *Eur. J. Inorg. Chem.*, 1998, **1998**, 203-210.

33. F. Cheng, A. L. Hector, W. Levason, G. Reid, M. Webster and W. Zhang, *Inorg. Chem.*, 2010, **49**, 752-760.

34. C. Gurnani, A. L. Hector, E. Jager, W. Levason, D. Pugh and G. Reid, *Dalton Trans.*, 2013, **42**, 8364-8374.

35. K. George, M. Jura, W. Levason, M. E. Light and G. Reid, *Dalton Trans.*, 2014, **43**, 3637-3648.

36. H. R. Hudson, in *The Chemistry of Organophosphorus Compounds*, ed. F. R. Hartley, John Wiley and Sons, Chichester, 1990, vol. 1, pp. 475-479.

37. A. R. Barron, *J. Chem. Soc., Dalton Trans.*, 1988, 3047-3050.

38. F. Cheng, H. L. Codgbrook, A. L. Hector, W. Levason, G. Reid, M. Webster and W. Zhang, *Polyhedron*, 2007, **26**, 4147-4155.

39. F. Cheng, S. I. Friend, A. L. Hector, W. Levason, G. Reid, M. Webster and W. Zhang, *Inorg. Chem.*, 2008, **47**, 9691-9700.

40. G. A. Olah and C. W. McFarland, *J. Org. Chem.*, 1969, **34**, 1832-1834.

41. M. Sigl, A. Schier and H. Schmidbaur, *Z. Naturforsch., B: Chem. Sci.*, 1998, **53**, 1313-1315.

42. W. Levason, D. Pugh and G. Reid, *Inorg. Chem.*, 2013, **52**, 5185-5193.

43. F. H. Allen, *Acta Crystallogr., Sect. B: Struct. Sci.*, 2002, **58**, 380-388.

44. A. Dimitrov, D. Heidemann and E. Kemnitz, *Inorg. Chem.*, 2006, **45**, 10807-10814.

45. H. Hatop, H. W. Roesky, T. Labahn, C. Röpken, G. M. Sheldrick and M. Bhattacharjee, *Organometallics*, 1998, **17**, 4326-4328.

46. R. Bhalla, W. Levason, S. K. Luthra, G. McRobbie, F. M. Monzittu, J. Palmer, G. Reid, G. Sanderson and W. Zhang, *Dalton Trans.*, 2015, **44**, 9569-9580.

47. R. Bhalla, C. Darby, W. Levason, S. K. Luthra, G. McRobbie, G. Reid, G. Sanderson and W. Zhang, *Chem. Sci.*, 2014, **5**, 381-391.

48. S. Ng, *Acta Crystallogr., Sect. E: Struct. Rep. Online*, 2009, **65**, 1431.

49. C. Loschen, K. Voigt, J. Frunzke, A. Diefenbach, M. Diedenhofen and G. Frenking, *Z. Anorg. Allg. Chem.*, 2002, **628**, 1294-1304.

50. E. F. Murphy, R. Murugavel and H. W. Roesky, *Chem. Rev.*, 1997, **97**, 3425-3468.

51. K. O. Christe and W. W. Wilson, *J. Fluorine Chem.*, 1990, **47**, 117-120.

52. S. L. Benjamin, W. Levason, D. Pugh, G. Reid and W. Zhang, *Dalton Trans.*, 2012, **41**, 12548-12557.

53. S. L. Benjamin, W. Levason and G. Reid, *Chem. Soc. Rev.*, 2013, **42**, 1460-1499.

54. CCDC, *Vista - A Program for the Analysis and Display of Data Retrieved from the CSD*, Cambridge, England, 1994.

Chapter 3: Coordination Complexes of Boron(III) Halides with Phosphine and Arsine Ligands

3.1 Introduction

The formation of $[BX_3(PR_3)]$ complexes is long established, yet almost exclusively limited to monodentate phosphine adducts, while recent work in the area is limited.[1] Given the current interest in the Lewis acidity trends of the boron(III) halides[1,2] this chapter sets out to synthesise and characterise a series of BX_3 complexes for all X (X = F, Cl, Br, I) with neutral phosphine ligands, in order to determine the effect of the halide on complex formation, whilst establishing the behaviour of BX_3 towards diphosphine and diarsine ligands.

3.1.1 Properties and uses of the boron(III) halides

The BX_3 (X = F, Cl, Br, I) are highly reactive, volatile, trigonal planar molecules that possess D_{3h} symmetry. At standard ambient temperature and pressure they are strictly monomeric; BF_3 and BCl_3 are gases, BBr_3 is a liquid and BI_3 is a solid.[3] Single crystal X-ray structure determinations of BX_3 (X = Cl, Br, I) reveal isomorphous hexagonal structures with the space group $P6_3/m$, containing two molecules in the unit cell. The structures are layered, with large intermolecular separations.[4-6] BF_3 however crystallises at 142 K in the space group $P2_1/c$, with eight molecules in the unit cell.[7] There are weak B···F interactions between the molecules (with distances of 2.68 and 2.71 Å, which are more than twice that of the intramolecular BF_3 bond lengths (mean d(B–F) = 1.29 Å), but within the sum of the Van der Waals radii for B and F, 3.39 Å),[8] yielding a [3+2] coordination geometry that has been described as (distorted) trigonal bipyramidal.[7] *Ab initio* calculations suggest that $X_2B(\mu\text{-}X)_2BX_2$ (X = Cl, Br, I) dimers (D_{2h} symmetry) can exist in the solid state at high pressures,[9] with $I_2B(\mu\text{-}I)_2BI_2$ already thought to have been isolated at pressures above 6.2 GPa.[10,11] The dimer $F_2B(\mu\text{-}F)_2BF_2$ (C_{2h} symmetry) has been identified by IR spectroscopy in a low temperature inert gas matrix isolation study.[12]

The boron(III) halides are good Lewis acids whose acidity is generally stated as increasing $BF_3 < BCl_3 < BBr_3 < BI_3$, though there has been much work (a lot of it computational) over the past fifteen years devoted to exploring the factors involved, the results of which are often subtle.[1,2] A discussion of the factors influencing the Lewis acidity of BX_3 is given in

Section 1.5.1. It is important to note that the properties of both the Lewis acid and Lewis base in a complex must be taken in consideration, and that calculations usually deal with gas phase molecules, meaning solvation or solid state effects may mask Lewis acidity trends in solution/crystal structures.[1] With neutral ligands, most four-coordinate complexes of BX_3 are of the type $[BX_3(L)]$ or $[(BX_3)_2\{\mu\text{-}(L–L)\}]$, but there are also examples where cationic $[BX_2(L)_2]^+$ or, more commonly, $[BX_2(L–L)]^+$ are formed. For the latter, direct combination is normally only successful with a rigid chelating ligand,[13] as seen for $[BF_2(L–L)][BF_4]$, where L–L = 1,8-bis(dimethylamino)naphthalene.[14] Fluoroboron cations with more flexible neutral ligands (e.g. $[BF_2\{Me_2N(CH_2)_2NMe_2\}]^+$) have been obtained through displacement reactions from mixed BX_3 adducts of monodentate ligands (such as $[BF_nCl_{(3-n)}(py)]$), or by the stepwise displacement of pyridine from $[BF_2(py)_2]^+$ (which itself is made by the displacement of the heavier halide in $[BF_nX_{(3-n)}(py)]$ (X = Cl or Br) using excess pyridine).[13,15]

Due to their innate Lewis acidity, boron(III) halides have found widespread use in organic syntheses and catalysis. All BX_3 can be used to cleave C–O bonds in ethers, though BBr_3 is usually chosen as it provides very mild reaction conditions, good functional group compatibility and high regioselectivities.[16] BF_3 is used to initiate epoxide polymerisation reactions, which proceed via the formation of an adduct with the epoxide monomer.[17] The reaction of BX_3 with chiral ligands yields chiral boron Lewis acid catalysts which can be used to induce chirality in other molecules, such as in enantioselective Diels-Alder reactions.[16] They can also be used as to activate catalysts, for example BCl_3 can be used to coordinate to and activate a ruthenium dithiolate alkylidene complex so that it can perform olefin metathesis reactions.[18] Halide abstraction from the adduct $[BCl_3(acridine)]$ using $AlCl_3$ yields the three-coordinate borocation $[BCl_2(acridine)][AlCl_4]$ which could be reacted with 2,4,6-tri-*tert*-butylpyridine to give a frustrated Lewis pair that heterolytically cleaves H_2 at 100 °C.[19] Recently, novel probes for positron emission tomography (PET) that are resistant to hydrolytic fluoride release have been synthesised by the radiofluorination of N-heterocyclic carbene (NHC) adducts of BF_3.[20]

3.1.2 Coordination complexes with phosphine and arsine ligands

Coordination complexes of BX_3 (X = F, Cl, Br or I) with PR_3 and AsR_3 (R = alkyl or aryl group) have long been investigated, with a lot of experimental work carried out between 1960 and 1980.[1] The complexes have attracted a lot of spectroscopic study (mainly by IR, Raman and multinuclear NMR spectroscopy), with crystallographic data, if collected, often

being reported in separate papers. Some systems, notably $[BX_3(PMe_3)]$, have been revisited several times over the decades as characterisation techniques have improved and ideas about relative complex stabilities and Lewis acidities have been questioned and addressed. Phosphine complexes have also been characterised as by-products from other reactions involving B(III) species and phosphine ligands; for instance, small amounts of $[BF_3(PMe_3)]$ was identified by multinuclear NMR spectroscopy in the reaction mixture of $[B_2H_4(PMe_3)_2]$ and $[C(C_6H_5)_3][BF_4]$,[21] while $[BCl_3(PR_3)]$ (R_3 = Me_3, Et_3, Me_2Ph, $^tBu_3$, Cy_3, $MePh_2$, Ph_3) were obtained at different rates as rearrangement products from the reaction of the phosphines with 2-chloro-1,3,2-benzodioxaborole (ClBcat).[22] Importantly, crystals of $[(BCl_3)_2(\mu\text{-}Ph_2PCH_2PPh_2)]$, the only reported example of a diphosphine ligand complex of BX_3, were isolated from the reaction of $[Pt_2(Ph_2PCH_2PPh_2)_3]$ and BCl_3.[23] Similarly, reactions between $[Pt(PR_3)_4]$ (R_3 = Me_3, Me_2Ph, $MePh_2$, Ph_3) and BCl_3 yielded $[BCl_3(PR_3)]$ as by-products ($[BCl_3(PR_3)]$ (R_3 = Me_2Ph, Ph_3) were crystallographically characterised),[23] while $[BI_3(PCy_3)]$ was obtained from the reaction of $[Pt(PCy_3)_2]$ with BI_3.[24] The frustrated Lewis pair [MesP-C(=CH-Ph)-Al$(CMe_3)_2$] (Mes = 2,4,6-$C_6H_2Me_3$) forms adducts with BX_3 (X = F, Cl, Br, I) where the phosphorus atom is coordinated to the boron centre and one of the halogen atoms to aluminium so that a five-membered heterocycle (BPCAlX) is created.[25]

All purposefully synthesised BX_3 complexes involve monodentate phosphine or arsine ligands, and feature C_{3v} boron(III) centres. Though other BF_3 complexes like $[BF_3(PMe_3)]$ have been spectroscopically identified, the only crystallographically authenticated BF_3 complex is $[BF_3(PEt_3)]$.[26] The crystal structures of the other $[BX_3(PMe_3)]$ (X = Cl, Br, I)[27] are known, as are $[BBr_3(P^nPr_3)]$,[28] $[BBr_3(PPh_3)]$,[29] $[BBr_3(PMePh_2)]$,[30] $[BBr_3(PHPh_2)]$[30] and the arsine complexes $[BX_3(AsMe_3)]$ (X = Cl, Br, I).[31] Trivinylphosphine forms the stable adducts $[BX_3\{P(CH{=}CH_2)_3\}]$ for X = Cl, Br and I, but reaction with BF_3 resulted in the polymerisation of the phosphine and its adduct.[26] The secondary phosphine adducts $[BX_3(PH^tBu_2)]$ (X = Cl, Br) are known; the chloride complex is unstable in air and readily converts into the corresponding phosphine oxide complex.[32] The complexes $[BX_3\{E(SiMe_3)_3\}]$ (X = Cl, Br, I; E = P, As) are isolable, with crystal structures reported for all but $[BI_3\{P(SiMe_3)_3\}]$, but they are susceptible to dehalosilylation (-Me_3SiX), forming dimeric $[\{BX_2(E(SiMe_3)_2)\}_2]$.[33-35] For complexes with a common phosphine/arsine ligand, the *d*(B–P/As) bond length decreases Cl > Br > I.[1]

3.2 Results and Discussion

Given the difficulties in handling corrosive BF_3 gas, often more conveniently handled adducts are used as the source of BF_3. Though the liquid $[BF_3(OEt_2)]$ is more commonly used as the BF_3 source for the synthesis of complexes[26] and for applications in e.g. organic transformations,[36] for this work $[BF_3(SMe_2)]$ (also a commercially available liquid) was chosen, as the calculated (*ab initio*) complex interaction energy for $[BF_3(SMe_2)]$ is smaller (–93.64 kJ mol^{-1}) than for the corresponding ether $[BF_3(OMe_2)]$ (–116.63 kJ mol^{-1}).[37] This suggests that it will be easier to perform ligand exchange with $[BF_3(SMe_2)]$ than $[BF_3(OEt_2)]$, especially as phosphorus is a relatively soft donor atom while BF_3 is a hard Lewis acid,[38] meaning it should be easier to displace a soft (S donor) thioether from BF_3 than a hard (O donor) ether. The displaced SMe_2 is easily removed *in vacuo* at the end of the reaction. The white solid $[BCl_3(SMe_2)]$ was also used as a easily handled BCl_3 source.

All of the boron(III) halides and $[BX_3(SMe_2)]$ (X = F, Cl) are very moisture sensitive, and so rigorous inert atmosphere conditions and dry solvents were employed throughout all the syntheses, manipulations and spectroscopic measurements. The boron(III) halide reagents were found to give colourless solutions in the weakly coordinating solvent CH_2Cl_2; in contrast to the behaviour seen with $AlBr_3$ and AlI_3 (see Section 2.2.1) halide exchange with CH_2Cl_2 was usually not observed for the boron(III) halides and so this was the solvent of choice for all reactions with BF_3 and BCl_3, as well as for BBr_3 and BI_3, unless the complex formed was ionic (see Section 3.2.3). Unlike the aluminium(III) halide systems, phosphonium cations $[R_3PH]^+$ were rarely observed.

In the IR spectra of the complexes synthesised the B–X bands were often broad and sometimes difficult to assign, presumably caused in part by effects such as lower site symmetry in the solid state. The IR spectra were sometimes further complicated by the fact that boron has two naturally occurring isotopes, ^{10}B (19.9% natural abundance) and ^{11}B (80.1% natural abundance), meaning a ^{10}B–X bond has a different reduced mass and hence (when observed) a different (higher) vibrational frequency to a ^{11}B–X bond. For the BF_3 complexes the B–F bending modes are expected to be above 200 cm^{-1},[39] but were often hard to reliably assign among the neutral ligand bands. In ^{19}F NMR spectroscopy often two resonances were observed ~ 20 Hz apart, with relative intensities of 1:4, due to a ^{10}B–^{11}B (the latter of which is always quoted in the Experimental Section) isotope shift. In ^{11}B NMR spectroscopy the $[BX_4]^-$ were observed to give a sharp peak in CH_2Cl_2/CD_2Cl_2 at δ = 0.1 (X = F), 8.0 (X = Cl) and –23.3 (X = Br).

3.2.1 Complexes with phosphine oxide ligands

Though a large number of complexes of BX_3 (X = F, Cl, Br, I) with oxygen donor ligands are known, there has been comparatively little research on phosphine oxide and arsine oxide complexes. The complexes $[BX_3(OPPh_3)]$ (X = F, Cl, Br, I) have all been isolated,[40-42] and selected NMR spectroscopic data has been reported for X = F, Cl and I.[41,42] The $[BF_3(OEPh_3)]$ (E = P, As) have been characterised by single crystal X-ray diffraction; the two complexes are isostructural, featuring *pseudo*-tetrahedral boron centres and bent B–O–E linkages.[43] Multinuclear NMR spectra have also been recorded for $[BF_3(OER_3)]$ (E = P, As; R = Me, Et, ^{n}Pr, ^{n}Bu)[44] and $[BCl_3(OEEt_3)]$ (E = P, As).[45] There has been little recent activity in the area however, and there are no reported complexes with bidentate phosphine oxides, and so reactions with some key representative ligands were performed in order to gain further insight into the behaviour of boron(III) halides towards phosphine oxides.

The complexes $[BX_3(OPMe_3)]$ (X = F, Cl) were isolated as white powders from the reactions of the corresponding $[BX_3(SMe_2)]$ with $OPMe_3$ in CH_2Cl_2, with successful complexation confirmed by the spectroscopic data and microanalysis results collected. Table 3.1 summarises the NMR spectroscopic data collected on both the dimethyl sulfide adducts used as starting reagents, and the trimethylphosphine oxide complexes obtained.

Table 3.1 Selected NMR spectroscopic data for $[BX_3(SMe_2)]$ and $[BX_3(OPMe_3)]$ (X = F, Cl)

Complex	$\delta(^1H)$ / 295 K[a]	$\delta(^{19}F)$ / 295 K[a]	$\delta(^{31}P\{^1H\})$ / 295 K[a]	$\delta(^{11}B)$ / 295 K[b]
$[BF_3(SMe_2)]$	2.20 (s)	–138.5 (s)	–	+4.73 (s)
$[BCl_3(SMe_2)]$	2.49 (s)	–	–	+8.50 (s)
$[BF_3(OPMe_3)]$	1.85 (d)	–146.2 (br s)	69.2 (q)	+0.11 (s)
$[BCl_3(OPMe_3)]$	2.06 (d)	–	75.4 (s)	+7.03 (s)

[a] CD_2Cl_2; [b] CH_2Cl_2/CD_2Cl_2

The Me groups give rise to sharp doublets in the ^{1}H NMR spectra of $[BX_3(OPMe_3)]$, while the resonance in $^{31}P\{^1H\}$ NMR spectra of both complexes has shifted to a much higher frequency with respect to free $OPMe_3$ (δ = 36.9). The greater deshielding of the $OPMe_3$ ligand in the BCl_3 complex, a trend also observed with $OPEt_3$,[17] is consistent with an increase in Lewis acidity at boron. The quartet in the $^{31}P\{^1H\}$ NMR spectrum of $[BF_3(OPMe_3)]$ is the result of coupling to fluorine ($^3J_{PF}$ = 8 Hz), while the singlet in the ^{19}F

NMR spectrum at $\delta = -146.2$ (which is in good agreement with the literature value)[46] is too broad for coupling to be resolved. The singlet in the ^{11}B NMR spectrum of $[BF_3(OPMe_3)]$ is at a slightly lower frequency than that of free BF_3 ($\delta(BF_3) = 10.0$,[47] $\Delta = -9.9$), while the boron centre experiences a greater degree of shielding in $[BCl_3(OPMe_3)]$ ($\delta(BCl_3) = 46.5$,[47] $\Delta = -39.5$); these chemical shifts are similar to those observed for $[BX_3(OPPh_3)]$ (X = F, Cl).[41] There was no evidence of either $[BX_3(SMe_2)]$ or uncoordinated SMe_2 in any of the spectra collected.

In the IR spectra of $[BX_3(OPMe_3)]$ the ν(PO) stretch has fallen from 1165 cm^{-1} in free $OPMe_3$ to 1092 (X = F) and 1084 (X = Cl) cm^{-1}, consistent with coordination. Two ν(BX) stretching modes (a_1 and e) are expected as the complexes have C_{3v} symmetry; these can be identified in the IR spectrum of $[BCl_3(OPMe_3)]$ (bands at 712 and 370 cm^{-1}), but for $[BF_3(OPMe_3)]$ the very broad ν(PO) stretch obscures the region where the ν(BF) e mode is expected, so that only the ν(BF) a_1 mode is identifiable at 899 cm^{-1}.

To investigate the behaviour of boron(III) halides with bidentate phosphine oxide ligands, $[BF_3(SMe_2)]$ was reacted with the non-rigid $Ph_2P(O)CH_2P(O)Ph_2$ in CH_2Cl_2. A 2:1 (BF_3 : L–L) molar ratio was initially chosen because it was thought that the complex formed would be the ligand-bridged $[(BF_3)_2\{\mu\text{-}Ph_2P(O)CH_2P(O)Ph_2\}]$, similar to the complex formed by $AlCl_3$, $[(AlCl_3)_2\{\mu\text{-}Ph_2P(O)CH_2P(O)Ph_2\}]$.[48] This is because the B–F bond in BF_3 is the strongest known "single" bond (mean B–F bond energy = 646 kJ mol^{-1}),[3] so removing a fluoride from the boron(III) centre under such mild conditions seemed unlikely. However, crystals grown from the reaction were shown by a single crystal X-ray diffraction study to be the 3:1 complex $[BF_2\{Ph_2P(O)CH_2P(O)Ph_2\}][B_2F_7]$ (Figure 3.1). The cation features a BF_2 moiety with an almost symmetrically chelating $Ph_2P(O)CH_2P(O)Ph_2$ ligand, giving a tetrahedral boron centre overall that is only slightly distorted from an ideal tetrahedron. The first crystal structure containing the $[B_2F_7]^-$ anion, $[Pd\{Ph_2PCH_2C(O)Ph\}_2][BF_4][B_2F_7]$, was reported in 1992;[49] nevertheless $[BF_2\{Ph_2P(O)CH_2P(O)Ph_2\}][B_2F_7]$ remains a rare example of a crystallographically authenticated $[B_2F_7]^-$ fluoroanion. It is composed of a single fluorine atom bridging between two BF_3 fragments, resulting in two linked *pseudo*-tetrahedral boron centres. The terminal *d*(B–F) span the range 1.326(7) to 1.406(7) Å, while the bridging *d*(B–F) are 1.499(7) and 1.532(8) Å and the ∠B2–F6–B3 is 128.6(4)°, consistent with literature values.[49]

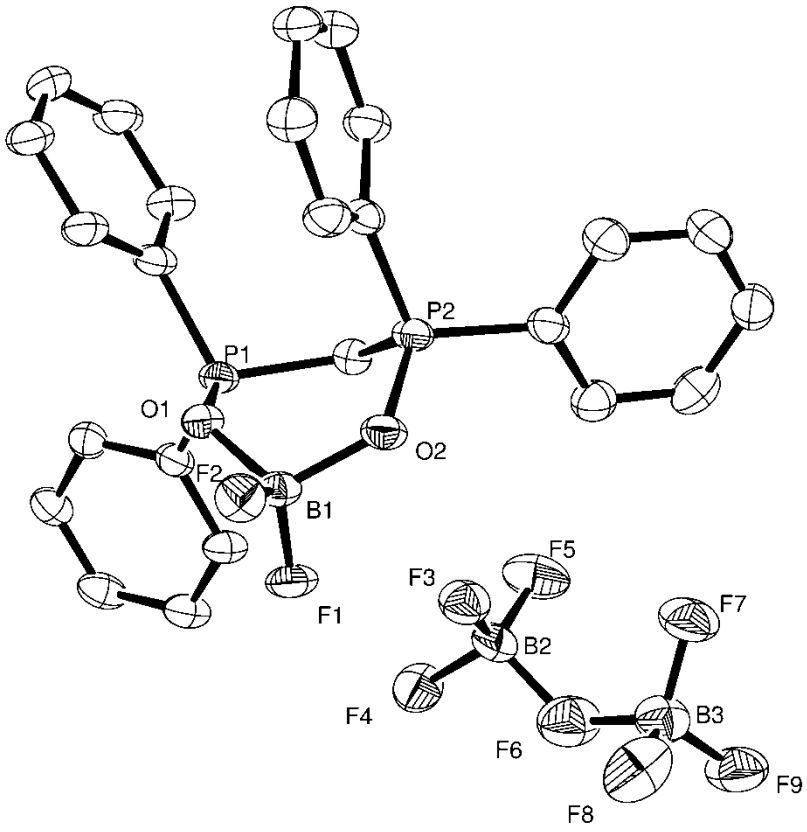

Figure 3.1 The structure of $[BF_2\{Ph_2P(O)CH_2P(O)Ph_2\}][B_2F_7]$ showing the atom labelling scheme. Ellipsoids are drawn at the 50% probability level and H atoms are omitted for clarity.

Table 3.2 Selected bond lengths (Å) and angles (°) for $[BF_2\{Ph_2P(O)CH_2P(O)Ph_2\}]^+$

B1–O1	1.517(6)	F1–B1–F2	114.7(4)
B1–O2	1.512(6)	F1–B1–O1	110.0(4)
B1–F1	1.353(5)	F1–B1–O2	108.0(4)
B1–F2	1.351(6)	F2–B1–O1	107.4(4)
P1–O1	1.538(3)	F2–B1–O2	109.0(4)
P2–O2	1.542(3)	O1–B1–O2	107.6(4)
		B1–O1–P1	127.6(3)
		B1–O2–P2	127.5(3)

The NMR spectra in CD_2Cl_2 of the white powder isolated from the above reaction reveal that there are two complexes present, $[BF_2\{Ph_2P(O)CH_2P(O)Ph_2\}]^+$ and $[(BF_3)_2\{\mu\text{-}Ph_2P(O)CH_2P(O)Ph_2\}]$, with the integrals being roughly 1:1 in the ^1H and $^{31}P\{^1H\}$ NMR

spectra. In the ^{1}H NMR spectrum two triplets (corresponding to the CH_2 group of $Ph_2P(O)CH_2P(O)Ph_2$) are observed, with the triplet for $[BF_2\{Ph_2P(O)CH_2P(O)Ph_2\}]^+$ appearing at a higher frequency; this is also true for its corresponding resonances in the ^{19}F and $^{31}P\{^{1}H\}$ NMR spectra. In the $^{31}P\{^{1}H\}$ NMR spectrum the ionic chelating ligand complex appears as a triplet ($^{3}J_{PF}$ = 9 Hz) at δ = 50.0 while the neutral bridging ligand complex is a singlet at δ = 44.2, both of which have shifted to a significantly higher frequency than free $Ph_2P(O)CH_2P(O)Ph_2$ (δ = 24.2). The ^{19}F NMR spectrum consists of a doublet ($^{3}J_{FP}$ = 6 Hz) at δ = –142.9 for $[(BF_3)_2\{\mu\text{-}Ph_2P(O)CH_2P(O)Ph_2\}]$, a triplet ($^{3}J_{FP}$ = 9 Hz) at δ = –138.2 for $[BF_2\{Ph_2P(O)CH_2P(O)Ph_2\}]^+$ and a singlet at δ = –149.8 assigned as $[BF_4]^-$ as the peak integral is too small for $[B_2F_7]^-$. The sharp singlet for $[BF_4]^-$ is located at δ = 0.15 in the ^{11}B NMR spectrum, right next to a very broad resonance centred at δ = 0.51; here separate peaks for the ionic and neutral complexes (which are thought to have similar chemical shifts)[50] cannot be distinguished.

In an attempt to isolate a pure sample of $[BF_2\{Ph_2P(O)CH_2P(O)Ph_2\}][B_2F_7]$ the reaction was repeated in a 3:1 (BF_3 : L–L) molar ratio. NMR spectroscopic analysis of the white powder isolated however revealed that both the chelating- and bridging ligand complexes were still present, though by integrating the spectra it was found that there was now more $[BF_2\{Ph_2P(O)CH_2P(O)Ph_2\}]^+$ present than the bridging ligand complex, with the new ratio being roughly 2:1. Otherwise the spectra remained similar, except, importantly, a large peak had grown alongside the $[BF_4]^-$ resonance in the ^{19}F NMR spectrum at δ = –148.4 (this resonance is evident but is very small in the 2:1 spectrum), while in the ^{11}B NMR spectrum the resonance corresponding to $[BF_4]^-$ had broadened and partially split, with two peaks evident at δ = 0.14 and 0.20. The new resonances were assigned as $[B_2F_7]^-$; no resonance for the bridging fluorine was observed in the ^{19}F NMR spectrum due to fast chemical exchange.[51,52] It therefore appears that increasing the amount of BF_3 in the system favours the formation of $[BF_2\{Ph_2P(O)CH_2P(O)Ph_2\}][B_2F_7]$.

This behaviour can be explained if the equations (1), (2) and (3) below are considered (in this case, L–L = $Ph_2P(O)CH_2P(O)Ph_2$):

$$2BF_3 + L\text{–}L \rightleftarrows [(BF_3)_2\{\mu\text{-}(L\text{–}L)\}] \quad (1)$$

$$[(BF_3)_2\{\mu\text{-}(L\text{–}L)\}] \rightleftarrows [BF_2(L\text{–}L)]^+ + [BF_4]^- \quad (2)$$

$$[BF_4]^- + BF_3 \rightleftarrows [B_2F_7]^- \quad (3)$$

Related equilibria have been used to help explain the observation (by NMR spectroscopy) of small amounts of the ionic species $[BF_2L_2]^+$ (L = $OP(Me_2N)_3$[50] and $EC(NMe_2)_2$ (E = S, Se)[53]) in these adduct systems. At low BF_3 concentrations (i.e. the 2:1 (BF_3 : L–L) ratio reaction) there is no real drive to form $[B_2F_7]^-$ and so the main ionic species formed is $[BF_2\{Ph_2P(O)CH_2P(O)Ph_2\}][BF_4]$, which is in equilibrium with the neutral bridging ligand complex. Some $[BF_2\{Ph_2P(O)CH_2P(O)Ph_2\}][B_2F_7]$ is still formed though, and is presumably the least soluble species in the system, preferentially crystallising out of solution. Increasing the BF_3 concentration (i.e. the 3:1 reaction) leads to the formation of more $[B_2F_7]^-$ (as seen in the ^{19}F NMR spectrum), which consumes $[BF_4]^-$ according to equation (3) and in turn forces equation (2) to the right, resulting in more of the ionic complex forming. Evidence for these equilibria comes from the fact that upon performing the reaction in a 6:1 (BF_3 : L–L) molar ratio, the NMR spectra of the isolated powder were little changed with respect to the 3:1 reaction; the order of addition of the reagents (i.e. the local concentration at the beginning of the reaction) had little effect also.

It is unusual to observe the $[B_2F_7]^-$ fluoroanion by NMR spectroscopy at room temperature as it is widely reported[51,53] to only exist in solution at low temperatures, readily dissociating to give BF_3 and $[BF_4]^-$ upon warming. At 118 K the ^{19}F NMR spectrum of $[B_2F_7]^-$ in $CHFCl_2$ consists of a doublet at $\delta = -151.4$, which is shifted by 2.1 ppm to high frequency with respect to the observed $[BF_4]^-$ resonance, and a broad resonance at $\delta = -117$ for the bridging fluorine.[51] However $[B_2F_7]^-$ has been observed by ^{19}F NMR spectroscopy at room temperature before, as in CD_3CN the biruthenocenium salt $[Ru(C_5H_5)(C_5H_4C_5H_4)(C_5H_5)Ru(NCC_2H_5)][BF_4][B_2F_7]$ gives two resonances at $\delta = -146$ and –147 (no resonance is observed for the bridging fluorine).[52] The $[B_2F_7]^-$ fluoroanion is thought to be stabilised by large, bulky cations because their interaction with the $[BF_4]^-$ counterion becomes so weak that $[BF_4]^-$ can better coordinate to a free BF_3 molecule.[54] The $[BF_2\{Ph_2P(O)CH_2P(O)Ph_2\}]^+$ cation must therefore be sufficiently stable to allow $[B_2F_7]^-$ to exist on the NMR timescale at room temperature, and this stability presumably stems from a number of factors, including the chelate effect and the low steric hindrance of the phosphoryl groups.[50]

The reaction of $[BCl_3(SMe_2)]$ with $Ph_2P(O)CH_2P(O)Ph_2$ in a 2:1 molar ratio yielded crystals of $[(BCl_3)_2\{\mu\text{-}Ph_2P(O)CH_2P(O)Ph_2\}]$ (Figure 3.2). The compound is triclinic, *P*-1, a = 9.516(2), b = 10.612(2), c = 14.591(4) Å, α = 93.387(2), β = 106.504(4), γ = 97.135(3)°, *Z* = 2. Though the identity of the bridging ligand complex is not in doubt,

unfortunately the data set completeness is low (82%) which precludes detailed structural analysis, and so full X-ray crystallographic data are not reported.

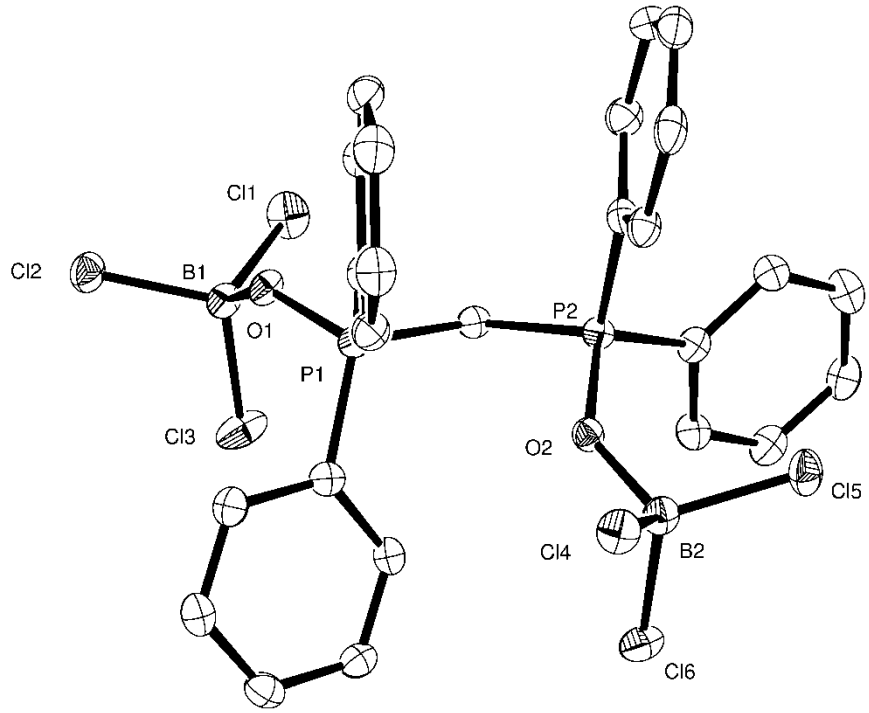

Figure 3.2 The structure of $[(BCl_3)_2\{\mu\text{-}Ph_2P(O)CH_2P(O)Ph_2\}]$. Ellipsoids are drawn at the 50% probability level and H atoms are omitted for clarity.

The major species in the NMR spectra of the white powder isolated from the reaction is the neutral bridging ligand complex. As seen with $[BX_3(OPMe_3)]$ (X = F, Cl), the triplet in the ^{1}H NMR spectrum and the singlet in the $^{31}P\{^1H\}$ NMR spectrum are to a higher frequency (Δ = +0.45 and +5.3 respectively) than the resonances observed for $[(BF_3)_2\{\mu\text{-}Ph_2P(O)CH_2P(O)Ph_2\}]$. $[(BCl_3)_2\{\mu\text{-}Ph_2P(O)CH_2P(O)Ph_2\}]$ gives a singlet in the ^{11}B NMR spectrum at δ = 7.78; the lack of a strong $[BCl_4]^-$ peak in the spectrum rules out the formation of significant amounts of an ionic complex. There is evidence however of a minor species in the NMR spectra, and these extra peaks have been tentatively assigned as the κ^1-coordinated complex on the basis of the doublet of doublets centred at δ = 4.39 ($^2J_{HP}$ = 12.0, 18.8 Hz) in the ^{1}H NMR spectrum and resonances of equal intensity in the $^{31}P\{^1H\}$ NMR spectrum at δ = 22.9 and 53.1 (these do not change in the ^{1}H-coupled ^{31}P NMR spectrum) which correspond to the free and coordinated ends of the diphosphine dioxide. The microanalysis results confirm that the white powder isolated has a 2:1 (BCl_3 : L–L) ratio, meaning that the amount of κ^1-complex present is very small. This is supported by IR spectroscopy as while a very strong ν(PO) stretch for coordinated $Ph_2P(O)CH_2P(O)Ph_2$ is observed at 1065 cm^{-1}, there is no ν(PO) stretch for free phosphine oxide evident at 1186

cm^{-1}. That there is no detectable ionic chelating ligand complex present in the BCl_3 system may be in part due to the fact that, while the formation of $[B_2F_7]^-$ helped to drive ionic complex formation in the fluoride system, the analogous $[B_2Cl_7]^-$ anion is unknown (*ab initio* calculations predict that $[B_2Cl_7]^-$ is an energetically stable species, but likely to dissociate at room temperature).[55]

3.2.2 Neutral complexes with phosphine ligands

3.2.2.1 $[BF_3(PMe_3)]$

While $[BF_3(PMe_3)]$ has been known for over 60 years, with multinuclear NMR spectroscopic data reported as early as 1965,[56] the X-ray crystal structure of the complex has never been reported, as previous attempts to grow a single crystal have failed.[27] Upon layering with hexane a CH_2Cl_2 solution containing $[BF_3(SMe_2)]$ and PMe_3 in a 1:1 molar ratio, colourless crystals of $[BF_3(PMe_3)]$ were obtained. The crystals decomposed rapidly on exposure to air, but fast manipulations enabled a single crystal X-ray diffraction study to be performed. The structure (Figure 3.3) reveals the expected C_{3v} geometry; it adopts the same space group ($P2_1/m$) as $[BX_3(PMe_3)]$ (X = Cl, Br),[27] but unlike the staggered conformation of the chloro and bromo complexes $[BF_3(PMe_3)]$ has an eclipsed conformation, as observed for the isomorphous $[AlCl_3(PMe_3)]$ (see Section 2.2.2). An *ab initio* study of the structure of $[BF_3(PMe_3)]$ found that the staggered conformer is preferred,[57] suggesting that the observed eclipsed arrangement is a result of crystal packing effects. The *d*(B–P) and *d*(B–F) are in good agreement (within 0.02 Å) with theoretically (*ab initio*) calculated values.[57,58] The B–P bond length in $[BF_3(PMe_3)]$ (2.029(10) Å) is significantly longer than in $[BCl_3(PMe_3)]$ (1.957(5) Å),[27] consistent with the order of Lewis acidity being $BCl_3 > BF_3$. Theoretical calculations also establish this order when the Lewis base is PMe_3, with the greater Lewis acidity of BCl_3 being attributed not to the deformation energy (the energy needed to convert the trigonal planar BX_3 into a pyramidal fragment) but instead the intrinsic interaction energy between the Lewis acid and base.[58] The *d*(B–P) and *d*(B–F) are identical (within bond error margins) to those found in $[BF_3(PEt_3)]$,[26] indicating a similar phosphine donor strength.

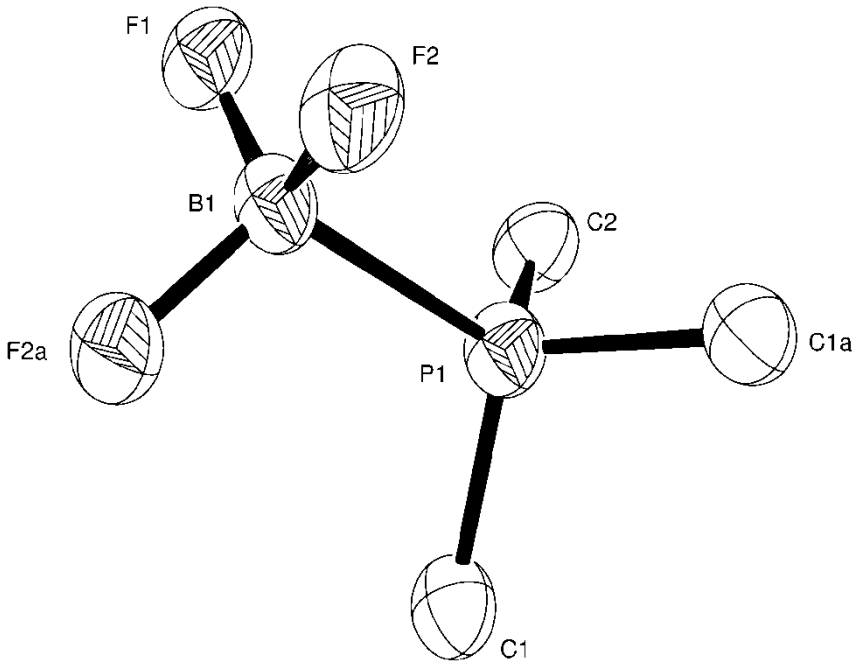

Figure 3.3 The structure of $[BF_3(PMe_3)]$ showing the atom labelling scheme. The molecule lies on a mirror plane going through C2, P1, B1 and F1. Ellipsoids are drawn at the 50% probability level and H atoms are omitted for clarity. Symmetry operation: a = x, 1/2 – y, z.

Table 3.3 Selected bond lengths (Å) and angles (°) for $[BF_3(PMe_3)]$

B1–F1	1.376(11)	F1–B1–F2	110.3(5)
B1–F2	1.396(7)	F2–B1–F2a	110.5(7)
B1–P1	2.029(10)	F1–B1–P1	108.4(6)
		F2–B1–P1	108.6(5)

Though the microanalysis of the dried crystals confirmed that $[BF_3(PMe_3)]$ had been isolated, the complex was found to be susceptible to both oxidation and hydrolysis in solution, evidenced by minor resonances corresponding to $[BF_3(OPMe_3)]$ (characterised in Section 3.2.1) and $[Me_3PH][BF_4]$ (see Section 2.2.4) in the NMR spectra. The ^{11}B, ^{19}F and $^{31}P\{^1H\}$ NMR spectra of $[BF_3(PMe_3)]$ are shown in Figure 3.4; the chemical shifts and coupling constants are in good agreement with literature values.[21,46,56] In the IR spectrum the antisymmetric (e) ν(BF) stretch is broad and centred at 1060 cm^{-1}; the band at 521 cm^{-1} suggests there is some $[BF_4]^-$ present[59] which has a t_2 stretching mode at ~1070 cm^{-1} and so will complicate the region. The symmetric (a_1) ν(BF) stretch for $[BF_3(PMe_3)]$ is at 768 cm^{-1} while the symmetric (a_1) bending mode is observed as a strong band at 635 cm^{-1}.[57]

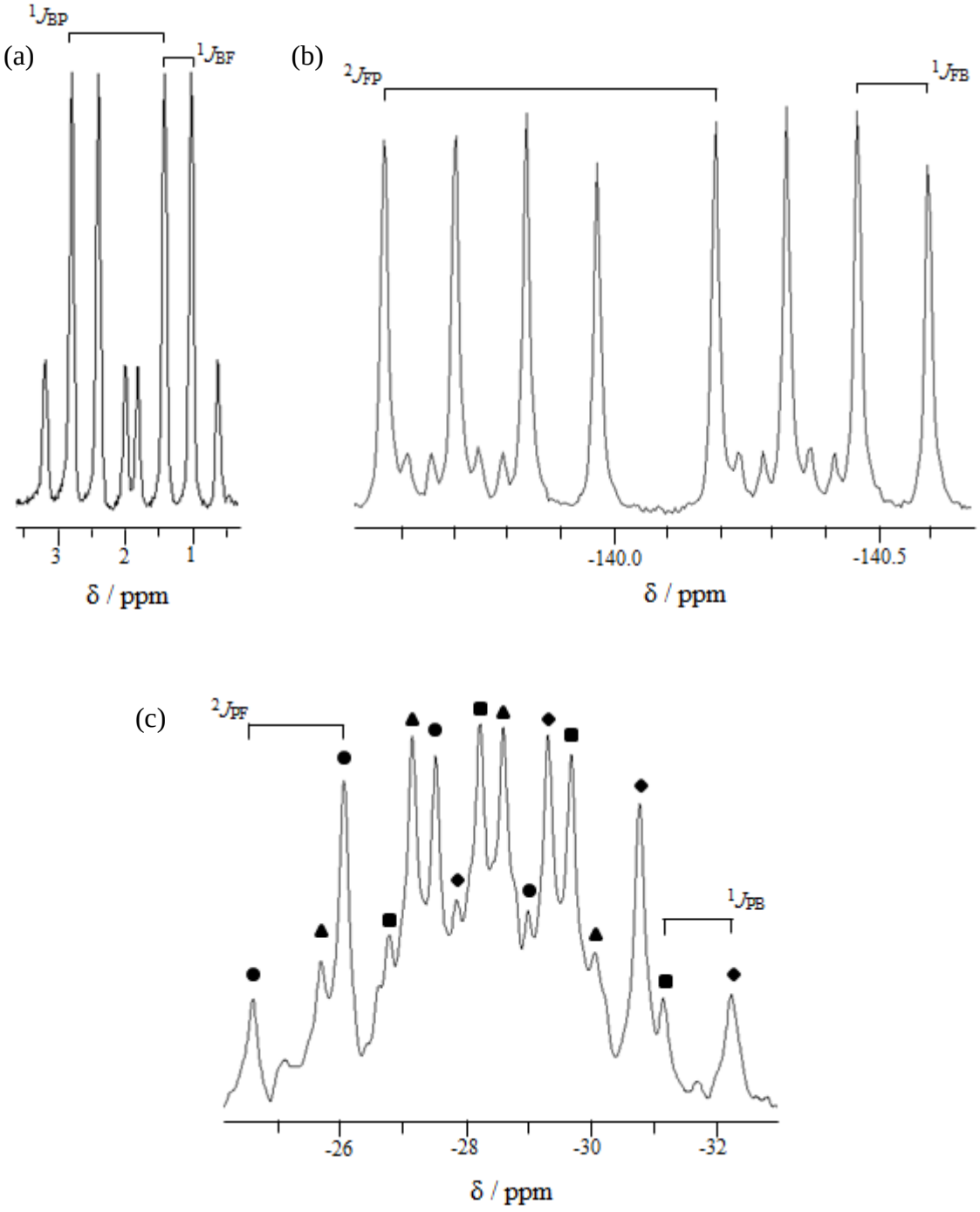

Figure 3.4 (a) ^{11}B NMR, (b) ^{19}F NMR and (c) ^{31}P{^{1}H} NMR spectra of [$BF_3(PMe_3)$] in CD_2Cl_2 at 295 K. The four types of marker each highlight one of the quartets.

3.2.2.2 Complexes with $R_2P(CH_2)_2PR_2$ (R = Me, Et)

Despite the crystal structure of [$(BCl_3)_2(\mu$-$Ph_2PCH_2PPh_2)$] having been reported as a by-product in 2007,[23] there has been no purposeful research into BX_3 complexes with bidentate phosphine ligands. Thus a systematic study of these complexes was undertaken, and initially the reactions of BX_3 with the flexible alkyl diphosphine ligand $Et_2P(CH_2)_2PEt_2$ were examined, chosen because of its strong σ-donating ability and

relatively small steric requirements, as well as its tendency to increase the solubility of its complexes in weakly coordinating organic solvents such as CH_2Cl_2 relative to other readily available diphosphine ligands. The reaction of two molar equivalents of $[BX_3(SMe_2)]$ (X = F, Cl) or BX_3 (X = Br, I) with one equivalent of $Et_2P(CH_2)_2PEt_2$ yielded colourless crystals of $[(BX_3)_2\{\mu\text{-}Et_2P(CH_2)_2PEt_2\}]$. X-ray structure determinations revealed that $[(BF_3)_2\{\mu\text{-}Et_2P(CH_2)_2PEt_2\}]$ (Figure 3.5), $[(BCl_3)_2\{\mu\text{-}Et_2P(CH_2)_2PEt_2\}]$ (Figure 3.6) and $[(BBr_3)_2\{\mu\text{-}Et_2P(CH_2)_2PEt_2\}]$ (Figure 3.7) are all centrosymmetric and adopt the monoclinic space group $P2_1/c$, with the isomorphous chloro and bromo complexes having near-identical unit cell dimensions. There are two similar but independent molecules in the asymmetric unit of $[(BI_3)_2\{\mu\text{-}Et_2P(CH_2)_2PEt_2\}]$ (Figure 3.8), which crystallises in the triclinic space group P-1.

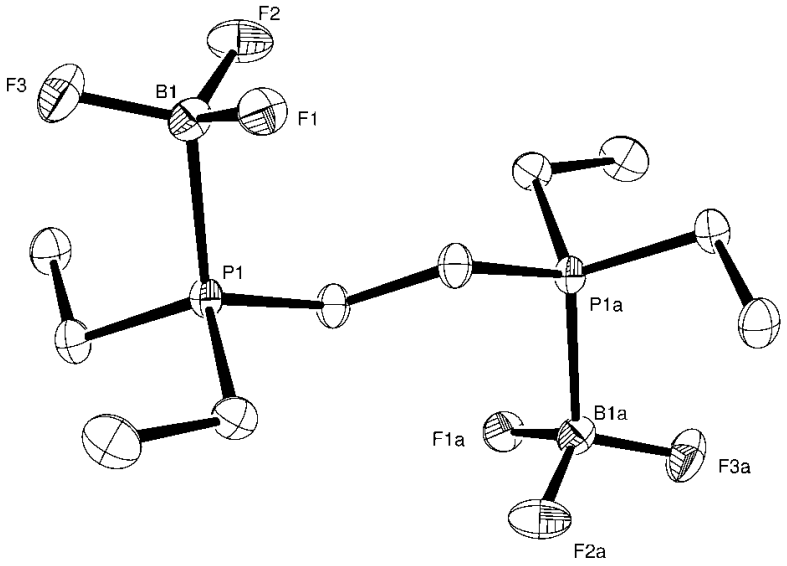

Figure 3.5 The structure of centrosymmetric $[(BF_3)_2\{\mu\text{-}Et_2P(CH_2)_2PEt_2\}]$ showing the atom labelling scheme. Ellipsoids are drawn at the 50% probability level and H atoms are omitted for clarity. Symmetry operation: a = 2 – x, – y, 1 – z.

Table 3.4 Selected bond lengths (Å) and angles (°) for $[(BF_3)_2\{\mu\text{-}Et_2P(CH_2)_2PEt_2\}]$

B1–F1	1.388(2)	F1–B1–F2	110.57(15)
B1–F2	1.385(2)	F1–B1–F3	110.96(14)
B1–F3	1.373(2)	F2–B1–F3	111.68(15)
B1–P1	2.028(2)	F1–B1–P1	107.00(12)
		F2–B1–P1	107.89(12)
		F3–B1–P1	108.55(13)

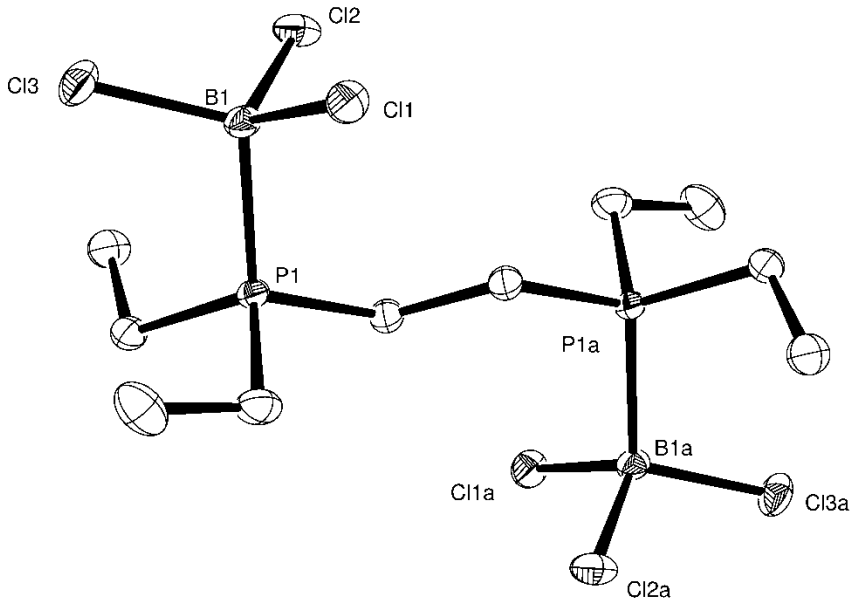

Figure 3.6 The structure of centrosymmetric $[(BCl_3)_2\{\mu\text{-}Et_2P(CH_2)_2PEt_2\}]$ showing the atom labelling scheme. Ellipsoids are drawn at the 50% probability level and H atoms are omitted for clarity. Symmetry operation: a = 1 – x, – y, – z.

Table 3.5 Selected bond lengths (Å) and angles (°) for $[(BCl_3)_2\{\mu\text{-}Et_2P(CH_2)_2PEt_2\}]$

B1–Cl1	1.8536(18)	Cl1–B1–Cl2	111.15(10)
B1–Cl2	1.8470(19)	Cl1–B1–Cl3	110.55(9)
B1–Cl3	1.834(2)	Cl2–B1–Cl3	111.03(8)
B1–P1	1.9701(18)	Cl1–B1–P1	107.47(8)
		Cl2–B1–P1	107.30(9)
		Cl3–B1–P1	109.21(8)

All four complexes feature staggered, *pseudo*-tetrahedral boron(III) centres with similar ∠X–B–X. The *d*(B–P) decrease as the halide gets heavier (F > Cl > Br > I), which is consistent with the generally established order of (increasing) Lewis acidity for BX_3. However the differences in bond length are within the uncertainty range (apart from the difference between the fluoro and chloro complexes) and so cannot be reliably used to discuss the relative Lewis acidities of BX_3. Furthermore, DFT calculations have shown for strongly bonded BX_3 complexes that bond length does not always correlate with bond strength, and that bond strength does not always correlate with the intrinsic interaction energy (i.e. donor-acceptor strength).[58,60] While the *d*(B–P) of $[(BX_3)_2\{\mu\text{-}Et_2P(CH_2)_2PEt_2\}]$ and $[BX_3(PMe_3)]$ are identical when X = F, and similar when X = Cl (1.9701(18) and

1.957(5)[27] Å respectively), the *d*(B–P) when X = Br and I are considerably shorter for [$BX_3(PMe_3)$] (1.967(3) *vs.* 1.924(12) Å for X = Br; 1.950(4)–1.966(4) *vs.*1.918(15) Å for X = I).[27] This can be attributed to the greater steric bulk of the diphosphine ligand, which prevents $Et_2P(CH_2)_2PEt_2$ approaching the boron centre as closely as PMe_3 does when the halide involved is large. The *d*(B–X) are comparable in [$(BX_3)_2\{\mu\text{-}Et_2P(CH_2)_2PEt_2\}$] and [$BX_3(PMe_3)$][27] (X = F, Cl, Br and I), indicating a similar phosphine donor strength.

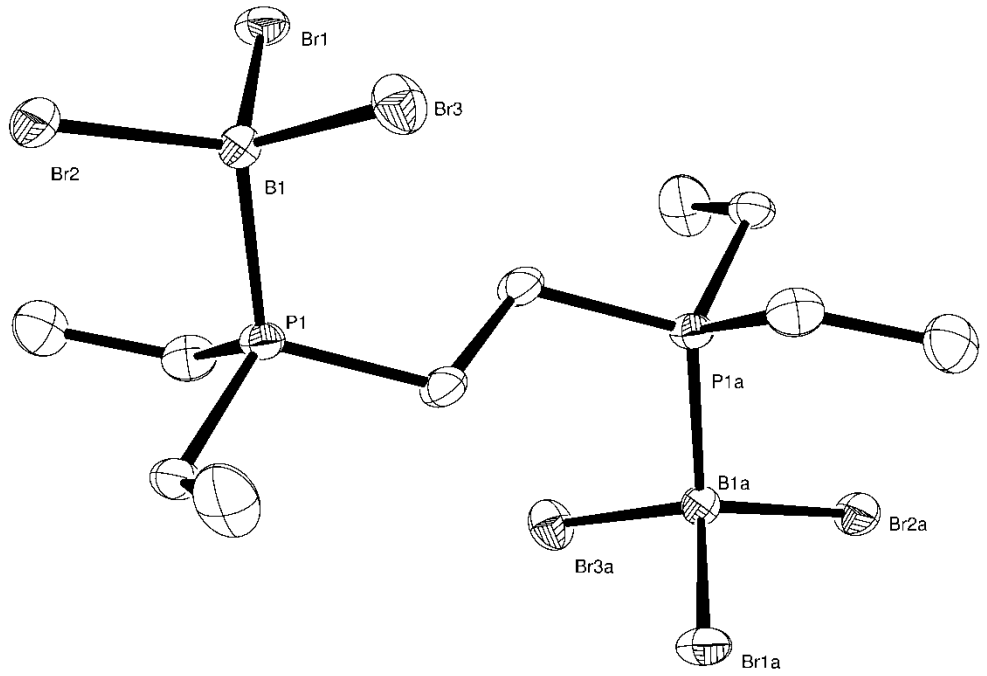

Figure 3.7 The structure of centrosymmetric [$(BBr_3)_2\{\mu\text{-}Et_2P(CH_2)_2PEt_2\}$] showing the atom labelling scheme. Ellipsoids are drawn at the 50% probability level and H atoms are omitted for clarity. Symmetry operation: a = 1 – x, 1 – y, – z.

Table 3.6 Selected bond lengths (Å) and angles (°) for [$(BBr_3)_2\{\mu\text{-}Et_2P(CH_2)_2PEt_2\}$]

B1–Br1	2.013(3)	Br1–B1–Br2	110.84(16)
B1–Br2	2.007(3)	Br1–B1–Br3	111.25(16)
B1–Br3	2.017(4)	Br2–B1–Br3	110.25(15)
B1–P1	1.967(3)	Br1–B1–P1	107.21(15)
		Br2–B1–P1	108.62(16)
		Br3–B1–P1	108.55(16)

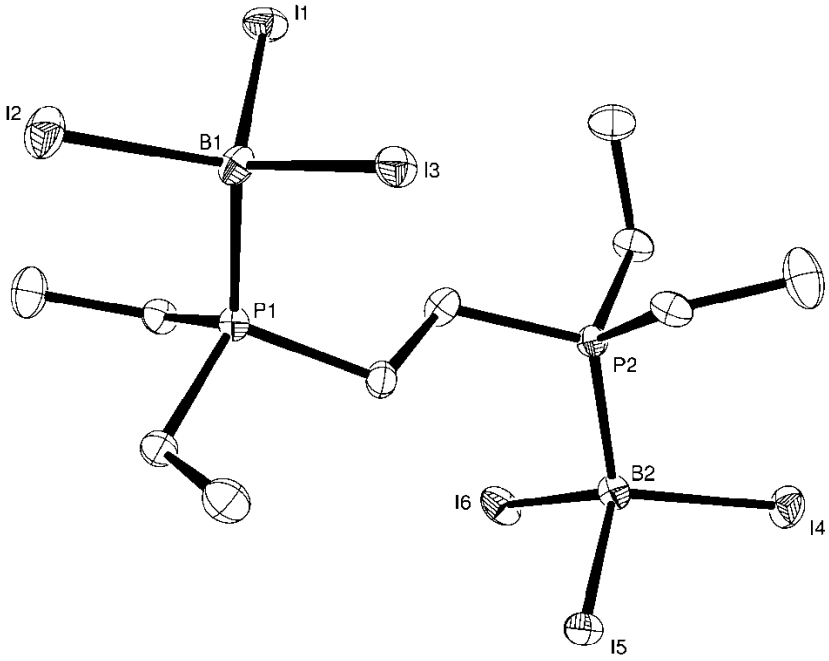

Figure 3.8 The structure of the B1/B2 centred molecule of $[(BI_3)_2\{\mu\text{-}Et_2P(CH_2)_2PEt_2\}]$ showing the atom labelling scheme. Ellipsoids are drawn at the 50% probability level and H atoms are omitted for clarity. The other molecule is similar.

Table 3.7 Selected bond lengths (Å) and angles (°) for $[(BI_3)_2\{\mu\text{-}Et_2P(CH_2)_2PEt_2\}]$

B1–I1	2.253(4)	I1–B1–I2	109.31(14)
B1–I2	2.238(3)	I1–B1–I3	111.72(16)
B1–I3	2.224(3)	I2–B1–I3	110.55(14)
B1–P1	1.966(4)	I1–B1–P1	108.49(15)
B2–I4	2.239(3)	I2–B1–P1	108.48(17)
B2–I5	2.236(4)	I3–B1–P1	108.21(15)
B2–I6	2.237(3)	I4–B2–I5	109.14(15)
B2–P2	1.950(4)	I4–B2–I6	109.78(14)
		I5–B2–I6	112.51(15)
		I4–B2–P2	108.93(16)
		I5–B2–P2	109.49(15)
		I6–B2–P2	106.92(16)

Despite several attempts the crystals of $[(BF_3)_2\{\mu\text{-}Et_2P(CH_2)_2PEt_2\}]$ could not be isolated from the mother liquor, nor the complex be obtained as a solid directly. Invariably a colourless oil was isolated, which was shown by multinuclear NMR spectroscopy to be largely the mono-protonated $[Et_2HP(CH_2)_2PEt_2][BF_4]$ ($\delta(^{31}P)$ = –17.1 (s), 21.9 (d, $^1J_{PH}$ = 512 Hz); $\delta(^{19}F)$ = –150.9), suggesting that the complex is very susceptible to hydrolysis.

However the $[(BX_3)_2\{\mu\text{-}Et_2P(CH_2)_2PEt_2\}]$ (X = Cl, Br, I) could all be isolated as white powders that did not show evidence of hydrolysis (or halide exchange) having occurred in the NMR spectra collected. Multinuclear NMR spectroscopic data are given in Table 3.8; in each case there was a single species present in solution, identified as the neutral bridging ligand complex on the basis of the coupling patterns and the absence of a $[BX_4]^-$ resonance in the ^{11}B NMR spectrum. The IR spectra show the expected ν(BX) stretches for complexes possessing C_{3v} symmetry at boron (for X = Br and I only the antisymmetric (e) stretch is clearly located above 200 cm^{-1}).[61] In the IR spectrum of the iodo complex both ν(^{10}BI) and ν(^{11}BI) stretches are evident at 559 and 535 cm^{-1}. Given the flexibility of $Et_2P(CH_2)_2PEt_2$, it is not surprising that it does not chelate to the small boron centre (covalent radius of 0.84 Å)[62] to give an ionic complex; similar behaviour that has also been observed for flexible neutral multidentate amine ligands such as $Me_2N(CH_2)_2NMe_2$ when reacted directly with the boron trihalide.[13]

Table 3.8 Selected NMR spectroscopic data for $[(BX_3)_2\{\mu\text{-}Et_2P(CH_2)_2PEt_2\}]$ (X = Cl, Br, I)

Complex	$\delta(^1H)$ / 295 K[a]	$\delta(^{31}P\{^1H\})$ / 295 K[a,c]	$\delta(^{11}B)$ / 295 K[b]
$[(BCl_3)_2\{\mu\text{-}Et_2P(CH_2)_2PEt_2\}]$	1.30 (dt) 2.02-2.17 (m) 2.36 (d)	+3.0 $^1J_{PB}$ = 155 Hz	+3.39 (d) $^1J_{BP}$ = 155 Hz
$[(BBr_3)_2\{\mu\text{-}Et_2P(CH_2)_2PEt_2\}]$	1.34 (dt) 2.13-2.28 (m) 2.55 (d)	–0.8 $^1J_{PB}$ = 146 Hz	–14.82 (d) $^1J_{BP}$ = 146 Hz
$[(BI_3)_2\{\mu\text{-}Et_2P(CH_2)_2PEt_2\}]$	1.41 (dt) 2.29-2.45 (m) 2.82 (d)	–11.6 $^1J_{PB}$ = 120 Hz	–72.11 (d) $^1J_{BP}$ = 129 Hz

[a] CD_2Cl_2; [b] CH_2Cl_2/CD_2Cl_2; [c] the expected quartet shows further splitting due to AA'XX' spin system (*vide infra*)

As observed for $[BX_3(PMe_3)]$ (X = F, Cl, Br, I),[42] the resonances in the ^{1}H NMR spectra of $[(BX_3)_2\{\mu\text{-}Et_2P(CH_2)_2PEt_2\}]$ (X = Cl, Br, I) move to successively higher frequencies as the halide gets heavier (Table 3.8). Conversely, though the resonances in the $^{31}P\{^1H\}$ NMR spectra are all to a high frequency of free $Et_2P(CH_2)_2PEt_2$ ($\delta = -18$), this shift gets smaller with increasing halogen atomic number, trends that have also been reported for $[BX_3\{P(CH{=}CH_2)_3\}]$ (X = Cl, Br, I).[26] As expected, the increased shielding of the boron centre upon ligand coordination is seen in the ^{11}B NMR spectra, with $[(BI_3)_2\{\mu\text{-}Et_2P(CH_2)_2PEt_2\}]$ showing the greatest degree of shielding ($\delta(BI_3) = -7.9$,[47] $\Delta = -64.2$; $\delta(BBr_3) = 38.7$,[47] $\Delta = -53.5$; $\delta(BCl_3) = 46.5$,[47] $\Delta = -43.1$), parallel to the generally accepted order of Lewis acidity. Each ^{11}B NMR spectrum consists of a doublet, with the $^1J_{BP}$ coupling constant decreasing as the halide gets heavier. This reduction in $^1J_{BP}$ has been reported for a number of neutral phosphine adducts of BX_3,[26,42,47] and has been attributed to a decrease in the *s* character of the P–B bond with decreasing electronegativity of X,[26] but given the crystallographically determined *d*(B–P) and the modest differences in bond angles between the complexes there are probably several factors influencing the magnitude of $^1J_{BP}$ that are not obvious.[42]

The resonance in the $^{31}P\{^1H\}$ NMR spectrum of $[(BCl_3)_2\{\mu\text{-}Et_2P(CH_2)_2PEt_2\}]$ was not a simple four line pattern as expected from coupling to the quadrupolar ^{11}B nucleus, but instead appeared to be an eight line pattern that could be described as a 'quartet of doublets'. Similar behaviour was observed in the $^{31}P\{^1H\}$ NMR spectra of $[(BX_3)_2\{\mu\text{-}Et_2P(CH_2)_2PEt_2\}]$ (X = Br, I), though the splitting was less well resolved. In order to investigate whether this splitting occurred with other diphosphine ligands, the complex $[(BCl_3)_2\{\mu\text{-}Me_2P(CH_2)_2PMe_2\}]$ was synthesised in an analogous reaction. A microanalysis confirmed the 2:1 (BCl_3 : L–L) stoichiometry of the white powder isolated, while the ν(BCl) stretches in the IR spectrum fell at similar wavenumbers to the corresponding $Et_2P(CH_2)_2PEt_2$ complex. Though less soluble than $[(BCl_3)_2\{\mu\text{-}Et_2P(CH_2)_2PEt_2\}]$, NMR spectra could still be recorded for the $Me_2P(CH_2)_2PMe_2$ complex in CD_2Cl_2, which revealed that the only species present was the bridging ligand complex. The resonances in the ^{1}H and $^{31}P\{^1H\}$ NMR spectra have shifted to much higher frequencies relative to free $Me_2P(CH_2)_2PMe_2$ ($\Delta(^{31}P\{^1H\}) = +44.5$). The doublet in the ^{11}B NMR spectrum has an almost identical chemical shift ($\delta = 3.42$) and $^1J_{BP}$ coupling constant (160 Hz) to the doublet recorded for $[(BCl_3)_2\{\mu\text{-}Et_2P(CH_2)_2PEt_2\}]$ (see Table 3.8), confirming that the boron centre is in a very similar tetrahedral coordination environment.

Importantly, the $^{31}P\{^{1}H\}$ NMR spectrum of $[(BCl_3)_2\{\mu\text{-}Me_2P(CH_2)_2PMe_2\}]$ also showed a similar eight line pattern, with comparable coupling constants. To improve the spectral resolution, a $^{31}P\{^{1}H\}$ NMR spectrum (Figure 3.9) was obtained at 202 MHz by Dr. N. Wells (University of Southampton) using a Bruker AVIIIHD500 FT-NMR spectrometer, which clearly shows an eight line pattern, with coupling constants of 160 and 33 Hz.

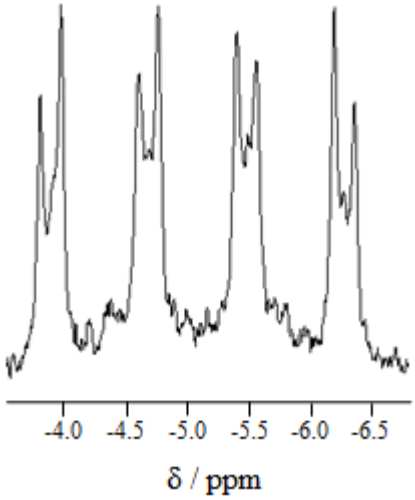

Figure 3.9 $^{31}P\{^{1}H\}$ NMR spectrum of $[(BCl_3)_2\{\mu\text{-}Me_2P(CH_2)_2PMe_2\}]$ in CD_2Cl_2 at 295 K.

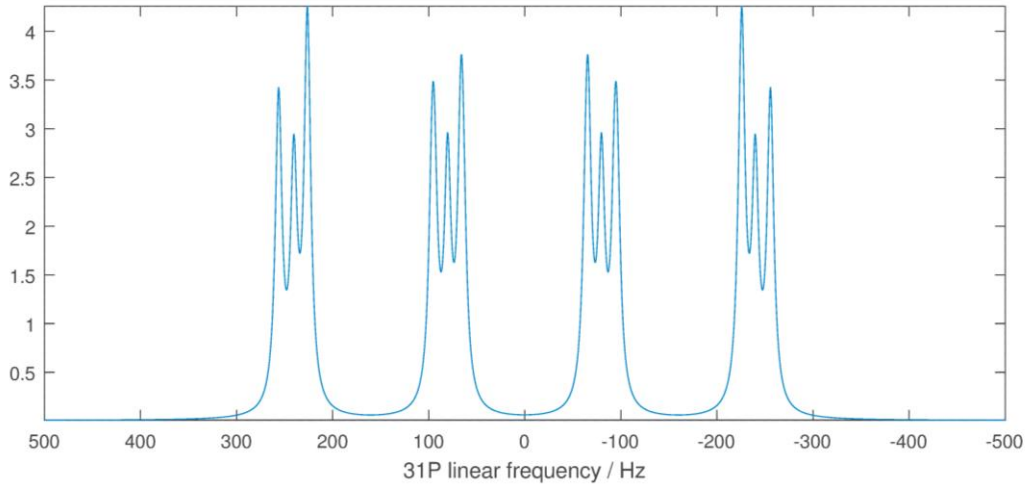

Figure 3.10 Simulated ^{31}P NMR spectrum for an AA'XX' spin system where A = ^{31}P and X = ^{11}B with $J_{AX} = J_{A'X'} = 160$ Hz and $J_{AA'} = 30$ Hz.

This behaviour can be explained if the system is considered to be an AA'XX' spin system where A = ^{31}P and X = ^{11}B. The two phosphorus nuclei are symmetrically equivalent but are not magnetically equivalent and so couple to one another, causing the extra splitting in the spectrum (normally this effect is too small to be observed). To test this theory the ^{31}P NMR spectrum was simulated by Prof. J. Emsley (University of Southampton) using Spinach,[63] a spin dynamics simulation software library. The predicted spectrum with J_{AX} =

$J_{A'X'}$ = 160 Hz, $J_{AA'}$ = 30 Hz (to match the experimentally observed coupling constants) and all other couplings at zero can be seen in Figure 3.10. It is clear that the simulated and recorded spectra are similar, confirming that the extra splitting can be accorded to $^3J_{PP}$ coupling; the lines of lower height between the stronger peaks seen in the simulated spectrum are presumably broadened by a quadrupolar relaxation mechanism to the extent that their existence is only hinted at in the recorded spectrum.

In an attempt to obtain spectroscopic data on a BF_3 complex with a diphosphine ligand, $[BF_3(SMe_2)]$ was reacted with $Me_2P(CH_2)_2PMe_2$ in a 2:1 molar ratio. Microanalysis data on the resulting white powder suggested it was a mixture of species. Though poorly soluble, NMR spectra could be obtained in CD_2Cl_2 which revealed that the major species present in solution was the ligand bridging complex $[(BF_3)_2\{\mu\text{-}Me_2P(CH_2)_2PMe_2\}]$. More strongly coordinating solvents such as CD_3CN caused complex decomposition. At room temperature in CD_2Cl_2 the peaks were broad and unresolved, but once the solution was cooled below 273 K coupling could clearly be seen in the ^{19}F and ^{11}B NMR spectra, and was partially resolved in the $^{31}P\{^1H\}$ NMR spectrum. The chemical shifts and coupling constants of the doublet of quartets in the ^{11}B NMR spectrum (δ = 1.90, $^1J_{BF}$ = 51 Hz , $^1J_{BP}$ = 176 Hz) and the ^{19}F NMR spectrum (δ = –137.2, $^1J_{FB}$ = 51 Hz , $^2J_{FP}$ = 229 Hz) are very similar to those observed for $[BF_3(PMe_3)]$, suggesting that the boron centre is in a comparable tetrahedral coordination environment. Though still shifted to a higher frequency relative to free $Me_2P(CH_2)_2PMe_2$ ($\Delta(^{31}P\{^1H\})$ = ~ +32), the resonance in the $^{31}P\{^1H\}$ NMR spectrum is to a lower frequency of the analogous chloro complex. The fluoroanion $[BF_4]^-$ could also be identified in the ^{19}F and ^{11}B NMR spectra, and these peaks grew in intensity, while in the $^{31}P\{^1H\}$ NMR spectrum a relatively sharp singlet appeared and also grew in intensity over time at δ = –42. This, and the lack of other peaks in the multinuclear NMR spectra, suggests that the complex is decomposing in solution over time, and makes the coexistence of another (e.g ionic) complex unlikely, though further analysis is hampered by solubility issues. In the IR spectrum ν(BF) bands could be identified for both $[(BF_3)_2\{\mu\text{-}Me_2P(CH_2)_2PMe_2\}]$ and $[BF_4]^-$.

3.2.3 Ionic complexes with phosphine ligands

It has been shown that rigid ligands that are preorganised for chelation will react directly with a BF_3 source to form an ionic complex; for example the reaction of $[BF_3(Et_2O)]$ with the bidentate imine ligand 1,10-phenanthroline yielded $[BF_2(phen)][BF_4]$, with no evidence of neutral complex formation.[64] It was therefore decided to react $[BF_3(SMe_2)]$ with

o-$C_6H_4(PMe_2)_2$ (a strong σ-donating diphosphine ligand that is preorganised for chelation and has small steric demands) in a 2:1 molar ratio in CH_2Cl_2, which led to the immediate precipitation of a white powder, the microanalysis results matching the composition $C_{10}H_{16}B_2F_6P_2$. The powder was insoluble in CD_2Cl_2 and decomposed in CD_3CN, and so useful NMR spectroscopic data could not be obtained on the compound. Strong bands corresponding to $[BF_4]^-$ are however evident in the IR spectrum, leading to the formulation of the complex as $[BF_2\{o\text{-}C_6H_4(PMe_2)_2\}][BF_4]$, with a chelating diphosphine ligand. The $[BF_2\{o\text{-}C_6H_4(PMe_2)_2\}]^+$ cation would be expected to possess C_{2v} symmetry, which would result in two IR active ν(BF) stretches. The bands at 1039 and 923 cm^{-1} are assignable as the ν(BF) a_1 and b_1 modes, while a ν(BF) bend is also identifiable at 655 cm^{-1}.

In an attempt to grow crystals of $[BF_2\{o\text{-}C_6H_4(PMe_2)_2\}][BF_4]$, and thereby confirm its structure, the N_2 atmosphere in a Schlenk containing a very dilute solution of *o*-$C_6H_4(PMe_2)_2$ in hexane was replaced with BF_3 gas. A white phase at the top of the hexane was immediately visible, which rapidly led to the precipitation of a white powder. This was shown by microanalysis and IR spectroscopy to be the same compound as the powder obtained from the reaction with $[BF_3(SMe_2)]$ in CH_2Cl_2. That no single crystals could be grown via this diffusion technique highlights how rapid the reactions between boron(III) halides and phosphine ligands are.

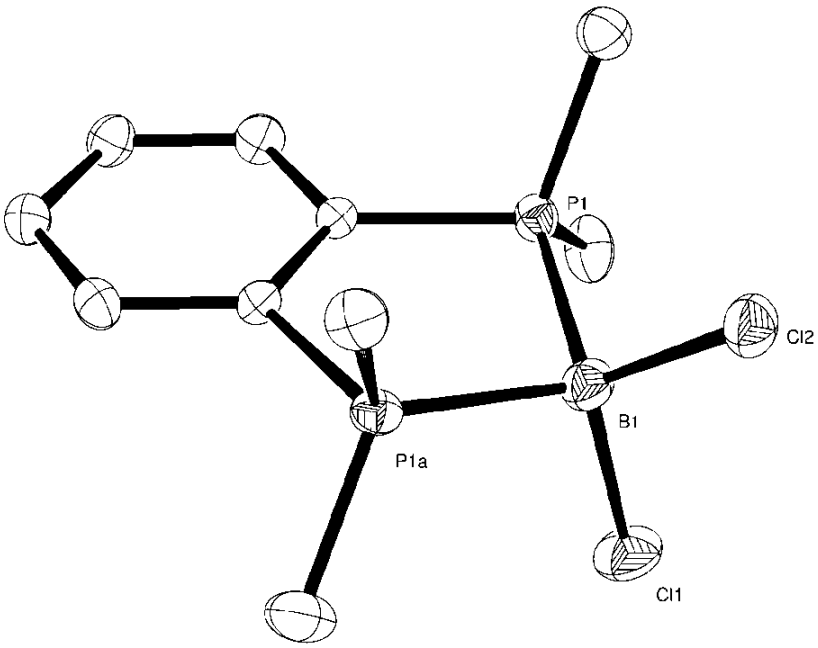

Figure 3.11 The structure of the cation in $[BCl_2\{o\text{-}C_6H_4(PMe_2)_2\}][BCl_4]$ showing the atom labelling scheme. Ellipsoids are drawn at the 50% probability level and H atoms are omitted for clarity. Symmetry operation: a = – x, y, z.

Table 3.9 Selected bond lengths (Å) and angles (°) for $[BCl_2\{o\text{-}C_6H_4(PMe_2)_2\}]^+$

B1–Cl1	1.836(5)	Cl1–B1–Cl2	115.0(3)
B1–Cl2	1.832(4)	Cl1–B1–P1	109.22(17)
B1–P1	1.990(3)	Cl2–B1–P1	111.24(18)
		P1–B1–P1a	99.8(2)

The reaction of two equivalents of $[BCl_3(SMe_2)]$ with one equivalent of $o\text{-}C_6H_4(PMe_2)_2$ in CH_2Cl_2 yielded crystals (upon layering with hexane) which X-ray analysis identified as $[BCl_2\{o\text{-}C_6H_4(PMe_2)_2\}][BCl_4]$ (Figure 3.11). Crystals grown in an analogous reaction with BBr_3 were shown to be $[BBr_2\{o\text{-}C_6H_4(PMe_2)_2\}][BBr_4]$ (Figure 3.12), while the reaction with BI_3 (which was kept covered to avoid unnecessary exposure to light) yielded crystals of $[BI_2\{o\text{-}C_6H_4(PMe_2)_2\}][I_3]$ (Figure 3.13). While there are numerous crystal structures containing $[BCl_4]^-$, and several with $[BBr_4]^-$, there is only one crystallographically authenticated example of $[BI_4]^-$ in $[Ph_3PCH_2P(OBI_3)Ph_2][BI_4]$,[65] suggesting that it does not readily crystallise. Instead the counterion is a *pseudo*-linear $[I_3]^-$ anion, formed presumably by the decomposition of $[BI_4]^-$ and/or BI_3. These complexes are the first crystallographically authenticated examples of boronium cations with a neutral phosphine ligand.

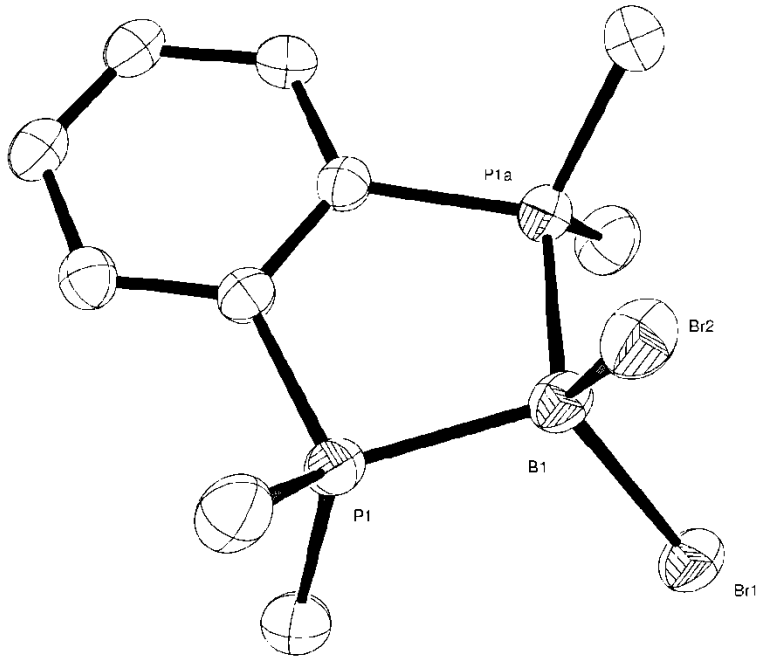

Figure 3.12 The structure of the cation in $[BBr_2\{o\text{-}C_6H_4(PMe_2)_2\}][BBr_4]$ showing the atom labelling scheme. Ellipsoids are drawn at the 50% probability level and H atoms are omitted for clarity. Symmetry operation: a = x, 1/2 – y, z.

Table 3.10 Selected bond lengths (Å) and angles (°) for $[BBr_2\{o\text{-}C_6H_4(PMe_2)_2\}]^+$

B1–Br1	2.003(6)	Br1–B1–Br2	114.8(3)
B1–Br2	2.007(6)	Br1–B1–P1	111.7(2)
B1–P1	1.974(4)	Br2–B1–P1	108.3(2)
		P1–B1–P1a	101.1(3)

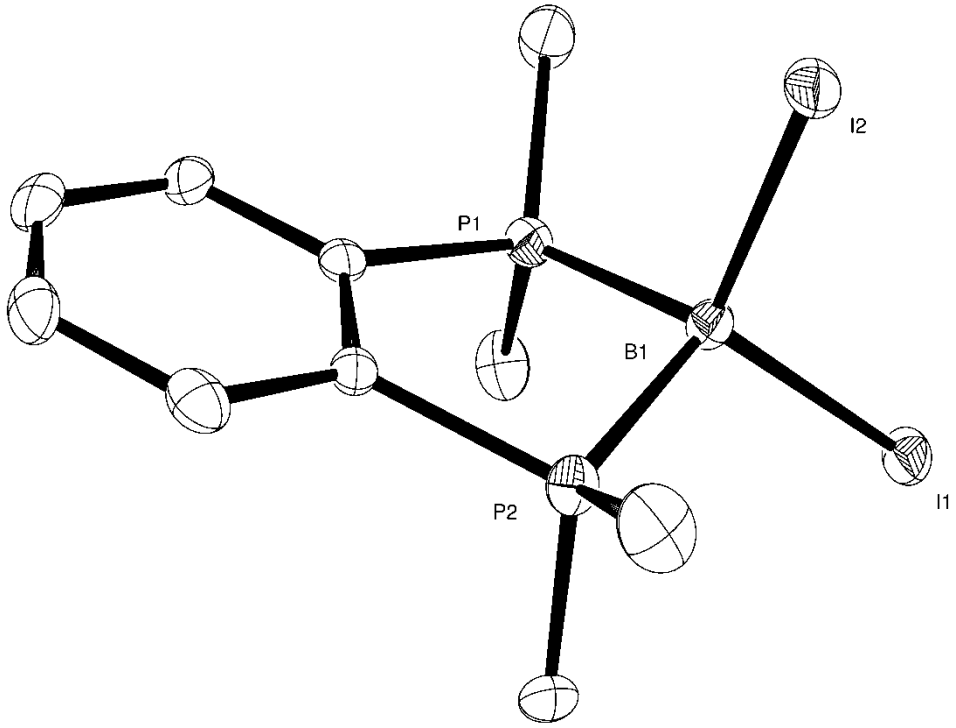

Figure 3.13 The structure of the cation in $[BI_2\{o\text{-}C_6H_4(PMe_2)_2\}][I_3]$ showing the atom labelling scheme. Ellipsoids are drawn at the 50% probability level and H atoms are omitted for clarity.

Table 3.11 Selected bond lengths (Å) and angles (°) for $[BI_2\{o\text{-}C_6H_4(PMe_2)_2\}]^+$

B1–I1	2.197(6)	I1–B1–I2	114.1(3)
B1–I2	2.224(6)	I1–B1–P1	113.5(3)
B1–P1	1.961(6)	I2–B1–P1	107.6(3)
B1–P2	1.930(7)	I1–B1–P2	112.6(3)
		I2–B1–P2	108.5(3)
		P1–B1–P2	99.4(3)

All three $[BX_2\{o\text{-}C_6H_4(PMe_2)_2\}]^+$ cations have tetrahedral boron centres (C_{2v} geometry), distorted by the small chelate bite of $o\text{-}C_6H_4(PMe_2)_2$ (∠P–B–P = ~ 100°). The angles around the boron are little affected by the halide present. Unlike the symmetric chelation seen in the chloro and bromo complexes, in $[BI_2\{o\text{-}C_6H_4(PMe_2)_2\}]^+$ the diphosphine is asymmetrically chelated, with *d*(B–P) = 1.961(6) and 1.930(7) Å. As the halide gets heavier there is a decrease in the *d*(B–P), but, as seen for $[(BX_3)_2\{\mu\text{-}Et_2P(CH_2)_2PEt_2\}]$ (X = Cl, Br, I), the difference is not significant once the bond length errors are taken into account. As a cation, the *d*(B–X) are ~0.02 Å shorter in $[BX_2\{o\text{-}C_6H_4(PMe_2)_2\}]^+$ compared to $[BX_3(PMe_3)]$ (X = Cl, Br, I).[27] The tetrahedral $[BCl_4]^-$ and $[BBr_4]^-$ anions have slightly longer *d*(B–X) than the cations. The $[I_3]^-$ anion has *d*(I–I) of 2.8851(7) and 2.9459(7) Å and a ∠I–I–I of 175.77(2)°, similar to other reported crystal structures containing $[I_3]^-$.[66]

Though multinuclear NMR spectroscopy confirmed that the bulk powders obtained from the reaction of BX_3 (X = Br, I) with $o\text{-}C_6H_4(PMe_2)_2$ in CH_2Cl_2 contained the corresponding $[BX_2\{o\text{-}C_6H_4(PMe_2)_2\}]^+$ cation, the microanalysis data were not consistent with the X-ray structures. It has been reported that CH_2Cl_2 will undergo halide exchange with halogens other than fluorine when present either as X^- or $[BX_4]^-$.[67] For the bromo and iodo complexes halogen exchange between anion and solvent therefore presumably occurred, which explains the inconsistent microanalysis data and the discolouration of the reaction solutions over time. To obtain a pure bulk sample of $[BBr_2\{o\text{-}C_6H_4(PMe_2)_2\}][BBr_4]$, BBr_3 was reacted with $o\text{-}C_6H_4(PMe_2)_2$ in hexane. This led to the immediate precipitation of the desired complex in high yield, which analysed correctly by microanalysis. Given the successes of this method with BF_3 and BBr_3 it suggests that an alternative route to obtaining boron(III) halide – phosphine complexes in good yield therefore is by direct reaction in hexane.

Once the bulk powders had been isolated, NMR spectroscopic analysis could be performed on them in CD_2Cl_2 (in which they show modest solubility), with no evidence of halide exchange or hydrolysis of the complexes occurring. The IR and ^{11}B NMR spectra of $[BX_2\{o\text{-}C_6H_4(PMe_2)_2\}][BX_4]$ (X = Cl, Br) confirm the presence of $[BX_4]^-$ in the bulk powders.[59,67] IR and ^{11}B NMR spectroscopic analysis of the bulk powder obtained from the reaction of BI_3 and $o\text{-}C_6H_4(PMe_2)_2$ in CH_2Cl_2 confirm that no $[BI_4]^-$ (or any other mixed tetrahaloborate anion) is present,[67,68] suggesting that the $[BI_4]^-$ anion is either not formed during the reaction or decomposes rapidly to form I_2 and (poly)iodides. Multinuclear NMR spectroscopic data for the $[BX_2\{o\text{-}C_6H_4(PMe_2)_2\}]^+$ (X = Cl, Br, I) cations are given in Table 3.12. The coupling patterns seen in the $^{31}P\{^1H\}$ and ^{11}B NMR spectra are consistent

with a BX_2 moiety coordinated to a chelating diphosphine ligand. The resonances in the ^1H NMR spectra shift to higher frequency as the halide gets heavier, while the resonances in the $^{31}P\{^1H\}$ NMR spectra have shifted to a much higher frequency from free *o*-$C_6H_4(PMe_2)_2$ ($\delta = -55$) and differ very little with X. Consistent with other phosphine complexes, the $^1J_{BP}$ coupling constant gets smaller as the atomic number of the halogen increases. There is however no clear trend in the shielding of the boron centre when moving from a $[BX_3L]$ to a $[BX_2(L–L)]+$ complex as the resonance in the ^{11}B NMR spectrum of $[BCl_2\{o\text{-}C_6H_4(PMe_2)_2\}]^+$ is to a lower frequency of that of $[(BCl_3)_2\{\mu\text{-}Et_2P(CH_2)_2PEt_2\}]$, but $[BI_2\{o\text{-}C_6H_4(PMe_2)_2\}]^+$ is at a much higher frequency than $[(BI_3)_2\{\mu\text{-}Et_2P(CH_2)_2PEt_2\}]$.

Table 3.12 Selected NMR spectroscopic data for $[BX_2\{o\text{-}C_6H_4(PMe_2)_2\}]^+$ (X = Cl, Br, I)

Complex Cation	$\delta(^1H)$ CH_3 / 295 K[a]	$\delta(^{31}P\{^1H\})$ / 295 K[b]	$\delta(^{11}B)$ / 295 K[b]
$[BCl_2\{o\text{-}C_6H_4(PMe_2)_2\}]^+$	2.06 (t)	+7.5 (q) $^1J_{PB}$ = 125 Hz	–3.17 (t) $^1J_{BP}$ = 125 Hz
$[BBr_2\{o\text{-}C_6H_4(PMe_2)_2\}]^+$	2.23 (t)	+7.7 (q) $^1J_{PB}$ = 119 Hz	–14.02 (t) $^1J_{BP}$ = 119 Hz
$[BI_2\{o\text{-}C_6H_4(PMe_2)_2\}]^+$	2.34-2.37 (m)	+7.2 (q) $^1J_{PB}$ = 110 Hz	–43.5 (t) $^1J_{BP}$ = 111 Hz

[a] CD_2Cl_2; [b] CH_2Cl_2/CD_2Cl_2

The reaction of $[BCl_3(SMe_2)]$ with *o*-$C_6H_4(PPh_2)_2$ in a 2:1 molar ratio in CH_2Cl_2 resulted in the recovery of uncoordinated *o*-$C_6H_4(PPh_2)_2$ at the end of the reaction. Though *o*-$C_6H_4(PPh_2)_2$ is preorganised for chelation its much greater steric bulk must prevent it from coordinating to the small boron centre, either as a chelating or κ^1-coordinating ligand. Electronic effects are unlikely to be involved as PPh_3, a monodentate phosphine with a similar σ-donor strength, readily forms complexes with BX_3.[69] This result highlights the requirement of phosphine ligands to be sterically small, particularly for diphosphine ligands able to chelate to boron.

3.2.4 Complexes with the diarsine ligand *o*-$C_6H_4(AsMe_2)_2$

While $[BX_3(AsR_3)]$ (R = Me, Ph; X = F, Cl, Br, I) have been studied by IR and NMR spectroscopy,[69-71] and the crystal structures of $[BX_3(AsMe_3)]$ (X = Cl, Br, I) are known,[31] there have been no reported syntheses of boron(III) halide complexes with neutral

bidentate arsine ligands. Focus therefore was on reactions with the rigid diarsine, *o*-$C_6H_4(AsMe_2)_2$, with the expectation that it would form ionic complexes like its phosphine analogue. The reaction of $[BCl_3(SMe_2)]$ with *o*-$C_6H_4(AsMe_2)_2$ in a 2:1 molar ratio yielded a few colourless single crystals of $[BCl_2\{o\text{-}C_6H_4(AsMe_2)_2\}][BCl_4]$ (Figure 3.14), with a *pseudo*-tetrahedral cation and a tetrahedral anion. The complex is the first example of a boron(III) halide complex with a neutral diarsine ligand, and also the first example of an boronium cation with a neutral arsine ligand.

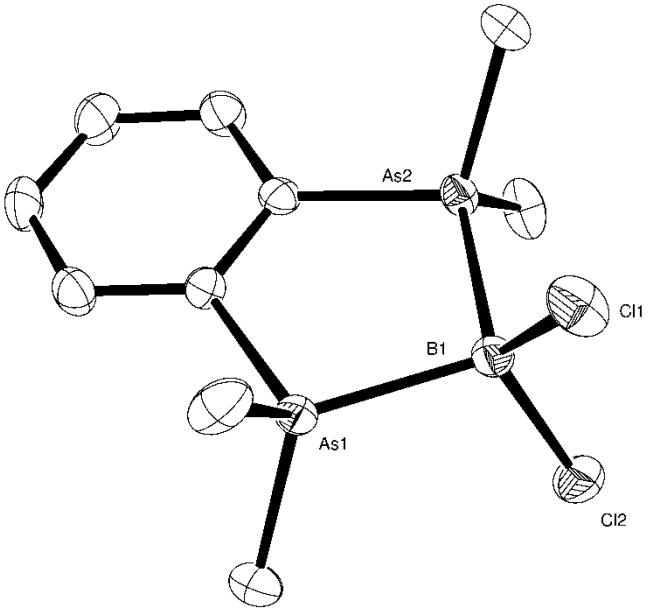

Figure 3.14 The structure of the cation in $[BCl_2\{o\text{-}C_6H_4(AsMe_2)_2\}][BCl_4]$ showing the atom labelling scheme. Ellipsoids are drawn at the 50% probability level and H atoms are omitted for clarity.

Table 3.13 Selected bond lengths (Å) and angles (°) for $[BCl_2\{o\text{-}C_6H_4(AsMe_2)_2\}]^+$

B1–Cl1	1.819(3)	Cl1–B1–Cl2	114.51(16)
B1–Cl2	1.815(3)	Cl1–B1–As1	110.20(16)
B1–As1	2.067(3)	Cl2–B1–As1	110.54(15)
B1–As2	2.083(3)	Cl1–B1–As2	110.05(15)
		Cl2–B1–As2	110.97(16)
		As1–B1–As2	99.57(13)

Though the chelating *o*-$C_6H_4(AsMe_2)_2$ ligand is asymmetrically coordinated, the coordination environment around the boron centre in $[BCl_2\{o\text{-}C_6H_4(EMe_2)_2\}]^+$ (E = P, As)

is otherwise little affected by the change in donor atom from phosphorus to arsenic; the cations feature similar angles around the boron centre, and the differences in *d*(B–Cl) are small (the *d*(B–Cl) are ~0.015 Å shorter for the diarsine, consistent with its weaker Lewis basicity). As expected for ligands that only coordinate relatively weakly to boron, the *d*(B–As) and *d*(B–Cl) are comparable to those seen for $[BCl_3(AsMe_3)]$.[31]

It was not possible to isolate either the crystals or a pure bulk solid from several reaction attempts either in CH_2Cl_2 or hexane, with spectroscopic data on the sticky white solids recovered showing either uncoordinated *o*-$C_6H_4(AsMe_2)_2$ or a mixture of compounds that were difficult to identify. Similarly, free *o*-$C_6H_4(AsMe_2)_2$ was the only product isolated from the reaction of $[BF_3(SMe_2)]$ with *o*-$C_6H_4(AsMe_2)_2$ in a 2:1 molar ratio in CH_2Cl_2, suggesting that the diarsine may not be a good enough donor to displace the SMe_2 from BF_3, while the small amount of white powder isolated from the direct reaction of BF_3 with *o*-$C_6H_4(AsMe_2)_2$ was difficult to characterise owing to its poor solubility in weakly coordinating NMR solvents. The difficulties encountered in isolating a pure bulk solid from these reactions of *o*-$C_6H_4(AsMe_2)_2$ with BX_3 (X = F, Cl) are most probably caused by the greater orbital size mismatch between arsenic and boron, and the ionic nature of the complexes, which means that several anions (such as $[BX_4]^-$ or X^-) are possible. Similar issues were encountered when trying to isolate solids from the reactions of *o*-$C_6H_4(AsMe_2)_2$ with AlX_3 (X = Cl, Br, I) (see Section 2.2.5).

3.3 Conclusions

The boron(III) halides have been shown to complex to a number of neutral alkyl phosphine ligands, with several novel four-coordinate diphosphine complexes having been synthesised and characterised both structurally and spectroscopically. The X-ray crystal structure of $[BF_3(PMe_3)]$ has been solved for the first time, allowing structural comparisons to be made with $[BX_3(PMe_3)]$ (X = Cl, Br, I).[27] It was shown that with the flexible diphosphine ligands $R_2P(CH_2)_2PR_2$ (R = Me, Et) the only complexes observed were the neutral bridging ligand complexes $[(BX_3)_2\{\mu\text{-}R_2P(CH_2)_2PR_2\}]$ (X = F, Cl, Br, I). Ionic complexes are exclusively formed however with sterically small and rigid bidentate ligands that are preorganised for chelation, and this work includes the first structurally authenticated examples of ionic boron(III) halide complexes with chelating neutral diphosphine and diarsine ligands, $[BX_2\{o\text{-}C_6H_4(PMe_2)_2\}]^+$ (X = Cl, Br, I) and $[BCl_2\{o\text{-}C_6H_4(AsMe_2)_2\}]^+$, which possess C_{2v} symmetry at boron. The phosphine complexes all show very large high frequency shifts relative to free ligand in their $^{31}P\{^1H\}$ NMR spectra, which are much larger in magnitude than those observed in the corresponding AlX_3 systems (see Section 2.2). In the ^{11}B NMR spectra $^1J_{BP}$ decreases as the atomic number of the halogen increases, a trend that has been reported for a number of neutral phosphine adducts of BX_3.[26,42,47] Although the differences are sometimes small (and may not be considered significant once the bond length errors are taken into account), for all the X-ray structures reported the *d*(B–P) decrease as the halide gets heavier, which is consistent with the order of Lewis acidity being $BI_3 > BBr_3 > BCl_3 > BF_3$.

The behaviour of BX_3 (X = F, Cl) towards the neutral phosphine oxide ligands $OPMe_3$ and $Ph_2P(O)CH_2P(O)Ph_2$ has also been investigated, the latter of which was of particular interest as diphosphine dioxide complexes have not been studied before. Unexpectedly for a flexible bidentate ligand, the X-ray crystal structure of the ionic chelating ligand complex $[BF_2\{Ph_2P(O)CH_2P(O)Ph_2\}][B_2F_7]$ was obtained. However multinuclear NMR spectroscopic data showed that in solution the ionic complex was actually in equilibrium with the neutral bridging ligand complex $[(BF_3)_2\{\mu\text{-}Ph_2P(O)CH_2P(O)Ph_2\}]$. In the BCl_3 system there was no evidence of the ionic complex forming, and so its existence in the BF_3 system was attributed to the formation of the unusual $[B_2F_7]^-$ anion.

The phosphine complexes with BX_3 (X = Cl, Br, I) were found to be robust, showing little sign of oxidation or hydrolysis in CH_2Cl_2 solution or when stored over time under an inert atmosphere. Complexes with BF_3 were found to be more prone to hydrolysis in solution.

3.4 Experimental

The general experimental techniques used in this chapter can be found in Appendix 1 at the end of the thesis.

[$BF_3(OPMe_3)$]

To a solution of $OPMe_3$ (0.100 g, 1.09 mmol) in CH_2Cl_2 (5 mL) was added [$BF_3(SMe_2)$] (0.141 g, 1.09 mmol) in CH_2Cl_2 (5 mL). The resulting colourless solution was stirred for 3 h. The solvent was then removed *in vacuo* and the resulting white precipitate was washed with hexane (1 mL) and dried *in vacuo* to give a white powder. Yield: 0.092 g (53%). Anal. Calc. for $C_3H_9BF_3OP$: C, 22.5; H, 5.7. Found: C, 22.5; H, 5.8%. ^{1}H NMR (CD_2Cl_2, 295 K): δ = 1.85 (d, $^2J_{HP}$ = 12.0 Hz, CH_3). ^{19}F NMR (CD_2Cl_2, 295 K): δ = –146.2 (br s). ^{31}P{^{1}H} NMR (CD_2Cl_2, 295 K): δ = 69.2 (q, $^3J_{PF}$ = 8 Hz). ^{11}B NMR (CH_2Cl_2/CD_2Cl_2, 295 K): δ = 0.11 (s). IR (Nujol): ν = 1092 (vs, br) (PO), 899 (s, br) (BF) cm^{-1}.

[$BCl_3(OPMe_3)$]

To a solution of $OPMe_3$ (0.035 g, 0.38 mmol) in CH_2Cl_2 (5 mL) was added [$BCl_3(SMe_2)$] (0.068 g, 0.38 mmol) in CH_2Cl_2 (5 mL). The resulting colourless solution was stirred for 2 h, then the solvent volume was reduced to about 3 ml *in vacuo*, onto which hexane (7 mL) was layered. The white precipitate that formed was isolated by filtration and dried *in vacuo*. Yield: 0.056 g (71%). Anal. Calc. for $C_3H_9BCl_3OP$: C, 17.2; H, 4.3. Found: C, 17.1; H, 4.2%. ^{1}H NMR (CD_2Cl_2, 295 K): δ = 2.06 (d, $^2J_{HP}$ = 13.5 Hz, CH_3). ^{31}P{^{1}H} NMR (CD_2Cl_2, 295 K): δ = 75.4 (s). ^{11}B NMR (CH_2Cl_2/CD_2Cl_2, 295 K): δ = 7.03 (s). IR (Nujol): ν = 1084 (vs, br) (PO), 712 (vs, br), 371 (m) (BCl) cm^{-1}.

Reaction of [$BF_3(SMe_2)$] with $Ph_2P(O)CH_2P(O)Ph_2$

To a solution of $Ph_2P(O)CH_2P(O)Ph_2$ (0.200 g, 0.48 mmol) in CH_2Cl_2 (5 mL) was added [$BF_3(SMe_2)$] (0.124 g, 0.95 mmol) in CH_2Cl_2 (5 mL) to form a colourless solution which was stirred for 1 h. The solvent volume was reduced to about 5 mL *in vacuo*, onto which hexane (10 mL) was layered. Colourless crystals formed which were identified as [$BF_2\{Ph_2P(O)CH_2P(O)Ph_2\}$][$B_2F_7$] by single crystal X-ray diffraction study. These were isolated by filtration, washed with Et_2O (10 mL) and dried *in vacuo* to give a white

powder. Yield: 0.121 g. ^{1}H NMR (CD_2Cl_2, 295 K): δ = 4.38 (t, $^{2}J_{HP}$ = 14.8 Hz, CH_2), 4.55 (t, $^{2}J_{HP}$ = 12.6 Hz, CH_2), 7.52-7.90 (m, C_6H_5). ^{19}F NMR (CD_2Cl_2, 295 K): δ = –149.8 (s, $[BF_4]^-$), –142.9 (d, $^{3}J_{FP}$ = 6 Hz), –138.2 (t, $^{3}J_{FP}$ = 9 Hz). ^{31}P{^{1}H} NMR (CD_2Cl_2, 295 Hz): δ = 44.2 (s), 50.0 (t, $^{3}J_{PF}$ = 9 Hz). ^{11}B NMR (CH_2Cl_2/CD_2Cl_2, 295 K): 0.15 (s, $[BF_4]^-$), 0.51 (br s).

[$(BCl_3)_2${μ-$Ph_2P(O)CH_2P(O)Ph_2$}]

To a solution of $Ph_2P(O)CH_2P(O)Ph_2$ (0.100 g, 0.24 mmol) in CH_2Cl_2 (5 mL) was added [$BCl_3(SMe_2)$] (0.086 g, 0.48 mmol) in CH_2Cl_2 (5 mL) and the resulting solution was stirred for 1.5 h. The solvent volume was reduced to about 2 mL *in vacuo* whereupon a white precipitate formed. This was isolated by filtration and dried *in vacuo* to yield a white powder. Yield: 0.037 g (24%). Anal. Calc. for $C_{25}H_{22}B_2Cl_6O_2P_2$: C, 46.1; H, 3.4. Found: C, 46.1; H, 3.4%. Small colourless crystals suitable for single crystal X-ray diffraction study were grown by layering the filtrate with hexane (5 mL). ^{1}H NMR (CD_2Cl_2, 295 K): δ = 4.83 (t, $^{2}J_{HP}$ = 14.9 Hz, CH_2), 7.55-7.79 (m, C_6H_5). ^{31}P{^{1}H} NMR (CD_2Cl_2, 295 K): δ = 49.5 (s). ^{11}B NMR (CH_2Cl_2/CD_2Cl_2, 295 K): δ = 7.78 (s). IR (Nujol): ν = 1065 (vs) (PO), 718 (s, br), 472 (m) (BCl) cm^{-1}.

[$BF_3(PMe_3)$]

To a solution of PMe_3 (0.098 g, 1.29 mmol) in CH_2Cl_2 (5 mL) was added [$BF_3(SMe_2)$] (0.170 g, 1.31 mmol) in CH_2Cl_2 (5 mL) to give a colourless solution which was stirred for 2.5 h. The solvent volume was reduced to about 5 mL *in vacuo*, onto which hexane (8 mL) was layered. Colourless crystals suitable for single crystal X-ray diffraction study formed. These were isolated by filtration and dried *in vacuo* to give a white powder. Yield: 0.089 g (48%). Anal. Calc. for $C_3H_9BF_3P$: C, 25.0; H, 6.3. Found: C, 24.9; H, 6.2%. ^{1}H NMR (CD_2Cl_2, 295 K): 1.41 (d, $^{2}J_{HP}$ = 11.3 Hz, CH_3). ^{19}F NMR (CD_2Cl_2, 295 K): δ = –140.1 (dq, $^{1}J_{FB}$ = 51 Hz , $^{2}J_{FP}$ = 236 Hz). ^{31}P{^{1}H} NMR (CD_2Cl_2): δ = –28.5 (qq, $^{1}J_{PB}$ = 176 Hz, $^{2}J_{PF}$ = 236 Hz). ^{11}B NMR (CH_2Cl_2/CD_2Cl_2, 295 K): δ = 1.88 (dq, $^{1}J_{BF}$ = 50 Hz, $^{1}J_{BP}$ = 176 Hz). IR (Nujol): ν = 1060 (vs, br), 768 (s), 635 (vs) (BF) cm^{-1}.

[$(BF_3)_2${μ-$Et_2P(CH_2)_2PEt_2$}]

To a solution of [$BF_3(SMe_2)$] (0.128 g, 0.99 mmol) in CH_2Cl_2 (5 mL) was added $Et_2P(CH_2)_2PEt_2$ (0.102 g, 0.49 mmol) in CH_2Cl_2 (5 mL) to give a colourless solution which was stirred for 2 h. The solvent volume was reduced to about 5 mL *in vacuo*, then the solution was layered with hexane (8 mL) whereupon small colourless crystals suitable for single crystal X-ray diffraction study grew. Despite several attempts the crystals could not be isolated for satisfactory spectroscopic analysis, with a colourless oil instead being obtained.

[$(BCl_3)_2${μ-$Et_2P(CH_2)_2PEt_2$}]

To a solution of [$BCl_3(SMe_2)$] (0.130 g, 0.72 mmol) in CH_2Cl_2 (5 mL) was added $Et_2P(CH_2)_2PEt_2$ (0.075 g, 0.36 mmol) in CH_2Cl_2 (5 mL) to give a colourless solution which was stirred for 2 h. The solvent volume was reduced to about 2.5 mL *in vacuo* whereupon a white powder precipitated out. The powder was isolated by filtration and dried *in vacuo*. Yield: 0.082 g (51%). Anal. Calc. for $C_{10}H_{24}B_2Cl_6P_2$: C, 27.3; H, 5.5. Found: C, 27.4; H, 5.6%. ^{1}H NMR (CD_2Cl_2, 295 K): δ = 1.30 (dt, [12H], CH_3), 2.02-2.17 (m, [8H], CH_2), 2.36 (d, [4H], CH_2). ^{31}P{^{1}H} NMR (CD_2Cl_2, 295 K): δ = 3.0 (*see Section 3.2.2*, $^1J_{PB}$ = 155 Hz). ^{11}B NMR (CH_2Cl_2/CD_2Cl_2, 295 K): δ = 3.39 (d, $^1J_{BP}$ = 155 Hz). IR (Nujol): ν =710 (vs), 389 (m) (BCl) cm^{-1}. Small colourless crystals suitable for single crystal X-ray diffraction study were obtained from layering the filtrate with hexane (5 mL).

[$(BBr_3)_2${μ-$Et_2P(CH_2)_2PEt_2$}]

To a solution of BBr_3 (0.124 g, 0.50 mmol) in CH_2Cl_2 (5 mL) was added $Et_2P(CH_2)_2PEt_2$ (0.053 g, 0.26 mmol) in CH_2Cl_2 (5 mL) to give a colourless solution which was stirred for 2 h. The solvent volume was reduced to about 3 mL *in vacuo* whereupon a white powder precipitated out. The powder was isolated by filtration and dried *in vacuo*. Small colourless crystals suitable for single crystal X-ray diffraction study were obtained from layering the filtrate with hexane (7 mL). Concentrating the filtrate *in vacuo* to about 3 mL afforded a second crop of white powder, which was isolated by filtration and dried *in vacuo*. The overall yield was 0.110 g (63%). Anal. Calc. for $C_{10}H_{24}B_2Br_6P_2$: C, 17.0; H, 3.4. Found: C, 17.1; H, 3.4%. ^{1}H NMR (CD_2Cl_2, 295 K): δ = 1.34 (dt, [12H], CH_3), 2.13-2.28 (m, [8H], CH_2), 2.55 (d, [4H], CH_2). ^{31}P{^{1}H} NMR (CD_2Cl_2, 295 K): δ = –0.8 (*see Section 3.2.2*,

$^{1}J_{PB}$ = 146 Hz). ^{11}B NMR (CH_2Cl_2/CD_2Cl_2, 295 K): δ = –14.82 (d, $^{1}J_{BP}$ = 146 Hz). IR (Nujol): ν = 613 (vs) (BBr) cm^{-1}.

[$(BI_3)_2${μ-$Et_2P(CH_2)_2PEt_2$}]

To a solution of BI_3 (0.114 g, 0.29 mmol) in CH_2Cl_2 (5 mL) was added $Et_2P(CH_2)_2PEt_2$ (0.031 g, 0.15 mmol) in CH_2Cl_2 (5 mL) to give a colourless solution which was stirred for 2 h. The solvent volume was reduced to about 3 mL *in vacuo*, then the solution was layered with hexane (5 mL). Large colourless block crystals suitable for single crystal X-ray diffraction study were obtained. The solvent volume was reduced to about 2 mL *in vacuo*, and the resulting white powder was isolated by filtration and dried *in vacuo*. Yield: 0.089 g (62%). Anal. Calc. for $C_{10}H_{24}B_2I_6P_2$: C, 12.1; H, 2.5. Found: C, 12.3; H, 2.5%. ^{1}H NMR (CD_2Cl_2, 295 K): δ = 1.41 (dt, [12H], CH_3), 2.29-2.45 (m, [8H], CH_2), 2.82 (d, [4H], CH_2). ^{31}P{^{1}H} NMR (CD_2Cl_2, 295 K): δ = –11.6 (*see Section 3.2.2*, $^{1}J_{PB}$ = 120 Hz). ^{11}B NMR (CH_2Cl_2/CD_2Cl_2, 295 K): δ = –72.11 (d, $^{1}J_{BP}$ = 129 Hz). IR (Nujol): ν = 559 (vs), 535 (vs) (BI) cm^{-1}.

Reaction of $[BF_3(SMe_2)]$ with $Me_2P(CH_2)_2PMe_2$

To a solution of $[BF_3(SMe_2)]$ (0.130 g, 1.00 mmol) in CH_2Cl_2 (5 mL) was added $Me_2P(CH_2)_2PMe_2$ (0.075 g, 0.50 mmol) in CH_2Cl_2 (5 mL) which immediately led to the precipitation of a white solid. The reaction was stirred for 1 h, then the white powder was isolated by filtration and dried *in vacuo*. Yield: 0.053 g. *Spectroscopic data obtained for [$(BF_3)_2${μ-$Me_2P(CH_2)_2PMe_2$}] from mixture:* ^{1}H NMR (CD_2Cl_2, 295 K): δ = 1.37 (br s, [12H], CH_3), 1.84 (br s, [4H], CH_2). ^{19}F NMR (CH_2Cl_2/CD_2Cl_2, 295 K): δ = –137.2 (br d); (273 K): –137.2 (dq, $^{1}J_{FB}$ = 51 Hz , $^{2}J_{FP}$ = 229 Hz). ^{31}P{^{1}H} NMR (CH_2Cl_2/CD_2Cl_2, 295 K): δ = –17.7 (br s); (223 K): –20.4 - –13.0 (m). ^{11}B NMR (CH_2Cl_2/CD_2Cl_2, 295 K): δ = 2.08 (br s); (223 K): 1.90 (dq, $^{1}J_{BF}$ = 51 Hz , $^{1}J_{BP}$ = 176 Hz). IR (Nujol): ν = 1039 (vs), 852 (s), 634 (s) (BF) cm^{-1}.

[$(BCl_3)_2${μ-$Me_2P(CH_2)_2PMe_2$}]

To a solution of $[BCl_3(SMe_2)]$ (0.119 g, 0.66 mmol) in CH_2Cl_2 (5 mL) was added $Me_2P(CH_2)_2PMe_2$ (0.050 g, 0.33 mmol) in CH_2Cl_2 (5 mL) which immediately led to the

precipitation of a white solid. The reaction was stirred for 1 h, then the white powder was isolated by filtration and dried *in vacuo*. Yield: 0.072 g (56%). Anal. Calc. for $C_6H_{16}B_2Cl_6P_2$: C, 18.7; H, 4.2. Found: C, 18.8; H, 4.1%. ^{1}H NMR (CD_2Cl_2, 295 K): δ = 1.63 (d, [12H], CH_3), 2.36 (d, [4H], CH_2). ^{31}P{^{1}H} NMR (CD_2Cl_2, 295 K): δ = –4.5 (*see Section 3.2.2*, $^1J_{PB}$ = 160 Hz). ^{11}B NMR (CH_2Cl_2/CD_2Cl_2, 295 K): δ = 3.42 (d, $^1J_{BP}$ = 160 Hz). IR (Nujol): ν = 699 (vs), 408 (s) (BCl) cm^{-1}.

[BF_2{*o*-$C_6H_4(PMe_2)_2$}][BF_4]

Method 1: To a solution of [$BF_3(SMe_2)$] (0.140 g, 1.08 mmol) in CH_2Cl_2 (5 mL) was added *o*-$C_6H_4(PMe_2)_2$ (0.104 g, 0.52 mmol) in CH_2Cl_2 (5 mL) which caused the immediate precipitation of a white solid. The reaction was stirred for 1.5 h, then the white powder was isolated by filtration and dried *in vacuo*. Yield: 0.108 g (61%). Anal. Calc. for $C_{10}H_{16}B_2F_6P_2$: C, 36.0; H, 4.8. Found: C, 36.0; H, 4.8%. IR (Nujol): ν = 1054 (vs, br) ([BF_4]$^-$), 1039 (sh), 923 (s), 655 (s) (BF), 520 ([BF_4]$^-$) cm^{-1}.

Method 2: The N_2 atmosphere inside a Schlenk containing a drop of *o*-$C_6H_4(PMe_2)_2$ in hexane (5 mL) was replaced with BF_3 gas, which caused the immediate precipitation of a large amount of white powder. The reaction was allowed to sit overnight. After returning the Schlenk atmosphere to N_2, the white powder was isolated by filtration and dried *in vacuo*. Yield: 0.054 g. Anal. Calc. for $C_{10}H_{16}B_2F_6P_2$: C, 36.0; H, 4.8. Found: C, 35.8; H, 4.7%. IR spectroscopic data on the white powder were as for Method 1.

[BCl_2{*o*-$C_6H_4(PMe_2)_2$}][BCl_4]

To a solution of [$BCl_3(SMe_2)$] (0.096 g, 0.53 mmol) in CH_2Cl_2 (5 mL) was added *o*-$C_6H_4(PMe_2)_2$ (0.051 g, 0.26 mmol) in CH_2Cl_2 (5 mL) to give a colourless solution which was stirred for 2 h. The solvent volume was reduced to about 3 mL *in vacuo*, onto which hexane (6 mL) was layered. Colourless crystals suitable for single crystal X-ray diffraction study formed. These were isolated by filtration and dried *in vacuo* to give a white powder. Concentrating the filtrate to dryness *in vacuo* afforded a second crop of the product. The overall yield was 0.072 g (65%). Anal. Calc. for $C_{10}H_{16}B_2Cl_6P_2$: C, 27.8; H, 3.7. Found: C, 27.6; H, 3.6%. ^{1}H NMR (CD_2Cl_2, 295 K): δ = 2.06 (t, $^{2+5}J_{HP}$ = 6.0 Hz, [12H], CH_3), 8.03-8.13 (m, [4H], C_6H_4). ^{31}P{^{1}H} NMR (CH_2Cl_2/CD_2Cl_2, 295 K): δ = 7.5 (q, $^1J_{PB}$ = 125 Hz).

^{11}B NMR (CH_2Cl_2/CD_2Cl_2, 295 K): δ = –3.17 (t, $^1J_{BP}$ = 125 Hz), 8.05 (s, $[BCl_4]^-$). IR (Nujol): ν = 700 (vs) (BCl), 667 (vs) ($[BCl_4]^-$), 477 (m) (BCl) cm^{-1}.

$[BBr_2\{o\text{-}C_6H_4(PMe_2)_2\}][BBr_4]$

To a solution of *o*-$C_6H_4(PMe_2)_2$ (0.050 g, 0.25 mmol) in hexane (8 mL) was added BBr_3 (0.129 g, 0.51 mmol) which immediately led to the precipitation of a white solid. The reaction was stirred for 2 h, then the white powder was isolated by filtration and dried *in vacuo*. Yield: 0.157 g (89%). Anal. Calc. for $C_{10}H_{16}B_2Br_6P_2$: C, 17.2; H, 2.3. Found: C, 17.3; H, 2.2%. ^{1}H NMR (CD_2Cl_2, 295 K): δ = 2.23 (t, $^{2+5}J_{HP}$ = 6.0 Hz, [12H], CH_3), 8.02-8.45 (m, [4H], C_6H_4). $^{31}P\{^1H\}$ NMR (CH_2Cl_2/CD_2Cl_2, 295 K): δ = 7.7 (q, $^1J_{PB}$ = 119 Hz). ^{11}B NMR (CH_2Cl_2/CD_2Cl_2, 295 K): δ = –14.02 (t, $^1J_{BP}$ = 119 Hz), –23.27 (s, $[BBr_4]^-$). IR (Nujol): ν = 607 (vs) ($[BBr_4]^-$), 595 (vs), 584 (vs) (BBr) cm^{-1}. Small colourless single crystals of $[BBr_2\{o\text{-}C_6H_4(PMe_2)_2\}][BBr_4]$ were grown from a similar reaction where hexane was layered onto a filtered CH_2Cl_2 solution of the reagents.

Reaction of BI_3 with *o*-$C_6H_4(PMe_2)_2$

To a solution of BI_3 (0.121 g, 0.31 mmol) in CH_2Cl_2 (5 mL) was added *o*-$C_6H_4(PMe_2)_2$ (0.031 g, 0.16 mmol) in CH_2Cl_2 (5 ml) which immediately led to the precipitation of a white solid. The reaction was covered and stirred for 1.5 h, then the white powder was isolated by filtration and dried *in vacuo*. Yield: 0.048 g. ^{1}H NMR (CD_2Cl_2, 295 K): δ = 2.34-2.37 (m, [12H], CH_3), 7.99-8.50 (m, [4H], C_6H_4). $^{31}P\{^1H\}$ NMR (CH_2Cl_2/CD_2Cl_2, 295 K): δ = 7.2 (q, $^1J_{PB}$ = 110 Hz). ^{11}B NMR (CH_2Cl_2/CD_2Cl_2, 295 K): δ = –43.5 (t, $^1J_{BP}$ = 111 Hz). IR (Nujol): ν = 551 (s) (BI) cm^{-1}. Small yellow single crystals of $[BI_2\{o\text{-}C_6H_4(PMe_2)_2\}][I_3]$ were grown from layering the filtrate with hexane (7 mL).

$[BCl_2\{o\text{-}C_6H_4(AsMe_2)_2\}][BCl_4]$

To a solution of $[BCl_3(SMe_2)]$ (0.094 g, 0.52 mmol) in CH_2Cl_2 (5 mL) was added *o*-$C_6H_4(AsMe_2)_2$ (0.075 g, 0.26 mmol) in CH_2Cl_2 (5 mL) to give a colourless solution which was stirred for 2 h. The solvent volume was reduced to about 2 mL *in vacuo*, then the solution was layered with hexane (5 mL) whereupon a few small colourless crystals suitable for single crystal X-ray diffraction study grew.

3.5 Appendix – X-Ray Crystallographic Data

Compound	$[BF_2\{Ph_2P(O)CH_2P(O)Ph_2\}][B_2F_7]$	$[BF_3(PMe_3)]$	$[(BF_3)_2\{\mu\text{-}Et_2P(CH_2)_2PEt_2\}]$
Formula	$C_{25}H_{22}B_3F_9O_2P_2$	$C_3H_9BF_3P$	$C_{10}H_{24}B_2F_6P_2$
M	619.80	143.88	341.85
Crystal system	triclinic	monoclinic	monoclinic
Space group (no.)	*P*-1 (2)	$P2_1/m$ (11)	$P2_1/c$ (14)
a /Å	10.446(4)	5.838(6)	6.636(2)
b /Å	10.871(4)	9.170(9)	19.987(8)
c /Å	12.470(5)	6.675(7)	6.556(2)
α /°	71.531(13)	90	90
β /°	86.113(14)	113.359(11)	108.286(9)
γ /°	85.936(15)	90	90
U /Å^3	1338.2(9)	328.1(5)	826.9(5)
Z	2	2	2
μ(Mo-K$_\alpha$) /mm^{-1}	0.250	0.373	0.308
F(000)	628	148	356
Total no. reflns	12131	2502	3715
R_{int}	0.083	0.132	0.038
Unique reflns	6040	611	1860
No. of params, restraints	370, 0	49, 3	93, 0
R_1, wR_2 [$I > 2\sigma(I)$][a]	0.080, 0.198	0.097, 0.226	0.035, 0.085
R_1, wR_2 (all data)	0.149, 0.240	0.123, 0.240	0.048, 0.091

Common items: T = 100 K; wavelength (Mo-Kα) = 0.71073 Å; θ(max) = 27.5°.

[a] $R_1 = \Sigma||F_o| - |F_c|| / \Sigma|F_o|$; $wR_2 = [\Sigma w(F_o^2 - F_c^2)^2 / \Sigma wF_o^4]^{1/2}$.

Compound	$[(BCl_3)_2\{\mu\text{-}Et_2P(CH_2)_2PEt_2\}]$	$[(BBr_3)_2\{\mu\text{-}Et_2P(CH_2)_2PEt_2\}]$	$[(BI_3)_2\{\mu\text{-}Et_2P(CH_2)_2PEt_2\}]$
Formula	$C_{10}H_{24}B_2Cl_6P_2$	$C_{10}H_{24}B_2Br_6P_2$	$C_{10}H_{24}B_2I_6P_2$
M	440.55	707.31	989.25
Crystal system	monoclinic	monoclinic	triclinic
Space group (no.)	$P2_1/c$ (14)	$P2_1/c$ (14)	P-1 (2)
a /Å	11.138(6)	11.412(7)	10.7029(19)
b /Å	6.934(4)	7.255(4)	11.820(2)
c /Å	13.505(8)	14.002(9)	19.582(4)
α /°	90	90	85.694(6)
β /°	110.741(7)	112.219(7)	85.145(6)
γ /°	90	90	77.051(5)
U /Å^3	975.5(9)	1073.2(11)	2401.6(7)
Z	2	2	4
μ(Mo-K$_\alpha$) /mm^{-1}	1.032	11.362	7.885
F(000)	452	668	1768
Total no. reflns	8022	9120	21164
R_{int}	0.068	0.052	0.030
Unique reflns	2212	2452	10864
No. of params, restraints	93, 0	93, 0	369, 0
R_1, wR_2 [$I > 2\sigma(I)$][a]	0.029, 0.057	0.025, 0.055	0.019, 0.039
R_1, wR_2 (all data)	0.032, 0.058	0.030, 0.056	0.022, 0.040

Common items: T = 100 K; wavelength (Mo-Kα) = 0.71073 Å; θ(max) = 27.5°.

[a] $R_1 = \Sigma||F_o| - |F_c|| / \Sigma|F_o|$; $wR_2 = [\Sigma w(F_o^2 - F_c^2)^2 / \Sigma wF_o^4]^{1/2}$.

Compound	$[BCl_2\{o\text{-}C_6H_4(PMe_2)_2\}][BCl_4]$	$[BBr_2\{o\text{-}C_6H_4(PMe_2)_2\}][BBr_4]$	$[BI_2\{o\text{-}C_6H_4(PMe_2)_2\}][I_3]$
Formula	$C_{10}H_{16}B_2Cl_6P_2$	$C_{10}H_{16}B_2Br_6P_2$	$C_{10}H_{16}BI_5P_2$
M	432.49	699.25	843.48
Crystal system	orthorhombic	orthorhombic	monoclinic
Space group (no.)	*Cmc*2_1 (36)	*Pnma* (62)	*P*2_1/*c* (14)
a /Å	10.3485(15)	14.745(4)	9.702(2)
b /Å	13.475(2)	10.796(3)	17.454(3)
c /Å	13.740(2)	13.068(3)	12.615(2)
α /°	90	90	90
β /°	90	90	97.751(4)
γ /°	90	90	90
U /Å^3	1916.1(5)	2080.3(9)	2116.7(7)
Z	4	4	4
μ(Mo-K$_\alpha$) /mm^{-1}	1.049	11.721	7.484
F(000)	872	1304	1504
Total no. reflns	4450	17176	18682
R_{int}	0.037	0.081	0.045
Unique reflns	1590	2491	4150
No. of params, restraints	102, 1	102, 0	167, 0
R_1, wR_2 [$I > 2\sigma(I)$][a]	0.028, 0.069	0.032, 0.070	0.028, 0.060
R_1, wR_2 (all data)	0.030, 0.069	0.045, 0.073	0.040, 0.065

Common items: T = 100 K; wavelength (Mo-Kα) = 0.71073 Å; θ(max) = 27.5°.

[a] $R_1 = \Sigma||F_o| - |F_c|| / \Sigma|F_o|$; $wR_2 = [\Sigma w(F_o^2 - F_c^2)^2 / \Sigma wF_o^4]^{1/2}$.

Compound	$[BCl_2\{o\text{-}C_6H_4(AsMe_2)_2\}][BCl_4]$
Formula	$C_{10}H_{16}As_2B_2Cl_6$
M	520.39
Crystal system	orthorhombic
Space group (no.)	$P2_12_12_1$ (19)
a /Å	8.277(3)
b /Å	14.406(4)
c /Å	16.214(5)
α /°	90
β /°	90
γ /°	90
U /Å^3	1933.3(10)
Z	4
μ(Mo-K$_\alpha$) /mm^{-1}	4.272
F(000)	1016
Total no. reflns	17649
R_{int}	0.055
Unique reflns	4421
No. of params, restraints	185, 0
R_1, wR_2 [$I > 2\sigma(I)$][a]	0.021, 0.041
R_1, wR_2 (all data)	0.023, 0.041

Common items: T = 100 K; wavelength (Mo-Kα) = 0.71073 Å; θ(max) = 27.5°.

[a] $R_1 = \Sigma||F_o| - |F_c|| / \Sigma|F_o|$; $wR_2 = [\Sigma w(F_o^2 - F_c^2)^2 / \Sigma wF_o^4]^{1/2}$.

3.6 References

1. J. Burt, W. Levason and G. Reid, *Coord. Chem. Rev.*, 2014, **260**, 65-115.
2. J. A. Plumley and J. D. Evanseck, *J. Phys. Chem. A*, 2009, **113**, 5985-5992.
3. N. N. Greenwood and A. Earnshaw, *Chemistry of the Elements*, Butterworth-Heinemann, Oxford, 2 edn., 1997.
4. G. Santiso-Quiñones and I. Krossing, *Z. Anorg. Allg. Chem.*, 2008, **634**, 704-707.
5. M. Atoji and W. N. Lipscomb, *J. Chem. Phys.*, 1957, **27**, 195-195.
6. C. Spencer and W. N. Lipscomb, *J. Chem. Phys.*, 1958, **28**, 355.
7. D. Mootz and M. Steffen, *Angew. Chem., Int. Ed. Engl.*, 1980, **19**, 483-484.
8. M. Mantina, A. C. Chamberlin, R. Valero, C. J. Cramer and D. G. Truhlar, *J. Phys. Chem. A*, 2009, **113**, 5806-5812.
9. S. Patchkovskii, D. D. Klug and Y. Yao, *Inorg. Chem.*, 2011, **50**, 10472-10475.
10. N. Hamaya, M. Ishizuka, S. Onoda, J. Guishan, A. Ohmura and K. Shimizu, *Phys. Rev. B*, 2010, **82**, 094506.
11. Y. Yao, D. D. Klug, R. Martoňák and S. Patchkovskii, *Phys. Rev. B*, 2011, **83**, 214105.
12. L. M. Nxumalo and T. A. Ford, *Vib. Spectrosc.*, 1994, **6**, 333-343.
13. J. A. W. Shoemaker and J. S. Hartman, *Can. J. Chem.*, 1999, **77**, 1856-1868.
14. T. Onak, H. Rosendo, G. Siwapinyoyos, R. Kubo and L. Liauw, *Inorg. Chem.*, 1979, **18**, 2943-2945.
15. M. J. Farquharson and J. S. Hartman, *Can. J. Chem.*, 1996, **74**, 1309-1320.
16. M.-L. Yao and G. W. Kabalka, in *Boron Science: New Technologies and Applications*, ed. N. S. Hosmane, CRC Press, Florida, 2012, pp. 579-623.
17. M. A. Beckett, G. C. Strickland, J. R. Holland and K. Sukumar Varma, *Polymer*, 1996, **37**, 4629-4631.
18. A. M. McKinty, C. Lund and D. W. Stephan, *Organometallics*, 2013, **32**, 4730-4732.
19. E. R. Clark and M. J. Ingleson, *Organometallics*, 2013, **32**, 6712-6717.
20. K. Chansaenpak, M. Wang, Z. Wu, R. Zaman, Z. Li and F. P. Gabbai, *Chem. Commun.*, 2015, **51**, 12439-12442.
21. M. Kameda and G. Kodama, *Inorg. Chem.*, 1997, **36**, 4369-4371.
22. R. B. Coapes, F. E. S. Souza, M. A. Fox, A. S. Batsanov, A. E. Goeta, D. S. Yufit, M. A. Leech, J. A. K. Howard, A. J. Scott, W. Clegg and T. B. Marder, *J. Chem. Soc., Dalton Trans.*, 2001, 1201-1209.

23. J. P. H. Charmant, C. Fan, N. C. Norman and P. G. Pringle, *Dalton Trans.*, 2007, 114-123.

24. H. Braunschweig, K. Radacki and K. Uttinger, *Inorg. Chem.*, 2007, **46**, 8796-8800.

25. W. Uhl, C. Appelt, A. Wollschläger, A. Hepp and E.-U. Würthwein, *Inorg. Chem.*, 2014, **53**, 8991-8999.

26. U. Monkowius, S. Nogai and H. Schmidbaur, *Dalton Trans.*, 2003, 987-991.

27. D. L. Black and R. C. Taylor, *Acta Crystallogr., Sect. B: Struct. Sci.*, 1975, **31**, 1116-1120.

28. C. Aubauer, K. Davidge, T. M. Klapötke, P. Mayer, H. Piotrowski and A. Schulz, *Z. Anorg. Allg. Chem.*, 2000, **626**, 2373-2378.

29. F. Weller, M. Möhlen and K. Dehnicke, *Z. Kristallogr. - New Cryst. Struct.*, 1997, **212**, 159-160.

30. F. Dornhaus, M. Bolte, H.-W. Lerner and M. Wagner, *Eur. J. Inorg. Chem.*, 2006, **2006**, 1777-1785.

31. R. Chadha, J. Chehayber and J. Drake, *J. Crystallogr. Spectrosc. Res.*, 1985, **15**, 53-60.

32. F. Dornhaus, S. Scholz, I. Sänger, M. Bolte, M. Wagner and H.-W. Lerner, *Z. Anorg. Allg. Chem.*, 2009, **635**, 2263-2272.

33. M. S. Lube, R. L. Wells and P. S. White, *Inorg. Chem.*, 1996, **35**, 5007-5014.

34. M. S. Lube, R. L. Wells and P. S. White, *Main Group Met. Chem.*, 1996, **19**, 733-741.

35. M. Lube, R. Jouet, R. Wells, P. Whtte and V. Young, *Main Group Chem.*, 1997, **2**, 89-96.

36. A. K. Mandal and S. W. Mahajan, *Tetrahedron Lett.*, 1985, **26**, 3863-3866.

37. T. A. Ford, *J. Mol. Struct.*, 2007, **834–836**, 30-41.

38. R. G. Pearson, *J. Am. Chem. Soc.*, 1963, **85**, 3533-3539.

39. R. L. Amster and R. C. Taylor, *Spectrochim. Acta*, 1964, **20**, 1487-1502.

40. M. J. Frazer, W. Gerrard and R. Twaits, *J. Inorg. Nucl. Chem.*, 1963, **25**, 637-640.

41. N. Burford, B. W. Royan, R. E. v. H. Spence, T. S. Cameron, A. Linden and R. D. Rogers, *J. Chem. Soc., Dalton Trans.*, 1990, 1521-1528.

42. M. L. Denniston and D. R. Martin, *J. Inorg. Nucl. Chem.*, 1974, **36**, 1461-1464.

43. N. Burford, R. E. v. H. Spence, A. Linden and T. S. Cameron, *Acta Crystallogr. Sect. C: Cryst. Struct. Commun.*, 1990, **46**, 92-95.

44. R. Bravo, M. Durand and J. P. Laurent, *Org. Magn. Reson.*, 1973, **5**, 357-360.

45. R. Bravo and J. P. Laurent, *J. Chem. Res., Synop.*, 1983, 61.

46. M. J. Bula, J. S. Hartman and C. V. Raman, *Can. J. Chem.*, 1975, **53**, 326-331.

47. H. Nöth and B. Wrackmeyer, *NMR 14, Nuclear Magnetic Resonance Spectroscopy of Boron Compounds*, Springer-Verlag, Berlin, 1978.

48. S. A. Sangokoya, B. Lee, M. F. Self, W. T. Pennington and G. H. Robinson, *Polyhedron*, 1989, **8**, 1497-1502.

49. P. Braunstein, L. Douce, J. Fischer, N. C. Craig, G. Goetz-Grandmont and D. Matt, *Inorg. Chim. Acta*, 1992, **194**, 151-156.

50. J. S. Hartman and P. Stilbs, *J. Chem. Soc., Dalton Trans.*, 1980, 1142-1144.

51. J. S. Hartman and P. Stilbs, *J. Chem. Soc., Chem. Commun.*, 1975, 566-567.

52. M. Watanabe, M. Sato, A. Nagasawa, M. Kai, I. Motoyama and T. Takayama, *Bull. Chem. Soc. Jpn.*, 1999, **72**, 715-723.

53. J. S. Hartman, G. J. Schrobilgen and P. Stilbs, *Can. J. Chem.*, 1976, **54**, 1121-1129.

54. J. J. Harris, *Inorg. Chem.*, 1966, **5**, 1627-1629.

55. S. D. Williams, W. Harper, G. Mamantov, L. J. Tortorelli and G. Shankle, *J. Comput. Chem.*, 1996, **17**, 1696-1711.

56. C. W. Heitsch, *Inorg. Chem.*, 1965, **4**, 1019-1024.

57. T. A. Ford, *J. Phys. Chem. A*, 2008, **112**, 7296-7302.

58. C. Loschen, K. Voigt, J. Frunzke, A. Diefenbach, M. Diedenhofen and G. Frenking, *Z. Anorg. Allg. Chem.*, 2002, **628**, 1294-1304.

59. K. Nakamoto, *Infrared and Raman Spectra of Inorganic and Coordination Compounds*, Wiley-Interscience, NY, 4 edn., 1986.

60. F. Bessac and G. Frenking, *Inorg. Chem.*, 2006, **45**, 6956-6964.

61. J. E. Drake, J. L. Hencher and B. Rapp, *Inorg. Chem.*, 1977, **16**, 2289-2294.

62. B. Cordero, V. Gomez, A. E. Platero-Prats, M. Reves, J. Echeverria, E. Cremades, F. Barragan and S. Alvarez, *Dalton Trans.*, 2008, 2832-2838.

63. H. J. Hogben, M. Krzystyniak, G. T. P. Charnock, P. J. Hore and I. Kuprov, *J. Magn. Reson.*, 2011, **208**, 179-194.

64. J. S. Hartman and J. A. W. Shoemaker, *Polyhedron*, 2000, **19**, 165-176.

65. W. Petz, F. Öxler, K. Aicher and B. Neumüller, *Z. Anorg. Allg. Chem.*, 2010, **636**, 1751-1759.

66. M. Di Vaira, M. Peruzzini and P. Stoppioni, *Acta Crystallogr. Sect. C: Cryst. Struct. Commun.*, 1983, **39**, 1210-1211.

67. J. S. Hartman and G. J. Schrobilgen, *Inorg. Chem.*, 1972, **11**, 940-951.

68. T. C. Waddington and J. A. White, *Proc. Chem. Soc.*, 1960, 315.

69. E. Muylle, G. P. Van Der Kelen and E. G. Claeys, *Spectrochim. Acta, Part A*, 1976, **32**, 1149-1154.

70. J. E. Drake, L. N. Khasrou and A. Majid, *Can. J. Chem.*, 1981, **59**, 2417-2428.

71. D. C. Mente and J. L. Mills, *Inorg. Chem.*, 1975, **14**, 1862-1865.

Chapter 4: Exploring Fluoroanion Coordination in Lead(II) Di- and Tri-Imine Complexes

4.1 Introduction

Fluoroanions, such as $[BF_4]^-$ and $[PF_6]^-$, are known to coordinate weakly to a range of metal ions, and there has been recent interest in the variety of different coordination modes these anions can exhibit.[1,2] As Pb(II) will readily form compounds with high coordination numbers and irregular geometries[3] it was an ideal choice of metal ion to further explore the coordination behaviour of both monoanionic $[BF_4]^-$ and the little studied dianionic $[SiF_6]^{2-}$ fluoroanions, whilst synthesising and characterising some new di- and tri-imine complexes of Pb(II).

4.1.1 Properties and coordination chemistry of lead(II)

As a large metal centre with a covalent radius of 1.46 Å,[4] lead(II) is able to form complexes with a variety of geometries, and coordination numbers ranging from two to twelve.[3,5] A discussion of the Lewis acidity, bonding trends and lone pair activity of Group 14 is given in Section 1.6. Lead(II) forms stable complexes with a wide range of neutral and charged donor ligands across Groups 14-17; the majority of complexes are with hard oxygen and nitrogen donor ligands, though there is considerable chemistry with softer sulfur (and to a lesser extent, selenium) donor ligands as well.[3,5,6] There is a tendency for lead(II) to form extended structures in the solid state, resulting in the poor solubility of many Pb(II) complexes in most solvents, including water.[3] However, once dissolved, complexes are often extensively dissociated in solution, which is attributed to the low charge to radius ratio of lead(II).[2]

There are a vast number of known coordination complexes of lead(II) with neutral nitrogen donor ligands, many of which contain the imines used in this chapter: 2,2'-bipyridyl (bipy), 1,10-phenanthroline (phen) or 2,2':6',2''-terpyridyl (terpy). The majority of these complexes are with oxoanions (such as $[NO_3]^-$, $[ClO_4]^-$ or $[O_2CR]^-$),[3] but there also examples with halides, including the $(\mu\text{-}X)_2$-linked one-dimensional polymers $[PbX_2(bipy)]$ (X = Cl, I) and $[PbX_2(phen)]$ (X = Cl, Br, I),[7] and the dimeric $[PbI_2(terpy)]$.[8] Complexes with thioanions are also known, such as the binuclear $[Pb(bipy)\{S_2P(OEt_2)\}_2]$,[9] and polymeric $[Pb(bipy)(SCN)_2]$.[7] However, the only structurally authenticated examples

with a fluoroanion are $[Pb(bipy)_2(PF_6)_2]$, $[Pb(bipy)_4][PF_6]_2 \cdot bipy$ and the mixed-anion one-dimensional chain polymer complex $[Pb(bipy)_2(\mu\text{-}NO_3)][PF_6]$,[10] which are described further in Section 4.1.3.

4.1.2 Weakly coordinating anions

Due to the ease of their displacement, weakly coordinating anions can enhance the chemical reactivity of metal complexes.[11] Complexes containing weakly coordinating anions are commonly used as catalysts (for example, $Li[B(Ar^F)_4]$ ($Ar^F = C_6H_3\text{-}3,5\text{-}(CF_3)_2$) has been used to catalyse Diels-Alder reactions);[12] other applications include being used as supporting electrolytes in electrochemistry, in ionic liquids and in lithium-ion batteries.[13] Weakly coordinating anions are also often more simply a valuable tool for synthesising novel complexes, particularly when very poor donor ligands are used.[11] In Pb(II) imine chemistry, a wider range of coordination numbers and motifs can be accessed with more weakly coordinating anions; for instance the dimeric 1:2 adducts $[Pb(bipy)_2Y_2]$ ($Y = NO_3$, ClO_4) are nine-coordinate,[14] while with strongly coordinating halide anions, adducts such as $[PbX_2(bipy)]$ (X = Cl, I) have a 1:1 stoichiometry with six-coordinate Pb(II).[7]

Fluoroanions typically have a weaker coordinating ability than oxoanions like $[ClO_4]^-$ and $[NO_3]^-$ as the accessible (fluorine) atoms are less basic (than oxygen).[11] While larger, robust fluoroanions such as $[B(C_6F_5)_4]^-$ and $[B(Ar^F)_4]^-$ are more weakly coordinating (as the negative charge is delocalised over more atoms),[11] the simpler $[BF_4]^-$ and $[PF_6]^-$ are much more readily available and are chemically inert in most systems. In the present study, the use of small (and therefore more sterically similar) fluoroanions will also enable a closer comparison to be made with the known Pb(II) imine oxoanion complexes. The dianionic $[SiF_6]^{2-}$ anion is little studied, presumably because when designing a weakly coordinating anion it is better to have a low overall charge;[11] nevertheless it merits investigation as a weakly coordinating anion as its coordination behaviour may be different to the monoanionic fluoroanions. While there are no known complexes of lead(II) hexafluorosilicate, the $[SiF_6]^{2-}$ anion has been shown to coordinate to other metal ions, including Zn(II) in $[Zn(phen)_2(SiF_6)]$[15] and Cu(II) in $[CuL(SiF_6)]$, where L = 1,2-bis{3-(2-pyridyl)pyrazol-1-ylmethyl}benzene.[16]

4.1.3 Fluoroanion coordination in lead(II) complexes

There are few crystallographically characterised examples of fluoroanion coordination to lead(II) in the literature, and even when present, it is not always recognised by the authors.

In order to be considered an interaction the Pb–F distance must be less than 3.49 Å, i.e. the sum of the Van der Waals radii of Pb and F,[17] though crystal packing effects must also be considered when the bond length is near the limit. In a recent study[2] into complexes of $Pb(BF_4)_2$ and $Pb(PF_6)_2$ with crown ethers, oxathia- and oxaselena-macrocycles, the fluoroanions were found to readily enter the first coordination sphere of the lead, where they exhibit a range of coordination modes. Asymmetrically bridging $[BF_4]^-$ groups with *d*(Pb–F) = 2.677(5) and 2.813(4) Å were observed in $[\{Pb(18\text{-crown-6})(H_2O)(\mu^2\text{-}BF_4)\}_2][BF_4]_2$. The organolead complex $[\{Pb(\eta^5\text{-}C_5Me_5)(\mu^2\text{-}BF_4)\}_2]$ is the only other example of Pb(II) with bridging $[BF_4]^-$ groups, with *d*(Pb–F) = 2.831(9) and 2.901(9) Å.[18] Asymmetrical chelating (κ^2-coordination) behaviour was observed for the coordinated $[BF_4]^-$ groups in $[Pb([18]aneO_4S_2)(H_2O)_2(BF_4)][BF_4]$ and $[Pb([18]aneO_4Se_2)(BF_4)_2]$, though in the latter (which has two-fold symmetry) the Pb–F distances differ by ~0.5 Å.[2] Similar κ^2-coordination is also observed in $[Pb\{HC(pz)_3\}_2(BF_4)_2]$ (pz = pyrazolyl ring), with Pb–F distances of ~3.0 Å, while in $[Pb\{HC(3,5\text{-}Me_2pz)_3\}(BF_4)_2]$ there are five Pb–F interactions (two κ^2, one κ^1) ranging in length from 2.685(10) to 3.046(8) Å from three $[BF_4]^-$ groups, two of which are bridging between different Pb(II) centres.[19]

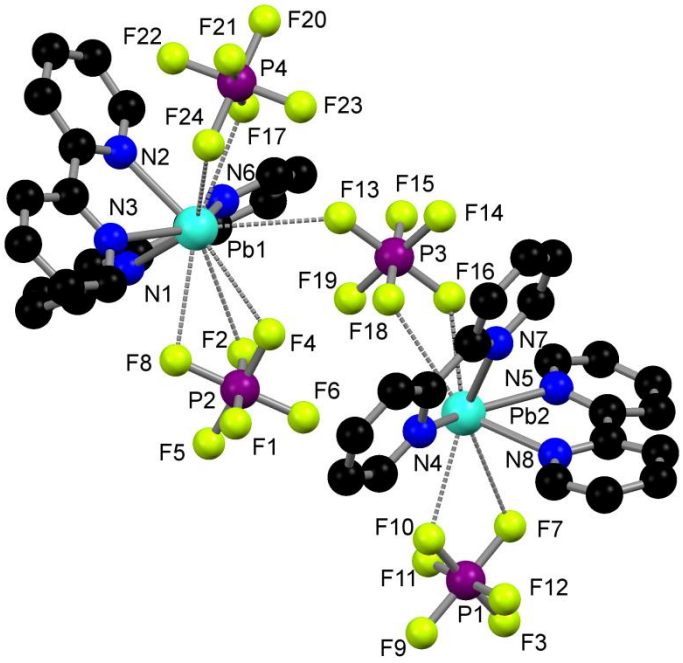

Figure 4.1 View showing the fluoroanion coordination in $[Pb(bipy)_2(PF_6)_2]$.[10]

Sykes *et al.*[10] report the crystal structures of some bipy complexes of lead(II) hexafluorophosphate, but do not discuss any interactions with $[PF_6]^-$ in detail; while no Pb–F interactions are present in $[Pb(bipy)_4][PF_6]_2\cdot bipy$, and the closest Pb–F contact in $[Pb(bipy)_2(\mu\text{-}NO_3)][PF_6]$ is very long at ~3.4 Å, there are several Pb–F interactions in the

dimeric [Pb(bipy)$_2$(PF$_6$)$_2$]. The structure (Figure 4.1) reveals each Pb(II) κ^2-coordinated by a [PF$_6$]$^-$ group with *d*(Pb–F) of ~3.0 Å, with a third [PF$_6$]$^-$ asymmetrically κ^3-coordinated and the fourth [PF$_6$]$^-$ κ^2-coordinated to one (eight-coordinate) Pb(II) centre, whilst bridging to the other (ten-coordinate) Pb(II) centre via a long (~3.3 Å) Pb–F contact. Similarly, with crown ether and oxaselena-macrocycle complexes of Pb(PF$_6$)$_2$, κ^2- (in [Pb(18-crown-6)(H$_2$O)$_2$(PF$_6$)][PF$_6$] and [Pb([18]aneO$_4$Se$_2$)(PF$_6$)$_2$]) and κ^3-coordinated (in [Pb(18-crown-6)(NO$_3$)(PF$_6$)]) [PF$_6$]$^-$ groups were observed, though the macrocyclic complexes degraded over a period of a few days due to hydrolysis of the [PF$_6$]$^-$ anions, a process thought to be promoted by the lead.[2]

4.2 Results and Discussion

Identification of what are the first examples of di- and tri-imine complexes of lead(II) tetrafluoroborate and lead(II) hexafluorosilicate has been driven by solid state characterisation, the key technique being single crystal X-ray diffraction, supported by identification of the fluoroanion using infrared spectroscopy. Microanalysis was used to confirm the stoichiometries of the bulk samples. Due to the labile nature of Pb(II) in solution, the information provided by NMR spectroscopy is quite limited. There was no evidence for decomposition of the fluoroanions in any of the reactions, which were performed under an air atmosphere.

The lead(II) salts used for the syntheses were obtained commercially as a 50% aqueous solution of $Pb(BF_4)_2$ and solid $Pb(SiF_6)\cdot 2H_2O$. The $Pb(BF_4)_2$ solution, as supplied, contains some excess acid to prevent hydroxide formation at Pb(II), and was found to protonate terpy (see Section 4.2.2); bipy and phen were unaffected. The structure of $Pb(SiF_6)\cdot 2H_2O$ contains nine-coordinate Pb(II) in two environments, one involving three water molecules and six fluorines, the other four water molecules and five fluorines.[20] Table 4.1 gives selected spectroscopic data for $Pb(BF_4)_2$ and $Pb(SiF_6)\cdot 2H_2O$. The resonances in the ^{19}F NMR spectra have similar shifts to 'free' $[BF_4]^-$ and $[SiF_6]^{2-}$,[21] indicating that the lead(II) salts are extensively dissociated in solution.

Table 4.1 Selected spectroscopic data for $Pb(BF_4)_2$ and $Pb(SiF_6)\cdot 2H_2O$

Lead(II) Salt	ν(SiF) / cm^{-1} [a]	δ(^{19}F) / 295 K[b]	δ(^{29}Si) / 295 K[b,c]	δ(^{207}Pb) / 295 K[b]
$Pb(BF_4)_2$	–	–149.8 (s)[d]	–	–2903.3 (s)
$Pb(SiF_6)\cdot 2H_2O$	720, 698 (vs, br) 463, 436 (s)	–129.3 (s) $^1J_{FSi}$ = 108 Hz	–188.2 (septet) $^1J_{SiF}$ = 108 Hz	–2862.0 (s)

[a] nujol mull; [b] D_2O; [c] ^{29}Si: I = ½, N.A. = 4.7%; [d] resonances for $[^{10}BF_4]^-$ and $[^{11}BF_4]^-$ (quoted) are observed ~ 20 Hz apart, with relative intensities of 1:4

Due to the poor solubility of the lead(II) salts in organic solvents the reactions were performed by combining a CH_3CN solution of the di- or tri-imine with an aqueous solution of the Pb(II) salt ($Pb(SiF_6)\cdot 2H_2O$ is sparingly soluble in water). The complexes were isolated as white, beige or pale pink air-stable solids, while single crystals suitable for X-ray diffraction were obtained by allowing portions of the reaction solutions to evaporate slowly in air.

4.2.1 Complexes with bidentate imines

Crystals grown from the reaction of 2,2'-bipyridyl with $Pb(BF_4)_2$ in a 2:1 molar ratio were shown to be $[\{Pb(bipy)_2(BF_4)_2(H_2O)_{0.25}\}_2]$ (Figure 4.2), which has a fractionally occupied (50%) water molecule site located between the lead centres. The bipy ligands are chelating and are "*cis*" disposed on one hemisphere of the lead. As with $[Pb(bipy)_2Y_2]$ (Y = NO_3, ClO_4) the structure is dimeric, but while the PbN_4 geometry is closely comparable with the centrosymmetric $[Pb(bipy)_2(ClO_4)_2]$ (*d*(Pb–N) = 2.512(7)–2.560(8) Å, ∠N–Pb–N = 64.4(2)–65.4(2)°),[14] the anion coordination is much more complicated. In $[Pb(bipy)_2Y_2]$ (Y = NO_3, ClO_4) the oxoanions are κ^2-coordinated to Pb(II), with one oxoanion per Pb(II) also bridging through a third oxygen to the other Pb(II) centre, giving nine-coordinate lead(II) overall.[14] In $[\{Pb(bipy)_2(BF_4)_2(H_2O)_{0.25}\}_2]$ however, each Pb(II) centre interacts with four fluorines from three $[BF_4]^-$ anions, to give eight- (or nine- when the water is present) coordinate lead(II). One $[BF_4]^-$ is κ^1, one is κ^2, one is μ^2, while the fourth $[BF_4]^-$ is κ^2-coordinated to one Pb(II) centre whilst bridging through another fluorine to the other Pb(II) centre. The *d*(Pb–F) span the range 2.725(6)–3.028(9) Å, which are all well within 3.49 Å, the sum of the Van der Waals radii for Pb and F.[17] The arrangement gives a Pb···Pb distance of 5.059(2) Å, which is much shorter than in $[Pb(bipy)_2(NO_3)_2]$ (6.062(2) Å), and nearly 2 Å shorter than in $[Pb(bipy)_2(ClO_4)_2]$ (7.010(1) Å).[14]

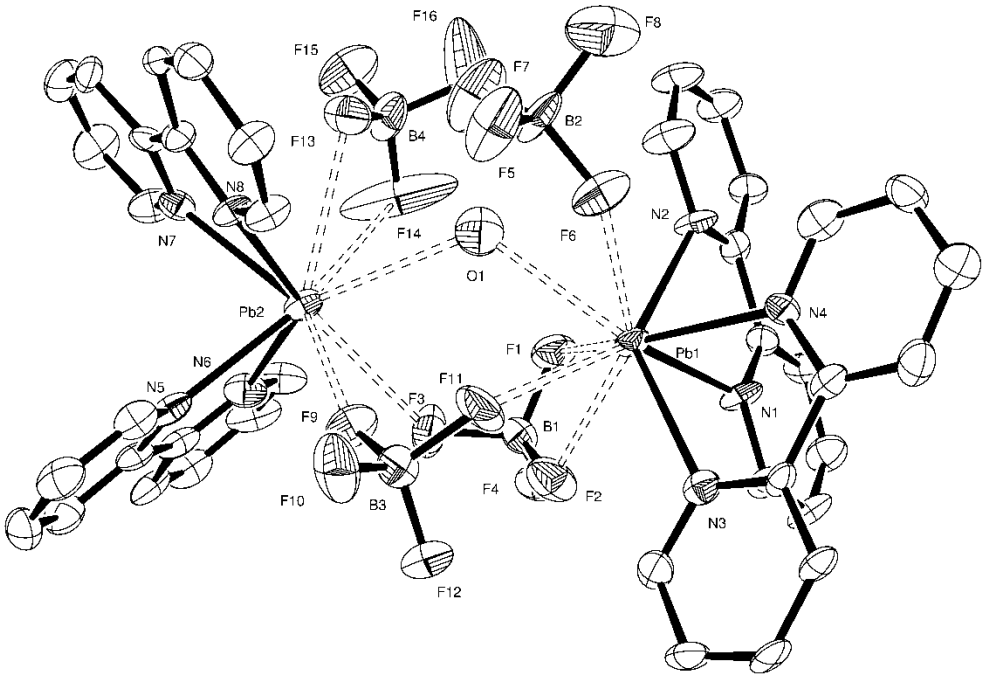

Figure 4.2 The structure of $[\{Pb(bipy)_2(BF_4)_2(H_2O)_{0.25}\}_2]$ showing the atom labelling scheme. Ellipsoids are drawn at the 50% probability level and H atoms are omitted for clarity.

Table 4.2 Selected bond lengths (Å) and angles (°) for [{Pb(bipy)$_2$(BF$_4$)$_2$(H$_2$O)$_{0.25}$}$_2$]

Pb1–N1	2.516(8)	N1–Pb1–N2	64.8(3)
Pb1–N2	2.503(8)	N3–Pb1–N4	64.7(3)
Pb1–N3	2.558(8)	N5–Pb2–N6	64.5(3)
Pb1–N4	2.514(9)	N7–Pb2–N8	65.1(3)
Pb1–O1	2.836(8)		
Pb1–F1	3.017(10)		
Pb1–F2	2.802(9)		
Pb1–F6	2.767(10)		
Pb1–F11	3.007(8)		
Pb2–N5	2.533(9)		
Pb2–N6	2.509(9)		
Pb2–N7	2.541(9)		
Pb2–N8	2.486(8)		
Pb2–O1	2.916(8)		
Pb2–F3	2.958(8)		
Pb2–F9	2.725(6)		
Pb2–F13	2.946(11)		
Pb2–F14	3.028(9)		

Crystals from the analogous reaction with Pb(SiF$_6$)·2H$_2$O revealed [Pb(bipy)$_2$(SiF$_6$)] to be a centrosymmetric dimer (Figure 4.3), with a similar core PbN$_4$ geometry to those observed for the other bipy complexes.[14] The [SiF$_6$]$^{2-}$ anions bridge between the Pb(II) centres, with four of the fluorines coordinating; three fluorines (F4, F5 and F6) interact with a single Pb(II) centre (*d*(Pb–F) = 2.811(2), 2.750(2) and 2.723(4) Å respectively), while F1 asymmetrically bridges the two Pb(II) centres with longer bonds (*d*(Pb1–F1) = 2.974(2) Å, *d*(Pb1–F1a) = 2.911(2) Å). The distance between the Pb(II) centres is 4.769(5) Å. Like [Pb(bipy)$_2$Y$_2$] (Y = NO$_3$, ClO$_4$),[14] overall the lead is in a nine-coordinate environment; the dimerisation and similarity in the geometries of these bipy complexes

suggest that, irrespective of the anion geometry (planar, tetrahedral or octahedral), this arrangement maximises the interactions between the lead(II) and the donor groups present.

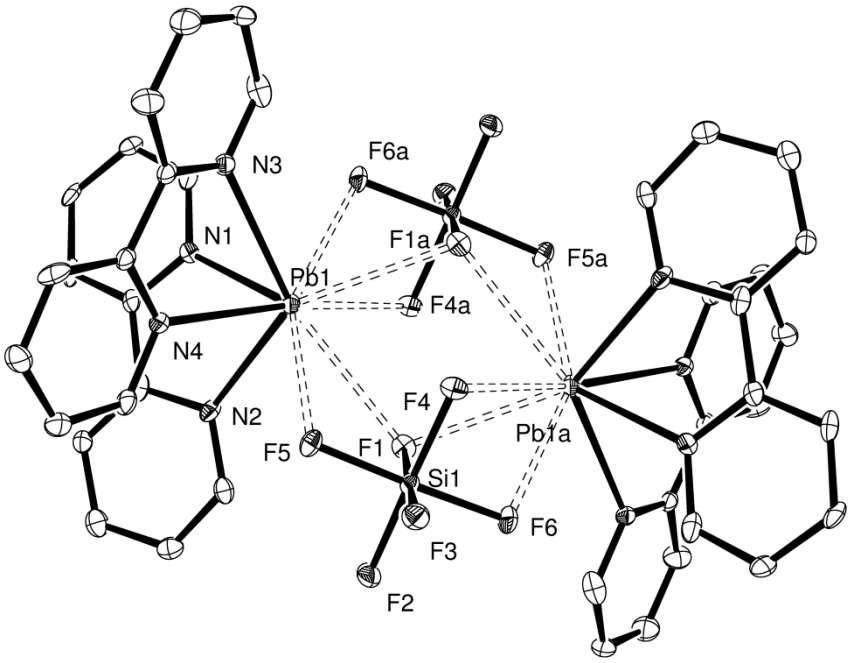

Figure 4.3 The structure of the centrosymmetric dimer present in $[Pb(bipy)_2(SiF_6)]$ showing the atom labelling scheme. Ellipsoids are drawn at the 50% probability level and H atoms are omitted for clarity. Symmetry operation: a = 2 – x, – y, 1 – z.

Table 4.3 Selected bond lengths (Å) and angles (°) for $[Pb(bipy)_2(SiF_6)]$

Pb1–N1	2.531(5)	N1–Pb1–N2	63.92(16)
Pb1–N2	2.553(5)	N3–Pb1–N4	60.64(16)
Pb1–N3	2.760(5)		
Pb1–N4	2.643(5)		
Pb1–F1	2.974(2)		
Pb1–F5	2.750(2)		
Pb1–F1a	2.911(2)		
Pb1–F4a	2.811(2)		
Pb1–F6a	2.723(4)		

The reaction of $Pb(SiF_6)\cdot 2H_2O$ with two molar equivalents of 1,10-phenanthroline yielded single crystals that were found to be $[\{Pb(phen)_2(SiF_6)\}_2]\cdot[Pb(phen)_2(H_2O)_2(SiF_6)]\cdot 11H_2O$, which contains two lead complexes and eleven lattice water molecules. The expected hydrogen bonding for the lattice waters could not be satisfactorily modelled, suggesting that the network varies throughout the crystal. Although not centrosymmetric, the dimeric unit in $[Pb(phen)_2(SiF_6)]$ (Figure 4.4) is very similar to $[Pb(bipy)_2(SiF_6)]$ (Figure 4.3), with comparable $[SiF_6]^{2-}$ coordination and nine-coordinate Pb(II) centres. The range of Pb–F distances are alike in both complexes, while the Pb···Pb distance (4.706(1) Å) is also short. The PbN_4 geometries of $[Pb(phen)_2(SiF_6)]$ are similar to those in the monomeric $[Pb(phen)_2Y_2]$ (Y = NO_3, ClO_4), where eight-coordinate Pb(II) is achieved by both oxoanions chelating in a bidentate fashion.[22]

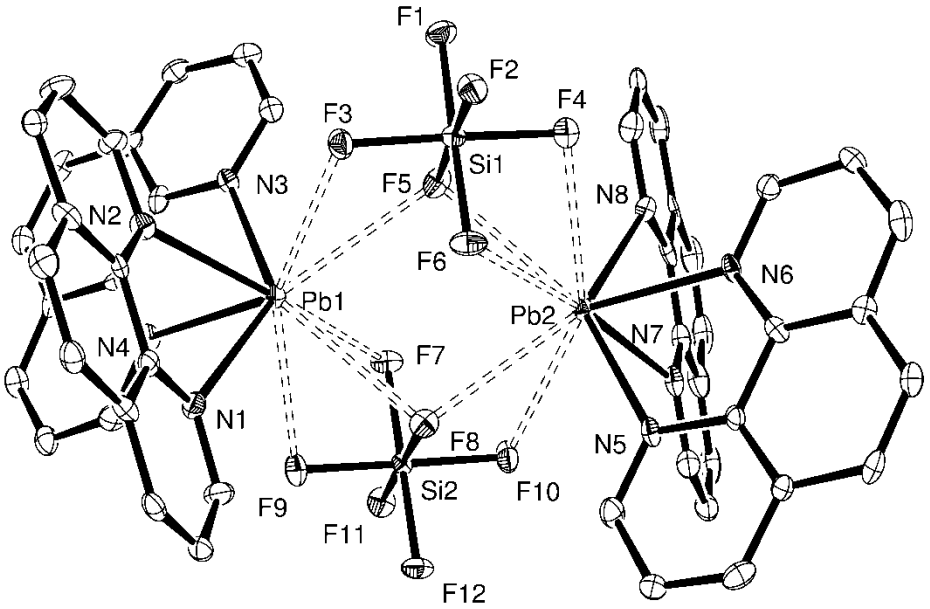

Figure 4.4 The structure of $[\{Pb(phen)_2(SiF_6)\}_2]$ present in the crystal structure of $[\{Pb(phen)_2(SiF_6)\}_2]\cdot[Pb(phen)_2(H_2O)_2(SiF_6)]\cdot 11H_2O$ showing the atom labelling scheme. Ellipsoids are drawn at the 50% probability level and H atoms are omitted for clarity.

Table 4.4 Selected bond lengths (Å) and angles (°) for [{Pb(phen)$_2$(SiF$_6$)}$_2$]

Pb1–N1	2.667(5)	N1–Pb1–N2	62.77(14)
Pb1–N2	2.603(5)	N3–Pb1–N4	65.27(15)
Pb1–N3	2.591(5)	N5–Pb2–N6	65.59(15)
Pb1–N4	2.509(5)	N7–Pb2–N8	64.37(16)
Pb1–F3	2.724(3)		
Pb1–F5	3.072(5)		
Pb1–F7	2.791(4)		
Pb1–F8	2.948(4)		
Pb1–F9	2.836(5)		
Pb2–N5	2.536(5)		
Pb2–N6	2.522(4)		
Pb2–N7	2.542(5)		
Pb2–N8	2.627(5)		
Pb2–F4	2.894(4)		
Pb2–F5	2.951(4)		
Pb2–F6	2.875(4)		
Pb2–F8	3.060(5)		
Pb2–F10	2.817(4)		

The monomeric [Pb(phen)$_2$(H$_2$O)$_2$(SiF$_6$)] (Figure 4.5) also present in the X-ray crystal structure reveals a very asymmetrically κ^2-coordinated [SiF$_6$]$^{2-}$ anion (*d*(Pb–F) = 2.701(5) and 3.272(5) Å), and two coordinated water molecules, so that overall the lead(II) is eight-coordinate. The core PbN$_4$ geometry, with its "*cis*" disposed phen ligands, is very similar to those of the dimeric unit [{Pb(phen)$_2$(SiF$_6$)}$_2$]. Although relatively weak interactions, the *d*(Pb–O) fall within the range of lengths seen in PbSiF$_6$·2H$_2$O (2.357(10)–2.858(13) Å),[20] and are still well within the sum of the Van der Waals radii for Pb and O (3.54 Å).[17] The weakly coordinating behaviour of the [SiF$_6$]$^{2-}$ anions has little effect on the actual fluoroanion, as in all the PbSiF$_6$ diimine complexes discussed the *d*(Si–F) and ∠F–Si–F are

not significantly different from those found in either $PbSiF_6 \cdot 2H_2O$[20] or the free anion (~ 1.70 Å, 90°).[23]

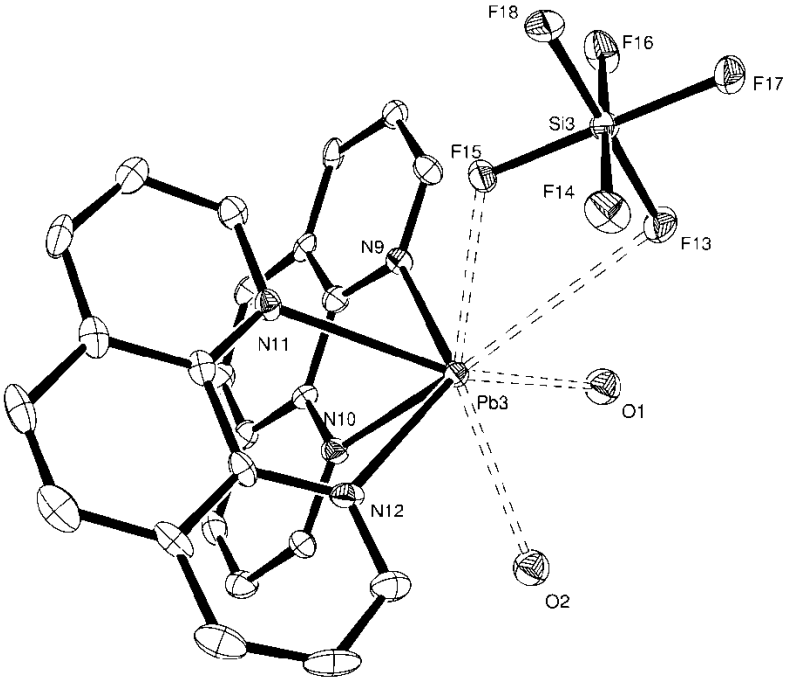

Figure 4.5 The structure of $[Pb(phen)_2(H_2O)_2(SiF_6)]$ present in the crystal structure of $[\{Pb(phen)_2(SiF_6)\}_2] \cdot [Pb(phen)_2(H_2O)_2(SiF_6)] \cdot 11H_2O$ showing the atom labelling scheme. Ellipsoids are drawn at the 50% probability level and H atoms are omitted for clarity.

Table 4.5 Selected bond lengths (Å) and angles (°) for $[Pb(phen)_2(H_2O)_2(SiF_6)]$

Pb3–N9	2.561(5)	N9–Pb3–N10	65.44(14)
Pb3–N10	2.513(5)	N11–Pb3–N12	61.95(14)
Pb3–N11	2.677(5)		
Pb3–N12	2.654(5)		
Pb3–O1	2.778(5)		
Pb3–O2	2.800(3)		
Pb3–F13	3.272(5)		
Pb3–F15	2.702(3)		

Crystals of the monomeric $[Pb(phen)_2(BF_4)_2]$ were obtained from the analogous reaction with $Pb(BF_4)_2$; as with the other diimine structures it contains a core PbN_4 geometry, with "*cis*" disposed ligands occupying one hemisphere of the lead, which is little affected by the

anions present. The remaining coordination sphere is filled with longer contacts to the anions, resulting in highly irregular and varying geometries around the lead(II). In $[Pb(phen)_2(BF_4)_2]$ (Figure 4.6) both of the $[BF_4]^-$ anions are κ^2-coordinating, though the *d*(Pb–F) are ~0.2 Å different between the two anions, and this gives an eight-coordinate lead(II) centre overall that is closely related to $[Pb(phen)_2(H_2O)_2(SiF_6)]$ (Figure 4.5).

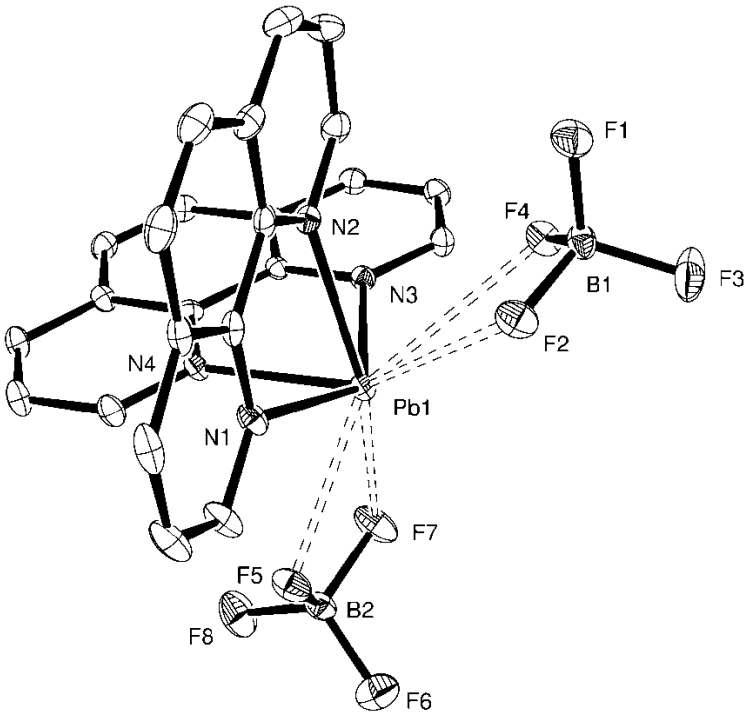

Figure 4.6 The structure of $[Pb(phen)_2(BF_4)_2]$ showing the atom labelling scheme. Ellipsoids are drawn at the 50% probability level and H atoms are omitted for clarity.

Table 4.6 Selected bond lengths (Å) and angles (°) for $[Pb(phen)_2(BF_4)_2]$

Pb1–N1	2.539(2)	N1–Pb1–N2	66.40(7)
Pb1–N2	2.483(2)	N3–Pb1–N4	66.62(6)
Pb1–N3	2.549(2)		
Pb1–N4	2.445(2)		
Pb1–F2	3.038(17)		
Pb1–F4	3.010(14)		
Pb1–F5	2.751(11)		
Pb1–F7	2.845(15)		

Though water is present in several of the X-ray crystal structures collected, the dried bulk products isolated from the reactions were found to be anhydrous by both IR spectroscopy and microanalysis, i.e. the bulk product from the reaction of $Pb(SiF_6)\cdot 2H_2O$ with two molar equivalents of 1,10-phenthroline was found to be $[Pb(phen)_2(SiF_6)]$. Bands corresponding to the fluoroanions are easily identified in the IR spectra of the complexes (see Table 4.7). The bands observed for $[Pb(phen)_2(BF_4)_2]$ are in good agreement with IR spectroscopic data that has been previously reported for this complex.[24] Upon coordination to a metal ion the symmetry of the fluoroanions will be lowered, which should result in band splitting.[1] However resolved splittings are not observed (instead the fluoroanion stretching modes are significantly broadened); this is in part due to overlap with bands corresponding to the diimine ligands,[25] but presumably is mostly because the interactions between the fluoroanions and the lead(II) are weak. The anion coordination modes cannot therefore be reliably distinguished using IR spectroscopy.

Table 4.7 IR spectroscopic data for the fluoroanions in the Pb(II) diimine complexes

Complex	ν(BF) / cm^{-1} [a,b]	ν(SiF) / cm^{-1} [a,c]
$[Pb(bipy)_2(BF_4)_2]$	1066 (vs, br), 520 (m)	–
$[Pb(phen)_2(BF_4)_2]$	1058 (vs, br), 523 (s)	–
$[Pb(bipy)_2(SiF_6)]$	–	755 (vs, br), 482 (m), 474 (s), 460 (m)
$[Pb(phen)_2(SiF_6)]$	–	735 (vs, br), 473 (s, br)

[a] nujol mull; [b] literature[26] values for $[BF_4]^-$ = 1070, 533 cm^{-1}; literature[26] values for $[SiF_6]^{2-}$ = 741, 483 cm^{-1}

While the NMR spectra of the $Pb(BF_4)_2$ diimine complexes were recorded in CD_3CN, the $Pb(SiF_6)$ diimine complexes were found to be insoluble in CH_3CN and so NMR spectra on these complexes were recorded in D_2O. The ^1H NMR spectra show the imine resonances shifted to high frequency, confirming that they are coordinated. However, the resonances in the $^{19}F\{^1H\}$ NMR spectra are consistent with 'free' $[BF_4]^-$ or $[SiF_6]^{2-}$,[21] indicating that the fluoroanion coordination seen in the solid state does not persist significantly in solution. Instead, the fluoroanions are probably displaced by the NMR solvent; more weakly coordinating solvents, such as CH_2Cl_2, cannot be used due to the insolubility of the complexes in these solvents. Presumably due to the dissociative, dynamic nature of the complexes in solution, no resonances were observed in the ^{207}Pb NMR spectra collected.

4.2.2 Complexes with the tridentate imine 2,2':6',2''-terpyridyl

In contrast to the Pb(II) diimine structures, most of the structures with terpy reported in the literature are 1:1 adducts. The complexes $[Pb(terpy)(Y)_2]$ (Y = ClO_4, NO_3, NO_2) are all one-dimensional chain polymers with bridging oxoanions.[8] The reaction of $Pb(SiF_6)\cdot 2H_2O$ with terpy in a 1:1 molar ratio afforded single crystals with the stoichiometry $[Pb(terpy)(H_2O)(SiF_6)]$ (Figure 4.7). The terpy ligand is chelating through all three nitrogen atoms and is planar, while there is a water molecule disordered above and below the PbN_3 plane that is weakly coordinating, with *d*(Pb–O) of 2.87(2) and 3.05(1) Å.

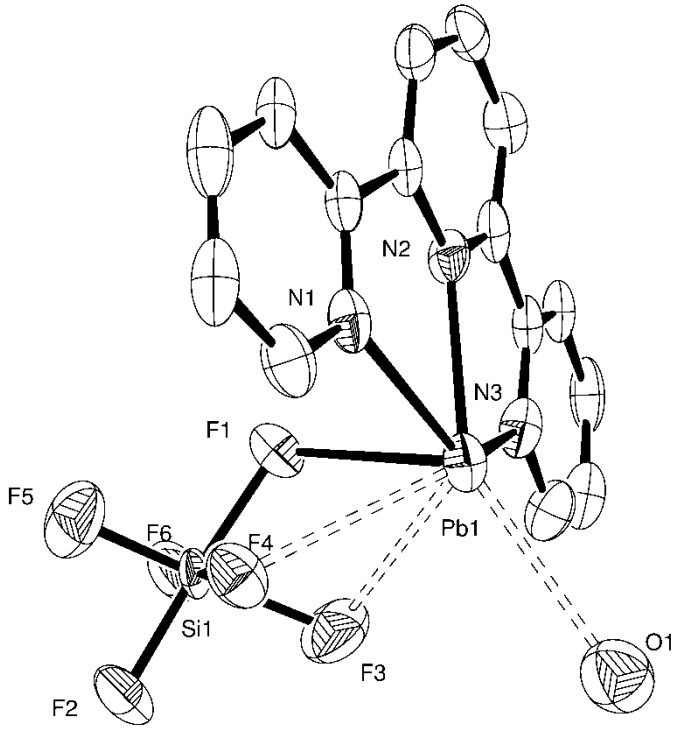

Figure 4.7 The structure of $[Pb(terpy)(H_2O)(SiF_6)]$ showing the atom labelling scheme. Ellipsoids are drawn at the 50% probability level and H atoms are omitted for clarity. The SiF_6 is rotationally disordered roughly about the F1–Si–F2 axis (only one orientation is shown).

Table 4.8 Selected bond lengths (Å) and angles (°) for $[Pb(terpy)(H_2O)(SiF_6)]$

Pb1–N1	2.550(6)	N1–Pb1 –N2	64.62(18)
Pb1–N2	2.491(6)	N2–Pb1–N3	65.73(19)
Pb1–N3	2.480(7)		

The $[SiF_6]^{2-}$ anion is also disordered, but appears to adopt two distinct and reasonably well-defined orientations, both with ~ 50% occupancy. Like the $[Pb(terpy)(Y)_2]$ (Y = ClO_4,

NO_3, NO_2),[8] the $[SiF_6]^{2-}$ fluoroanions bridge between the lead-terpy units to form a one-dimensional chain polymer, with π-stacking between the terpy ligands (distance between planes = 3.566 Å) in neighbouring chains (see Figure 4.8(a)) being evident. One orientation (Figure 4.8(a)) sees all six of the fluorines in the $[SiF_6]^{2-}$ group involved in bridging the lead-terpy units in a $\kappa^3\kappa'^3$ fashion, giving a ten-coordinate lead(II) centre, with the Pb–F distances ranging between ~2.54 and ~3.13 Å. In the other orientation (Figure 4.8(b)) the $[SiF_6]^{2-}$ groups are bridging via planar SiF_4 units ($\kappa^2\kappa'^2$-coordinated), resulting in an eight-coordinate lead(II) centre with Pb–F distances in the range ~2.43 to ~3.12 Å. As with the diimine complexes the bulk solid is anhydrous (i.e. $[Pb(terpy)(SiF_6)]$) by IR spectroscopy and microanalysis; its ^{1}H NMR spectrum shows resonances for the terpy shifted to high frequency, while the resonance in the $^{19}F\{^1H\}$ NMR spectrum is consistent with 'free' $[SiF_6]^{2-}$, consistent with dissociation in solution.

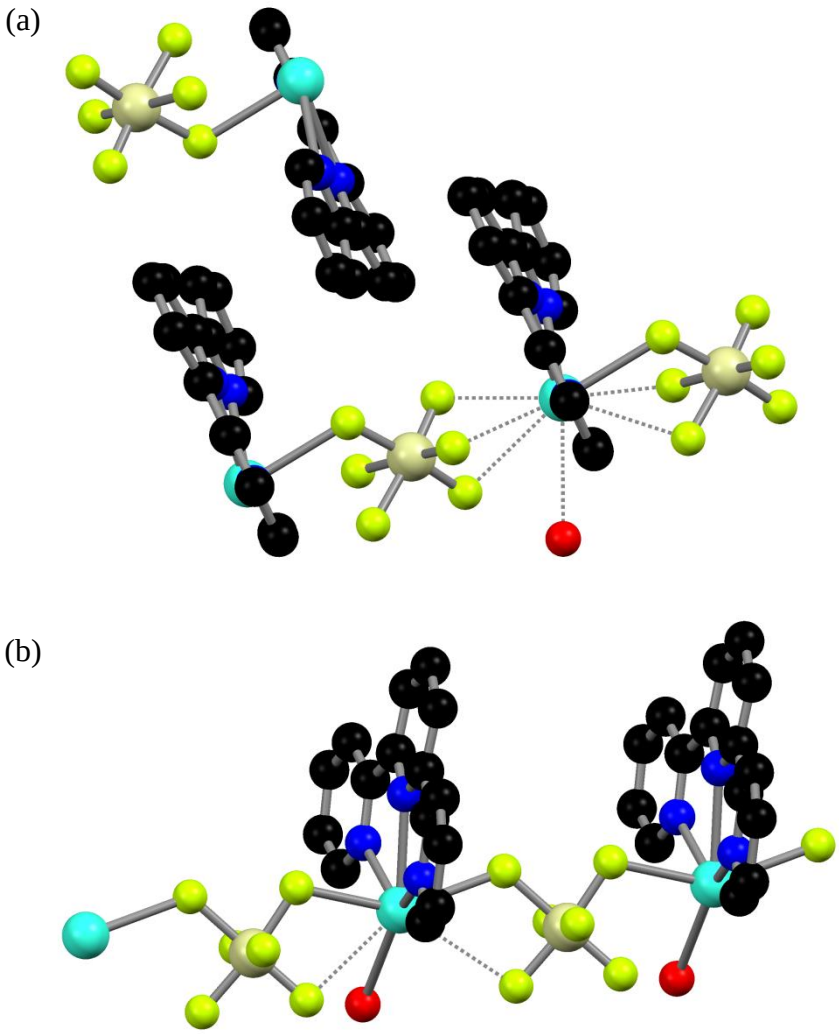

Figure 4.8 View of (a) the $\kappa^3\kappa'^3$ and (b) the $\kappa^2\kappa'^2$ orientation of the $[SiF_6]^{2-}$ fluoroanion in $[Pb(terpy)(H_2O)(SiF_6)]$. Colour key: light blue = Pb, blue = N, red = O, beige = Si, green = F, black = C.

Crystals obtained from the reaction of $Pb(BF_4)_2$ with terpy in a 1:1 molar ratio were reproducibly found by single crystal X-ray structure determination to be $[terpyH_2][BF_4]_2$, the cation of which is shown in Figure 4.9. The compound is triclinic, *P*-1, a = 8.363(3), b = 9.166(3), c = 12.212(5) Å, α = 83.125(16), β = 87.397(18), γ = 63.789(10)°, *Z* = 2. Unfortunately the data set collected is of insufficient quality (R_1 = 0.098, wR_2 = 0.312) to allow detailed structural analysis, and so full X-ray crystallographic data are not reported. The $[BF_4]^-$ anions are located on either side of the $[terpyH_2]^+$ cation and there is evidence of both N–H···F and C–H···F hydrogen bonding interactions between the cation and nearby fluoroanions, resulting in a supramolecular network. The cation is similar to the cation in the reported $[4'\text{-}ClterpyH_2][Cl][BF_4]$, which also exhibits an extensive hydrogen bonding network involving both the chloride and $[BF_4]^-$ fluoroanion.[27]

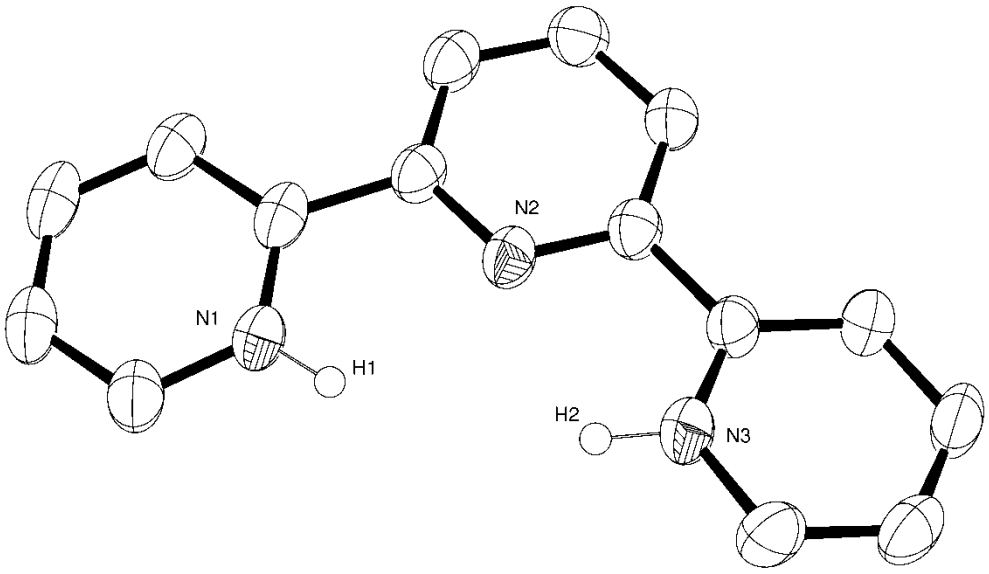

Figure 4.9 The structure of the cation in $[terpyH_2][BF_4]_2$. Ellipsoids are drawn at the 50% probability level and H atoms bonded to C are omitted for clarity.

To remove the excess acid in the supplied aqueous $Pb(BF_4)_2$ solution it was stirred with basic lead carbonate ($2PbCO_3 \cdot Pb(OH)_2$) for fifteen minutes, then filtered and the filtrate used immediately. Reaction of this filtrate with terpy in a 1:1 molar ratio yielded $[Pb(terpy)_3][BF_4]_2$, which has a nine-coordinate lead(II) centre. A single crystal X-ray structure determination (Figure 4.10) reveals the cation to be disordered around the three-fold axis, with the coordinated terpy ligands forming both a left and a right handed spiral, each with 50% occupancy. The non-coordinating $[BF_4]^-$ anions are also disordered about the three-fold axis. The cation has been reported before in $[Pb(terpy)_3][ClO_4]_2$,[28] which also shows disorder. For $[Pb(terpy)_3][BF_4]_2$ the disorder has been modelled in the

alternative space group *P*-3*c*1, as this avoids the unreasonably close approach of some atoms in the reported structure.[28] The isolated bulk white solid was found by microanalysis to also be $[Pb(terpy)_3][BF_4]_2$. The information available from spectroscopic techniques is limited, but the data are consistent with the non-coordination of the $[BF_4]^-$ anions.

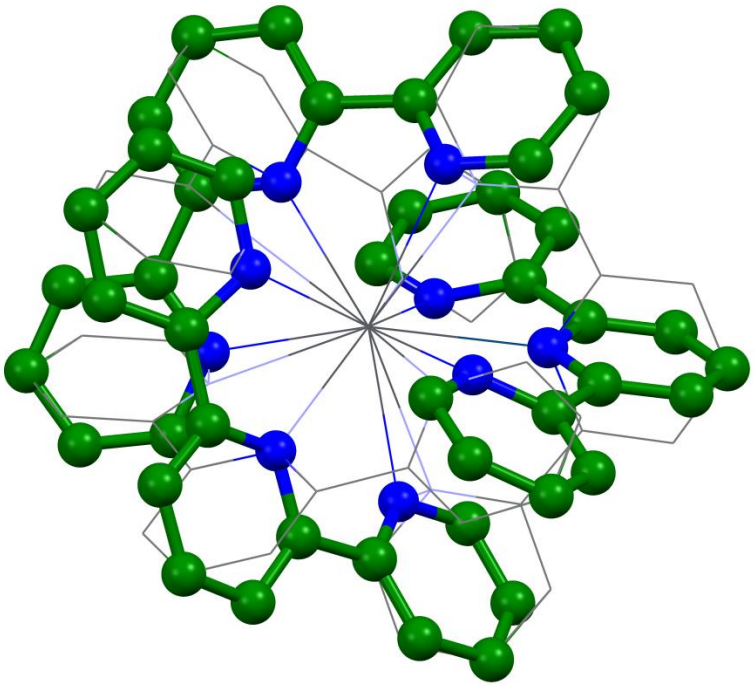

Figure 4.10 The structure of the disordered cation in $[Pb(terpy)_3][BF_4]_2$, showing the right and left handed spiral formed by the coordinated terpy ligands.

4.3 Conclusions

A number of new diimine complexes of the lead(II) salts $Pb(BF_4)_2$ and $Pb(SiF_6)$ have been synthesised which, along with the triimine complex $[Pb(terpy)(SiF_6)]$, show long but significant Pb–F interactions in the solid state. In solution the fluoroanions dissociate and are thought to be displaced by the solvent. The diimine complexes all feature two bipy or phen ligands "*cis*" disposed on one hemisphere of the lead, while the remaining coordination sphere is filled with longer contacts to $[BF_4]^-$ or $[SiF_6]^{2-}$, and sometimes water as well.

That fluoroanion coordination to Pb(II) is prevalent in these imine complexes, as well as in other systems, such as the complexes with crown ether, oxathia- and oxaselena-macrocycles,[2] demonstrates that Pb–F coordination is favoured. Four different $[BF_4]^-$ coordination modes (κ^1, κ^2, $\kappa^2\kappa'^1$ and μ^2) have been observed, all of which are present in $[\{Pb(bipy)_2(BF_4)_2(H_2O)_{0.25}\}_2]$. The dianionic $[SiF_6]^{2-}$ is capable of generating different structural motifs to the monoanionic fluoroanions, with examples of monomer, dimer and chain polymer Pb(II) complexes all having been formed.

Overall the complexes synthesised exhibit highly irregular geometries, while the lead(II) coordination numbers are large, ranging from eight to ten. What geometry is observed is probably largely dictated by the lead(II) centre accommodating the steric demands of the imine ligands and fluoroanions, whilst maximising Pb–donor interactions and minimising ligand repulsion. It is not possible to predict which fluoroanion coordination mode(s) will be observed for a given complex; the fact that four different modes were observed in $[\{Pb(bipy)_2(BF_4)_2(H_2O)_{0.25}\}_2]$ indicates that there is little difference between them on bond energy grounds. Therefore the structures adopted may also reflect packing within the crystal lattice (so as to maximise lattice energy), rather than any strong directional preference.

4.4 Experimental

The general experimental techniques used in this chapter can be found in Appendix 1 at the end of the thesis.

$[Pb(bipy)_2(BF_4)_2]$

$Pb(BF_4)_2$ as a 50% aqueous solution (0.206 g, 0.27 mmol) was added to a solution of 2,2'-bipyridyl (0.081 g, 0.52 mmol) in CH_3CN (5 mL), leading to the precipitation of a small amount of fine white powder. The reaction mixture was stirred for 24 h, then it was filtered and a portion was removed for crystal growth. From the remaining solution, the solvent was removed *in vacuo* to yield a pale pink powder, which was washed with Et_2O (5 mL) and dried *in vacuo*. Yield: 0.113 g, 60%. Anal. Calc. for $C_{20}H_{16}B_2F_8N_4Pb$: C, 34.7; H, 2.3; N, 8.1. Found: C, 34.7; H, 2.4; N, 8.2%. ^1H NMR (CD_3CN, 295 K): δ = 7.78 (ddd, [2H]), 8.29 (td, [2H]), 8.42 (d, [2H]), 8.74 (dd, [2H]). $^{19}F\{^1H\}$ NMR (CD_3CN, 295 K): δ = –150.6 (s). IR (Nujol): ν = 1066 (vs, br), 520 (m) (BF_4) cm^{-1}. Slow evaporation of a portion of the reaction mixture yielded colourless crystals of $[\{Pb(bipy)_2(BF_4)_2(H_2O)_{0.25}\}_2]$.

$[Pb(bipy)_2(SiF_6)]$

A solution of 2,2'-bipyridyl (0.081 g, 0.52 mmol) in CH_3CN (5 mL) was added to $Pb(SiF_6)\cdot 2H_2O$ (0.100 g, 0.26 mmol) dissolved in deionised water (15 mL), leading to the precipitation of a small amount of fine white powder. The reaction mixture was stirred for 1 h, then it was filtered and a portion of the filtrate removed for crystal growth. From the remaining solution, the solvent was removed *in vacuo* to yield a pale pink powder, which was washed with Et_2O (5 mL) and dried *in vacuo*. Yield: 0.062 g, 36%. Anal. Calc. for $C_{20}H_{16}F_6N_4PbSi$: C, 36.3; H, 2.4; N, 8.5. Found: C, 36.7; H, 2.5; N, 8.5%. ^1H NMR (D_2O, 295 K): δ = 7.57 (br s, [2H]), 8.03 (br s, [2H]), 8.09 (t, [2H]), 8.61 (br s, [2H]). $^{19}F\{^1H\}$ NMR (D_2O, 295 K): δ = –130.1 (s, $^1J_{FSi}$ = 109 Hz). IR (Nujol): ν = 755 (vs, br), 482 (m), 474 (s), 460 (m) (SiF_6) cm^{-1}. Slow evaporation of a portion of the reaction mixture yielded colourless crystals of $[Pb(bipy)_2(SiF_6)]$.

$[Pb(phen)_2(BF_4)_2]$

$Pb(BF_4)_2$ as a 50% aqueous solution (0.197 g, 0.26 mmol) was added to a solution of 1,10-phenanthroline (0.095 g, 0.52 mmol) in CH_3CN (5 mL), leading to the precipitation of a small amount of fine white powder. The reaction mixture was stirred for 2 h, then it was filtered and a small aliquot of the filtrate removed for crystal growth. From the remaining solution, the solvent was removed *in vacuo* to yield a white powder, which was washed with Et_2O (5 mL) and dried *in vacuo*. Yield: 0.107 g, 56%. Anal. Calc. for $C_{24}H_{16}B_2F_8N_4Pb$: C, 38.9; H, 2.2; N, 7.6. Found: C, 38.7; H, 2.1; N, 7.4%. ^{1}H NMR (CD_3CN, 295 K): δ = 8.03 (br s, [2H]), 8.12 (br s, [2H]), 8.75 (s, [2H]), 9.11 (br s, [2H]). $^{19}F\{^1H\}$ NMR (CD_3CN, 295 K): δ = –150.4 (s). IR (Nujol): ν = 1058 (vs, br), 523 (s) (BF_4) cm^{-1}. Slow evaporation of a portion of the reaction mixture yielded colourless crystals of $[Pb(phen)_2(BF_4)_2]$.

$[Pb(phen)_2(SiF_6)]$

A solution of 1,10-phenanthroline (0.100 g, 0.55 mmol) in CH_3CN (5 mL) was added to $Pb(SiF_6)\cdot 2H_2O$ (0.102 g, 0.26 mmol) dissolved in deionised water (15 mL), giving a colourless solution. The reaction mixture was stirred for 2 h, then the solvent volume was reduced *in vacuo* until a white powder precipitated, which was isolated by filtration, washed with CH_3CN and dried *in vacuo*. Yield: 0.045 g, 23%. Anal. Calc. for $C_{24}H_{16}F_6N_4PbSi$: C, 40.6; H, 2.3; N, 7.9. Found: C, 40.5; H, 2.2; N, 7.5%. ^{1}H NMR (D_2O, 295 K): δ = 7.93 (dd, [2H]), 7.97 (s, [2H]), 8.62 (dd, [2H]), 9.03 (dd, [2H]). $^{19}F\{^1H\}$ NMR (D_2O, 295 K): δ = –129.7 (s, $^1J_{FSi}$ = 109 Hz). IR (Nujol): ν = 735 (vs, br), 473 (s, br) (SiF_6) cm^{-1}. Slow evaporation of a portion of the reaction mixture yielded colourless crystals of $[\{Pb(phen)_2(SiF_6)\}_2]\cdot[Pb(phen)_2(H_2O)_2(SiF_6)]\cdot 11H_2O$.

$[Pb(terpy)(SiF_6)]$

A solution of 2,2’:6’,2”-terpyridyl (0.061 g, 0.26 mmol) in CH_3CN (5 mL) was added to $Pb(SiF_6)\cdot 2H_2O$ (0.100 g, 0.26 mmol) dissolved in deionised water (15 mL), giving a pale yellow solution. The reaction mixture was stirred for 1.5 h, then a portion was removed for crystal growth. From the remaining solution, the solvent was removed *in vacuo* to yield a beige powder, which was washed with Et_2O (5 mL) and dried *in vacuo*. Yield: 0.075 g,

49%. Anal. Calc. for $C_{15}H_{11}F_6N_3PbSi$: C, 30.9; H, 1.9; N, 7.2. Found: C, 30.8; H, 1.8; N, 7.1%. ^{1}H NMR (D_2O, 295 K): δ = 7.89 (t, [2H]), 8.29 (t, [2H]), 8.50 (t, [1H]), 8.55 (d, [2H]), 8.62 (d, [2H]), 8.91 (d, 2H). $^{19}F\{^1H\}$ NMR (D_2O, 295 K): δ = –129.8 (s, $^1J_{FSi}$ = 109 Hz). IR (Nujol): ν = 716 (vs, br), 469 (s, br) (SiF_6) cm^{-1}. Slow evaporation of a portion of the reaction mixture yielded colourless crystals of [Pb(terpy)(H_2O)(SiF_6)].

[Pb(terpy)$_3$][BF$_4$]$_2$

To $Pb(BF_4)_2$ as a 50% aqueous solution (0.201 g, 0.26 mmol) in deionised water (5 mL) was added a few crystals of basic lead carbonate. The resulting colourless solution was stirred for 15 min., filtered and 2,2':6',2"-terpyridyl (0.061 g, 0.26 mmol) in CH_3CN (5 mL) added. The colourless reaction mixture was stirred for 1.5 h, then the CH_3CN was removed *in vacuo* which caused the precipitation of a white solid. The solid was isolated by filtration, washed with Et_2O (3 mL) and dried *in vacuo*. Yield: 0.028 g, 30%. Anal. Calc. for $C_{45}H_{33}B_2F_8N_9Pb$: C, 50.0; H, 3.1; N, 11.7. Found: C, 49.9; H, 3.0; N, 11.8%. ^{1}H NMR (CD_3CN, 295 K): δ = 7.38 (td, [2H]), 8.05 (td, [2H]), 8.35 (t, [1H]), 8.47 (d, [2H]), 8.50 (d, [2H]), 8.55 (d, [2H]). $^{19}F\{^1H\}$ NMR (CD_3CN, 295 K): δ = –151.2 (s). IR (Nujol): ν = 1049 (vs, br), 520 (m) (BF_4) cm^{-1}. Slow evaporation of a portion of the reaction mixture yielded colourless crystals of [Pb(terpy)$_3$][BF_4]$_2$.

[terpyH$_2$][BF$_4$]$_2$

$Pb(BF_4)_2$ as a 50% aqueous solution (0.207 g, 0.27 mmol) was added to a solution of 2,2':6',2"-terpyridyl (0.062 g, 0.27 mmol) in CH_3CN (5 mL) to give a pale yellow solution. The reaction mixture was stirred for 1.5 h, over which time precipitation of a small amount of white powder occurred. The reaction was filtered, and then a portion of the filtrate was removed for crystal growth. From the remaining solution, the solvent was removed *in vacuo* to yield a pale yellow powder, which was dried *in vacuo*. Yield: 0.041 g. ^{1}H NMR (CD_3CN, 295 K): δ = 2.61 (br s, NH), 7.94 (t, [2H]), 8.33 (t, [2H]), 8.62-8.54 (m, [3H]), 8.66 (d, [2H]), 9.01 (d, [2H]). $^{19}F\{^1H\}$ NMR (CD_3CN, 295 K): δ = –150.3 (s). IR (Nujol): ν = 3236 (s, br), 3185 (s, br), 3109 (m) (NH), 1067 (vs, br), 521 (s) (BF_4) cm^{-1}. Slow evaporation of a portion of the reaction mixture yielded colourless crystals of [terpyH$_2$][BF_4]$_2$.

4.5 Appendix – X-Ray Crystallographic Data

Compound	[{Pb(bipy)$_2$(BF$_4$)$_2$-(H$_2$O)$_{0.25}$}$_2$]	[Pb(bipy)$_2$(SiF$_6$)]	[Pb(phen)$_2$(BF$_4$)$_2$]
Formula	$C_{20}H_{16.50}B_2F_8N_4O_{0.25}Pb$	$C_{20}H_{16}F_6N_4PbSi$	$C_{24}H_{16}B_2F_8N_4Pb$
M	697.68	661.65	741.22
Crystal system	triclinic	monoclinic	triclinic
Space group (no.)	*P*-1 (2)	*P*2$_1$/*n* (14)	*P*-1 (2)
a /Å	12.796(5)	10.748(13)	7.830(5)
b /Å	12.894(5)	14.188(16)	11.971(7)
c /Å	13.958(5)	13.599(15)	12.983(8)
α /°	83.820(12)	90	90.592(12)
β /°	83.697(11)	104.037(15)	96.972(12)
γ /°	89.317(12)	90	95.428(17)
U /Å^3	2275.7(15)	2012(4)	1202.2(13)
Z	4	4	2
μ(Mo-K$_\alpha$) /mm^{-1}	7.497	8.517	7.102
F(000)	1322	1256	704
Total no. reflns	20215	6769	10707
R_{int}	0.093	0.034	0.019
Unique reflns	10140	3552	5444
No. of params, restraints	635, 0	283, 0	352, 0
R_1, wR_2 [$I > 2\sigma(I)$][a]	0.072, 0.171	0.034, 0.059	0.016, 0.031
R_1, wR_2 (all data)	0.090, 0.183	0.041, 0.063	0.018, 0.032

Common items: T = 100 K; wavelength (Mo-Kα) = 0.71073 Å; θ(max) = 27.5°.

[a] $R_1 = \Sigma||F_o| - |F_c|| / \Sigma|F_o|$; $wR_2 = [\Sigma w(F_o^2 - F_c^2)^2 / \Sigma wF_o^4]^{1/2}$.

Compound	$[\{Pb(phen)_2(SiF_6)\}_2]\cdot[Pb(phen)_2(H_2O)_2(SiF_6)]\cdot 11H_2O$	$[Pb(terpy)(H_2O)\text{-}(SiF_6)]$	$[Pb(terpy)_3][BF_4]_2$
Formula	$C_{72}H_{74}F_{18}N_{12}O_{13}Pb_3Si_3$	$C_{15}H_{13}F_6N_3OPbSi$	$C_{45}H_{33}B_2F_8N_9Pb$
M	2363.27	600.56	1080.61
Crystal system	monoclinic	triclinic	trigonal
Space group (no.)	$P2_1/c$ (14)	$P\bar{1}$ (2)	$P\bar{3}c1$ (165)
a /Å	12.289(3)	6.938(4)	13.0853(19)
b /Å	31.837(6)	8.888(5)	13.0853(19)
c /Å	20.399(4)	13.345(8)	14.558(3)
α /°	90	98.936(13)	90
β /°	100.658(4)	90.905(12)	90
γ /°	90	90.119(10)	120
U /Å^3	7844(3)	812.8(8)	2158.7(8)
Z	4	2	2
μ(Mo-K$_\alpha$) /mm^{-1}	6.583	10.529	3.988
F(000)	4576	564	1060
Total no. reflns	36217	7418	4520
R_{int}	0.034	0.081	0.033
Unique reflns	17354	3709	1645
No. of params, restraints	1090, 0	270, 136	104, 368
R_1, wR_2 [$I > 2\sigma(I)$][a]	0.042, 0.074	0.062, 0.132	0.024, 0.062
R_1, wR_2 (all data)	0.055, 0.080	0.069, 0.136	0.033, 0.065

Common items: T = 100 K; wavelength (Mo-Kα) = 0.71073 Å; θ(max) = 27.5°.

[a] $R_1 = \Sigma||F_o| - |F_c|| / \Sigma|F_o|$; $wR_2 = [\Sigma w(F_o^2 - F_c^2)^2 / \Sigma wF_o^4]^{1/2}$.

4.6 References

1. W. Beck and K. Suenkel, *Chem. Rev.*, 1988, **88**, 1405-1421.
2. P. Farina, T. Latter, W. Levason and G. Reid, *Dalton Trans.*, 2013, **42**, 4714-4724.
3. E. S. Claudio, H. A. Godwin and J. S. Magyar, *Prog. Inorg. Chem.*, 2003, **51**, 1-144.
4. B. Cordero, V. Gomez, A. E. Platero-Prats, M. Reves, J. Echeverria, E. Cremades, F. Barragan and S. Alvarez, *Dalton Trans.*, 2008, 2832-2838.
5. J. Parr, in *Comprehensive Coordination Chemistry II*, eds. J. A. McCleverty and T. J. Meyer, Elsevier, Oxford, 2004, vol. 3, pp. 545-608.
6. R. L. Davidovich, V. Stavila and K. H. Whitmire, *Coord. Chem. Rev.*, 2010, **254**, 2193-2226.
7. G. Bowmaker, J. Harrowfield, H. Miyamae, T. Shand, B. Skelton, A. Soudi and A. White, *Aust. J. Chem.*, 1996, **49**, 1089-1097.
8. L. Engelhardt, J. Harrowfield, H. Miyamae, J. Patrick, B. Skelton, A. Soudi and A. White, *Aust. J. Chem.*, 1996, **49**, 1135-1146.
9. P. G. Harrison, M. G. Begley, T. Kikabhai, A. T. Steel and M. I. Khalil, *J. Chem. Soc., Dalton Trans.*, 1989, 2443-2448.
10. M. Kadarkaraisamy, D. P. Engelhart, P. N. Basa and A. G. Sykes, *J. Coord. Chem.*, 2010, **63**, 2261-2267.
11. S. H. Strauss, *Chem. Rev.*, 1993, **93**, 927-942.
12. K. Fujiki, S. Ikeda, H. Kobayashi, A. Mori, A. Nagira, J. Nie, T. Sonoda and Y. Yagupolskii, *Chem. Lett.*, 2000, **29**, 62-63.
13. I. Krossing and I. Raabe, *Angew. Chem. Int. Ed.*, 2004, **43**, 2066-2090.
14. L. Engelhardt, J. Harrowfield, H. Miyamae, J. Patrick, B. Skelton, A. Soudi and A. White, *Aust. J. Chem.*, 1996, **49**, 1111-1119.
15. R. W. Seidel, C. Dietz, J. Breidung, R. Goddard and I. M. Oppel, *Acta Crystallogr. Sect. C: Cryst. Struct. Commun.*, 2013, **69**, 1112-1115.
16. J. S. Fleming, K. L. V. Mann, S. M. Couchman, J. C. Jeffery, J. A. McCleverty and M. D. Ward, *J. Chem. Soc., Dalton Trans.*, 1998, 2047-2052.
17. M. Mantina, A. C. Chamberlin, R. Valero, C. J. Cramer and D. G. Truhlar, *J. Phys. Chem. A*, 2009, **113**, 5806-5812.
18. P. Jutzi, R. Dickbreder and H. Nöth, *Chem. Ber.*, 1989, **122**, 865-870.
19. D. L. Reger, J. E. Collins, A. L. Rheingold, L. M. Liable-Sands and G. P. A. Yap, *Inorg. Chem.*, 1997, **36**, 345-351.
20. A. M. Golubev, A. M. Il'inets, A. N. Tsvigunov and L. G. Makarevich, *Kristallografiya*, 1991, **36**, 214-216.

21. D. Zopes, S. Kremer, H. Scherer, L. Belkoura, I. Pantenburg, W. Tyrra and S. Mathur, *Eur. J. Inorg. Chem.*, 2011, **2011**, 273-280.

22. I. Bytheway, L. Engelhardt, J. Harrowfield, D. Kepert, H. Miyamae, J. Patrick, B. Skelton, A. Soudi and A. White, *Aust. J. Chem.*, 1996, **49**, 1099-1110.

23. B. Neumüller and K. Dehnicke, *Z. Anorg. Allg. Chem.*, 2008, **634**, 2567-2571.

24. A. N. Chebotarev, M. V. Shestakova, V. F. Khorunov and O. M. Sabadash, *Ukr. Khim. Zh. (Russ. Ed.)*, 2000, **66**, 88-92.

25. M. S. Atanassova and G. D. Dimitrov, *Spectrochim. Acta, Part A*, 2003, **59**, 1655-1662.

26. K. Nakamoto, *Infrared and Raman Spectra of Inorganic and Coordination Compounds*, Wiley-Interscience, NY, 4 edn., 1986.

27. W. Huang and H. Qian, *J. Mol. Struct.*, 2007, **832**, 108-116.

28. D. Kepert, J. Patrick, B. Skelton and A. White, *Aust. J. Chem.*, 1988, **41**, 157-158.

Chapter 5: Coordination Complexes of Lead(II) Salts with Phosphine Ligands

5.1 Introduction

While there is considerable lead(II) coordination chemistry with oxygen, nitrogen, sulfur and selenium donor ligands,[1] complex formation with phosphine ligands has been largely overlooked.[2] The aim of this chapter was to find suitable lead(II) precursors and reaction conditions to enable the synthesis of some Pb(II) diphosphine complexes, and to characterise these new complexes as fully as possible in order to establish trends in their behaviour and structures adopted as a function of the phosphine ligand and anion present.

5.1.1 Pb(II) coordination complexes with phosphine ligands

Though Pb(IV) is almost certainly too strongly oxidising to form phosphine complexes (evidenced by the rapid decomposition of the uncharacterised solid that was obtained from the reaction of $PbCl_4$ with PPh_3),[3] DFT calculations predict that Pb(II) will form viable complexes with neutral phosphine ligands, as ΔG was calculated to be negative for the reactions $PbCl_2 + PR_3 \rightarrow [PbCl_2(PR_3)]$ (R = H, Me, Ph).[4] Furthermore, Pb(II) is classed as an intermediate Lewis acid[5] (see Section 1.6), and so is expected to be able to form complexes with a broad range of donor atoms, including soft neutral phosphorus donor ligands. It is therefore surprising that there are very few phosphine complexes known for lead, one of the most common p-block metals, especially when other heavy p-block elements are considered. The coordination chemistry of Ga(III), In(III), Ge(II), Ge(IV), Sb(III) and Bi(III) with phosphine ligands is well established,[2] and while a large number of Sn(IV) phosphine complexes have long been known, recent work on Sn(II) has also yielded several diphosphine complexes of $SnCl_2$.[6]

The only structurally characterised examples of neutral Pb(II) diphosphine complexes are the Pb(II) thiolates, $[(2,6\text{-}Me_2C_6H_3S)_2Pb]_2\{\mu\text{-}Ph_2P(CH_2)_2PPh_2\}$ (Figure 5.1(a)) and $[(2,6\text{-}Me_2C_6H_3S)_2Pb]_3\{Me_2P(CH_2)_2PMe_2\}$ (Figure 5.1(b)), the latter of which consists of a chain of three lead centres linked by thiolate bridges, with the $Me_2P(CH_2)_2PMe_2$ chelated to the central Pb(II).[7] The complexes $[PbBr_2\{Et_2P(CH_2)_2PEt_2\}]$ and $[Pb\{Et_2P(CH_2)_2PEt_2\}_2][ClO_4]_2$ were reported in 1960, but characterisation was limited to partial microanalysis.[8] Several $Pb(SbF_6)_2$ complexes with polydentate phosphine ligands,

including $Ph_2P(CH_2)_2PPh_2$ and $MeC(CH_2PPh_2)_3$, have been studied by *in situ* $^{31}P\{^1H\}$ and ^{207}Pb NMR spectroscopy in $MeNO_2$ solution. Although no complexes were isolated, the data suggest that the major species present were the 1:1 adducts, with ^{31}P–^{207}Pb couplings ($^1J_{PbP}$ = ~ 1800 Hz) usually being resolved at room temperature.[9,10]

(a)

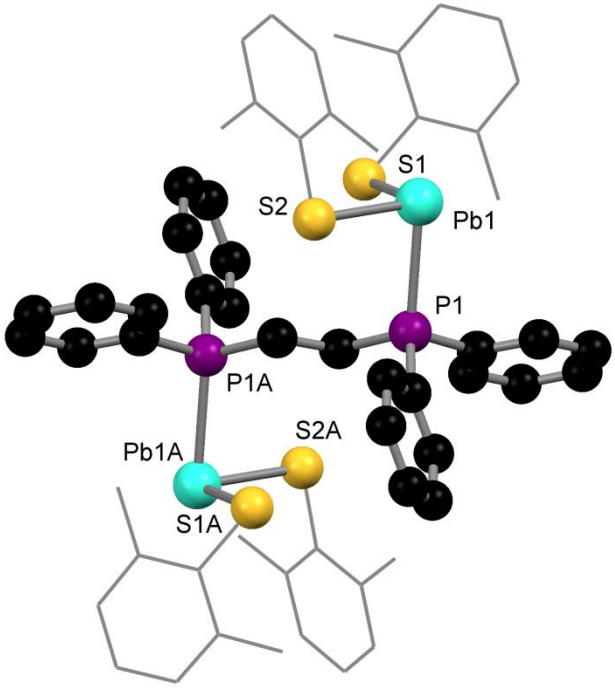

(b)

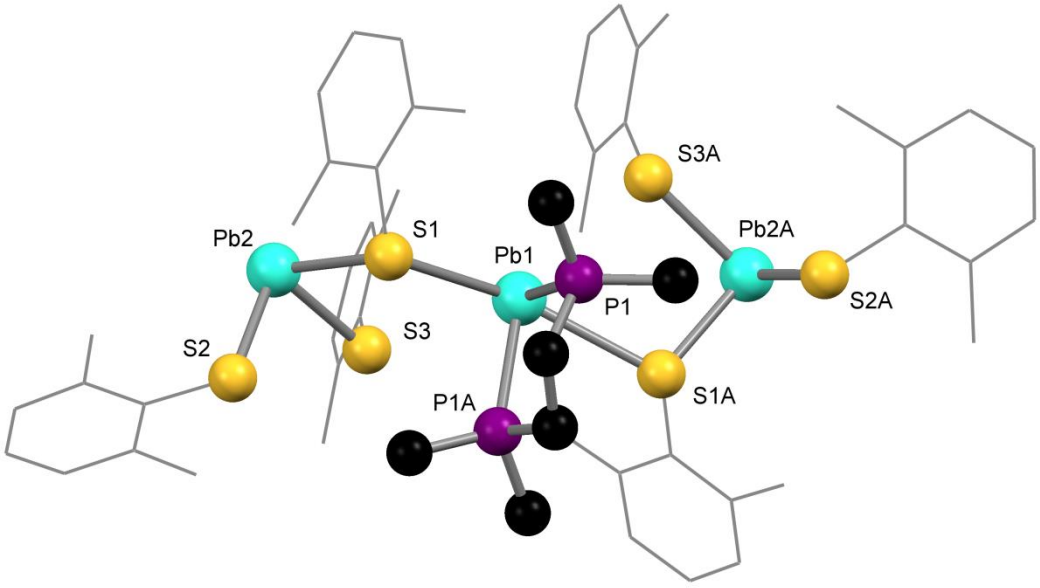

Figure 5.1 View of (a) $[(2,6\text{-}Me_2C_6H_3S)_2Pb]_2\{\mu\text{-}Ph_2P(CH_2)_2PPh_2\}$ and (b) $[(2,6\text{-}Me_2C_6H_3S)_2Pb]_3\{Me_2P(CH_2)_2PMe_2\}$.[7]

The reaction of $PbBr_2$ and monodentate PEt_3 with $[(Me_3Si)_2KSi(SiMe_2)_2SiK(SiMe_3)_2]$ yielded the cyclic disilylated plumbylene phosphine adduct

[(Et_3P)Pb{(Me_3Si)$_2$Si($SiMe_2$)$_2$Si($SiMe_3$)$_2$}], which has a Pb–P bond length of 2.740(2) Å.[11] Coordinated phosphino-groups are also present in complexes of Pb(II) with anionic ligands, where the charge is on N or S. The phosphinothiolate complexes [Pb{2-(Ph_2P)C_6H_4S}$_2$] and [Pb{2-(Ph_2P)-6-(Me_3Si)C_6H_3S}$_2$] were obtained by the anodic dissolution of lead in a CH_3CN solution of the ligand,[12] while [Pb{2-(R_2P)C_6H_4S}$_2$] (R = ^{i}Pr, ^{t}Bu, Ph) were synthesised from MeOH solution using $PbCl_2$ and excess NEt_3.[13] The Pb(II) phosphanamide complex [Pb{2-(Ph_2PCH)C_5H_4N}{$N(SiMe_3)_2$}] is also known.[14] There are no known complexes of Pb(II) with arsine ligands.

Though limited in number, these examples clearly show that Pb(II) will form complexes with mono- and bi-dentate phosphine ligands, with both bridging and chelating coordination modes having been observed for the latter. However, there has been no detailed and systematic investigation into Pb(II) phosphine coordination chemistry; for most of the complexes reported, the nature of the phosphine coordination to Pb(II) is not the main focus of the studies, and characterisation is often limited.

Main group phosphine chemistry is usually performed with metal halides,[2] but the lead dihalides are largely insoluble and intractable in nature;[1] the isomorphous $PbCl_2$ and $PbBr_2$ have nine-coordinate Pb(II) centres, while PbI_2 forms a layer lattice with six-coordinate Pb(II) centres.[15] Solvent adducts (that have favourable properties such as increased solubility or reactivity) have been successfully used as precursors in lighter p-block phosphine chemistry; for example, [$SnCl_2$(1,4-dioxane)] was used to synthesise some diphosphine complexes of Sn(II).[6] For PbX_2 (X = Cl, Br, I), numerous solvent adducts (e.g. [$PbX_2(DMSO)_2$]) have been reported, having usually been synthesised by direct reaction with the parent ligand.[16] However, typically the adducts were found to be insoluble in common organic solvents, presumably due to having polymeric structures with extensive halide bridging. The lead dihalides therefore do not provide a good entry point into Pb(II) phosphine coordination chemistry.

The initial challenge therefore is to find suitable lead precursors and reaction conditions to enable the synthesis of Pb(II) phosphine complexes, which the literature has shown often requires the use of less conventional solvents and reaction methods. The work in this chapter describes the synthesis and structures of some diphosphine complexes of $Pb(NO_3)_2$ and $Pb(SiF_6)\cdot 2H_2O$, and probes their behaviour in solution and in the solid state.

5.2 Results and Discussion

Lead(II) coordination chemistry is often performed with oxo-salts,[1] and so $Pb(NO_3)_2$ was investigated as a precursor. The structure of $Pb(NO_3)_2$ reveals twelve-coordinate Pb(II) centres, with Pb–O distances of 2.7482(6) and 2.8688(6) Å.[17] As di- and tri-imine complexes of the lead(II) fluoroanion salts $Pb(BF_4)_2$ and $Pb(SiF_6)\cdot 2H_2O$ were successfully synthesised (see Section 4.2), and found to exhibit a range of fluoroanion coordination modes, these salts were also reacted with bidentate phosphine ligands. In all but one experiment (see Section 5.2.3) the 50% aqueous solution of $Pb(BF_4)_2$ was found to protonate the phosphine ligand. Ligand protonation has been observed before when $[terpyH_2][BF_4]_2$ was repeatedly obtained from the reaction of $Pb(BF_4)_2$ with terpy (see Section 4.2.2), and is presumably caused by the excess acid added to the solution to prevent hydroxide formation at the lead. The diphosphine ligands *o*-$C_6H_4(PMe_2)_2$, $Me_2P(CH_2)_2PMe_2$ and $Et_2P(CH_2)_2PEt_2$ were chosen as they are strong σ-donating ligands that can form favourable five-membered chelate rings.

Both $Pb(NO_3)_2$ and $Pb(SiF_6)\cdot 2H_2O$ show negligible solubility in organic solvents, such as CH_2Cl_2 or toluene, which are commonly used for phosphine coordination chemistry. Reactions therefore involved dissolving $Pb(NO_3)_2$ or $Pb(SiF_6)\cdot 2H_2O$ in the minimum amount of water that had been degassed with N_2 (to prevent unwanted oxidation of the diphosphine ligand), to which a solution of the diphosphine in CH_3CN was added. The reactions were performed under an inert atmosphere, and the complexes were obtained as white powders. Crystals suitable for single crystal X-ray diffraction study were grown by carefully layering a miscible solvent (typically Et_2O) onto a solution of the pre-isolated complex (which was typically made up using the minimal amount of DMF). *In-situ* oxidation of the diphosphine ligands was occasionally observed (Section 5.2.3).

Characterisation of the complexes has been driven by solid state techniques: primarily single crystal X-ray diffraction, but supported by identification of the anion using infrared spectroscopy, and by microanalysis to confirm the stoichiometries of the bulk samples. Of the complexes isolated, multinuclear NMR spectroscopy could only be performed on $[Pb\{Et_2P(CH_2)_2PEt_2\}(NO_3)_2]$ (see Section 5.2.1), as it alone was sufficiently soluble in a weakly coordinating solvent (CD_2Cl_2). The other complexes were found to be insoluble in common NMR solvents, including CD_2Cl_2, CD_3CN, D_2O and CD_3OD, while in the strong donor solvent DMF (in which the complexes were soluble) the diphosphine ligand was partially displaced, meaning no useful NMR spectroscopic data were obtained.

5.2.1 Lead(II) nitrate complexes

The reaction of $Pb(NO_3)_2$ with $Me_2P(CH_2)_2PMe_2$ in a 1:2 molar ratio was found to form only the 1:1 adduct $[Pb\{Me_2P(CH_2)_2PMe_2\}(NO_3)_2]$, with the stoichiometry of the isolated bulk powder being confirmed by microanalysis. The X-ray crystal structure (Figure 5.2) reveals a symmetrically chelated $Me_2P(CH_2)_2PMe_2$ ligand, with *d*(Pb–P) ~0.05 Å shorter than in $[(2,6\text{-}Me_2C_6H_3S)_2Pb]_3\{Me_2P(CH_2)_2PMe_2\}$.[7] The $[NO_3]^-$ groups are asymmetrically κ^2-coordinated, with a difference in *d*(Pb–O) of ~0.2 Å.

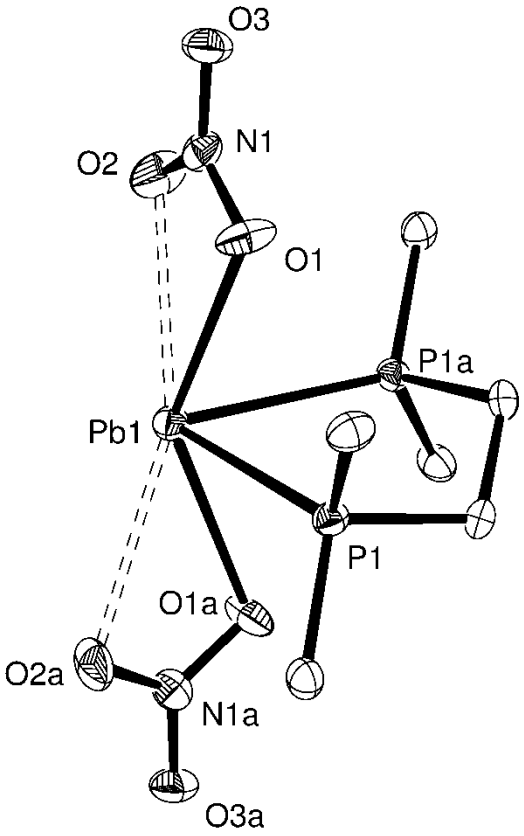

Figure 5.2 The structure of $[Pb\{Me_2P(CH_2)_2PMe_2\}(NO_3)_2]$ showing the atom labelling scheme. Ellipsoids are drawn at the 50% probability level and H atoms are omitted for clarity. Symmetry operation: a = x, y, – z.

Table 5.1 Selected bond lengths (Å) and angles (°) for $[Pb\{Me_2P(CH_2)_2PMe_2\}(NO_3)_2]$

Pb1–P1	2.7918(15)	P1–Pb1–P1a	74.19(6)
Pb1–O1	2.621(4)	O1–Pb1–O2	46.07(13)
Pb1–O2	2.859(5)	O1–Pb1–O1a	139.98(19)

Two further contacts (d(Pb–O) = 2.995(4) Å, well within the sum of the Van der Waal's radii of 3.54 Å[18] for Pb and O) from $[NO_3]^-$ groups on neighbouring molecules link the units into an infinite polymer network (Figure 5.3), so that overall the coordination number around the Pb(II) centre is eight. The ∠P–Pb–P is almost identical in both $[Pb\{Me_2P(CH_2)_2PMe_2\}(NO_3)_2]$ (74.19(6)°) and the *pseudo*-trigonal bipyramidal Pb1 centre in $[(2,6\text{-}Me_2C_6H_3S)_2Pb]_3\{Me_2P(CH_2)_2PMe_2\}$ (73.49(5)°),[7] suggesting that the nitrate complex is not sterically crowded.

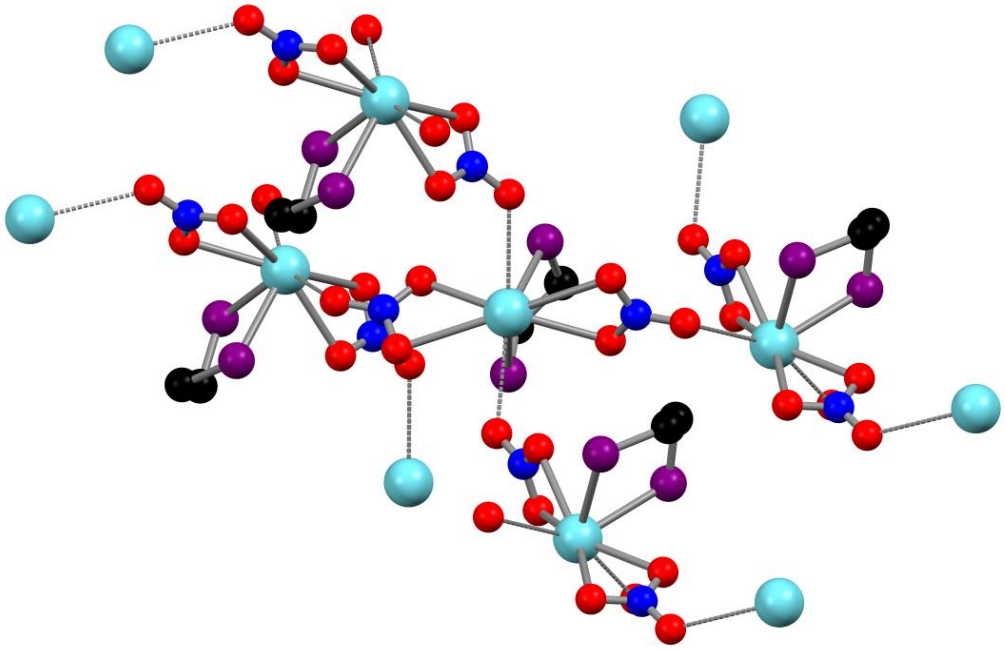

Figure 5.3 View of the extended structure of $[Pb\{Me_2P(CH_2)_2PMe_2\}(NO_3)_2]$. Methyl groups are omitted for clarity. Colour key: light blue = Pb, purple = P, blue = N, red = O, black = C.

The X-ray crystal structure of $[Pb\{o\text{-}C_6H_4(PMe_2)_2\}(NO_3)_2]$ (Figure 5.4), obtained from the reaction of $Pb(NO_3)_2$ and $o\text{-}C_6H_4(PMe_2)_2$ in a 1:1 molar ratio, has a very similar molecular unit to $[Pb\{Me_2P(CH_2)_2PMe_2\}(NO_3)_2]$, with a single chelating diphosphine ligand and asymmetrically κ^2-coordinated $[NO_3]^-$ anions. The Pb–P bond lengths are comparable in both complexes, while the ∠O–Pb–O for the nitrate oxygen atoms nearest the diphosphine is ~ 7° larger in $[Pb\{o\text{-}C_6H_4(PMe_2)_2\}(NO_3)_2]$. The third oxygen of the $[NO_3]^-$ groups again bridge to neighbouring Pb(II) centres with d(Pb–O) of 2.948(5) and 2.959(5) Å (Figure 5.5), so that an infinite chain structure is formed with the coordination number around Pb(II) being eight.

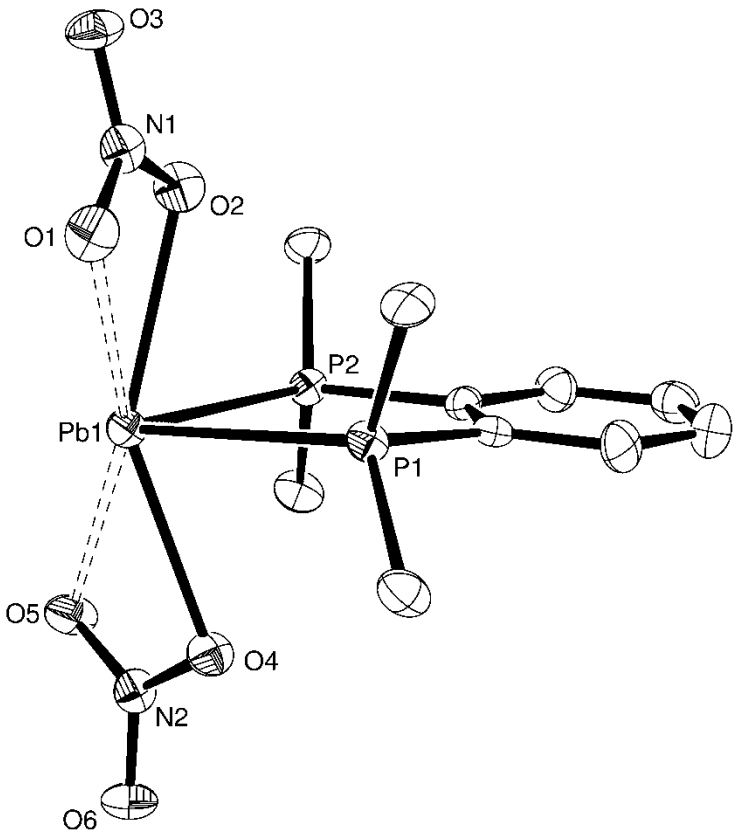

Figure 5.4 The structure of [Pb{*o*-$C_6H_4(PMe_2)_2$}$(NO_3)_2$] showing the atom labelling scheme. Ellipsoids are drawn at the 50% probability level and H atoms are omitted for clarity.

Table 5.2 Selected bond lengths (Å) and angles (°) for [Pb{*o*-$C_6H_4(PMe_2)_2$}$(NO_3)_2$]

Pb1–P1	2.806(2)	P1–Pb1–P2	71.95(6)
Pb1–P2	2.8088(19)	O1–Pb1–O2	46.56(15)
Pb1–O1	2.869(6)	O2–Pb1–O4	147.37(16)
Pb1–O2	2.611(6)	O4–Pb1–O5	46.83(15)
Pb1–O4	2.595(5)		
Pb1–O5	2.827(6)		

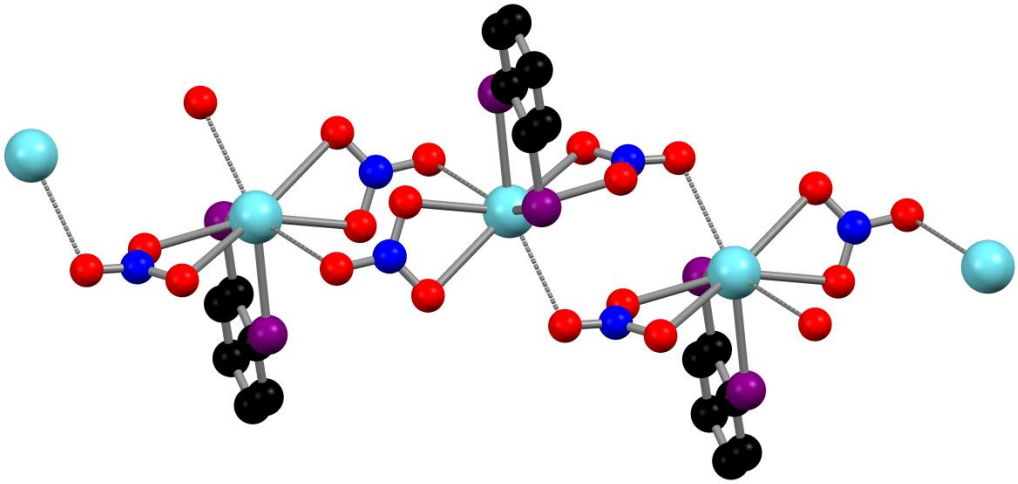

Figure 5.5 View of the chain structure of [Pb{*o*-$C_6H_4(PMe_2)_2$}$(NO_3)_2$]. Methyl groups are omitted for clarity. Colour key: light blue = Pb, purple = P, blue = N, red = O, black = C.

Looking at the X-ray crystal structures of both complexes, it becomes evident that there is a four-coordinate P_2O_2 core motif which occupies one hemisphere of the lead, with longer contacts to other nitrate oxygen atoms occupying much of the remaining coordination sphere. The *d*(Pb–O) for the core nitrate oxygen atoms are ~0.15 Å shorter than the shortest Pb–O distance in $Pb(NO_3)_2$.[17] If the κ^2-coordinated $[NO_3]^-$ groups are considered to occupy one (axial) coordination site each then the geometries around the lead(II) centres are very distorted from a regular octahedron. In [Pb{$Me_2P(CH_2)_2PMe_2$}$(NO_3)_2$] the ∠O–Pb–O between the (equatorial) nitrate oxygen atoms that are bridging from nearby molecules is 155.89(19)°, while the corresponding ∠O–Pb–O is 140.60(15)° in [Pb{*o*-$C_6H_4(PMe_2)_2$}$(NO_3)_2$]. These "voids" in the coordination spheres could indicate the presence of a stereochemically active lone pair on the Pb(II),[19] but because the structures are polymeric, crystal packing effects must also be taken into consideration, which could strongly influence the geometries observed.

Identification of the crystallographically characterised κ^2-coordinated $[NO_3]^-$ groups is possible in the IR spectra of the two complexes. Three IR active ν(NO) stretching modes ($2a_1$ and b_2) are expected as the nitrates have approximately C_{2v} symmetry.[20] Two stretches are observed at ~1310 and 1030 cm^{-1} (the stretch anticipated at ~1470 cm^{-1} is obscured by Nujol), while a bending mode[20] is also evident at ~815 cm^{-1}. The bands observed are similar to those reported for macrocyclic complexes of $Pb(NO_3)_2$ (such as [Pb(18-crown-6)$(NO_3)_2$]), which also exhibit high coordination numbers and

κ^2-coordinated $[NO_3]^-$ groups.[21] Splitting of some of the bands was seen in the IR spectra, though this was more clearly resolved for $[Pb\{o\text{-}C_6H_4(PMe_2)_2\}(NO_3)_2]$.

The reaction of $Pb(NO_3)_2$ with $Et_2P(CH_2)_2PEt_2$ in a 1:1 molar ratio yielded $[Pb\{Et_2P(CH_2)_2PEt_2\}(NO_3)_2]$ as a white powder; its stoichiometry was confirmed by microanalysis. The ligand $Et_2P(CH_2)_2PEt_2$ was used with the specific intention of increasing complex solubility in weakly coordinating organic solvents for NMR studies (*vide infra*). The system was susceptible to hydrolysis in solution, evidenced by several instances whereby crystals whose unit cells matched that of $[Pb_4(OH)_4][NO_3]_4$[22] grew either from the reaction solution or from crystallisation attempts on the phosphine complex. Despite several attempts, no crystals of $[Pb\{Et_2P(CH_2)_2PEt_2\}(NO_3)_2]$ were successfully grown (on one occasion a few crystals of the phosphine oxide complex $[Pb\{Et_2(O)P(CH_2)_2P(O)Et_2\}_2(NO_3)_2]$ were obtained – see Section 5.2.3). The IR spectrum of the white powder isolated indicates that the $[NO_3]^-$ groups are again κ^2-coordinated with bands corresponding to ν(NO) at 1300, 1029 and 816 cm^{-1}.

Unlike the other diphosphine complexes synthesised, $[Pb\{Et_2P(CH_2)_2PEt_2\}(NO_3)_2]$ was found to be freely soluble in the weakly coordinating solvent CD_2Cl_2. This enabled multinuclear NMR spectroscopy to be performed on the complex, as due to the dissociative nature of Pb(II) complexes in solution[7] meaningful NMR spectra can generally only be obtained in non-competitive solvents. The ^1H NMR spectrum shows the diphosphine resonances having shifted to significantly higher frequencies (relative to free $Et_2P(CH_2)_2PEt_2$), confirming its successful coordination. The spectrum is complex, with J_{HH} and J_{HP} coupling evident. That the CH_3CH_2 ethyl protons appear as two separate complex multiplets that are ~ 0.3 ppm apart is surprising (only three resonances are seen in the $^{13}C\{^1H\}$ NMR spectrum overall), but while unusual this splitting has been observed for $Et_2P(CH_2)_2PEt_2$ before, in some of the nitrile phosphine complexes of iron(II), *trans*-$[Fe(NCR)_2\{Et_2P(CH_2)_2PEt_2\}_2]^{2+}$, characterised by Martins *et al.*.[23] Given that NMR spectroscopic data are only available on a single complex and that the coordination environment around the lead(II) centre is uncertain, further assessment is not possible.

A sharp singlet at δ = 89.3 is observed in the $^{31}P\{^1H\}$ NMR spectrum, whose chemical shift varies little with temperature. This is a very large high frequency shift (Δ = +107.3) from uncoordinated $Et_2P(CH_2)_2PEt_2$ (δ = –18), which is similar in magnitude to the shift (Δ = +116.9) reported for the 1:1 complex of $Pb(SbF_6)_2$ with $Ph_2P(CH_2)_2PPh_2$ formed *in situ* (but not isolated).[9] The large $^{31}P\{^1H\}$ NMR deshielding is consistent with that typically

observed for five-membered chelate ring formation on late transition metal ions,[9,24] suggesting that, like the other diphosphine complexes synthesised, $Et_2P(CH_2)_2PEt_2$ also acts as a chelating ligand towards the Pb(II) centre.

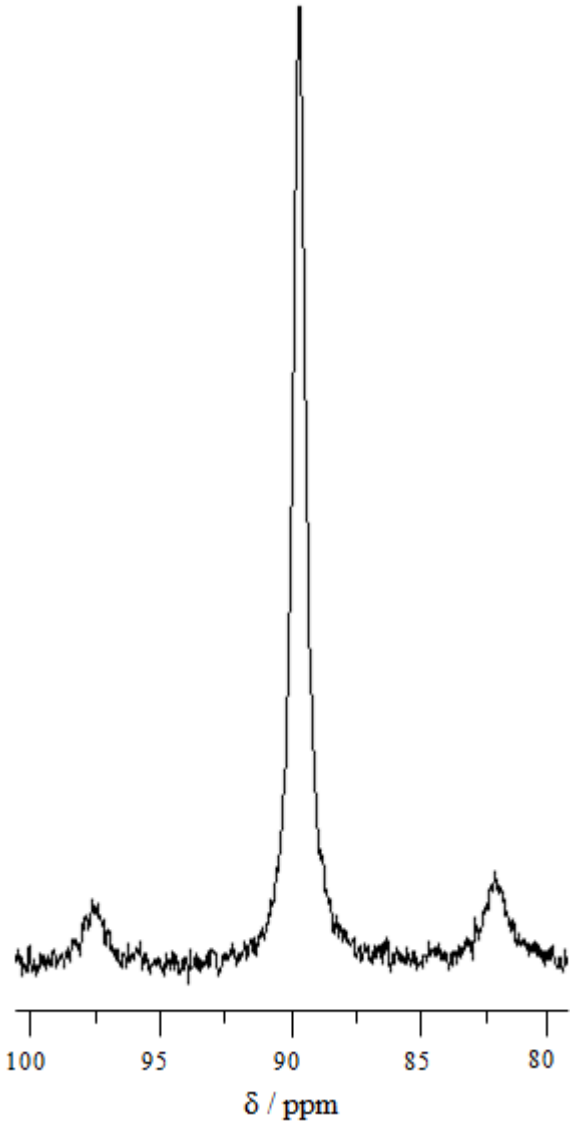

Figure 5.6 $^{31}P\{^1H\}$ NMR spectrum of $[Pb\{Et_2P(CH_2)_2PEt_2\}(NO_3)_2]$ at 193 K in CH_2Cl_2/CD_2Cl_2.

Upon cooling the solution to 223 K, ^{207}Pb satellites were observed in the $^{31}P\{^1H\}$ NMR spectrum, which sharpened upon further cooling to 193 K (Figure 5.6). Though large, the size of the coupling constant ($^1J_{PPb}$ = 2532 Hz) is comparable to the value ($^1J_{PPb}$ = 2680 Hz) reported for $[Pb\{2\text{-}(Ph_2PCH)C_5H_4N\}\{N(SiMe_3)_2\}]$.[14] The appearance of ^{207}Pb satellites only at low temperatures has been previously reported for $[Pb\{2\text{-}(R_2P)C_6H_4S\}_2]$ (R = ^{i}Pr, ^{t}Bu), and was attributed to ligand lability.[13] Similarly, as with $[Pb\{2\text{-}(R_2P)C_6H_4S\}_2]$,[13] no resonances could be observed in the ^{207}Pb NMR spectrum of $[Pb\{Et_2P(CH_2)_2PEt_2\}(NO_3)_2]$, even at low temperatures. This again is presumably due to

one or more fast dynamic processes happening at the Pb(II) centre and broadening the ^{207}Pb signal to undetectable levels, as suggested by P. A. W. Dean,[10] who reports only seeing a distinct ^{207}Pb NMR resonance for the 1:1 complex of $Pb(SbF_6)_2$ with $Ph_2P(CH_2)_2PPh_2$ upon cooling the solution to 260 K.

To ensure that the resonances observed were due to coordinated $Et_2P(CH_2)_2PEt_2$ (i.e. that oxidation of the ligand had not occurred), a $^{31}P\{^1H\}$ NMR spectrum of $[Pb\{Et_2P(CH_2)_2PEt_2\}(NO_3)_2]$ was also recorded in DMSO-d^6; this displaced the diphosphine, resulting in a resonance for uncoordinated $Et_2P(CH_2)_2PEt_2$ being identifiable. Overall, the IR and NMR spectroscopic data suggest that $[Pb\{Et_2P(CH_2)_2PEt_2\}(NO_3)_2]$ has a similar structure to the other diphosphine complexes of $Pb(NO_3)_2$.

Though $[Pb(L–L)(NO_3)_2]$ (L–L = *o*-$C_6H_4(PMe_2)_2$ or $Me_2P(CH_2)_2PMe_2$) dissolve completely in DMF, a property exploited for growing crystals of these complexes, NMR spectra collected in this solvent gave little information. For both complexes a single resonance was observed in $^{31}P\{^1H\}$ NMR spectra collected in DMF-d^7, with chemical shifts intermediate between those expected by analogy with $[Pb\{Et_2P(CH_2)_2PEt_2\}(NO_3)_2]$ and the uncoordinated diphosphine shifts. The chemical shifts were irreproducible and varied widely with concentration, indicating rapidly exchanging systems involving partial displacement of the diphosphine (DMF is a relatively strong[25] donor solvent). Similar behaviour was also observed for $[Pb\{Et_2P(CH_2)_2PEt_2\}(NO_3)_2]$ in DMF-d^7.

Under the same conditions (using CH_3CN/H_2O as the solvent) $Pb(NO_3)_2$ was found not to react with the weaker *σ*-donor diphosphine *o*-$C_6H_4(PPh_2)_2$. No identifiable complex could be isolated with the bidentate arsine ligand o-$C_6H_4(AsMe_2)_2$ either, suggesting that the affinity of lead(II) towards alkyl phosphines is much greater than for alkyl arsines in these systems; there still remains no known arsine complexes of Pb(II).

5.2.2 Lead(II) hexafluorosilicate complexes

The reaction of $Pb(SiF_6)\cdot 2H_2O$ with *o*-$C_6H_4(PMe_2)_2$ in a 1:1 molar ratio yielded a white powder from which small colourless crystals of $[Pb\{o\text{-}C_6H_4(PMe_2)_2\}(H_2O)(SiF_6)]\cdot H_2O$ were grown. The X-ray crystal structure (Figure 5.7) reveals an asymmetrically chelating diphosphine ligand, with a short bond (*d*(Pb–F) = 2.573(3) Å) to a κ^1-coordinated $[SiF_6]^{2-}$ group, and another short bond (*d*(Pb–O) = 2.496(3) Å) to a water molecule. This results in a four-coordinate P_2OF core motif occupying one hemisphere of the Pb(II) centre that is very similar to the core (P_2O_2) geometry observed in $[Pb\{o\text{-}C_6H_4(PMe_2)_2\}(NO_3)_2]$, though

there is a greater disparity (~0.03 Å) in the Pb–P bond lengths, and the ∠O–Pb–F (154.76(11)°) is large. Thus the core geometry appears to be little affected by the anion present. There are two more Pb–F distances (*d*(Pb1–F1) = 3.201(3), *d*(Pb1–F4) = 3.167(3) Å) that lie well within the sum of the Van der Waals radii for Pb and F (3.49 Å),[18] but these are probably the result of packing within the crystal lattice causing the fluorine atoms to sit close to the Pb(II) centre. Nonetheless the $[SiF_6]^{2-}$ group can also be described as being asymmetrically κ^3-coordinated.

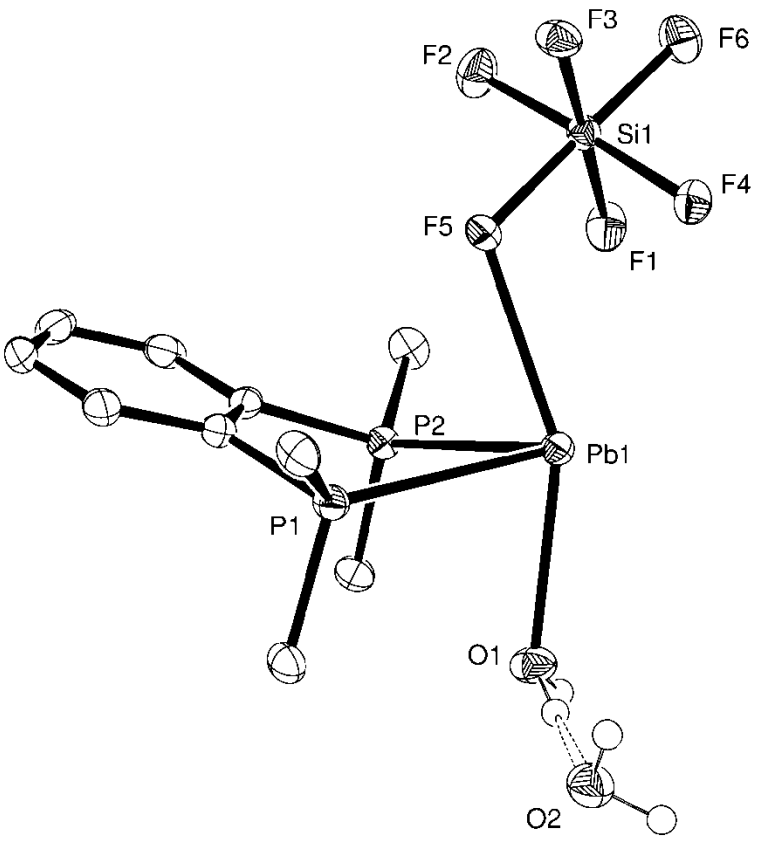

Figure 5.7 The structure of [Pb{*o*-$C_6H_4(PMe_2)_2$}(H_2O)(SiF_6)]·H_2O showing the atom labelling scheme. Ellipsoids are drawn at the 50% probability level and H atoms bonded to C are omitted for clarity.

Table 5.3 Selected bond lengths (Å) and angles (°) for [Pb{*o*-$C_6H_4(PMe_2)_2$}(H_2O)-(SiF_6)]·H_2O

Pb1–P1	2.8299(14)	P1–Pb1–P2	69.67(4)
Pb1–P2	2.7976(13)	O1–Pb1–F5	154.76(11)
Pb1–O1	2.496(3)		
Pb1–F5	2.573(3)		

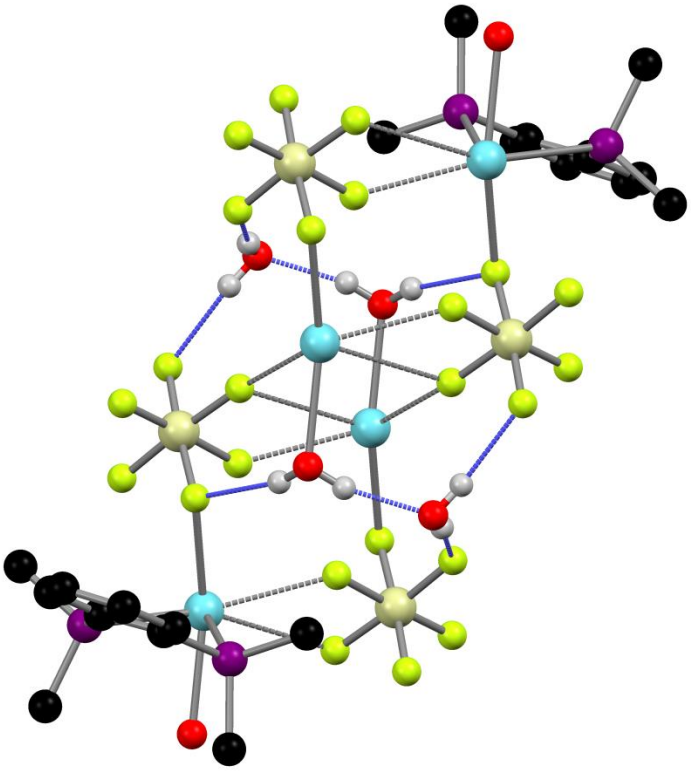

Figure 5.8 View of the polymeric chain structure of [Pb{*o*-$C_6H_4(PMe_2)_2$}(H_2O)-(SiF_6)]·H_2O. The intermolecular H-bonding network is shown in blue and the *o*-$C_6H_4(PMe_2)_2$ ligands on the two central lead atoms are omitted for clarity. Colour key: light blue = Pb, purple = P, red = O, beige = Si, green = F, black = C, white = H.

The [Pb{*o*-$C_6H_4(PMe_2)_2$}(H_2O)(SiF_6)] units are arranged into infinite strands by a Pb–F interaction with a neighbouring $[SiF_6]^{2-}$ group (*d*(Pb–F) = 2.815(3) Å). Two strands are then linked together by each Pb(II) centre forming two further interactions with a $[SiF_6]^{2-}$ group on a parallel strand (*d*(Pb–F) = 2.795(3) and 3.083(3) Å), so that overall a polymeric chain structure is created (Figure 5.8), with the *o*-$C_6H_4(PMe_2)_2$ ligands arranged so that they point outwards from the chain. The coordination number around the Pb(II) centre is seven (or nine if the $[SiF_6]^{2-}$ group is described as κ^3-coordinated). The arrangement gives a Pb···Pb distance of 4.038(1) Å, which is actually the sum of the Van der Waals radii (4.04 Å)[18] for two lead atoms. The coordinated water molecule is hydrogen bonded to a lattice water molecule (HO–H···OH_2 = 1.89(7) Å), and together with a number of hydrogen bonds (HO–H···F = 1.93(2), 2.05(6) and 2.14(3) Å) with fluorine atoms on nearby $[SiF_6]^{2-}$ groups, a hydrogen bonding network (Figure 5.8) is built up throughout the chain.

Similarly to the diimine complexes of $Pb(SiF_6)$ (see Section 4.2.1), bands corresponding to the $[SiF_6]^{2-}$ anion can be easily identified in the IR spectrum of the complex,[20] but the coordination mode cannot be reliably distinguished. The stretching mode is significantly broadened, indicating that the Pb–F interactions are too weak for the splittings expected for the coordinated (and thus lower symmetry) $[SiF_6]^{2-}$ anion to be resolved. Water is also visible in the IR spectrum, which suggests that the bulk solid is probably also $[Pb\{o\text{-}C_6H_4(PMe_2)_2\}(H_2O)(SiF_6)]\cdot xH_2O$, though a satisfactory microanalysis result could not be obtained. Poor solubility in non-donor solvents precluded NMR spectroscopic analysis of the complex.

A few small colourless crystals of $[Pb\{o\text{-}C_6H_4(PMe_2)_2\}(DMF)_2(SiF_6)]\cdot DMF$ were obtained when the reaction of $Pb(SiF_6)\cdot 2H_2O$ with $o\text{-}C_6H_4(PMe_2)_2$ was repeated in a 1:2 molar ratio. The 1:1 stoichiometry of the complex again demonstrates the preference of lead(II) to coordinate to just one diphosphine ligand. Again, the asymmetric unit has a four-coordinate (P_2OF) core motif, with bond lengths that are comparable to those found in $[Pb\{o\text{-}C_6H_4(PMe_2)_2\}(H_2O)(SiF_6)]\cdot H_2O$, though the H_2O molecule has been replaced by an O-bonded DMF molecule and the ∠O–Pb–F is smaller at 140.82(12)°. The orientation of a second DMF molecule close to the Pb(II) centre suggests that it is also interacting with the lead (*d*(Pb–O) = 3.263(6) Å); there is also a non-coordinating DMF solvate molecule in the structure.

The $[SiF_6]^{2-}$ group can be described as either κ^2- or κ^3-coordinated; the *d*(Pb1–F3) is ~0.3 Å shorter than the comparable distance in $[Pb\{o\text{-}C_6H_4(PMe_2)_2\}(H_2O)(SiF_6)]\cdot H_2O$, while the *d*(Pb1–F2) remains long at 3.081(4) Å. The $[SiF_6]^{2-}$ group also bridges to another Pb(II) centre through a single fluorine (*d*(Pb–F = 2.752(3) Å), so that overall the complex is a centrosymmetric dimer (Figure 5.9), with a Pb···Pb distance of 4.742(2) Å. This gives a coordination number for the Pb(II) of seven (or eight if the $[SiF_6]^{2-}$ group is described as κ^3-coordinated). The change in extended structure, moving from a polymeric chain in $[Pb\{o\text{-}C_6H_4(PMe_2)_2\}(H_2O)(SiF_6)]\cdot H_2O$ to a dimer in $[Pb\{o\text{-}C_6H_4(PMe_2)_2\}(DMF)_2(SiF_6)]$, is probably driven by the much greater size of the DMF molecule and the lack of hydrogen bonding in the latter complex.

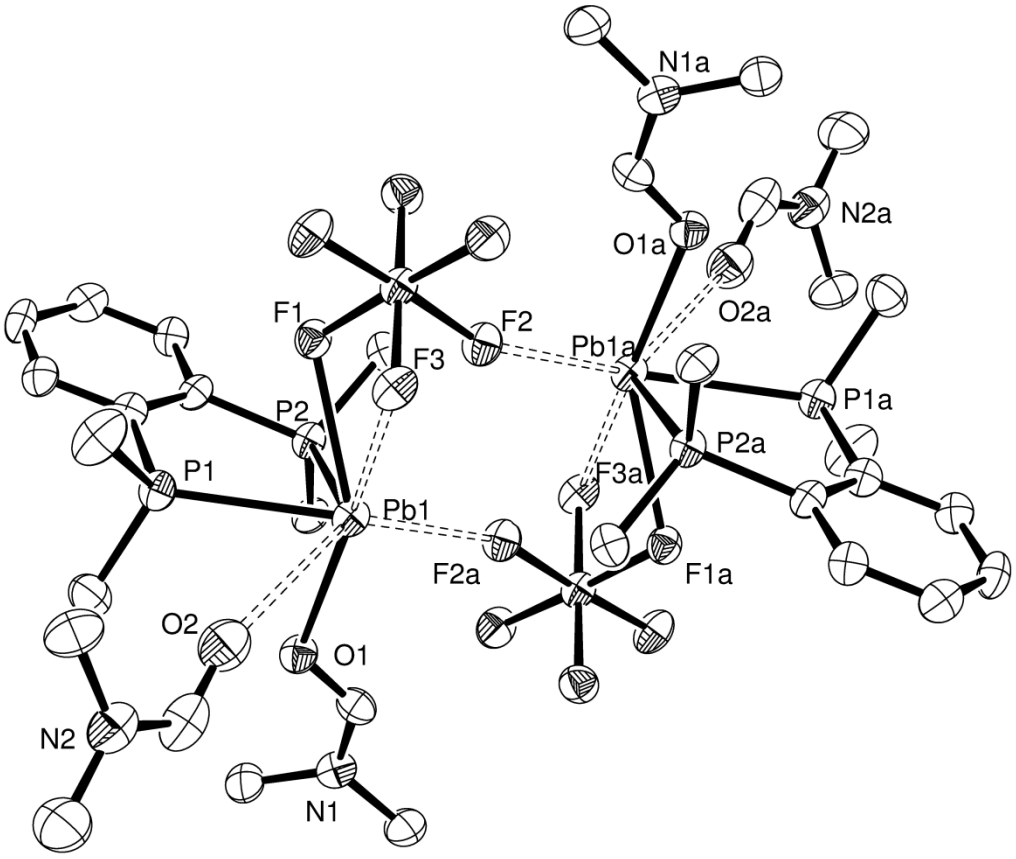

Figure 5.9 The structure of the SiF_6-bridged dimer present in [Pb{*o*-$C_6H_4(PMe_2)_2$}-$(DMF)_2(SiF_6)$]·DMF showing the atom labelling scheme. Ellipsoids are drawn at the 50% probability level. H atoms and solvate molecules are omitted for clarity. Symmetry operation: a = 2 – x, 2 – y, 1 – z.

Table 5.4 Selected bond lengths (Å) and angles (°) for [Pb{*o*-$C_6H_4(PMe_2)_2$}$(DMF)_2$-(SiF_6)]·DMF

Pb1–P1	2.7671(19)	P1–Pb1–P2	72.30(5)
Pb1–P2	2.7553(16)	F1–Pb1–O1	140.82(12)
Pb1–O1	2.463(4)	F1–Pb1–O2	109.10(12)
Pb1–O2	3.263(6)	F1–Pb1–F3	50.67(9)
Pb1–F1	2.585(3)	F1–Pb1–F2a	110.58(10)
Pb1–F3	2.894(3)		
Pb1–F2a	2.752(3)		

Formation of this complex highlights how readily DMF will coordinate to lead(II), and therefore why it is unsuitable as a NMR solvent in these systems. In DMF solution the Pb(II) ion is solvated by six DMF molecules, with a mean Pb–O distance of 2.56(1) Å.[25] In favourable cases DMF has even been known to displace halides from Pb(II), as seen in the X-ray crystal structure of $[Pr_3N(CH_2)_2NPr_3][Pb(DMF)_6][Pb_5I_{14}]\cdot DMF$.[26] Evidently, because of the lability of Pb(II) complexes in solution, the structure obtained is ultimately dependent on which complex crystallises out under the conditions employed.

These complexes of $Pb(SiF_6)$ with the diphosphine *o*-$C_6H_4(PMe_2)_2$ again show, as first seen in the di- and tri-imine complexes synthesised in Sections 4.2.1 and 4.2.2, that dianionic $[SiF_6]^{2-}$ will coordinate to Pb(II) in a variety of different coordination modes, forming dimer and polymer chain complexes. Though fluoroanions are generally more weakly coordinating than oxoanions like $[NO_3]^-$,[27] the two complexes each exhibit a very short Pb–F bond with lengths of ~2.58 Å, which are in fact shorter than the shortest Pb–O bonds in $[Pb(L–L)(NO_3)_2]$ (L–L = *o*-$C_6H_4(PMe_2)_2$ or $Me_2P(CH_2)_2PMe_2$); this may reflect the greater charge of the $[SiF_6]^{2-}$ anion. As observed for the diimine complexes, the geometries of these diphosphine complexes of $Pb(SiF_6)$ are highly irregular, and are probably largely dictated by the steric demands of the phosphine ligand, solvent molecules and fluoroanions, so that Pb–donor interactions are maximised while ligand repulsion is minimised.

5.2.3 Complexes with phosphine oxide ligands

During an attempt to recrystallise $[Pb\{Et_2P(CH_2)_2PEt_2\}(NO_3)_2]$ using CH_2Cl_2 and hexane, a few small colourless crystals of $[Pb\{Et_2(O)P(CH_2)_2P(O)Et_2\}_2(NO_3)_2]$ were isolated instead, evidently the result of *in-situ* oxidation of the ligand (by adventitious O_2). The *in-situ* oxidation of diphosphine ligands in the presence of heavy p-block metals has been previously reported,[2] including the SnI_4-catalysed oxidation of aryl phosphines to the corresponding phosphine oxides on reaction with dry air or O_2.[28] Another example is the oxidation of the 1:1 adduct of $BiCl_3$ and $Ph_2PCH_2PPh_2$ to the crystallographically identified $[BiCl_3\{Ph_2(O)PCH_2P(O)Ph_2\}]_2$, which occurred when trying to grow crystals of the phosphine complex.[29] The *in situ* oxidation of diphosphine ligands in the presence of Pb(II) has also been reported, when a few crystals of $[\{Pb_3(\mu\text{-}I)_6\}\{Ph_2(O)P(CH_2)_2P(O)Ph_2\}_3]\cdot EtOH$ were obtained from the solvothermal reaction of PbI_2 with I_2, KI and $Ph_2P(CH_2)_2PPh_2$. Introducing H_2O_2 into the reaction in an attempt to increase the yield of the phosphine oxide complex generated another three-dimensional

polymer, [{$Pb_2(\mu\text{-}I)_2(\mu^3\text{-}I)_2$}{$Ph_2(O)P(CH_2)_2P(O)Ph_2$}]. Both structures contain octahedrally coordinated Pb(II), with bridging $Ph_2(O)P(CH_2)_2P(O)Ph_2$ groups.[30]

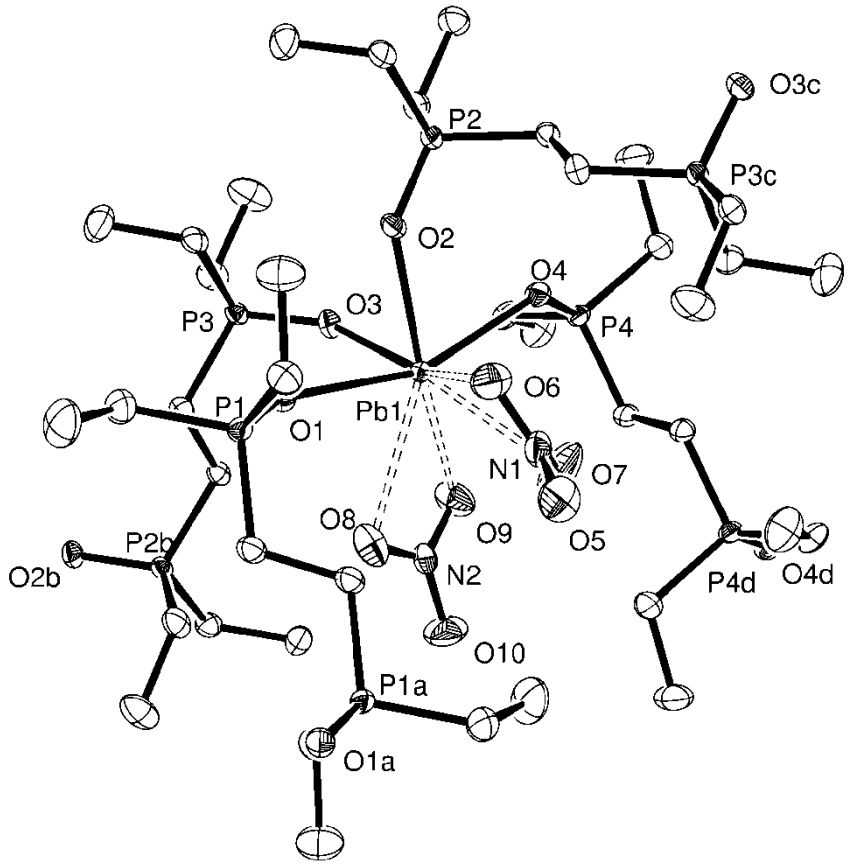

Figure 5.10 The structure of [Pb{$Et_2(O)P(CH_2)_2P(O)Et_2$}$_2(NO_3)_2$] showing the atom labelling scheme. Ellipsoids are drawn at the 50% probability level and H atoms are omitted for clarity. Symmetry operations: a = – x, 1 – y, 1 – z; b = x, 1/2 – y, 1/2 + z ; c = x, 1/2 – y, –1/2 + z; d = 1 – x, 1 – y, 1 – z.

Table 5.5 Selected bond lengths (Å) and angles (°) for [Pb{$Et_2(O)P(CH_2)_2P(O)Et_2$}$_2$-$(NO_3)_2$]

Pb1–O1	2.484(2)	O1–Pb1–O2	80.25(8)
Pb1–O2	2.429(2)	O1–Pb1–O3	83.96(8)
Pb1–O3	2.418(2)	O1–Pb1–O4	160.30(9)
Pb1–O4	2.589(2)	O2–Pb1–O3	81.05(9)
Pb1–O6	2.786(2)	O2–Pb1–O4	81.58(8)
Pb1–O7	2.912(3)	O3–Pb1–O4	85.75(8)
Pb1–O8	2.875(3)	O6–Pb1–O7	44.41(10)
Pb1–O9	2.891(3)	O8–Pb1–O9	43.97(8)
P1–O1	1.502(3)	Pb1–O1–P1	144.23(15)
P2–O2	1.504(2)	Pb1–O2–P2	137.26(14)
P3–O3	1.510(3)	Pb1–O3–P3	132.28(15)
P4–O4	1.504(3)	Pb1–O4–P4	131.86(14)

The X-ray structure determination of [Pb{$Et_2(O)P(CH_2)_2P(O)Et_2$}$_2$$(NO_3)_2$] (Figure 5.10) reveals that, despite the 1:1 stoichiometry of the parent phosphine complex, the phosphine oxide complex has a 2:1 (L–L:Pb) stoichiometry. Interestingly, though not crystallographically characterised, the adduct formed between $Pb(SbF_6)_2$ and $Ph_2(O)P(CH_2)_2P(O)Ph_2$ has a 1:1 stoichiometry (confirmed by microanalysis).[9] In [Pb{$Et_2(O)P(CH_2)_2P(O)Et_2$}$_2$$(NO_3)_2$] each $Et_2(O)P(CH_2)_2P(O)Et_2$ ligand bridges to a different Pb(II) centre so that overall each Pb(II) centre is linked to four others, resulting in an infinite polymer network (Figure 5.11). The bonds to the phosphine oxide ligands form a core PbO_4 geometry, with *d*(Pb–O) = 2.418(2)–2.589(2) Å, which are comparable bond lengths to those seen in [{$Pb_3(\mu$-$I)_6$}{$Ph_2(O)P(CH_2)_2P(O)Ph_2$}$_3$]·EtOH (average *d*(Pb–O) = 2.464(9) Å) and [{$Pb_2(\mu$-$I)_2(\mu^3$-$I)_2$}{$Ph_2(O)P(CH_2)_2P(O)Ph_2$}] (average *d*(Pb–O) = 2.408(3) Å).[30] The remainder of the coordination sphere is occupied by longer bonds to two κ^2-coordinated $[NO_3]^-$ groups (the third oxygen is uncoordinated), with Pb–O distances spanning the range 2.786(2)–2.912(3) Å, so that overall the lead(II) is eight-coordinate. If the κ^2-coordinated $[NO_3]^-$ groups are considered to occupy one coordination site each then

the geometry around the lead(II) centre is much less distorted from a regular octahedron than the geometries seen in $[Pb(L–L)(NO_3)_2]$ (L–L = *o*-$C_6H_4(PMe_2)_2$ or $Me_2P(CH_2)_2PMe_2$).

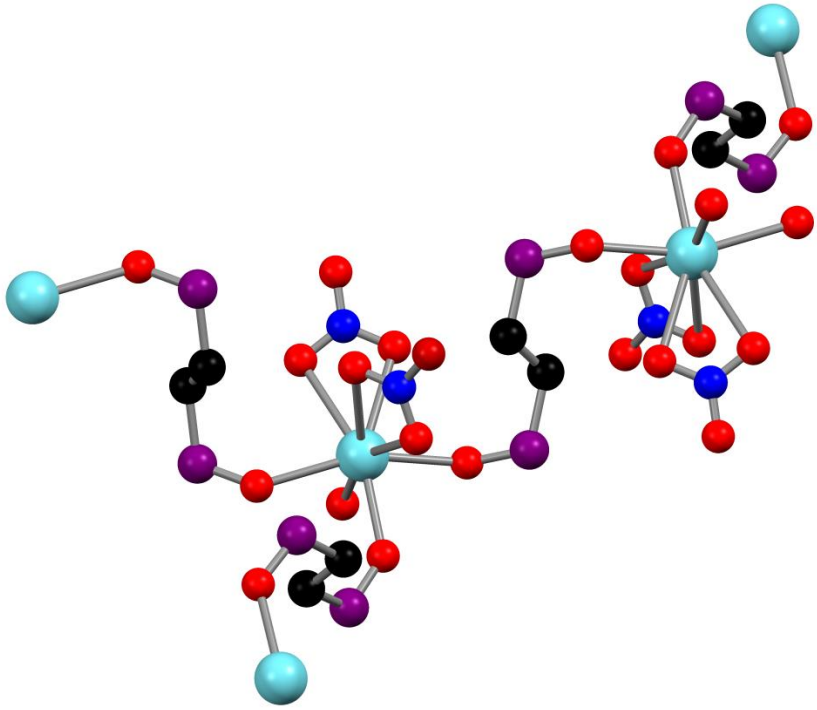

Figure 5.11 View of the extended structure of $[Pb\{Et_2(O)P(CH_2)_2P(O)Et_2\}_2(NO_3)_2]$. Ethyl groups are omitted for clarity. Colour key: light blue = Pb, purple = P, blue = N, red = O, black = C.

While several reactions of $Pb(BF_4)_2$ with diphosphine ligands were performed, the outcome was usually protonation of the ligand (almost certainly due to the aforementioned acidity of the aqueous $Pb(BF_4)_2$ solution). However, on one occasion, a few small crystals of $[Pb\{Me_2P(CH_2)_2PMe_2\}\{Me_2(O)P(CH_2)_2P(O)Me_2\}(BF_4)_2]\cdot 0.5MeNO_2$ were obtained from the reaction of $Pb(BF_4)_2$ with two molar equivalents of $Me_2P(CH_2)_2PMe_2$ in $MeNO_2$. The preferred coordination mode of both the diphosphine and the diphosphine dioxide to Pb(II) is evident, as the X-ray structure determination (Figure 5.12) reveals a chelating $Me_2P(CH_2)_2PMe_2$ ligand, while the $Me_2(O)P(CH_2)_2P(O)Me_2$ (from the *in situ* oxidation of the diphosphine ligand) bridges between Pb(II) centres to give a one-dimensional chain polymer (Figure 5.13).

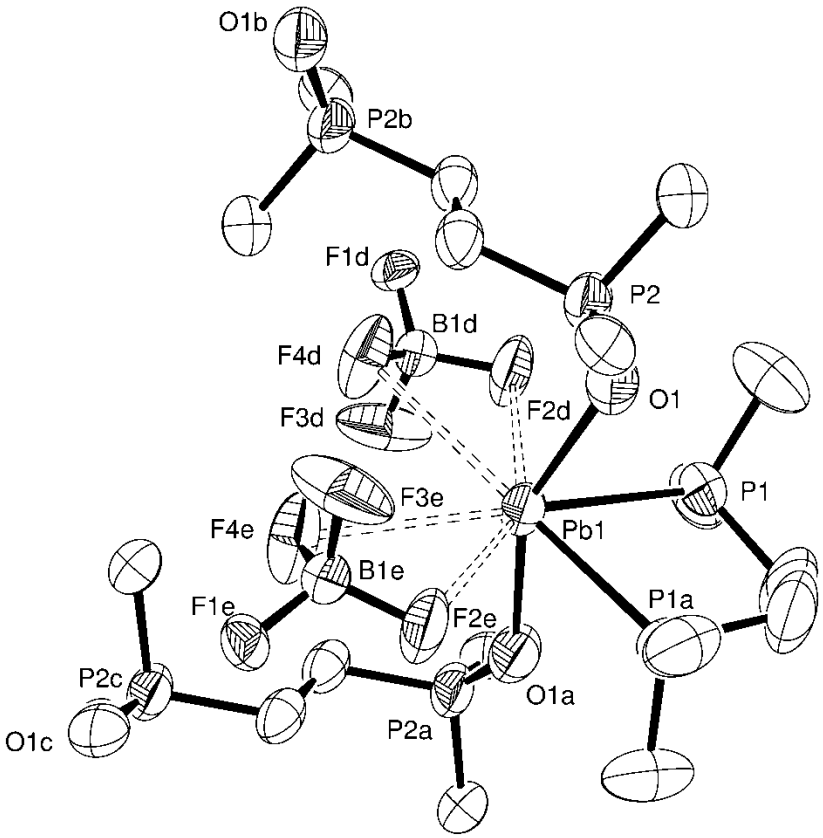

Figure 5.12 The structure of $[Pb\{Me_2P(CH_2)_2PMe_2\}\{Me_2(O)P(CH_2)_2P(O)Me_2\}\text{-}(BF_4)_2]\cdot 0.5MeNO_2$ showing the atom labelling scheme. Ellipsoids are drawn at the 50% probability level. H atoms and solvate molecules are omitted for clarity. Symmetry operations: a = 7/4 – x, 3/4 – y, z; b = 2 – x, 1 – y, – z; c = – 1/4 + x, –1/4 + y, – z; d = 2 – x, –1/4 + y, –1/4 + z; e = –1/4 + x, 1 – y, –1/4 + z. The $[BF_4]^-$ anion is disordered with two distinct orientations (only one orientation is shown).

Table 5.6 Selected bond lengths (Å) and angles (°) for $[Pb\{Me_2P(CH_2)_2PMe_2\}\text{-}\{Me_2(O)P(CH_2)_2P(O)Me_2\}(BF_4)_2]\cdot 0.5MeNO_2$

Pb1–P1	2.789(2)	P1–Pb1–P1a	72.86(9)
Pb1–O1	2.454(6)	O1–Pb1–O1a	154.5(3)
O1–P2	1.478(6)	Pb1–O1–P2	139.1(3)

The *d*(Pb–P) is identical (within bond error margins) to the Pb–P distance in $[Pb\{Me_2P(CH_2)_2PMe_2\}(NO_3)_2]$, while the *d*(Pb–O) is within the bond length range seen for the diphosphine dioxide ligands in $[Pb\{Et_2(O)P(CH_2)_2P(O)Et_2\}_2(NO_3)_2]$. This results in the complex having the expected core P_2O_2 geometry with a ∠O–Pb–O of 154.5(3)°; weak

interactions with the $[BF_4]^-$ anions fill the remaining coordination sphere. The asymmetric unit also contains a disordered $MeNO_2$ solvate molecule that has 50% occupancy. Though the symmetry related $[BF_4]^-$ groups are disordered, they appear to adopt two distinct and reasonably well-defined orientations, with two Pb–F interactions from both orientations that have similar distances of ~3.1 and ~3.3 Å. The $[BF_4]^-$ groups can therefore either be described as κ^1- or κ^2-coordinated, giving a coordination number of either six or eight for the lead(II) overall. $[Pb\{Me_2P(CH_2)_2PMe_2\}\{Me_2(O)P(CH_2)_2P(O)Me_2\}(BF_4)_2]\cdot 0.5MeNO_2$ is the first crystallographically authenticated example of a mixed phosphine-phosphine oxide complex of lead(II).

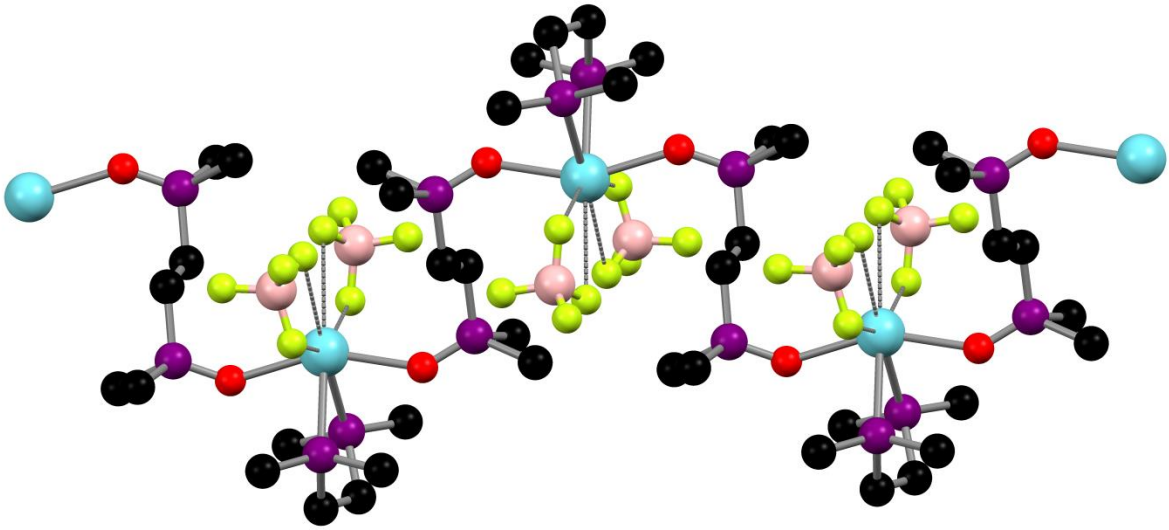

Figure 5.13 View of the extended structure of $[Pb\{Me_2P(CH_2)_2PMe_2\}\{Me_2(O)P(CH_2)_2P(O)Me_2\}(BF_4)_2]\cdot 0.5MeNO_2$. Only one orientation of the $[BF_4]^-$ anion is shown. Colour key: light blue = Pb, purple = P, red = O, pink = B, green = F, black = C.

5.3 Conclusions

Several new and rare complexes of $Pb(NO_3)_2$ and $Pb(SiF_6)$ with neutral diphosphine ligands have been synthesised and structurally authenticated by single crystal X-ray diffraction studies. The X-ray crystal structures reveal a clear preference for a single bidentate phosphine ligand to chelate to the Pb(II), even when the molar ratio of diphosphine used is greater than one. That no second diphosphine can be introduced to the Pb(II) coordination sphere is in marked contrast to the bis-ligand complexes (Section 4.2.1) that dominate Pb(II) diimine coordination chemistry, and presumably reflects the limited affinity of Pb(II) for phosphorus donors. As Pb(II) is a large metal centre that can accommodate coordination numbers up to twelve,[1] steric factors are unlikely to be involved. *In-situ* oxidation of the diphosphine ligands by adventitious O_2 can also occur, and yields diphosphine dioxide complexes, where the ligands bridge between lead(II) centres.

To access phosphine complexes of lead(II), syntheses have required the use of relatively unusual Pb(II) salt sources and reaction conditions to overcome the poor solubility of most Pb(II) salts and Pb(II) complexes in common organic solvents.[1] Of the complexes synthesised, only $[Pb\{Et_2P(CH_2)_2PEt_2\}(NO_3)_2]$ was found to be soluble in a weakly coordinating solvent (CD_2Cl_2), which allowed meaningful multinuclear NMR studies to be performed on the complex; a very large high frequency shift ($\Delta = +107.3$) was observed in the $^{31}P\{^1H\}$ NMR spectrum, which showed $^1J_{PPb}$ coupling at low temperatures. The use of donor solvents like DMF (in which all the complexes were found to be soluble) led to partial displacement of the diphosphine.

Though the geometries around the Pb(II) are highly irregular, a four-coordinate core motif arranged on one hemisphere of the lead can be identified in each complex, with longer contacts to anions or solvent molecules occupying much of the remaining coordination sphere. This usually results in polymeric chain or network structures, with coordination numbers of seven or eight around the Pb(II) centre overall. Multiple coordination modes have been observed for the little studied $[SiF_6]^{2-}$ fluoroanion; it will readily bond to a single lead via one or more Pb–F interactions, and can also bridge between metal centres. Once isolated the complexes are stable under an inert atmosphere; hydrolysis or degradation of the $[SiF_6]^{2-}$ anion did not occur in these systems.

5.4 Experimental

The general experimental techniques used in this chapter can be found in Appendix 1 at the end of the thesis. Aqueous solutions of the lead salts were degassed before use, by bubbling with N_2.

[Pb{*o*-$C_6H_4(PMe_2)_2$}$(NO_3)_2$]

To *o*-$C_6H_4(PMe_2)_2$ (0.090 g, 0.45 mmol) in CH_3CN (5 mL) was added a degassed solution of $Pb(NO_3)_2$ (0.150 g, 0.45 mmol) in deionised water (3 mL). A white precipitate formed rapidly on stirring; the reaction was stirred for 2 h, then the white powder was isolated by filtration and dried *in vacuo*. Yield: 0.056 g, 23%. Small colourless crystals suitable for single crystal X-ray diffraction study were grown by layering Et_2O onto a solution of the isolated complex dissolved in the minimal amount of DMF. Anal. Calc. for $C_{10}H_{16}N_2O_6P_2Pb$: C, 22.7; H, 3.1; N, 5.3. Found: C, 22.6; H, 3.1; N, 5.2%. IR (Nujol): ν = 1314 (s), 1295 (s), 1033 (s), 837 (sh), 818 (m) (NO_3) cm^{-1}.

[Pb{$Me_2P(CH_2)_2PMe_2$}$(NO_3)_2$]

To $Me_2P(CH_2)_2PMe_2$ (0.091 g, 0.60 mmol) in CH_3CN (5 mL) was added a degassed solution of $Pb(NO_3)_2$ (0.101 g, 0.30 mmol) in deionised water (5 mL), giving a colourless solution. The reaction was stirred for 1 h, then the solvent was concentrated *in vacuo* and the resulting white powder was filtered and dried *in vacuo*. Yield: 0.071 g, 48% based on Pb. Small colourless crystals suitable for single crystal X-ray diffraction study were grown by layering Et_2O onto a solution of the isolated powder dissolved in the minimal amount of DMF. Anal. Calc. for $C_6H_{16}N_2O_6P_2Pb$: C, 15.0; H, 3.4; N, 5.8. Found: C, 15.1; H, 3.3; N, 5.8%. IR (Nujol): ν = 1310 (vs, br), 1038 (s), 840 (w), 819 (m) (NO_3) cm^{-1}.

[Pb{$Et_2P(CH_2)_2PEt_2$}$(NO_3)_2$]

To a degassed solution of $Pb(NO_3)_2$ (0.162 g, 0.49 mmol) in deionised water (3 mL) was added $Et_2P(CH_2)_2PEt_2$ (0.101 g, 0.49 mmol) in CH_3CN (5 mL) to give a colourless solution. The reaction was stirred for 2 h, then the solvent volume was reduced to about 3 mL *in vacuo*. The resulting white precipitate was isolated by filtration and dried *in vacuo* to give a white powder. Yield: 0.092 g, 35%. Anal. Calc. for $C_{10}H_{24}N_2O_6P_2Pb$: C, 22.4; H,

4.5; N, 5.2. Found: C, 22.2; H, 4.6; N, 5.2%. ^{1}H NMR (CD_2Cl_2, 295 K): δ = 1.23 (dt, [12H], *J* = 7.6, 16.1 Hz, CH_3), 1.92-2.02 (m, [4H], CH_2), 2.20-2.35 (m, [4H], CH_2), 2.40 (d, [4H], *J* = 11.3 Hz, CH_2). ^{13}C{^{1}H} NMR (CD_2Cl_2, 295 K): δ = 8.44 (s, CH_3), 15.09 (t, J_{CP} = 5.1 Hz, CH_2), 25.47 (t, J_{CP} = 12.4 Hz, CH_2). ^{31}P{^{1}H} NMR (CH_2Cl_2/CD_2Cl_2, 295 K): δ = 89.3 (s); (223 K): 89.5 (s, $^{1}J_{PPb}$ = 2465 Hz); (193 K): 89.6 (s, $^{1}J_{PPb}$ = 2532 Hz). IR (Nujol): ν = 1300 (s, br), 1029 (s), 816 (m) (NO_3) cm^{-1}. Small colourless crystals of the phosphine oxide complex, [Pb{$Et_2(O)P(CH_2)_2P(O)Et_2$}$_2(NO_3)_2$], were grown from layering hexane onto a solution of the isolated powder dissolved in the minimal amount of CH_2Cl_2.

[Pb{*o*-$C_6H_4(PMe_2)_2$}$(H_2O)(SiF_6)$]·H_2O

To a degassed solution of $Pb(SiF_6)·2H_2O$ (0.151 g, 0.39 mmol) in deionised water (10 mL) was added *o*-$C_6H_4(PMe_2)_2$ (0.077 g, 0.39 mmol) in CH_3CN (5 mL), which caused the precipitation of a small amount of white solid. The reaction was stirred for 1.5 h, then the solid was removed by filtration to leave a colourless solution. The solvent was removed *in vacuo* and the resulting white powder was dried *in vacuo*. Yield: 0.110 g, 48%. IR (Nujol): ν = 3500 (br), 1628 (m, br) (H_2O), 721 (vs, br), 473 (s), 446 (s) (SiF_6) cm^{-1}. Small colourless crystals of [Pb{*o*-$C_6H_4(PMe_2)_2$}$(H_2O)(SiF_6)$]·H_2O were grown by layering Et_2O onto a solution of the isolated product dissolved in the minimal amount of DMF.

In a similar reaction where the *o*-$C_6H_4(PMe_2)_2$ to $Pb(SiF_6)·2H_2O$ molar ratio used was 2:1, small colourless crystals of [Pb{*o*-$C_6H_4(PMe_2)_2$}$(DMF)_2(SiF_6)$]·DMF were obtained.

[Pb{$Me_2P(CH_2)_2PMe_2$}{$Me_2(O)P(CH_2)_2P(O)Me_2$}$(BF_4)_2$]·0.5$MeNO_2$

To a degassed solution of $Me_2P(CH_2)_2PMe_2$ (0.087 g, 0.58 mmol) in $MeNO_2$ (6 mL) was added $Pb(BF_4)_2$ as a 50% aqueous solution (0.229 g, 0.30 mmol) that had been degassed beforehand. A small amount of white precipitate rapidly formed, which was removed by filtration, then Et_2O (10 mL) was layered onto the colourless filtrate, giving a few small colourless crystals suitable for single crystal X-ray diffraction study.

5.5 Appendix – X-Ray Crystallographic Data

Compound	$[Pb\{Me_2P(CH_2)_2PMe_2\}(NO_3)_2]$	$[Pb\{o\text{-}C_6H_4(PMe_2)_2\}(NO_3)_2]$
Formula	$C_6H_{16}N_2O_6P_2Pb$	$C_{10}H_{16}N_2O_6P_2Pb$
M	481.34	529.38
Crystal system	tetragonal	monoclinic
Space group (no.)	$P4_12_12$ (92)	$P2_1/n$ (14)
a /Å	8.2128(18)	10.182(4)
b /Å	8.2128(18)	10.863(3)
c /Å	20.989(7)	14.771(5)
α /°	90	90
β /°	90	91.614(5)
γ /°	90	90
U /Å^3	1415.7(6)	1633.0(9)
Z	4	4
μ(Mo-K$_\alpha$) /mm^{-1}	12.159	10.552
F(000)	904	1000
Total no. reflns	6585	7115
R_{int}	0.034	0.050
Unique reflns	1628	3709
No. of params, restraints	80, 0	188, 0
R_1, wR_2 [$I > 2\sigma(I)$][a]	0.026, 0.055	0.043, 0.101
R_1, wR_2 (all data)	0.029, 0.056	0.052, 0.104

Common items: T = 100 K; wavelength (Mo-Kα) = 0.71073 Å; θ(max) = 27.5°.

[a] $R_1 = \Sigma||F_o| - |F_c|| / \Sigma|F_o|$; $wR_2 = [\Sigma w(F_o^2 - F_c^2)^2 / \Sigma wF_o^4]^{1/2}$.

Compound	[Pb{*o*-$C_6H_4(PMe_2)_2$}(H_2O)-(SiF_6)]·H_2O	Pb{*o*-$C_6H_4(PMe_2)_2$}$(DMF)_2$-(SiF_6)]·DMF
Formula	$C_{10}H_{20}F_6O_2P_2PbSi$	$C_{19}H_{37}F_6N_3O_3P_2PbSi$
M	583.48	766.74
Crystal system	triclinic	triclinic
Space group (no.)	*P*-1 (2)	*P*-1 (2)
a /Å	6.6164(17)	8.404(2)
b /Å	10.637(3)	10.352(3)
c /Å	12.354(3)	15.994(5)
α /°	93.580(6)	87.522(7)
β /°	93.952(3)	89.782(6)
γ /°	100.854(6)	86.063(7)
U /Å^3	849.4(4)	1386.9(7)
Z	2	2
μ(Mo-K_α) /mm^{-1}	10.250	6.307
F(000)	552	752
Total no. reflns	7661	13101
R_{int}	0.035	0.069
Unique reflns	3848	6322
No. of params, restraints	219, 2	326, 0
R_1, wR_2 [$I > 2\sigma(I)$][a]	0.026, 0.064	0.043, 0.087
R_1, wR_2 (all data)	0.028, 0.065	0.048, 0.088

Common items: T = 100 K; wavelength (Mo-Kα) = 0.71073 Å; θ(max) = 27.5°.

[a] $R_1 = \Sigma||F_o| - |F_c|| / \Sigma|F_o|$; $wR_2 = [\Sigma w(F_o^2 - F_c^2)^2 / \Sigma wF_o^4]^{1/2}$.

Compound	$[Pb\{Et_2(O)P(CH_2)_2P(O)Et_2\}_2\text{-}(NO_3)_2]$	$[Pb\{Me_2P(CH_2)_2PMe_2\}\text{-}\{Me_2(O)P(CH_2)_2P(O)Me_2\}\text{-}(BF_4)_2]\cdot 0.5MeNO_2$
Formula	$C_{20}H_{48}N_2O_{10}P_4Pb$	$C_{12.50}H_{33.50}B_2F_8N_{0.50}O_3P_4Pb$
M	807.67	743.59
Crystal system	monoclinic	orthorhombic
Space group (no.)	$P2_1/c$ (14)	*Fddd* (70)
a /Å	15.1483(5)	16.938(6)
b /Å	13.8900(4)	24.212(9)
c /Å	16.2854(5)	25.686(10)
α /°	90	90
β /°	112.383(3)	90
γ /°	90	90
U /Å^3	3168.44(17)	10534(7)
Z	4	16
μ(Mo-K$_\alpha$) /mm^{-1}	5.576	6.719
F(000)	1616	5760
Total no. reflns	26042	11501
R_{int}	0.040	0.028
Unique reflns	7234	3021
No. of params, restraints	342, 0	212, 223
R_1, wR_2 [$I > 2\sigma(I)$][a]	0.031, 0.067	0.053, 0.103
R_1, wR_2 (all data)	0.045, 0.073	0.061, 0.108

Common items: T = 100 K; wavelength (Mo-Kα) = 0.71073 Å; θ(max) = 27.5°.

[a] $R_1 = \Sigma||F_o| - |F_c|| / \Sigma|F_o|$; $wR_2 = [\Sigma w(F_o^2 - F_c^2)^2 / \Sigma wF_o^4]^{1/2}$.

5.6 References

1. E. S. Claudio, H. A. Godwin and J. S. Magyar, *Prog. Inorg. Chem.*, 2003, **51**, 1-144.
2. J. Burt, W. Levason and G. Reid, *Coord. Chem. Rev.*, 2014, **260**, 65-115.
3. H. Clees and F. Huber, *Z. Anorg. Allg. Chem.*, 1967, **352**, 200-205.
4. D. J. D. Wilson, S. A. Couchman and J. L. Dutton, *Inorg. Chem.*, 2012, **51**, 7657-7668.
5. R. G. Pearson, *J. Am. Chem. Soc.*, 1963, **85**, 3533-3539.
6. C. Gurnani, A. L. Hector, E. Jager, W. Levason, D. Pugh and G. Reid, *Dalton Trans.*, 2013, **42**, 8364-8374.
7. A. J. Rossini, A. W. Macgregor, A. S. Smith, G. Schatte, R. W. Schurko and G. G. Briand, *Dalton Trans.*, 2013, **42**, 9533-9546.
8. C. E. Wymore and J. C. Bailar Jr, *J. Inorg. Nucl. Chem.*, 1960, **14**, 42-54.
9. P. A. W. Dean, D. D. Phillips and L. Polensek, *Can. J. Chem.*, 1981, **59**, 50-61.
10. P. A. W. Dean, *Can. J. Chem.*, 1983, **61**, 1795-1799.
11. H. Arp, J. Baumgartner, C. Marschner, P. Zark and T. Müller, *J. Am. Chem. Soc.*, 2012, **134**, 6409-6415.
12. P. Perez-Lourido, J. Romero, J. A. Garcia-Vazquez, A. Sousa, Y. Zheng, J. R. Dilworth and J. Zubieta, *J. Chem. Soc., Dalton Trans.*, 2000, 769-774.
13. B. M. Barry, B. W. Stein, C. A. Larsen, M. N. Wirtz, W. E. Geiger, R. Waterman and R. A. Kemp, *Inorg. Chem.*, 2013, **52**, 9875-9884.
14. A. Murso, M. Straka, M. Kaupp, R. Bertermann and D. Stalke, *Organometallics*, 2005, **24**, 3576-3578.
15. R. W. G. Wyckoff, *Crystal Structures – Volume 1*, Interscience Publishers, New York, 2 edn., 1963.
16. I. Wharf, T. Gramstad, R. Makhija and M. Onyszchuk, *Can. J. Chem.*, 1976, **54**, 3430-3438.
17. H. Nowotny and G. Heger, *Acta Crystallogr. Sect. C: Cryst. Struct. Commun.*, 1986, **42**, 133-135.
18. M. Mantina, A. C. Chamberlin, R. Valero, C. J. Cramer and D. G. Truhlar, *J. Phys. Chem. A*, 2009, **113**, 5806-5812.
19. L. Shimoni-Livny, J. P. Glusker and C. W. Bock, *Inorg. Chem.*, 1998, **37**, 1853-1867.
20. K. Nakamoto, *Infrared and Raman Spectra of Inorganic and Coordination Compounds*, Wiley-Interscience, NY, 4 edn., 1986.
21. P. Farina, T. Latter, W. Levason and G. Reid, *Dalton Trans.*, 2013, **42**, 4714-4724.

22. S. M. Grimes, S. R. Johnston and I. Abrahams, *J. Chem. Soc., Dalton Trans.*, 1995, 2081-2086.

23. L. M. D. R. S. Martins, M. Teresa Duarte, A. M. Galvao, C. Resende, A. J. L. Pombeiro, R. A. Henderson and D. J. Evans, *J. Chem. Soc., Dalton Trans.*, 1998, 3311-3318.

24. R. Mason and D. W. Meek, *Angew. Chem., Int. Ed. Engl.*, 1978, **17**, 183-194.

25. I. Persson, K. Lyczko, D. Lundberg, L. Eriksson and A. Płaczek, *Inorg. Chem.*, 2011, **50**, 1058-1072.

26. H. Krautscheid, F. Vielsack and N. Klaassen, *Z. Anorg. Allg. Chem.*, 1998, **624**, 807-812.

27. S. H. Strauss, *Chem. Rev.*, 1993, **93**, 927-942.

28. W. Levason, R. Patel and G. Reid, *J. Organomet. Chem.*, 2003, **688**, 280-282.

29. G. R. Willey, M. D. Rudd, C. J. Samuel and M. G. B. Drew, *J. Chem. Soc., Dalton Trans.*, 1995, 759-764.

30. Z.-J. Huang, H.-J. Cheng, M. Dai, C.-Y. Ni, H.-X. Li, K.-P. Hou, Z.-G. Ren and J.-P. Lang, *Inorg. Chem. Commun.*, 2013, **31**, 33-36.

Chapter 6: Development and Electrochemistry of Reagents for the Supercritical Fluid Electrodeposition of Tin and Lead

6.1 Introduction

The ability to deposit both tin and lead using SCFED opens up the possibility of new and exciting nanomaterials and devices.[1] As the electrodeposition of tin and lead has not been attempted using supercritical fluids before, the aim of this chapter was to design, synthesise and characterise Sn and Pb reagents that are compatible with the $scCH_2F_2$ system being investigated as part of the Programme Grant,[1] and to perform voltammetric and deposition studies on the most promising compounds in CH_2Cl_2 in order to determine key electrochemical properties and ultimately their likely suitability for SCFED.

6.1.1 Synthesis, properties and uses of tin and lead nanomaterials

Group 14 has long been of great importance to the electronics industry. Since the first experimental observation of transistor action in n-type polycrystalline germanium in 1947, and subsequently in polycrystalline silicon, both of these semiconductor elements have remained fundamental to transistor technology and integrated circuitry.[2] Meanwhile, graphene (a carbon allotrope consisting of a monolayer of carbon atoms arranged in a honeycomb lattice) has recently emerged as highly attractive material for numerous applications, including electronics, sensors and energy storage devices.[3] Though used in various compound semiconductors (e.g. SnTe, PbTe and PbSnTe),[4] the heavier Group 14 metallic elements tin and lead have received considerably less attention, but with the move towards the nanostructuring of materials at the extreme nanoscale, new and exciting properties and applications for these elements are likely to be discovered.

There are two common allotropes of tin, cubic α-Sn, a semimetal with a diamond structure, which undergoes a phase transition at temperatures above 13.2 °C to become the metallic form, tetragonal β-Sn.[5] In nanoparticles smaller than 50 nm the transition temperature is calculated to drop to below –20 °C. The same DFT study predicts that below 10 nm the near-hexagonal γ-Sn (usually only formed at temperatures above 170 °C) is the most stable phase at room temperature due to lower surface energies.[6] Bulk tin is ductile, a good

electrical conductor and is resistant to corrosion; its applications range from decorations and coatings to its alloys being used as solders.[7] Tin is also a very promising anode material for lithium-ion batteries as its theoretical specific capacity (993 mA h g^{-1}) is much higher than that of traditionally used graphite (372 mA h g^{-1}).[8] Reducing the tin particle size to the nanoscale makes it less prone to stress-induced structural degradation associated with the large volume changes that occur upon electrochemical reaction with lithium, while nanowires will provide a much shorter diffusion pathway for the Li ions than bulk tin.[8,9] The superconducting behaviour of single crystalline tin nanowires (T_c = 3.7 K) has also been studied.[10,11] By oxidising tin nanowires, highly sensitive SnO_2 nanowires capable of acting as gas sensors can be synthesised.[12]

A theoretical (DFT) study[5] has predicted that α-tin will undergo a semimetal to semiconductor transition in nanowires with diameters less than ~ 4 nm (the exact value depends on the nanowire orientation). The band gap arises due to quantum confinement and its energy increases as the diameter of the nanowire decreases. A further DFT study has shown that the application of uniaxial strain (by modifying the unit cell along the nanowire axis, which can be introduced mechanically or by alloying) to the α-Sn nanowires can also affect the band gap.[13] It is proposed that by thinning the central region of a semimetal Sn nanowire, to create a semiconducting channel region with a semimetallic source and drain on either side, a special type of dopant-free sub-5 nm field effect transistor could be created, dubbed the 'confinement modulated gap transistor.'[5]

Tin nanowires with diameters in the range ~ 15 to >100 nm have been fabricated by a number of methods, including physical vapour deposition (PVD),[11] templated hydraulic pressure injection,[7] template-assisted electrodeposition from aqueous electrolytes,[9,10,14] and templated[15] and template-free[16] electrodeposition from ionic liquids. There have however been no reports of the fabrication of sub-10 nm tin nanowires. SCFED is uniquely suited for deposition into high aspect ratio, small diameter nanopores[1] (see Section 1.2) and, if a compatible supercritical fluid and Sn precursor system can be found, presents a promising route to the formation of sub-10-, and even sub-4-, nm tin nanowires.

The stable phase of lead is face centred cubic and metallic. Bulk lead is ductile, soft, highly malleable, has a high density and is a relatively poor electrical conductor.[17] Bulk lead is an elementary superconductor below T_c = 7.2 K and so interest in Pb nanowires has primarily been focused on investigating and tailoring its superconducting behaviour at the nanoscale. Lead nanowires with diameters of ~ 5 nm, synthesised using a template-assisted chemical

vapour deposition (CVD) approach, have been shown to increase the T_c by 3-4 K above that of bulk Pb, while the upper critical field was almost two hundred times higher.[18] Other reported methods of fabricating Pb nanowires (of varying crystallinities and with diameters typically >20 nm) include pressure casting into templates,[19] template-assisted electrodeposition from aqueous electrolytes[20] and solution phase synthesis involving the thermal decomposition of a lead precursor salt.[21]

Tin and lead are present in many compound semiconductors, and so the ability to co-deposit them with other elements to obtain these materials on the nanoscale would be advantageous. For example, PbS, PbSe and PbTe are binary semiconductors with narrow band gaps that have potential uses in sensors, infrared photodetectors, solar photovoltaics and thermoelectric devices. Nanowires of these materials show improved carrier mobilities, larger absorption cross sections and better absorption and emission polarisation sensitivities.[22] A field effect transistor has been fabricated using a single PbTe nanowire.[23] Compound lead semiconductor nanowires have been synthesised using various methods including CVD and solution based approaches,[22] while SnSi nanowires with an average diameter of 100 nm have recently been synthesised via template-free electrodeposition from an ionic liquid containing $SnCl_2$ and $SiCl_4$.[24]

Through the use of compatible reagents SCFED is expected to be well suited for the co-deposition of two or more elements to form ultra-small diameter nanowires of compound semiconductors.[1] Access to higher temperatures through the use supercritical fluids also opens up the possibility of using a novel hybrid thermal-electrochemical method to deposit a wide range of compound semiconductors, where one component is electrodeposited (e.g. Pb) while the remaining components (e.g. S, Se, Te) are deposited by thermal decomposition. Single crystalline nanowires (~ 60 nm diameter) of InP have been deposited from $scCO_2$/hexane and $scCHF_3$ via the thermal decomposition of a single source precursor [$^nBu_2In(\mu\text{-}P^tBu_2)_2In^nBu_2$] at 773 K, but carbon contamination was significant.[25] With suitable (mutually compatible) precursors the hybrid approach could confer all the advantages of electrodeposition (see Section 1.2), while overcoming the need to deposit all the components at the same potential.

6.1.2 Precursor design considerations

The general properties of a good precursor (i.e. the reagent used to deliver the element to be electrodeposited) for SCFED are detailed in Section 1.2. Studies on halometallate

complexes of Ge(II) and Ge(IV) have revealed that the reduction potential is more accessible (less cathodic) for the lower oxidation state[26] and so only Sn(II) and Pb(II) compounds have been considered. The work undertaken in Chapters 4 and 5 has highlighted that Pb(II) tends to form complexes with large and varying coordination numbers that are very labile in solution, making it difficult to design a precursor that is coordinatively saturated. It was therefore decided to keep the systems as simple as possible, through the use of well-defined halometallate salts.

For tin, the tetrabutylammonium halometallate salts $[N^nBu_4][SnX_3]$ were chosen as previous studies[26,27] have shown that p-block halometallates can be readily synthesised in high yields and purity, are easily handled and are stable at high temperatures. They typically show a high solubility and stability in organic solvents, allowing high-concentration electrolytes to be prepared. By using well-defined molecular species it is easy to control the speciation in solution. Furthermore, the tetrabutylammonium chlorometallate salts exist for a wide range of the p-block elements, presenting the prospect of co-deposition from these mutually compatible reagents to form compound semiconductors and alloys. Investigations into the electrochemistry of $[N^nBu_4][MCl_4]$ (M = In, Sb, Bi) and $[N^nBu_4]_2[MCl_6]$ (M = Se, Te) in CH_2Cl_2, using $[N^nBu_4]Cl$ as the supporting electrolyte, found that they form stable and reproducible electrochemical systems from which the element can be electrodeposited. A thin film of crystalline InSb was also electrodeposited onto a planar TiN electrode from an electrolyte containing $[N^nBu_4][InCl_4]$ and $[N^nBu_4][SbCl_4]$.[27] Due to the poor solubility of the Pb(II) halides in organic solvents,[28] work with lead has focused on synthesising halometallate salts with solubilising cations, specifically using the $[PPh_4]^+$ cation.

6.2 Results and Discussion

The Sn(II) and Pb(II) halometallate precursors were synthesised using the relevant commercially obtained metal dihalide (MX_2) and either $[N^nBu_4]X$ or $[PPh_4]X$ in a dry solvent under an inert atmosphere so as to ensure no oxidation of the metal, or any other unwanted reactions, occurred. The products were also handled and stored in a N_2-filled glove box. Microanalysis was used to confirm the stoichiometries and check the purity of the synthesised precursors. The compounds were characterised by single crystal X-ray diffraction where suitable crystals were grown and by IR spectroscopy if the M–X stretching frequencies fell above 200 cm^{-1}. The $[N^nBu_4]^+$ and $[PPh_4]^+$ cations were easily identified using ^1H NMR spectroscopy and by a sharp singlet for $[PPh_4]^+$ at $\delta = 23.9$ in the $^{31}P\{^1H\}$ NMR spectra. $^{119}Sn\{^1H\}$ NMR spectroscopy was used to characterise the Sn precursors, and also to perform some speciation studies in CH_2Cl_2.

Detailed cyclic voltammetry and deposition studies (further details on the electrochemical techniques used can be found in Section 1.7.2) were then performed on the Sn and Pb reagents in dry CH_2Cl_2 in order to evaluate their electrochemical properties. Work by the group at the University of Southampton investigating SCFED has shown that the behaviour of a precursor in liquid CH_2Cl_2 is a good guide to its likely relative solubility and electrochemical behaviour in $scCH_2F_2$, thus providing a rapid screening process for potential reagents.[26] The supporting electrolyte used was accordingly either $[N^nBu_4]X$ or $[PPh_4]X$ (where X matches the halogen present in the precursor) to avoid unnecessary complications through the introduction of other ions into the system, as $[X]^-$ is expected to be liberated during the reduction of the halometallate precursor.

To allow the efficient exclusion of air and moisture the electrolyte preparation and electrochemical experiments were performed in a N_2-filled glove box. The electrochemical experiments in CH_2Cl_2 were performed at room temperature using a three-electrode system in a one compartment electrochemical cell. A Pt gauze was used as the counter electrode, and a Ag/AgCl electrode (in 0.1 M $[N^nBu_4]Cl$ in CH_2Cl_2) was used as the reference electrode. For the cyclic voltammetry experiments, the freshly polished working electrode used was a platinum (Pt, 0.5 mm diameter), gold (Au, 1.0 mm diameter) or glassy carbon (GC, 3.0 mm diameter) disk electrode. The cyclic voltammograms were recorded by starting at the open circuit potential and initially scanning negative to explore the metal reduction process first. Films of Sn and Pb were deposited potentiostatically onto planar gold or titanium nitride (TiN) slide electrodes. The latter is of interest because TiN is

regularly used in electronic applications as a conductive barrier layer between metallic contacts and semiconductors.[29] The electrolytes used were always homogenous (i.e. the precursor and supporting electrolyte had completely dissolved).

Using the information gained from the voltammetric and deposition studies of $[N^nBu_4][SnX_3]$ in CH_2Cl_2, the chlorometallate precursor was then studied in $scCH_2F_2$, chosen so as to be compatible with other p-block systems where the chlorometallate salts have been most widely studied. Details of the high pressure electrochemical cell and typical set-up used by Dr. P. Richardson from the University of Southampton to perform the SCFED of tin, plus the techniques (SEM, EDX and XRD) employed to characterise all the materials deposited in this chapter, can be found in the Experimental Section.

6.2.1 Synthesis and characterisation of the tin and lead precursors

The structural chemistry of the tin(II)- and lead(II) halides is complex and varied due to the stereochemical activity (or not) of the lone pair and their tendency to polymerise in the solid state.[30] Crystalline SnF_2 is composed of Sn_4F_8 tetramers interlinked by weaker Sn–F interactions so that each Sn centre is surrounded by six fluorine atoms in a very distorted [3+3] octahedron.[31] $SnCl_2$, $PbCl_2$ and $PbBr_2$ are all essentially isostructural, with a nine-coordinate metal centre, while the structure of eight-coordinate $SnBr_2$ is closely related.[32] The structure of $SnCl_2$ comprises of core chains of corner sharing trigonal pyramidal $\{SnCl_3\}$ units, with four medium and two long bonds to neighbouring chlorine atoms, while the coordination geometry of $PbCl_2$ and $PbBr_2$ is best described as [7+2]. The unique structure of SnI_2 consists of one third of the Sn atoms (with near-perfect octahedral coordination) in chains, which are cross-linked by double chains containing the remaining (seven-coordinate) Sn atoms, while PbI_2 has the CdI_2 hexagonal layer lattice structure.[30] Though formation of the halometallate anions *in situ* from MX_2 may be possible due to the large excess of $[X]^-$ ions in solution provided by the electrolyte, the poor solubility of PbX_2 in CH_2Cl_2 and the light, air and moisture sensitivity of $SnBr_2$, and particularly SnI_2,[33] means that the more stable and soluble $[N^nBu_4]^+$ or $[PPh_4]^+$ salts are easier to manipulate.

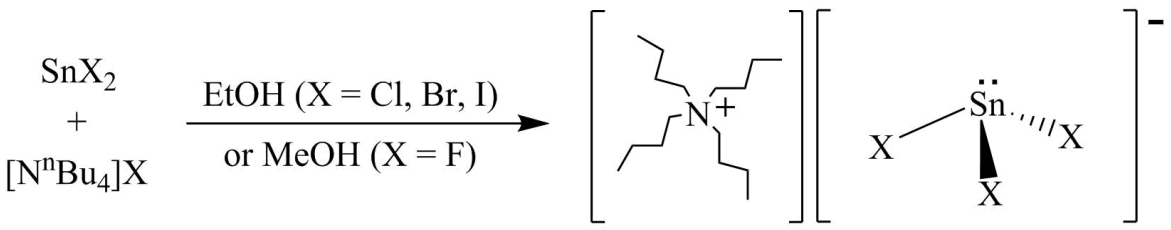

Scheme 6.1 Synthesis of $[N^nBu_4][SnX_3]$ (X = F, Cl, Br, I)

The precursors $[N^nBu_4][SnX_3]$ (X = Cl, Br, I) were synthesised as white or yellow powders using a modified literature route[34] used to prepare $[NEt_4][SnX_3]$, using ethanol as the solvent (Scheme 6.1). Due to the poor solubility of SnF_2 in most organic solvents, the synthesis of $[N^nBu_4][SnF_3]$ (a white powder) involved reacting SnF_2 with $[N^nBu_4]F$ (a 1.0 M solution in THF obtained commercially and used as supplied) in methanol, in which SnF_2 shows moderate solubility.[35] The crystal structures of $[N^nBu_4][SnX_3]$ (X = F, Cl, Br, I) have not been reported, but despite several attempts no single crystal X-ray diffraction data of sufficient quality could be collected. Though colourless crystals of $[N^nBu_4][SnCl_3]$ were grown by allowing a CH_2Cl_2 solution of the salt to evaporate, while the data indicate a discrete *pseudo*-trigonal pyramidal $[SnCl_3]^-$ anion, the butyl chains of the $[N^nBu_4]^+$ cation show heavy disorder that could not be satisfactorily modelled. The X-ray crystal structure of the closely related salt $[N^nPr_4][SnI_3]$ is known, and reveals the *pseudo*-trigonal pyramidal $[SnI_3]^-$ groups linked into infinite chains by long bridging $(\mu\text{-I})_2$ interactions.[36]

Over the period of a few days crystals grew in the EtOH filtrates kept after $[N^nBu_4][SnX_3]$ (X = Br, I) had been isolated from the reactions. Though the data were of poor quality and so full X-ray crystallographic data are not reported, single crystal X-ray diffraction studies showed that oxidation from Sn(II) to Sn(IV) had occurred as the crystals had the structure $[N^nBu_4][X_3Sn(\mu\text{-OEt})_3SnX_3]$ (X = Br, I). These bimetallic alkoxide clusters are structurally very similar to the crystallographically authenticated anion found in $[Ti_3(O^iPr)_{11}][I_3Sn(\mu\text{-}O^iPr)_3SnI_3]$.[37] Microanalysis of the yellow crystals isolated from the iodide reaction matched the formulation $[N^nBu_4][I_3Sn(\mu\text{-OEt})_3SnI_3]$. These findings highlight the importance of isolating the $[N^nBu_4][SnX_3]$ salts from the reaction solutions quickly if an alcohol is used as the solvent; the reaction of $[N^nBu_4]I$ and SnI_2 in CH_2Cl_2 was not clean as significant amounts of (poly)iodides and/or I_2 formed.

As trigonal pyramidal anions the $[SnX_3]^-$ anions possess C_{3v} symmetry and have two (a_1 and e) IR active stretching modes.[38] For X = Br and I these stretches fall below 200 cm^{-1}, but for X = F and Cl the observed stretching frequencies and their relative intensities are in good agreement with the literature.[38,39] Both ^{117}Sn and ^{119}Sn satellites can be clearly seen in the ^{19}F NMR spectrum of $[N^nBu_4][SnF_3]$ in CD_2Cl_2 (δ = –87.7), while in the $^{119}Sn\{^1H\}$ NMR spectrum a quartet is observed (δ = –528.7, $^1J^{119}_{SnF}$ = 3181 Hz), with the lines sharpening upon cooling the solution to 203 K (Figure 6.1). Though reports of NMR spectroscopic data for $[SnF_3]^-$ are rare, comparisons can be made with data reported for $[PhC(NH^tBu)_2][SnF_3]$ (the crystal structure of which reveals that the $[SnF_3]^-$ units dimerise), which at room temperature in THF-d^8 exhibited broad singlets at δ = –81.4 and

δ = –531.7 in the ^{19}F and ^{119}Sn NMR spectra respectively. Satellites ($^{1}J_{^{119}SnF}$ = 2959 Hz) were only observed in a ^{19}F NMR spectrum recorded at 193 K, suggesting that rapid fluorine exchange was occurring at higher temperatures.[40] The other $[N^nBu_4][SnX_3]$ all show singlets in the ^{119}Sn{^{1}H} NMR spectra (though the resonance for $[SnI_3]^-$ was only observed upon cooling the solution to 223 K), with the resonances sequentially moving to higher frequencies (δ = –40.8 (X = Cl), 134.3 (X = Br), 352.2 (X = I)) as the halide gets heavier, as reported by Taylor *et al.*[41] This trend is the opposite of that seen for SnX_4 and of that expected on halogen electronegativity grounds and has been attributed to the influence of the lone pair.[41] The NMR spectroscopic data suggest that the solution speciation of $[N^nBu_4][SnX_3]$ (X = F, Cl, Br, I) in CH_2Cl_2 is of discrete, mononuclear $[SnX_3]^-$ anions.

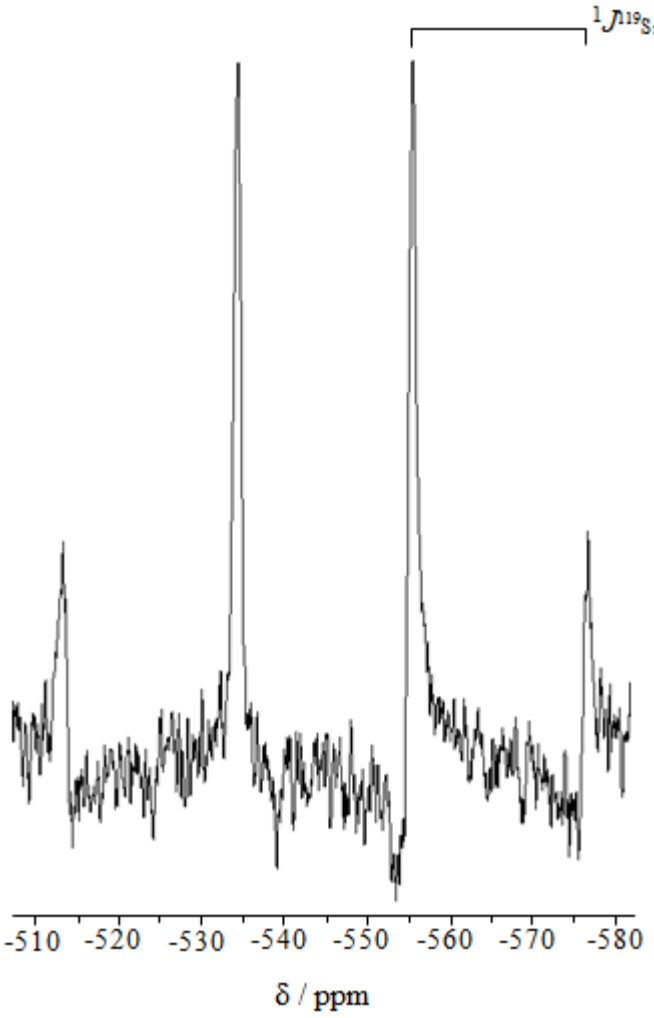

Figure 6.1 ^{119}Sn{^{1}H} NMR spectrum of $[N^nBu_4][SnF_3]$ at 203 K in CH_2Cl_2/CD_2Cl_2.

While the crystal structure of $[N^nBu_4][PbI_3]$ is known,[42,43] attempts to synthesise the salt based on the reported method (using a 1:1:1 molar ratio of PbI_2, NaI and $[N^nBu_4][PF_6]$ in acetone) resulted in the isolation of $[N^nBu_4]_8[Pb_{18}I_{44}]$ as a yellow powder,[42] confirmed by

microanalysis, which is too large and poorly soluble in CH_2Cl_2 to make a good precursor. Attempts to make $[N^nBu_4][PbCl_3]$ using either $PbCl_2$ or $Pb(NO_3)_2$ as the lead source were unsuccessful, and so the $[PPh_4]^+$ ion was studied as an alternative cation as its solubilising properties in organic solvents are well known and a number of lead(II) halide salts have already been isolated.[44-47]

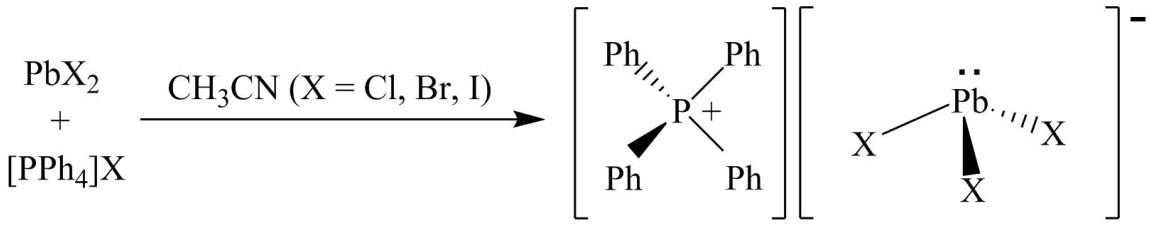

Scheme 6.2 Synthesis of $[PPh_4][PbX_3]$ (X = Cl, Br, I)

The reactions of PbX_2 and $[PPh_4]X$ (X = Cl, Br, I) in a 1:1 molar ratio using CH_3CN as the solvent resulted in the formation of $[PPh_4][PbCl_3]\cdot CH_3CN$, $[PPh_4][PbBr_3]$ and $[PPh_4]_2[Pb_2I_6]$ as white or yellow powders. Unit cell determinations on single crystals of both $[PPh_4][PbCl_3]\cdot CH_3CN$ and $[PPh_4]_2[Pb_2I_6]$ were consistent with the reported structures, the former anion containing $[PbCl_3]^-$ groups associated into chains via asymmetric $(\mu\text{-}Cl)_2$ chloro-bridges to give a distorted square pyramidal Pb(II) centre,[44] while the latter anion is a discrete $[Pb_2I_6]^{2-}$ dimer where the Pb(II) centres have a distorted seesaw coordination geometry.[46] The crystal structure of $[PPh_4][PbBr_3]$ reveals discrete cations and $(\mu\text{-}Br)_3$ bromo-bridged chain polymer anions (Figure 6.2). The Pb(II) centres have near-ideal octahedral coordination geometries (suggesting that the lone pair on the lead is stereochemically inactive) with a small range of Pb–Br bond lengths (2.9823(6)–3.0416(8) Å). The related compound, $[PPh_4]_2[Pb_3Br_8]$, formed by reacting $[PPh_4]Br$ and $PbBr_2$ in a 1:1 ratio in CH_3CN at 75 °C, contains both distorted tetrahedral and octahedral Pb(II) centres, the latter of which have very similar bond lengths and angles to the Pb(II) centres in $[PPh_4][PbBr_3]$.[45]

No resonance could be found for $[PPh_4]_2[Pb_2I_6]$ using ^{207}Pb NMR spectroscopy in CH_2Cl_2/CD_2Cl_2, even with the addition of excess $[PPh_4]I$, and so speciation studies on the lead precursors in CH_2Cl_2 could not be performed. However, given the dissociative nature of Pb(II) compounds,[28] the solution speciation of $[PPh_4][PbX_3]$ is likely to involve simple, possibly mononuclear species, which are in rapid equilibrium.

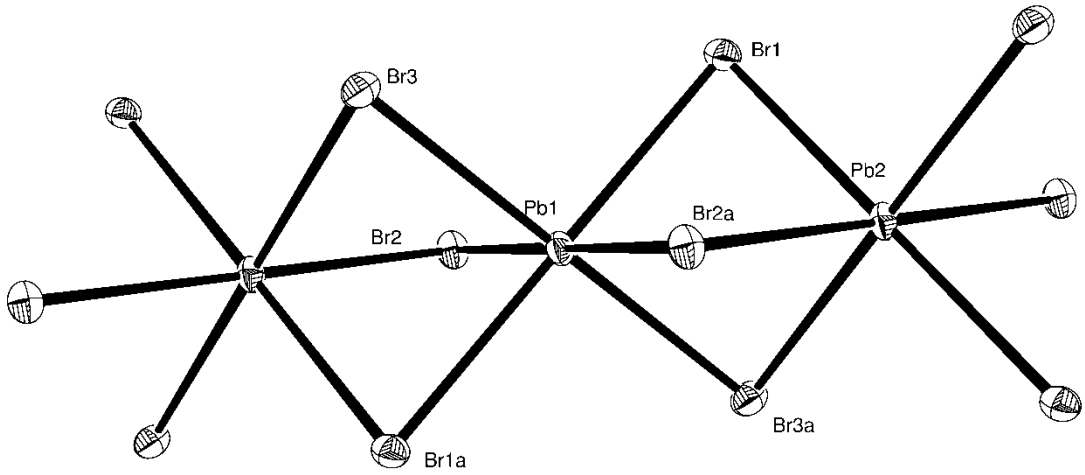

Figure 6.2 The structure of a portion of the chain polymer anion present in $[PPh_4][PbBr_3]$ showing the atom labelling scheme. Ellipsoids are drawn at the 50% probability level. Symmetry operation: a = – x, – y, – z.

Table 6.1 Selected bond lengths (Å) and angles (°) for $[PPh_4][PbBr_3]$

Pb1–Br1	3.0416(8)	Br1–Pb1–Br2	92.89(2)
Pb1–Br2	3.0332(8)	Br1–Pb1–Br3	96.094(16)
Pb1–Br3	2.9823(6)	Br2–Pb1–Br3	88.18(2)
Pb2–Br1	3.0179(7)	Br1–Pb1–Br2a	87.11(2)
Pb2–Br2a	3.0176(6)	Br1–Pb1–Br3a	83.906(16)
Pb2–Br3a	3.0296(7)	Br2–Pb1–Br3a	91.82(2)
		Br1–Pb2–Br2a	87.82(2)
		Br1–Pb2–Br3a	83.51(2)
		Br2a–Pb2–Br3a	87.60(2)

6.2.2 Cyclic voltammetry studies of $[N^nBu_4][SnX_3]$ in CH_2Cl_2

Initially cyclic voltammetry was performed on a CH_2Cl_2 solution containing 10 mM $[N^nBu_4][SnCl_3]$ with 100 mM $[N^nBu_4]Cl$ as the supporting electrolyte. A $^{119}Sn\{^1H\}$ NMR spectroscopic study showed that the resonance for $[N^nBu_4][SnCl_3]$ in CH_2Cl_2/CD_2Cl_2 was unchanged in the presence of a tenfold excess of $[N^nBu_4]Cl$, suggesting that its speciation with excess chloride present is the same. Previous voltammetric studies of the pure supporting electrolyte in CH_2Cl_2 have shown that $[N^nBu_4]Cl$ provides an excellent

potential window (current densities remain low between –1.5 and +1.5 V *vs*. Ag/AgCl) and good conductivity (σ = ~ 1 mS cm^{-1} for 100 mM [N^{n}Bu$_4$]Cl, comparable with a 10 mM KCl solution).[27] The voltammetry at a Pt disk electrode was reproducible and revealed typical metal deposition and stripping features, with a well-defined nucleation loop and stripping peak (Figure 6.3). The electrochemical window for the Sn(II)/Sn couple was found to be between –1.1 and +0.8 V (beyond these potentials other unwanted processes were observed). The single cathodic wave corresponds to the reduction of Sn(II) to Sn metal. A nucleation overpotential is observed as the tin needs to first nucleate and grow on the platinum surface before bulk deposition can proceed. This, and the absence of any underpotential deposition indicates that the deposition of tin is more thermodynamically favourable on itself than on platinum.[48] After a sharp deposition onset and peak the deposition then happens under diffusion controlled conditions until stripping starts to occur. The anodic wave (stripping peak) can be assigned to the oxidation of the Sn deposited during the preceding cathodic scan; the sharp drop in current on the right hand side of the peak is due to the tin running out at the same time over all of the electrode surface.[48] The deposition onset, peak deposition current and stripping onset occur at –0.49 V, –0.57 V and –0.41 V. The observed single deposition and stripping peak is comparable to that observed for the Sn(II)/Sn couple in other media, including ionic liquids.[48,49]

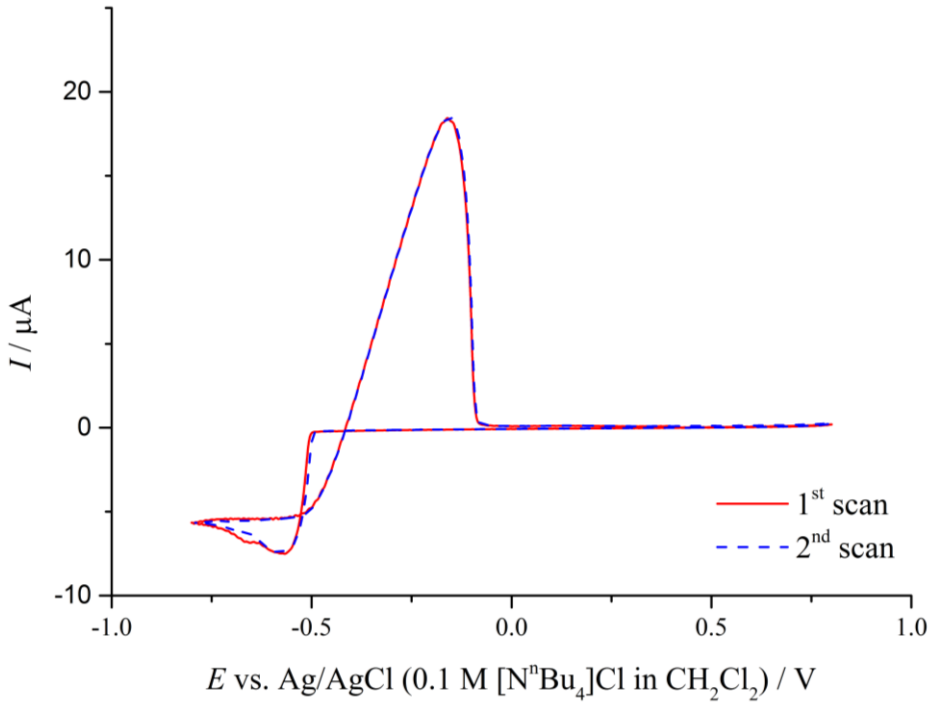

Figure 6.3 Cyclic voltammograms of 10 mM [N^{n}Bu$_4$][SnCl$_3$] in CH$_2$Cl$_2$ recorded at a 0.5 mm Pt disk working electrode. The supporting electrolyte used was 100 mM [N^{n}Bu$_4$]Cl and the potential scan rate was 50 mV s^{-1}.

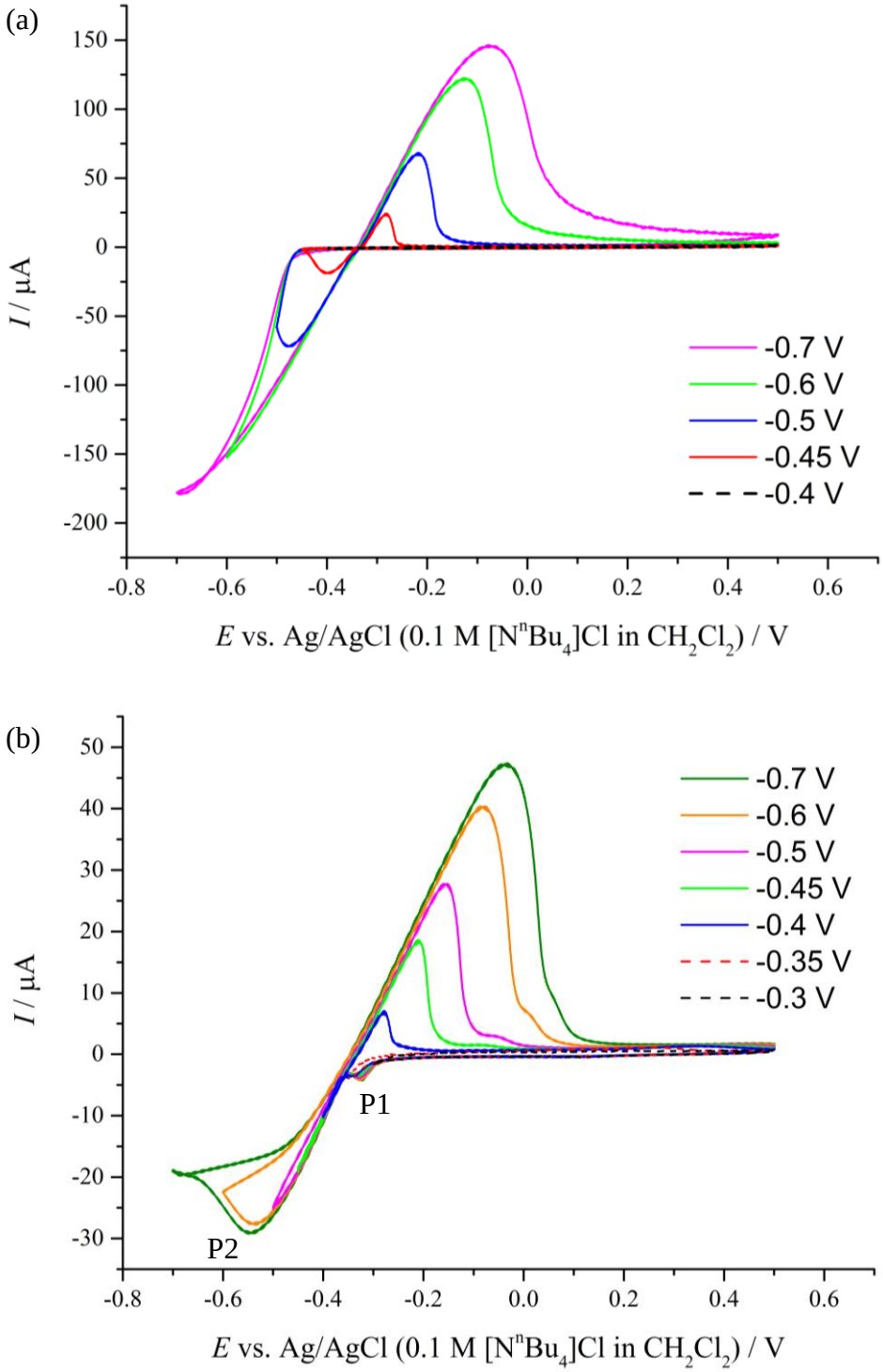

Figure 6.4 Cyclic voltammograms of 10 mM $[N^nBu_4][SnCl_3]$ in CH_2Cl_2 recorded at (a) a 3.0 mm GC disk and (b) a 1.0 mm Au disk working electrode. The cathodic potential was increased to more negative potentials with successive cycles. The supporting electrolyte used was 100 mM $[N^nBu_4]Cl$ and the potential scan rate was 100 mV s^{-1}.

Similar voltammetric behaviour (Figure 6.4(a)) was observed when a glassy carbon disk working electrode was instead used, though a definitive peak deposition current was not

reached, presumably due to the larger size (3.0 mm (GC) vs. 0.5 mm (Pt) diameter) of the electrode. With an Au disk working electrode, two reduction processes were observed, labelled P1 and P2 on Figure 6.4(b). The first reduction process (P1), which has a peak potential at –0.32 V, can be correlated to surface alloying processes and/or underpotential deposition on the Au surface.[15] The similar size of tin and gold atoms allows the substitution of gold atoms for tin to occur in the lattice, and the resulting Au–Sn binary alloy system is quite complicated, with several stable intermetallic compounds known in the solid state.[15,50] The second reduction process (P2), which has a peak potential at –0.55 V, is related to the bulk deposition of tin. On the anodic wave the expected tin stripping peak was observed; on fresh Au working electrodes a second, more positive, stripping peak was also observed, which became less pronounced as more cycles were performed, thought to be due to the change in the electrode surface.

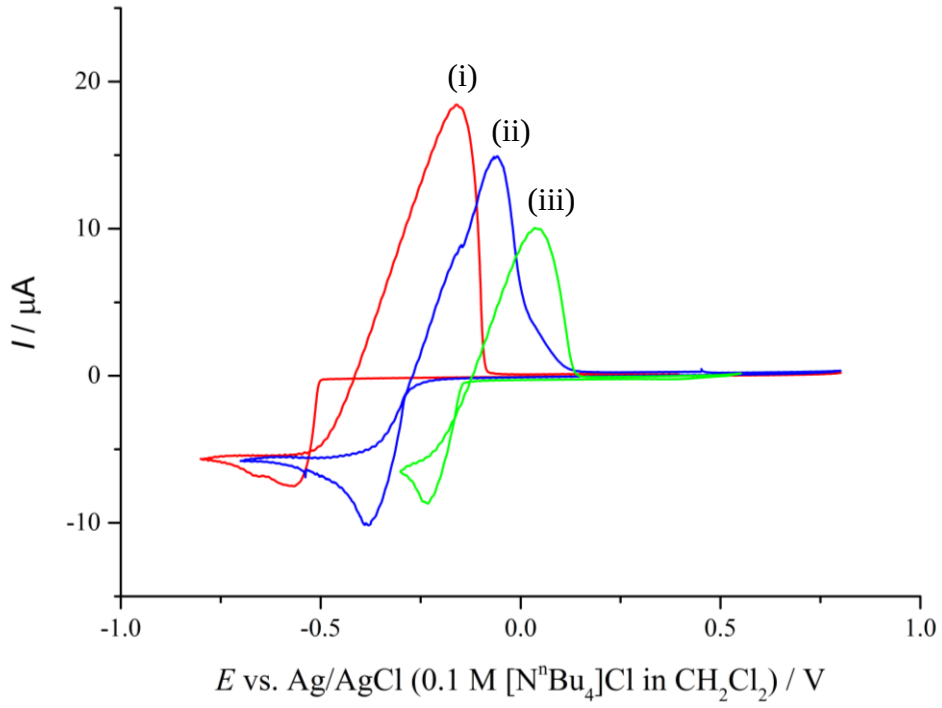

Figure 6.5 Cyclic voltammograms of $[N^nBu_4][SnX_3]$ (X = Cl, Br, I) in CH_2Cl_2 recorded at a 0.5 mm Pt disk working electrode. The composition of each electrolyte system was 10 mM $[N^nBu_4][SnX_3]$ and 100 mM $[N^nBu_4]X$, where (i) X = Cl, (ii) X = Br and (iii) X = I. The potential scan rate was 50 mV s^{-1}.

The effect of systematically changing the halide on the cyclic voltammetry of the tetrabutylammonium Sn(II) salts in CH_2Cl_2 was then investigated using Pt disk working electrodes. Cyclic voltammograms recorded for $[N^nBu_4][SnX_3]$ (X = Br, I), using the corresponding $[N^nBu_4]X$ as the supporting electrolyte, showed similar metal deposition

and stripping features to when X = Cl, though the nucleation overpotentials were much smaller. For X = I, additional oxidation features corresponding to iodide/iodine redox couples were seen if scanned positive beyond +0.6 V.[26] The deposition onset, peak deposition current and stripping onset were at –0.28 V, –0.38 V and –0.27 V for X = Br and –0.15 V, –0.23 V and –0.12 V for X = I. Importantly, it becomes clear that when X changes Cl → Br → I the reduction potential becomes significantly more positive (Figure 6.5), which means that that reduction of the $[SnI_3]^-$ anion is most accessible. A similar trend has been observed for [EMIM][GeX_3] (X = Cl, Br, I; EMIM = ethylmethylimidazolium) in CH_2Cl_2 (see Table 6.3).[26]

Upon performing cyclic voltammetry experiments on an electrolyte consisting of 10 mM $[N^nBu_4][SnF_3]$ and 100 mM $[N^nBu_4]F$ in CH_2Cl_2 no peaks were observed in either scan direction within the available electrochemical window (which was found to be –1.5 to +1.25 V *vs.* Ag/AgCl). Upon investigating the system using $^{119}Sn\{^1H\}$ NMR spectroscopy, it was found that in the presence of a tenfold excess of $[N^nBu_4]F$ the quartet corresponding to the $[SnF_3]^-$ ion disappeared (no resonances were observed), suggesting that the speciation had changed. For both the voltammetric and NMR spectroscopic studies the 1.0 M solution of $[N^nBu_4]F$ in THF was dried *in vacuo* beforehand to remove the THF, which yielded a yellow gum to which the precursor and CH_2Cl_2 was added immediately to give a colourless solution. This was done because THF is a coordinating solvent and so could react with the Sn precursor. However anhydrous $[N^nBu_4]F$ is known to be unstable in the solid state at room temperature,[51] making it potentially unsuitable as a supporting electrolyte. Therefore the readily available and stable solid $[N^nBu_4][BF_4]$ was also tested. In the presence of a tenfold excess of $[N^nBu_4][BF_4]$ the quartet of $[SnF_3]^-$ was still observable in the $^{119}Sn\{^1H\}$ NMR spectrum, but on performing cyclic voltammetry studies on an electrolyte consisting of 10 mM $[N^nBu_4][SnF_3]$ and 100 mM $[N^nBu_4][BF_4]$ in CH_2Cl_2 again no peaks were observed in either scan direction within the available electrochemical window, using either a Pt or Au disk working electrode. There was therefore no evidence that tin deposition could be achieved using $[N^nBu_4][SnF_3]$ as a precursor and so it was not investigated further.

6.2.3 Electrodeposition of tin from CH_2Cl_2 solution

Tin was deposited potentiostatically onto planar Au and TiN slide electrodes, using the same $[N^nBu_4][SnCl_3]$-containing electrolyte used for the voltammetric characterisations. The electrodes were held at a constant potential of –1.0 V *vs.* Ag/AgCl (0.1 M $[N^nBu_4]Cl$

in CH_2Cl_2), chosen to provide a large overpotential in order to obtain films of sufficient thickness (> 1 μm) for EDX and XRD analysis, whilst falling within the available electrochemical window. After deposition had finished, the electrodes with the deposited films were gently washed by dipping into CH_2Cl_2 to dissolve residual electrolyte salts. The silver-grey deposited films were analysed by Dr. P. Richardson (SEM and EDX) and M. Hasan (XRD) at the University of Southampton.

As the chronoamperogram data (Figure 6.6) shows, tin was electrodeposited potentiostatically onto a planar Au electrode by holding the potential at –1.0 V for 3600 s, which corresponded to 0.53 C of charge having passed. The area of the electrode that was electrodeposited onto was measured to be approximately 0.16 cm^2, giving an estimated deposit thickness of 2.8 μm. SEM images (Figure 6.7) of the deposited film show a fairly uniform morphology across the electrode surface, with the tin forming irregular shaped clusters of crystallites. These clusters are evidence of Sn nucleation having occurred at various points on the Au surface, followed by crystal growth from these points. Film adhesion to the gold was found to be good. EDX analysis of the deposited film detected only Sn, meaning the film thickness was sufficient to mask the Au substrate; there was no evidence of chloride contamination from the electrolyte.

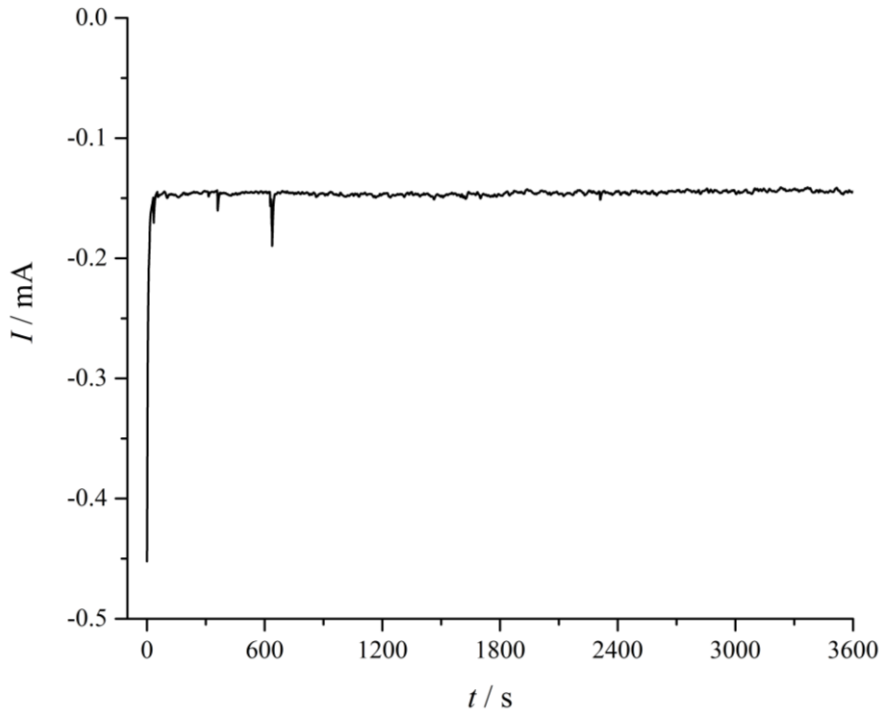

Figure 6.6 Chronoamperogram for the electrodeposition of Sn onto a planar Au electrode in CH_2Cl_2 from an electrolyte containing 10 mM $[N^nBu_4][SnCl_3]$ and 100 mM $[N^nBu_4]Cl$, using an applied potential of –1.0 V.

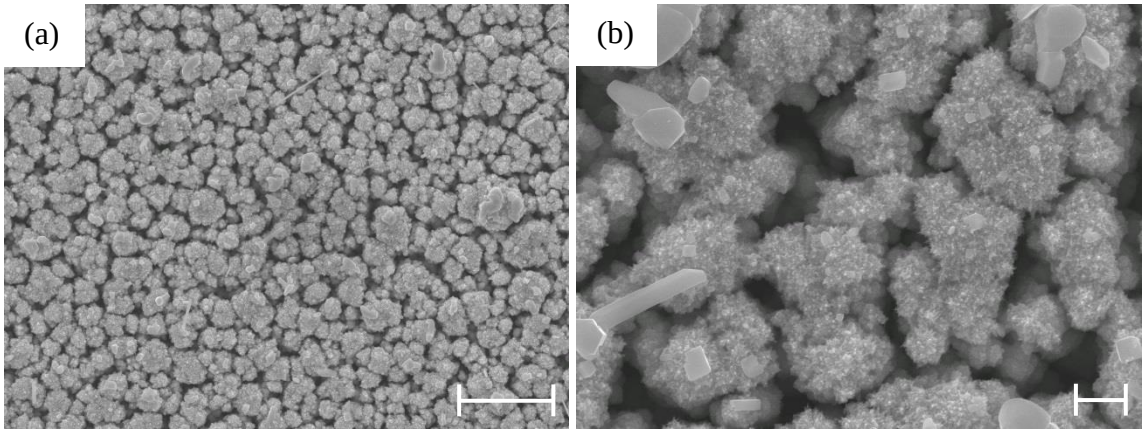

Figure 6.7 SEM micrographs of Sn electrodeposited on a planar Au electrode in CH_2Cl_2. The magnifications used are (a) x2000 (scale bar = 10 μm) and (b) x10000 (scale bar = 1 μm).

The structure of the film was investigated using XRD, which confirmed that the film was crystalline as-deposited. As well as the diffraction peaks expected for tetragonal *β*-tin, the 1° grazing incidence scan (Figure 6.8) reveals peaks corresponding to the cubic Au phase of the substrate, and an alloy phase, AuSn. The experimental and literature values for the observed phases are given in Table 6.2. Observation of an alloy phase supports the peak assignments made to the cyclic voltammograms on an Au disk working electrode (see Section 6.2.2). A symmetric (*θ*-2*θ*) XRD scan showed the normal distribution of intensities for the Sn phase (i.e. no preferred orientation was observed).

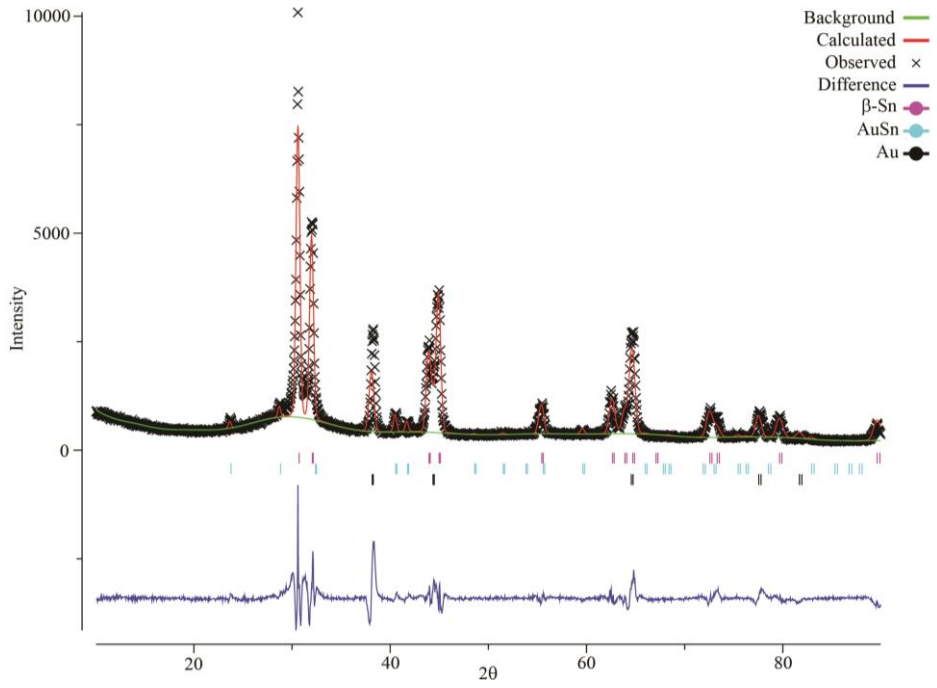

Figure 6.8 XRD pattern for Sn electrodeposited on a planar Au electrode in CH_2Cl_2 (1° grazing incidence scan). Comparison patterns come from the ICSD.

Table 6.2 Refined parameters from the XRD pattern for Sn on a planar Au electrode

Phase	Crystal structure and space group	Lattice parameters (Å)	Literature lattice parameters (Å)
Sn	tetragonal/$I4_1/amdS$ (141)	a = 5.8215(3) c = 3.1760(3)	a = 5.8318(3) c = 3.1819(3)[52]
AuSn	hexagonal/$P63/mmc$ (194)	a = 4.3159(18) c = 5.514(3)	a = 4.3218 c = 5.523[53]

The Sn film deposited on a planar TiN electrode (area = ~0.35 cm^2) by holding the electrode at –1 V for 2520 s (Q = 0.78 C) had an estimated thickness of 1.9 µm. The film was found to not adhere to the TiN surface well, with some flaking occurring when handled. The SEM images (Figure 6.9) reveal clusters of irregular shaped plates, with EDX analysis again finding only Sn. The X-ray diffraction data confirmed that the only Sn-containing phase present was tetragonal *β*-tin (refined lattice parameters: a = 5.8312(4), c = 3.1824(3) Å), with no preferred orientation.

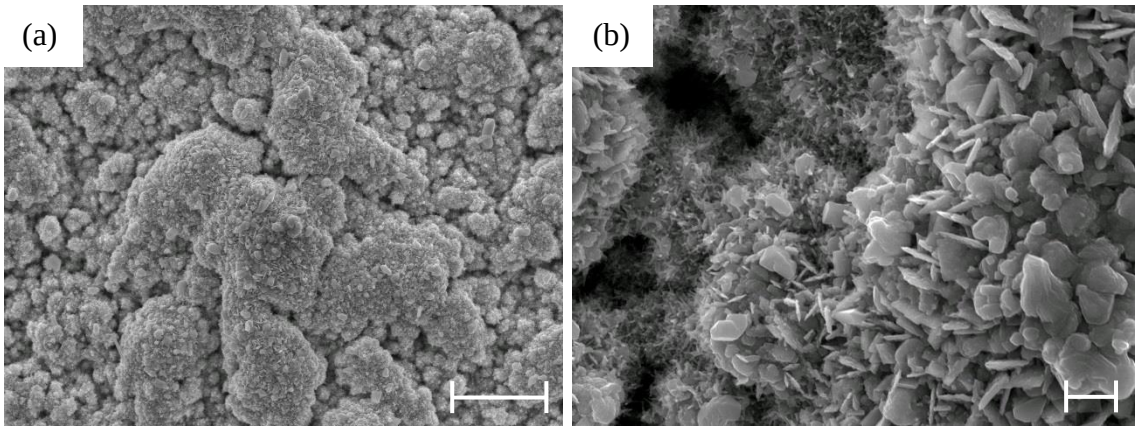

Figure 6.9 SEM micrographs of Sn electrodeposited on a planar TiN electrode in CH_2Cl_2. The magnifications used are (a) x2000 (scale bar = 10 µm) and (b) x10000 (scale bar = 1 µm).

6.2.4 Voltammetric and deposition studies of $[N^nBu_4][SnCl_3]$ in $scCH_2F_2$

The electrodeposition results in CH_2Cl_2 show that good quality films of tin can be successfully electrodeposited from an electrolyte containing $[N^nBu_4][SnCl_3]$ and $[N^nBu_4]Cl$, with no significant contamination from the precursor or supporting electrolyte occurring. Having screened the electrochemical properties of $[N^nBu_4][SnCl_3]$ in CH_2Cl_2,

the information gained was used by Dr. P. Richardson to perform cyclic voltammetry and deposition studies in supercritical difluoromethane using an electrolyte containing 2 mM $[N^nBu_4][SnCl_3]$ and 50 mM $[N^nBu_4]Cl$. These concentrations were chosen to ensure the precursor and supporting electrolyte were completely dissolved (i.e. to give a single homogenous fluid phase) whilst providing good conductivity in $scCH_2F_2$ at 358 K at 17.2 MPa, the conditions employed. The potential window when using $[N^nBu_4]Cl$ under these conditions was found to be between –2.0 and +1.0 V *vs*. Pt.

Initially the voltammetric characteristics of $[N^nBu_4][SnCl_3]$ in $scCH_2F_2$ were determined using an Au disk working electrode. The cyclic voltammogram (Figure 6.10) is similar to that observed in CH_2Cl_2 (thus confirming that the CH_2Cl_2-$scCH_2F_2$ electrochemistry analogy is effective), with a well-defined nucleation loop and stripping peak, but with a potential offset. The deposition onset and stripping onset occur at –1.11 V and –0.90 V. Compared to tin deposition in CH_2Cl_2, the deposition onset and stripping onset have shifted to more cathodic potentials by 0.62 V and 0.49 V respectively. The fluctuations in reduction current observed in the limiting current density region arise because of the effects of convection in the high pressure electrochemistry cell, caused by temperature gradients that are worsened by the low viscosity of the supercritical fluid.[1]

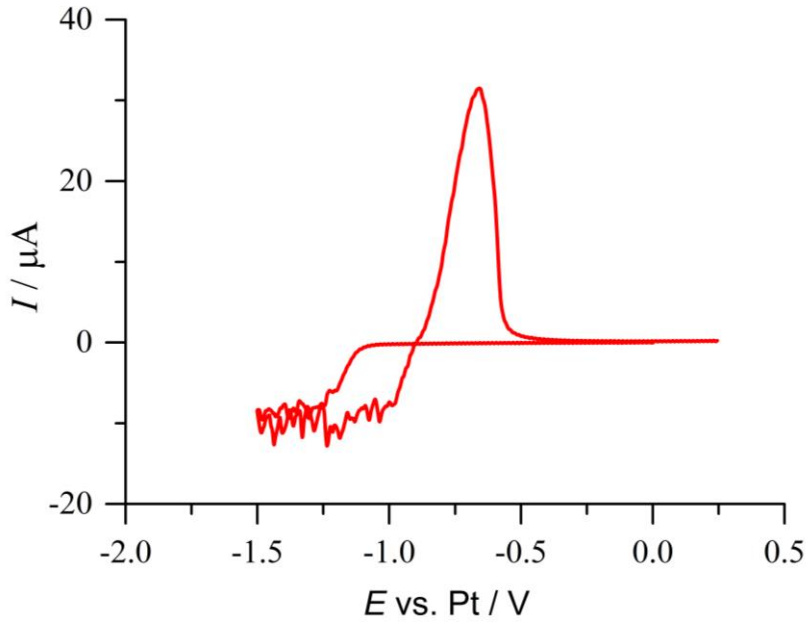

Figure 6.10 Cyclic voltammogram of 2 mM $[N^nBu_4][SnCl_3]$ in $scCH_2F_2$ (17.2 MPa and 358 K) recorded at a 0.5 mm Au disk working electrode. The supporting electrolyte used was 50 mM $[N^nBu_4]Cl$; the potential scan rate was 50 mV s^{-1}.

The potentiostatic electrodeposition of tin onto planar Au and TiN slides in $scCH_2F_2$, using the same electrolyte, was then performed. Using a deposition potential of either –1.25 V or

–1.5 V *vs*. Pt, good quality *β*-tin films were produced, with SEM analysis revealing similar irregular crystallite cluster morphologies to those deposited in CH_2Cl_2. Having proved that Sn can be deposited under these conditions, the electrodeposition of small diameter tin nanowires was attempted. An anodic aluminium oxide (AAO) membrane with nominal pore diameters of 13 nm was chosen to be the nanowire template. Anodic alumina membranes with aligned pore structures make good templates because they are robust, electrically and thermally insulating and optically transparent;[1] AAO templates have been successfully used for the electrodeposition of Sn nanowires before.[9] Using the same electrolyte and conditions, and a deposition potential of –1.5 V, tin was successfully deposited in the 13 nm pores, as seen by the cross-section SEMs shown in Figure 6.11. In this example the template was not completely filled, but it provides clear evidence for nanowires grown inside the pores. A symmetric scan XRD of the nanowires inside the template showed that the deposited material was tetragonal *β*-Sn, with a preferred orientation along the < 200 > plane.

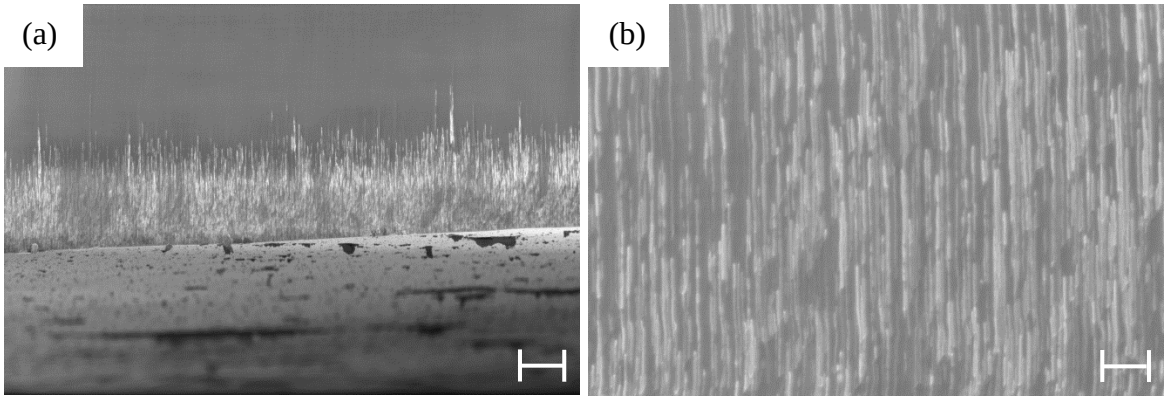

Figure 6.11 Cross-section SEM micrographs of a 13 nm AAO template containing Sn nanowires electrodeposited from $scCH_2F_2$. The magnifications used are (a) x843 (scale bar = 10 μm) and (b) x8690 (scale bar = 1 μm).

These results prove that crystalline tin can be electrodeposited from a supercritical fluid, $scCH_2F_2$, using $[N^nBu_4][SnCl_3]$ as a precursor (which has the advantage of being mutually compatible with other known p-block chlorometallate precursors), and that preliminary electrochemical measurements in CH_2Cl_2 can be used to screen reagents. The formation of 13 nm Sn nanowires, which is amongst the smallest known diameters of nanowires reported for Sn, highlights the applicability of supercritical fluid electrodeposition for the fabrication of ultrathin p-block nanowires, and work is ongoing in the Programme Grant to determine the best etching procedure for removal of the AAO template and to electrodeposit and characterise even smaller diameter Sn nanowires.

6.2.5 Cyclic voltammetry studies of $[PPh_4][PbX_3]$ in CH_2Cl_2

The solubility of the lead(II) precursors in CH_2Cl_2 was found to be much lower than for tin, and so, to ensure a homogenous solution, an electrolyte containing 0.5 mM $[PPh_4][PbCl_3]\cdot CH_3CN$ and 100 mM $[PPh_4]Cl$ in CH_2Cl_2 was prepared to investigate the electrochemical properties of the chlorometallate salt. The potential window available when $[PPh_4]Cl$ is used as the supporting electrolyte was established as being between –1.0 and +1.25 V *vs*. Ag/AgCl. Cyclic voltammograms recorded at a Pt disk working electrode (Figure 6.12) reveal very reproducible features, with a well-defined nucleation loop and stripping peak. Once the nucleation overpotential is reached the deposition onset is very steep and peaks almost straightaway; subsequent deposition behaviour is diffusion limited. The deposition onset, peak deposition current and stripping onset occur at –0.39 V, –0.40 V and –0.34 V. Comparable voltammograms were recorded with a GC disk working electrode, with the deposition onset, peak deposition current and stripping onset occurring at –0.39 V, –0.43 V and –0.34 V. As the concentration of the Pb precursor was lower the currents passed were much smaller in magnitude than those seen with the Sn precursors.

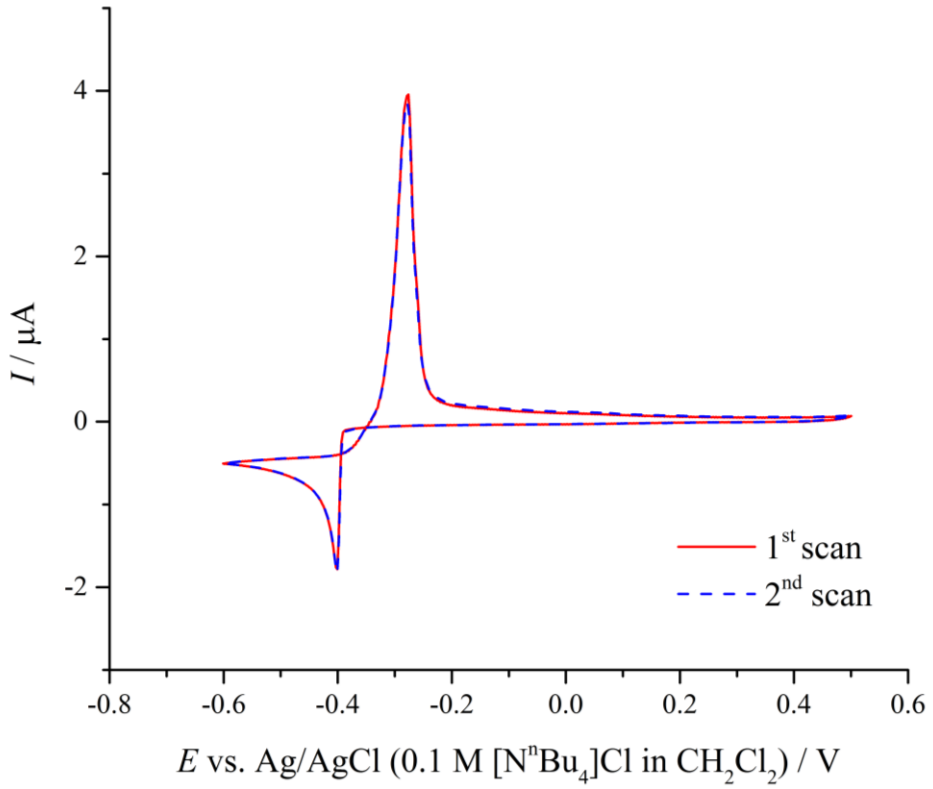

Figure 6.12 Cyclic voltammograms of 0.5 mM $[PPh_4][PbCl_3].CH_3CN$ in CH_2Cl_2 recorded at a 0.5 mm Pt disk working electrode. The supporting electrolyte used was 100 mM $[PPh_4]Cl$ and the potential scan rate was 50 mV s^{-1}.

Extra features were observed on cyclic voltammograms recorded at an Au disk working electrode (Figure 6.13). The first scan on a fresh electrode shows two reduction waves (P2 and P3), while on subsequent scans a third reduction process (P1) is also observed, presumably because the electrode surface has been altered. The underpotential deposition of Pb on gold in various media has been extensively studied,[54,55] while Pb is also known to form three Au alloys, Au_2Pb, $AuPb_2$ and $AuPb_3$.[56] Therefore P1 and P2 can be attributed to underpotential deposition and/or alloying processes, whilst P3 corresponds to the bulk deposition of Pb. The peak deposition current for bulk Pb occurs at –0.38 V, while the deposition and stripping onset are both at –0.34 V.

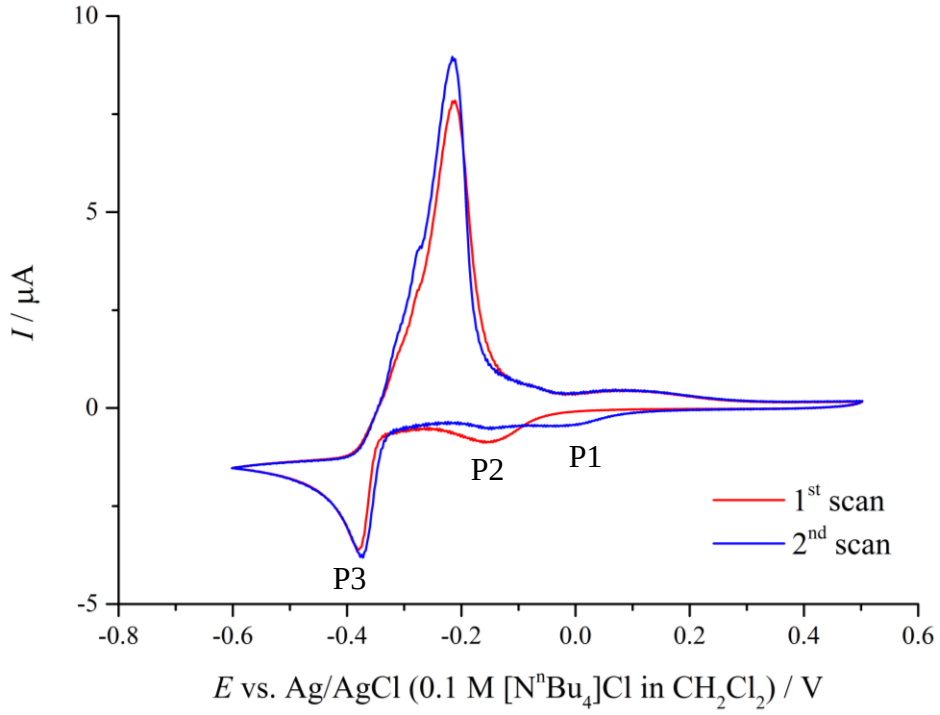

Figure 6.13 Cyclic voltammograms of 0.5 mM $[PPh_4][PbCl_3].CH_3CN$ in CH_2Cl_2 recorded at a 1.0 mm Au disk working electrode. The supporting electrolyte used was 100 mM $[PPh_4]Cl$ and the potential scan rate was 50 mV s^{-1}.

As with the Sn(II) precursors, the effect of systematically changing the halide on the cyclic voltammetry of the tetraphenylphosphonium Pb(II) salts in CH_2Cl_2, recorded at Pt disk working electrodes, was investigated. Cyclic voltammograms (Figure 6.14) recorded for $[PPh_4][PbBr_3]$ and $[PPh_4]_2[Pb_2I_6]$, using the corresponding $[PPh_4]X$ as the supporting electrolyte, showed similar metal deposition and stripping features as recorded for $[PPh_4][PbCl_3]\cdot CH_3CN$, with the Pb(II) to Pb(0) reduction potential becoming more accessible as the halide gets heavier. The deposition onset, peak deposition current and

stripping onset were at –0.25 V, –0.27 V and –0.23 V for $[PPh_4][PbBr_3]$ and –0.17 V, –0.19 V and –0.14 V for $[PPh_4]_2[Pb_2I_6]$.

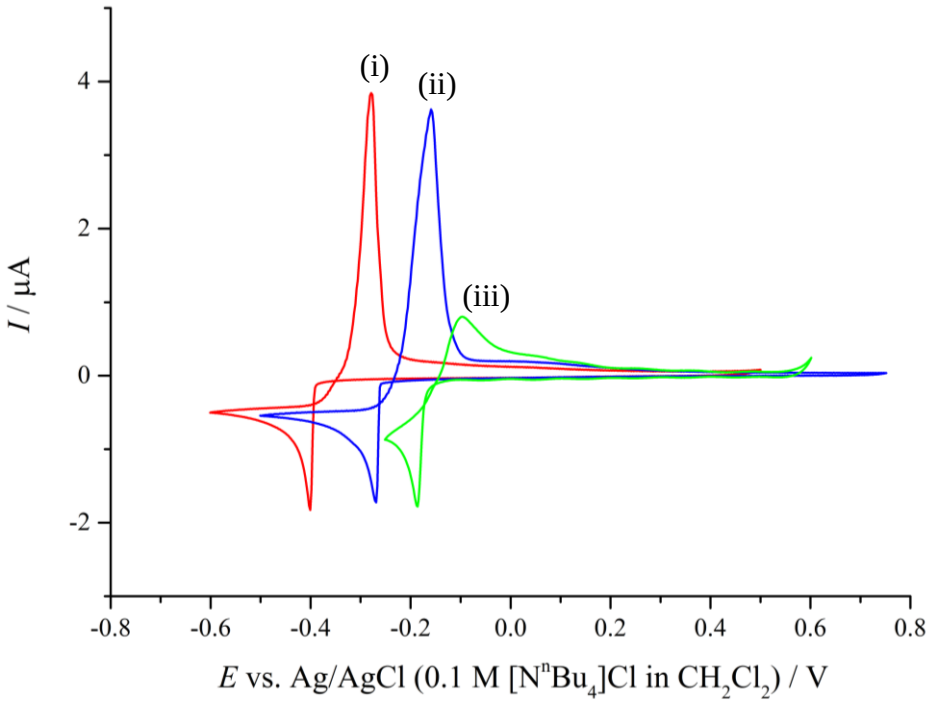

Figure 6.14 Cyclic voltammograms of $[PPh_4][PbX_3]$ (X = Cl, Br, I) in CH_2Cl_2 recorded at a 0.5 mm Pt disk working electrode. The composition of each electrolyte system was 0.5 mM of (i) $[PPh_4][PbCl_3]\cdot CH_3CN$, (ii) $[PPh_4][PbBr_3]$ and (iii) $[PPh_4]_2[Pb_2I_6]$ with 100 mM $[PPh_4]X$. The potential scan rate was 50 mV s^{-1}.

Looking at Table 6.3, it becomes clear that as well as the M(II) to M(0) reduction potential becoming more accessible Cl → Br → I, it also becomes systematically more accessible as Group 14 is descended. As the potentials required to deposit both Ge[57] and Sn from M(II) precursors in $scCH_2F_2$ are well within the potential window provided by $scCH_2F_2$, by using the CH_2Cl_2-$scCH_2F_2$ electrochemistry analogy the deposition potential of Pb in $scCH_2F_2$ should be easily accessible.

Table 6.3 M(II) (M = Ge, Sn, Pb) deposition peak potentials in CH_2Cl_2 recorded at a 0.5 mm Pt disk working electrode (E_{pc} *vs.* Ag/AgCl in V)

M(II) Precursor	X = Cl	X = Br	X = I
$[EMIM][GeX_3]$[26]	–0.81	–0.63	–0.35
$[N^nBu_4][SnX_3]$	–0.57	–0.38	–0.23
$[PPh_4][PbX_3]$	–0.40	–0.27	–0.19

6.2.6 Electrodeposition of lead from CH_2Cl_2 solution

The potentiostatic electrodeposition of Pb in CH_2Cl_2 was investigated on Au and TiN slides using an electrolyte containing 0.5 mM $[PPh_4][PbCl_3].CH_3CN$ and 100 mM $[PPh_4]Cl$ (i.e. the same electrolyte used for the voltammetric characterisations). Details of the parameters involved in both deposition experiments are given in Table 6.4.

Table 6.4 Pb thin film deposition parameters in CH_2Cl_2 at different electrodes

	Au slide	TiN slide
Deposition potential (V)	–0.6	–1.0
Deposition time (s)	3600	3600
Area of electrode (cm^2)	0.25	0.30
Charge passed (C)	0.10	0.12
Estimated deposit thickness (μm)	0.39	0.38

The chronoamperogram for the deposition of Pb onto an Au slide is given in Figure 6.15. Due to the thinness of the film produced on the Au slide (a result of the concentration of Pb in the electrolyte having to be low to ensure complete solubility) a greater overpotential was used for the TiN slide, but this appeared to have little effect on the charge passed.

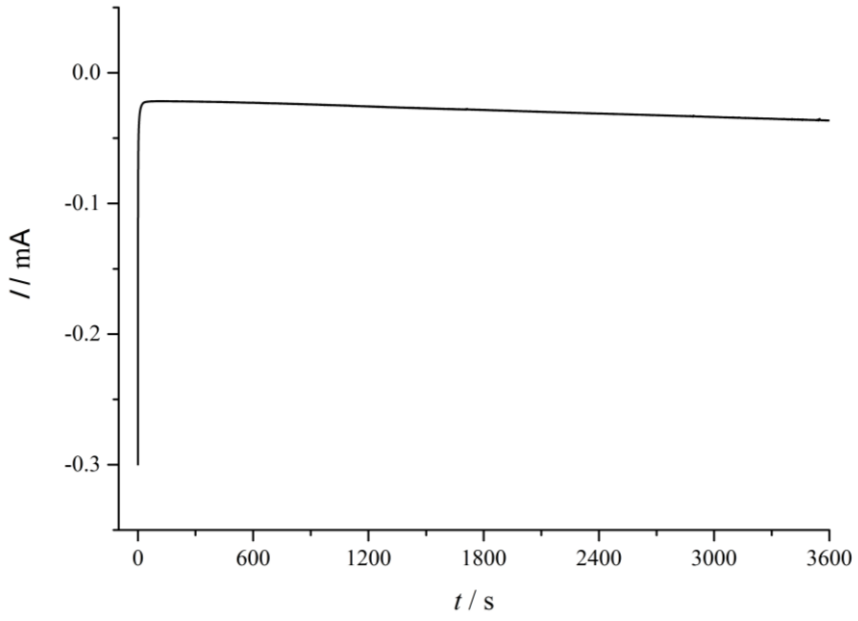

Figure 6.15 Chronoamperogram for the electrodeposition of Pb onto a planar Au electrode in CH_2Cl_2 from an electrolyte containing 0.5 mM $[PPh_4][PbCl_3]\cdot CH_3CN$ and 100 mM $[PPh_4]Cl$, using an applied potential of –0.6 V.

The resulting dark grey deposited films on the electrodes were gently washed by dipping into CH_2Cl_2 before being analysed by Dr. P. Richardson (SEM and EDX) and M. Hasan (XRD) at the University of Southampton. Despite the thinness of the deposited Pb films useful SEM, EDX and XRD data could be collected on both samples. SEM images (Figure 6.16) of the deposited Pb films show that the deposited material on the Au slide is of individual crystallites of differing sizes spread fairly uniformly across the electrode surface, while the crystallite morphology on the TiN slide is more regular. This difference in morphology may be the result of the different substrate types, or could be a result of the different deposition potentials that were used, which is known to often affect film morphology.[27] Unsurprisingly given the thinness of the deposited films, the EDX spectra show Pb as the dominant peak, but with Au or Ti and Si peaks from the Au or TiN substrate also evident. Again, no chloride was evident in any of the EDX spectra recorded.

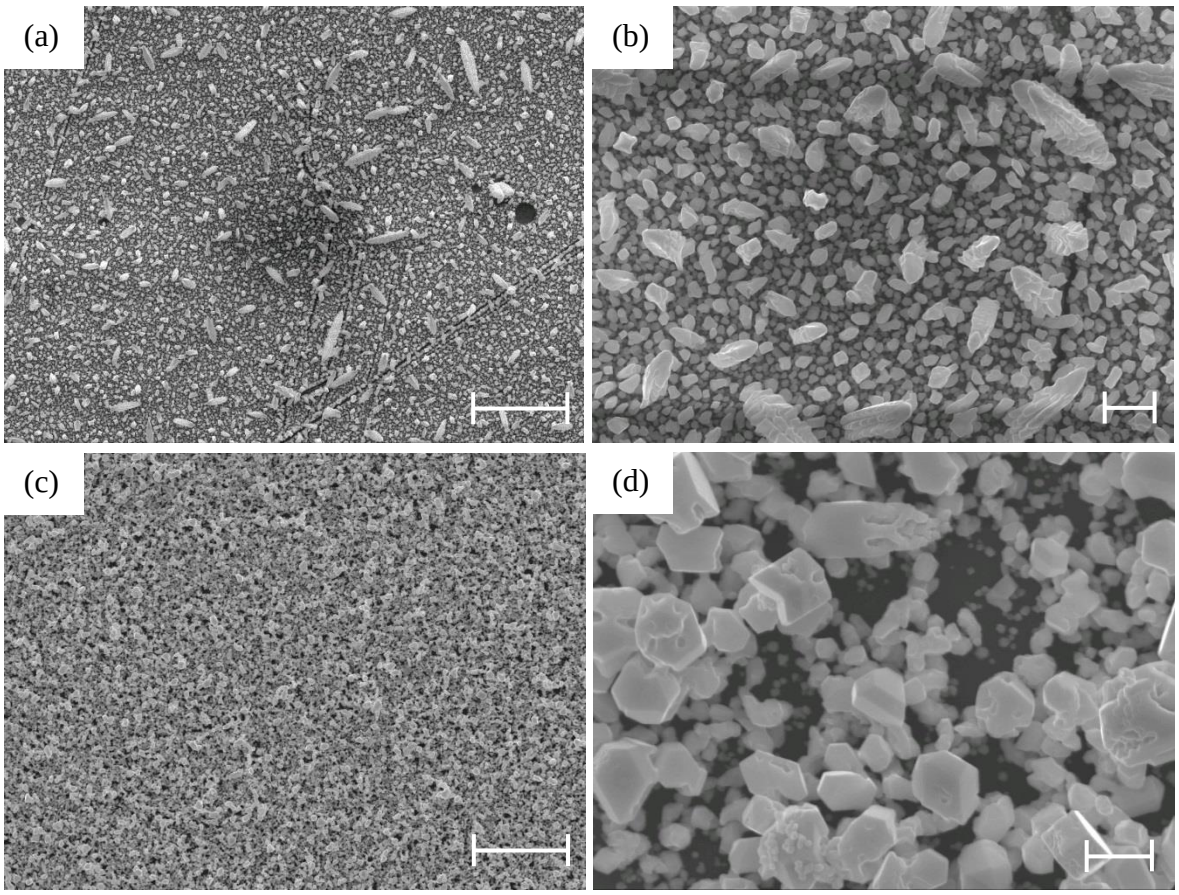

Figure 6.16 SEM micrographs of Pb electrodeposited on planar electrodes in CH_2Cl_2. The substrates and magnifications used are (a) Au, x2000 (scale bar = 10 μm), (b) Au, x10000 (scale bar = 1 μm), (c) TiN, x2000 (scale bar = 10 μm), (d) TiN, x13000 (scale bar = 1 μm).

The 1° grazing incidence X-ray diffraction data for the deposited films on both Au and TiN confirmed that cubic Pb had been deposited. In the case of the film deposited on TiN

(Figure 6.17(a)), peaks for the substrate (TiN and Si) were observed alongside the Pb peaks. The refined lattice parameter for the Pb phase observed was a = 4.9458(2) Å. The XRD pattern for the sample on Au (Figure 6.17(b)) was complicated by two alloy phases, $AuPb_2$ and $AuPb_3$, being observed as well as Pb and Au from the substrate. The experimental and literature values for the observed phases are given in Table 6.5. The observation of these alloy phases helps to explain the voltammetric behaviour observed on Au disk electrodes (see Section 6.2.5), which was also observed when cyclic voltammetry was run on a planar Au electrode similar to the one that was deposited onto.

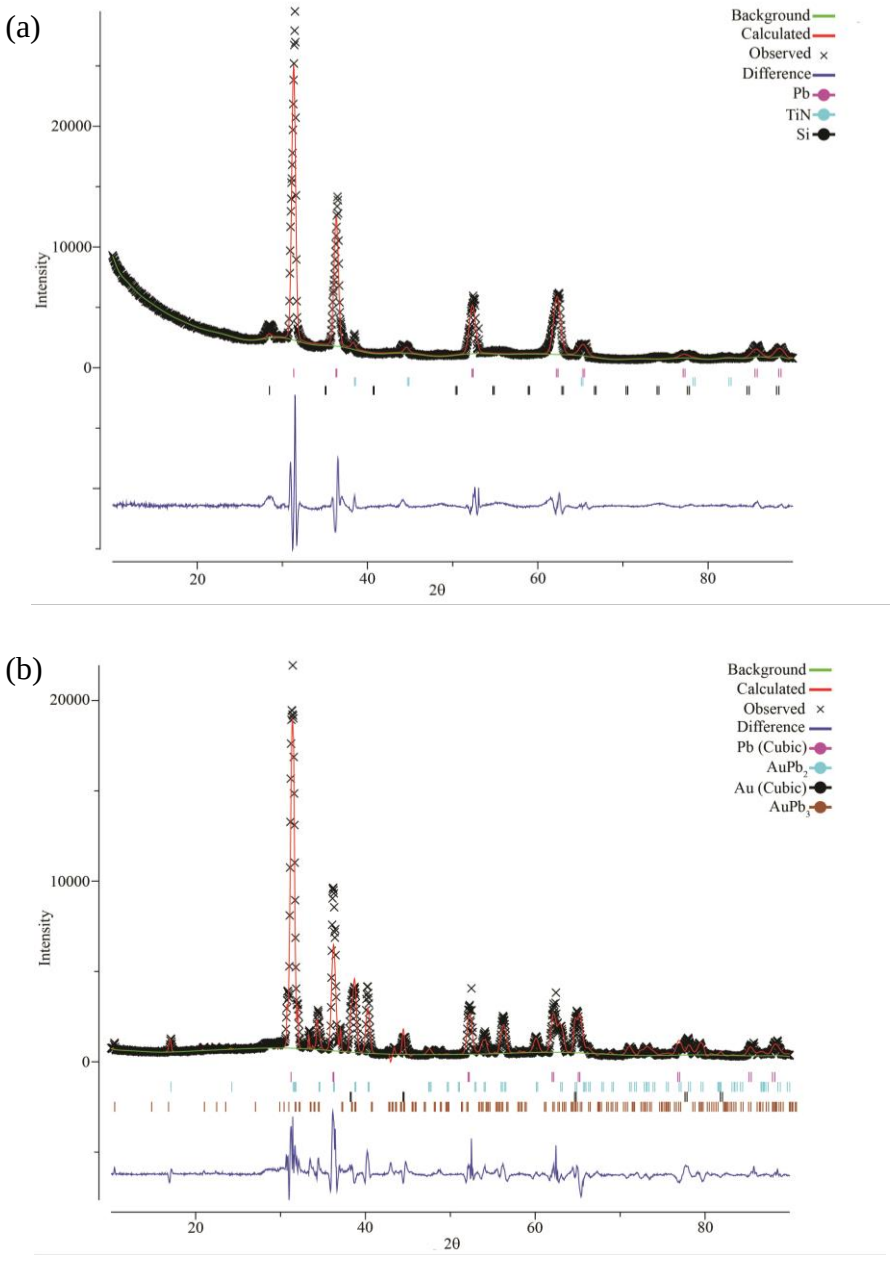

Figure 6.17 XRD patterns for Pb electrodeposited on planar (a) TiN and (b) Au electrodes in CH_2Cl_2 (1° grazing incidence scan). Comparison patterns come from the ICSD.

Table 6.5 Refined parameters from the XRD pattern for Pb on a planar Au electrode

Phase	Crystal structure and space group	Lattice parameters (Å)	Literature lattice parameters (Å)
Pb	cubic/*Fm*-3*m* (223)	a = 4.9616(4)	a = 4.9496(3)[58]
$AuPb_2$	tetragonal/*I*4/*mcm* (140)	a = 7.3396(9) c = 5.6347(11)	a = 7.338(4) c = 5.658(4)[59]
$AuPb_3$	tetragonal/*I*-42*m* (121)	a = 11.952(2) c = 5.880(1)	a = 11.959(5) c = 5.877(5)[60]

The specially designed precursor $[PPh_4][PbCl_3]\cdot CH_3CN$ has been shown to have a favourable Pb(II) to Pb(0) deposition potential and shows good, reproducible voltammetric behaviour in CH_2Cl_2, with films of Pb having been successfully electrodeposited using this precursor. The results suggest that, with some optimisation of deposition times, $[PPh_4][PbCl_3]\cdot CH_3CN$ is a promising candidate for the electrodeposition of Pb from $scCH_2F_2$. The co-deposition of lead (from $[PPh_4][PbCl_3]\cdot CH_3CN$) and tellurium (possibly from the known precursor $[N^nBu_4]_2[TeCl_6]$[27]) to form PbTe nanomaterials from supercritical fluids is a likely future target which will build upon the research detailed here. There is precedence for the co-electrodeposition of Pb and Te from a single electrolyte bath, with thin films of PbTe having been successfully deposited in aqueous media.[61,62]

6.3 Conclusions

The development and testing of suitable precursors for the electrodeposition of the p-block elements tin and lead has been the first step of an exciting investigation into what nanomaterials, and ultimately nanodevices, can be fabricated using SCFED. For tin, the well-defined and stable tetrabutylammonium halometallate salts $[N^nBu_4][SnX_3]$ (X = Cl, Br, I; X = F gave no voltammetric response) have been proven to produce characteristic and reproducible deposition voltammetry when combined with the supporting electrolytes $[N^nBu_4]X$ in CH_2Cl_2. EDX and XRD analyses showed that the Sn films electrodeposited onto both Au and TiN substrates using $[N^nBu_4][SnCl_3]$ in CH_2Cl_2 were of high purity. The translation of this electrolyte into $scCH_2F_2$ afforded comparable deposition voltammetry, good quality Sn thin films, and, through the use of a 13 nm AAO template, the fabrication of Sn nanowires, which were shown by XRD to have a preferred orientation along the < 200 > plane. The growth of some of the first examples of sub-20 nm Sn nanowires is an example of the strength and versatility of SCFED[1] as a nanomaterials deposition technique, and work is ongoing by the Programme Grant team to deposit even smaller diameter Sn nanowires and determine their properties. All of the tin samples deposited so far have been the tetragonal β-Sn phase, and so further research is warranted to see if cubic α-Sn can also be deposited, interesting due to its predicted semiconducting properties in nanowires with diameters less than ~ 4 nm.[5]

Through the use of a more solubilising cation, a series of tetraphenylphosphonium halometallate precursors for the electrodeposition of lead, $[PPh_4][PbX_3]$ (X = Cl, Br, I), have been synthesised and characterised, including by single crystal X-ray diffraction. Again, with the use of $[PPh_4]X$ as the supporting electrolyte, the deposition voltammetry of the precursors has been well characterised and Pb has been successfully electrodeposited on planar Au and TiN electrodes from $[PPh_4][PbCl_3]\cdot CH_3CN$ in CH_2Cl_2. These results suggest that Pb should be able to be electrodeposited from $scCH_2F_2$ using these precursors. The reduction potentials for the Group 14 M(II) → M(0) using $[MX_3]^-$ salts (M = Ge,[26] Sn, Pb; X = Cl, Br, I) have been observed to become less cathodic and therefore more accessible as both Groups 14 and 17 are descended. While deposition studies so far have used the $[MCl_3]^-$ salts (for mutual compatibility with other p-block systems),[27] with their favourable deposition potentials electrolytes containing the $[MI_3]^-$ salts are also worth investigating, and may produce deposits with different properties. The development of this simple and versatile electrolyte system for SCFED should enable the deposition of both elemental and compound p-block materials, with potential applications in e.g. electronics.

6.4 Experimental

6.4.1 Precursor synthesis and characterisation

The general experimental techniques used in this section can be found in Appendix 1 at the end of the thesis. The properties of commercial SnF_2 samples are known to vary greatly, and so the XRD pattern of the material used had been confirmed to be consistent with the literature data.[35]

$[N^nBu_4][SnF_3]$

To a suspension of SnF_2 (0.157 g, 1.00 mmol) in MeOH (10 mL) was added $[N^nBu_4]F$ in THF (1.0 M, 1 mL, 1.00 mmol) which immediately formed a colourless solution. The reaction was stirred for 19 h, then the solvent was removed *in vacuo*. The resulting solid was washed with Et_2O (5 mL) to give a white powder which was dried *in vacuo*. Yield: 0.313 g, 75%. Anal. Calc. for $C_{16}H_{36}F_3NSn$: C, 46.0; H, 8.7; N, 3.4. Found: C, 45.9; H, 8.9; N, 3.5%. ^{1}H NMR (CD_2Cl_2, 295 K): δ = 1.01 (t, [12H], CH_3), 1.39-1.49 (m, [8H], CH_2), 1.59-1.67 (m, [8H], CH_2), 3.22 (t, [8H], CH_2). ^{19}F NMR (CD_2Cl_2, 295K): δ = –87.7 (s, $^1J_{F^{117}Sn}$ = 3035 Hz, $^1J_{F^{119}Sn}$ = 3174 Hz). ^{119}Sn{^{1}H} NMR (CH_2Cl_2/CD_2Cl_2, 295 K): δ = –528.7 (q, $^1J^{119}_{SnF}$ = 3181 Hz); (203 K): –545.3 (q, $^1J^{119}_{SnF}$ = 3182 Hz). IR (Nujol): ν = 508 (s), 458 (vs) (SnF) cm^{-1}.

$[N^nBu_4][SnCl_3]$

$SnCl_2$ (0.380 g, 2.00 mmol) was dissolved in EtOH (5 ml) to form a colourless solution, to which $[N^nBu_4]Cl$ (0.556 g, 2.00 mmol) in EtOH (5 ml) was added. The resulting colourless solution was stirred for 17 h, then the solvent was removed *in vacuo* to yield a white powder which was dried *in vacuo*. Yield: 0.856 g, 91%. Anal. Calc. for $C_{16}H_{36}Cl_3NSn$: C, 41.1; H, 7.8; N, 3.0. Found: C, 41.2; H, 7.9; N, 3.1%. ^{1}H NMR (CD_2Cl_2, 295 K): δ = 1.02 (t, [12H], CH_3), 1.39-1.51 (m, [8H], CH_2), 1.59-1.70 (m, [8H], CH_2), 3.18 (t, [8H], CH_2). ^{119}Sn{^{1}H} NMR (CH_2Cl_2/CD_2Cl_2, 295 K): δ = –40.8 (s). IR (Nujol): ν = 297 (s), 260 (vs) (SnCl) cm^{-1}.

$[N^nBu_4][SnBr_3]$

$SnBr_2$ (0.278 g, 1.00 mmol) was dissolved in EtOH (5 ml) to form a colourless solution, to which $[N^nBu_4]Br$ (0.321 g, 1.00 mmol) in EtOH (5 ml) was added. The resulting colourless solution was stirred for 17 h, whereupon a white precipitate had formed which was isolated by filtration. The white powder was dried *in vacuo*. Yield: 0.242 g, 40%. Anal. Calc. for $C_{16}H_{36}Br_3NSn$: C, 32.0; H, 6.0; N, 2.3. Found: C, 31.8; H, 5.9; N, 2.4%. ^1H NMR (CD_2Cl_2, 295 K): δ = 1.03 (t, [12H], CH_3), 1.41-1.53 (m, [8H], CH_2), 1.61-1.69 (m, [8H], CH_2), 3.18 (t, [8H], CH_2). $^{119}Sn\{^1H\}$ NMR (CH_2Cl_2/CD_2Cl_2, 295 K): δ = 134.3 (s).

$[N^nBu_4][SnI_3]$

SnI_2 (0.185 g, 0.50 mmol) was dissolved in EtOH (15 ml) to form a bright yellow solution, to which $[N^nBu_4]I$ (0.182 g, 0.49 mmol) in EtOH (5 ml) was added. A yellow solid precipitated out after 10 min. stirring; the reaction was allowed to stir for a further hour, then the solid was isolated by filtration. The yellow powder was dried *in vacuo*. Yield: 0.114 g, 31%. Anal. Calc. for $C_{16}H_{36}I_3NSn$: C, 25.9; H, 4.9; N, 1.9. Found: C, 26.0; H, 4.9; N, 1.9%. ^1H NMR (CD_2Cl_2, 295 K): δ = 1.04 (t, [12H], CH_3), 1.44-1.52 (m, [8H], CH_2), 1.63-1.69 (m, [8H], CH_2), 3.18 (t, [8H], CH_2). $^{119}Sn\{^1H\}$ NMR (CH_2Cl_2/CD_2Cl_2, 295 K): no resonance; (223 K): δ = 352.2 (s).

After a few days block yellow crystals grew in the yellow filtrate, which single crystal X-ray diffraction indicated to have the structure $[N^nBu_4][I_3Sn(\mu\text{-}OEt)_3SnI_3]$. The crystals were isolated by filtration and dried *in vacuo* to give a deep yellow powder. Yield: 0.067 g. Anal. Calc. for $C_{22}H_{51}I_6NO_3Sn_2$: C, 19.2; H, 3.7; N, 1.0. Found: C, 19.1; H, 3.8; N, 1.1%.

$[PPh_4][PbCl_3]\cdot CH_3CN$

To a suspension of $PbCl_2$ (0.101 g, 0.36 mmol) in CH_3CN (20 mL) was added $[PPh_4]Cl$ (0.138 g, 0.37 mmol) to form a colourless solution. The reaction was stirred for 18 h, then the solvent volume was reduced to about 4 mL *in vacuo* whereupon a white solid precipitated out. The white powder was isolated by filtration and dried *in vacuo*. Meanwhile colourless crystals suitable for single crystal X-ray diffraction study grew in the filtrate which was stored at –18 °C. These were isolated by filtration and dried *in vacuo* to afford a second crop of the product. The overall yield was 0.133 g (53%). Anal. Calc.

for $C_{26}H_{23}Cl_3NPPb$: C, 45.0; H, 3.3; N, 2.0. Found: C, 44.9; H, 3.3; N, 2.0%. ^{1}H NMR (CD_2Cl_2, 295 K): δ = 1.97 (s, CH_3CN), 7.60-7.95 (m, C_6H_5). $^{31}P\{^1H\}$ NMR (CD_2Cl_2, 295 K): δ = 23.9 (s).

$[PPh_4][PbBr_3]$

To $PbBr_2$ (0.100 g, 0.27 mmol) and $[PPh_4]Br$ (0.115 g, 0.27 mmol) was added CH_3CN (20 mL) to initially form a suspension. Upon stirring for 0.5 h all the solid had dissolved to give a colourless solution. The reaction was stirred for 17 h, then the solvent volume was reduced to about 5 mL *in vacuo* whereupon a white solid precipitated out. The white powder was isolated by filtration and dried *in vacuo*. Meanwhile colourless needle-like crystals grew in the filtrate which was stored at –18 °C. These were isolated by filtration and dried *in vacuo* to afford a second crop of the product. The overall yield was 0.079 g (37%). Anal. Calc. for $C_{24}H_{20}Br_3PPb$: C, 36.7; H, 2.6. Found: C, 36.8; H, 2.5%. ^{1}H NMR (CD_2Cl_2, 295 K): δ = 7.60-7.95 (m, C_6H_5). $^{31}P\{^1H\}$ NMR (CD_2Cl_2, 295 K): δ = 23.9 (s). A very large colourless crystal suitable for single crystal X-ray diffraction study grew upon allowing a portion of the filtrate to evaporate.

$[PPh_4]_2[Pb_2I_6]$

To PbI_2 (0.227 g, 0.49 mmol) was added CH_3CN (20 mL) resulting in a yellow solution with evidence of some undissolved solid which did not change upon stirring for 0.5 h. To this was added $[PPh_4]I$ (0.229 g, 0.49 mmol) which immediately led to the precipitation of a large amount of yellow solid. The reaction was stirred for 18 h, then the yellow powder was isolated by filtration and dried *in vacuo*. Yield: 0.299 g (66%). Anal. Calc. for $C_{48}H_{40}I_6P_2Pb_2$: C, 31.1; H, 2.2. Found: C, 30.9; H, 2.1%. ^{1}H NMR (CD_2Cl_2, 295 K): δ = 7.60-7.95 (m, C_6H_5). $^{31}P\{^1H\}$ NMR (CD_2Cl_2, 295 K): δ = 23.9 (s). Yellow crystals suitable for single crystal X-ray diffraction study grew from a solution of the powder in CH_2Cl_2.

6.4.2 Electrochemical measurements

The electrolyte preparation and electrochemical experiments in dry CH_2Cl_2 were carried out under a dry dinitrogen atmosphere inside a glove box. The electrochemical measurements were performed at room temperature using a three-electrode system in a one-compartment electrochemical cell that had a volume of 10 mL. A Pt gauze was used as

the counter electrode, and an Ag/AgCl electrode (in 0.1 mol dm^{-1} $[N^nBu_4]Cl$ in CH_2Cl_2) was used as the reference electrode. For voltammetric characterisation of the compounds the working electrodes used were platinum (0.5 mm diameter), gold (1.0 mm diameter) or glassy carbon (3.0 mm diameter) disk electrodes sealed in glass. These were polished with alumina paste (1 and 0.3 μm) on a polishing cloth. Films were deposited potentiostatically onto either gold or TiN slides, prepared at the University of Southampton by Alistair Clarke and Dr. Akhtar Rind respectively. The evaporated gold slides consisted of microscope slides coated with a 15 nm chromium adhesion layer and 100 nm of gold. Details of how the TiN on Si slides were fabricated can be found in the literature.[63] A μAutolabIII potentiostat and Autolab GPES software was used to conduct the electrochemical measurements and data logging. After deposition the films were washed by holding them in a static solution of CH_2Cl_2 for thirty seconds.

A detailed description of the stainless steel high pressure cell and typical set-up used for the electrochemical studies in scCH_2F_2, performed by Dr. Peter Richardson at the University of Southampton, can be found in the literature.[63,64] The electrochemical experiments were performed using a three-electrode system, using a Pt mesh as the counter electrode and a 0.5 mm diameter Pt disk as the *pseudo*-reference electrode. The working electrode used for voltammetric characterisation was a 0.5 mm diameter Au disk, while films were deposited potentiostatically onto either TiN or Au slides, fabricated as described above. 60 μm thick Synkera AAO membranes with (nominally) 13 nm diameter pores were used as templates for the electrodeposition of Sn nanowires. The membranes were prepared as electrodes as described in the literature.[65] All experiments were carried out at 358 K and 17.2 MPa.

6.4.3 Characterisation of electrodeposited materials

Electrodeposited films were investigated using SEM, EDX and XRD. SEM and EDX measurements were carried out by Dr. Peter Richardson at the University of Southampton, while XRD measurements were performed by Mahboba Hasan, also at the University of Southampton. A Jeol JSM 6500F field emission gun scanning electron microscope (FEG-SEM) equipped with an Oxford Instruments EDX detector was used for the SEM and EDX analyses of electrodeposited films, for which an accelerating voltage of 20 keV was employed. The SEM analysis of the 13 nm Sn nanowires was performed by Dr. Jay Naik at the University of Southampton, using a Zeiss NVision 40 FIB system. XRD patterns were collected with a Rigaku Smartlab Thin Film (9 kW) diffractometer using a 0.1 mm parallel

X-ray beam (Cu-Kα) and DTex250 1D detector. Grazing incidence patterns were collected with a 1° incident angle, while preferred orientation was examined using symmetric (θ-2θ) scans. Data were modelled by Karl Kaye at the University of Southampton using the GSAS[66] software, refining the data as part of a Rietveld[67] refinement. Comparison patterns were obtained from the Inorganic Crystal Structure Database (ICSD).

6.5 Appendix – X-Ray Crystallographic Data

Compound	$[PPh_4][PbBr_3]$
Formula	$C_{24}H_{20}Br_3PPb$
M	786.29
Crystal system	triclinic
Space group (no.)	*P*-1 (2)
a /Å	7.402(2)
b /Å	12.192(3)
c /Å	14.520(4)
α /°	69.065(9)
β /°	86.790(12)
γ /°	73.933(9)
U /Å^3	1174.7(5)
Z	2
μ(Mo-K$_\alpha$) /mm^{-1}	12.361
F(000)	732
Total no. reflns	10181
R_{int}	0.033
Unique reflns	5254
No. of params, restraints	265, 0
R_1, wR_2 [$I > 2\sigma(I)$][a]	0.020, 0.041
R_1, wR_2 (all data)	0.024, 0.042

Common items: T = 100 K; wavelength (Mo-Kα) = 0.71073 Å; θ(max) = 27.5°.

[a] $R_1 = \Sigma||F_o| - |F_c|| / \Sigma|F_o|$; $wR_2 = [\Sigma w(F_o^2 - F_c^2)^2 / \Sigma wF_o^4]^{1/2}$.

6.6 References

1. P. N. Bartlett, D. A. Cook, M. W. George, A. L. Hector, J. Ke, W. Levason, G. Reid, D. C. Smith and W. Zhang, *Phys. Chem. Chem. Phys.*, 2014, **16**, 9202-9219.
2. H. R. Huff, *AIP Conf. Proc.*, 2003, **683**, 3-39.
3. K. Rana, J. Singh and J.-H. Ahn, *J. Mater. Chem. C*, 2014, **2**, 2646-2656.
4. J. O. Dimmock, I. Melngailis and A. J. Strauss, *Phys. Rev. Lett.*, 1966, **16**, 1193-1196.
5. L. Ansari, G. Fagas, J.-P. Colinge and J. C. Greer, *Nano Lett.*, 2012, **12**, 2222-2227.
6. N. G. Hörmann, A. Gross, J. Rohrer and P. Kaghazchi, *Appl. Phys. Lett.*, 2015, **107**, 123101.
7. C. Chien-Chon, Y. Bisrat, Z. P. Luo, R. E. Schaak, C. G. Chao and D. C. Lagoudas, *Nanotechnology*, 2006, **17**, 367-374.
8. Y. Xu, Q. Liu, Y. Zhu, Y. Liu, A. Langrock, M. R. Zachariah and C. Wang, *Nano Lett.*, 2013, **13**, 470-474.
9. B. Luo, D. Yang, M. Liang and L. Zhi, *Nanoscale*, 2010, **2**, 1661-1664.
10. A. Mingliang Tian, A. Jinguo Wang, A. Joseph Snyder, J. Kurtz, L. Ying, P. Schiffer, T. E. Mallouk and M. H. W. Chan, *Appl. Phys. Lett.*, 2003, **83**, 1620.
11. Y.-J. Hsu and S.-Y. Lu, *J. Phys. Chem. B*, 2005, **109**, 4398-4403.
12. A. Kolmakov, Y. Zhang, G. Cheng and M. Moskovits, *Adv. Mater.*, 2003, **15**, 997-1000.
13. L. Ansari, G. Fagas and J. C. Greer, *Appl. Phys. Lett.*, 2014, **105**, 123105.
14. T. Djenizian, I. Hanzu, M. Eyraud and L. Santinacci, *C. R. Chim.*, 2008, **11**, 995-1003.
15. A. M. R. Elbasiony, S. Zein El Abedin and F. Endres, *J. Solid State Electrochem.*, 2014, **18**, 951-957.
16. R. Al-Salman, H. Sommer, T. Brezesinski and J. Janek, *Chem. Mater.*, 2015, **27**, 3830-3837.
17. J. S. Casas and J. Sordo, eds., *Lead: Chemistry, Analytical Aspects, Environmental Impact and Health Effects*, Elsevier B.V., Amsterdam, 2006.
18. M. He, C. H. Wong, P. L. Tse, Y. Zheng, H. Zhang, F. L. Y. Lam, P. Sheng, X. Hu and R. Lortz, *ACS Nano*, 2013, **7**, 4187-4193.
19. C. Jung-Hsuan, L. Shen-Chuan, C. Chuen-Guang and L. Tzeng-Feng, *Jpn. J. Appl. Phys.*, 2008, **47**, 4815-4819.
20. G. Yi and W. Schwarzacher, *Appl. Phys. Lett.*, 1999, **74**, 1746-1748.
21. Y. Wang, T. Herricks and Y. Xia, *Nano Lett.*, 2003, **3**, 1163-1166.

22. A. C. Onicha, N. Petchsang, T. H. Kosel and M. Kuno, *ACS Nano*, 2012, **6**, 2833-2843.

23. J. So Young, K. Han Sung, P. Jeunghee, J. Minkyung, K. Jinhee, L. Seung Hyun, R. Jong Wook and L. Wooyoung, *Nanotechnology*, 2009, **20**, 415204.

24. A. M. Elbasiony, M. Olschewski, S. Z. El Abedin and F. Endres, *ChemElectroChem*, 2015, **2**, 1361-1365.

25. G. Aksomaityte, F. Cheng, A. L. Hector, J. R. Hyde, W. Levason, G. Reid, D. C. Smith, J. W. Wilson and W. Zhang, *Chem. Mater.*, 2010, **22**, 4246-4253.

26. P. N. Bartlett, C. Y. Cummings, W. Levason, D. Pugh and G. Reid, *Chem. Eur. J.*, 2014, **20**, 5019-5027.

27. P. N. Bartlett, D. Cook, C. H. de Groot, A. L. Hector, R. Huang, A. Jolleys, G. P. Kissling, W. Levason, S. J. Pearce and G. Reid, *RSC Adv.*, 2013, **3**, 15645-15654.

28. E. S. Claudio, H. A. Godwin and J. S. Magyar, *Prog. Inorg. Chem.*, 2003, **51**, 1-144.

29. Y. L. Jeyachandran, S. K. Narayandass, D. Mangalaraj, S. Areva and J. A. Mielczarski, *Mater. Sci. Eng., A*, 2007, **445–446**, 223-236.

30. N. N. Greenwood and A. Earnshaw, *Chemistry of the Elements*, Butterworth-Heinemann, Oxford, 2 edn., 1997.

31. R. C. McDonald, H. H. K. Hau and K. Eriks, *Inorg. Chem.*, 1976, **15**, 762-765.

32. I. Abrahams and D. Z. Demetriou, *J. Solid State Chem.*, 2000, **149**, 28-32.

33. N. Auner, in *Synthetic Methods of Organometallic and Inorganic Chemistry*, ed. W. A. Herrmann, Georg Thieme Verlag, Stuttgart, 1996, vol. 2, pp. 142-298.

34. R. J. H. Clark, L. Maresca and P. J. Smith, *J. Chem. Soc. A*, 1970, 2687-2690.

35. C. Gurnani, A. L. Hector, E. Jager, W. Levason, D. Pugh and G. Reid, *Dalton Trans.*, 2013, **42**, 8364-8374.

36. C. Lode and H. Krautscheid, *Z. Anorg. Allg. Chem.*, 2000, **626**, 326-331.

37. M. Veith, S. Mathur and V. Huch, *Chem. Commun.*, 1997, 2197-2198.

38. K. Nakamoto, *Infrared and Raman Spectra of Inorganic and Coordination Compounds*, Wiley-Interscience, NY, 4 edn., 1986.

39. M. Goldstein and G. C. Tok, *J. Chem. Soc. A*, 1971, 2303-2307.

40. P. P. Samuel, Y. Li, H. W. Roesky, V. Chevelkov, A. Lange, A. Burkhardt and B. Dittrich, *J. Am. Chem. Soc.*, 2014, **136**, 1292-1295.

41. J. M. Coddington and M. J. Taylor, *J. Chem. Soc., Dalton Trans.*, 1989, 2223-2227.

42. H. Krautscheid and F. Vielsack, *Angew. Chem., Int. Ed. Engl.*, 1995, **34**, 2035-2037.

43. Y.-J. She, S.-P. Zhao, Z.-F. Tian and X.-M. Ren, *Inorg. Chem. Commun.*, 2014, **46**, 29-32.

44. W. Czado and U. Müller, *Z. Anorg. Allg. Chem.*, 1998, **624**, 925-926.

45. T. M. Klapotke, B. Krumm, K. Polborn and C. M. Rienicker, *Z. Naturforsch., B: Chem. Sci.*, 2000, **55**, 377-382.

46. H. Krautscheid and F. Vielsack, *Z. Anorg. Allg. Chem.*, 1999, **625**, 562-566.

47. H. Krautscheid, J.-F. Lekieffre and J. Besinger, *Z. Anorg. Allg. Chem.*, 1996, **622**, 1781-1787.

48. B. C. M. Martindale, S. E. W. Jones and R. G. Compton, *Phys. Chem. Chem. Phys.*, 2010, **12**, 1827-1833.

49. N. Tachikawa, N. Serizawa, Y. Katayama and T. Miura, *Electrochim. Acta*, 2008, **53**, 6530-6534.

50. A. Dębski, W. Gąsior, Z. Moser and R. Major, *J. Alloys Compd.*, 2010, **491**, 173-177.

51. H. Sun and S. G. DiMagno, *J. Am. Chem. Soc.*, 2005, **127**, 2050-2051.

52. V. T. Deshpande and D. B. Sirdeshmukh, *Acta Crystallogr.*, 1961, **14**, 355-356.

53. J. P. Jan, W. B. Pearson, A. Kjekshus and S. B. Woods, *Can. J. Phys.*, 1963, **41**, 2252-2266.

54. B.-Y. Chang, E. Ahn and S.-M. Park, *J. Phys. Chem. C*, 2008, **112**, 16902-16909.

55. F.-X. Wang, G.-B. Pan, Y.-D. Liu and Y. Xiao, *Chem. Phys. Lett.*, 2010, **488**, 112-115.

56. A. Prince, *Bull. Alloy Phase Diagrams*, 1980, **1**, 59-62.

57. C. Y. Cummings, P. N. Bartlett, D. Pugh, G. Reid, W. Levason, M. M. Hasan, A. L. Hector, J. Spencer and D. C. Smith, *J. Electrochem. Soc.*, 2015, **162**, D619-D624.

58. E. A. Owen and E. L. Yates, *Philos. Mag.*, 1933, **15**, 472-488.

59. E. E. Havinga, H. Damsma and P. Hokkeling, *J. Less-Common Met.*, 1972, **27**, 169-186.

60. R. Wang and B. C. Giessen, *Metall. Trans.*, 1971, **2**, 2195-2197.

61. M. N. Mamedov, *Russ. J. Appl. Chem.*, 2002, **75**, 1075-1078.

62. F. Xiao, B. Yoo, M. A. Ryan, K.-H. Lee and N. V. Myung, *Electrochim. Acta*, 2006, **52**, 1101-1107.

63. P. N. Bartlett, J. Burt, D. A. Cook, C. Y. Cummings, M. W. George, A. L. Hector, M. M. Hasan, J. Ke, W. Levason, D. Pugh, G. Reid, P. W. Richardson, D. C. Smith, J. Spencer, N. Suleiman and W. Zhang, *Chem. Eur. J.*, 2016, **22**, 302-309.

64. J. Ke, P. N. Bartlett, D. Cook, T. L. Easun, M. W. George, W. Levason, G. Reid, D. Smith, W. Su and W. Zhang, *Phys. Chem. Chem. Phys.*, 2012, **14**, 1517-1528.

65. P. N. Bartlett, M. Perdjon-Abel, D. Cook, G. Reid, W. Levason, F. Cheng, W. Zhang, M. W. George, J. Ke, R. Beanland and J. Sloan, *ChemElectroChem*, 2014, **1**, 187-194.

66. A. C. Larson and R. B. Von Dreele, *General Structure Analysis System (GSAS)*, Los Alamos National Laboratory Report LAUR 86-748, 1994.

67. H. Rietveld, *J. Appl. Crystallogr.*, 1969, **2**, 65-71.

Chapter 7: Conclusions and Outlook

The systematic coordination chemistries of some mono- and bi-dentate neutral phosphine and arsine ligands with the trihalides of boron and aluminium have been explored, with the key features of the complexes established in the solid state by single crystal X-ray diffraction studies and IR spectroscopy, and probed in solution by multinuclear NMR spectroscopy. The interactions of some weakly coordinating fluoroanions with Pb(II) di- and tri-imine complexes have been investigated and found to exhibit several different coordination modes, while a number of very rare diphosphine complexes of Pb(II) have also been synthesised and characterised. Owing to the poor solubility and lability of Pb(II) complexes in solution these studies have been driven by X-ray crystallography, which have revealed favoured core geometries and complex extended structures. The design, synthesis and evaluation of the electrochemical properties of well-defined Sn(II) and Pb(II) precursors has led to the successful electrodeposition of good quality thin films of tin and lead from CH_2Cl_2. Furthermore, subsequent work in the group investigating SCFED at the University of Southampton has shown that, using the same Sn(II) precursor, 13 nm tin nanowires can be grown from supercritical CH_2F_2.

From a fundamental coordination chemistry perspective, future directions for this work may include the systematic chemistry of BX_3 with neutral chalcogenoether (S, Se, Te) ligands, another area of boron chemistry that has received little attention and which would provide an interesting comparison with the P/As systems described in this thesis. Extending the Group 15 coordination chemistry of BX_3 and AlX_3 to include stibine and bismuthine chemistry would provide further insight into the steric and electronic effects governing coordination.

Immediate opportunities to develop this work in terms of the SCFED project include studying the electrochemistry of lead in $scCH_2F_2$ and attempting to deposit tin in templates with sub-5 nm diameter pores. The versatility of the electrolyte system developed for the SCFED of tin and lead, combined with the information gained from fundamental studies, should enable mutually compatible precursors to be synthesised for a wide range of p-block elements, which can be easily and rapidly screened in CH_2Cl_2 before being studied in $scCH_2F_2$. This opens up the possibility of co-depositing compound semiconductors such as PbTe, which should ultimately enable the fabrication of technologically important materials and devices on the extreme nanoscale.

Appendix 1: General Experimental Techniques

Reactions were carried out under a dry dinitrogen atmosphere using Schlenk line and glove box techniques. The products were stored, and spectroscopic samples prepared, in a N_2-filled glove box. This excluded the reactions of lead(II) salts with 2,2'-bipyridyl, 1,10-phenanthroline and 2,2':6',2''-terpyridyl, as these were performed under a normal air atmosphere, with the products being stored in air. Solvents were dried and degassed prior to use. Hexane and toluene were distilled over Na; CH_2Cl_2 was distilled over CaH_2; CH_3CN was distilled over CaH_2 and stored over molecular sieves (4Å); Et_2O was distilled over Na/benzophenone ketyl; MeOH was distilled over $Mg/BrCH_2CH_2Br$ and stored over molecular sieves (4Å); EtOH was distilled over Mg/I_2 and stored over molecular sieves (4Å); $MeNO_2$ was stored over molecular sieves (4Å). Reagents were purchased from Sigma-Aldrich, Strem or Alfa Aesar. $OPPh_3$ and $OAsPh_3$ were dried by heating *in vacuo* and $OPMe_3$ was freshly sublimed prior to use; all other reagents were used as received. The aluminium trihalides used were anhydrous grade. $Ph_2P(O)CH_2P(O)Ph_2$ was prepared by oxidation of the parent phosphine via the literature method.[1] *o*-$C_6H_4(PMe_2)_2$ and *o*-$C_6H_4(PPh_2)_2$ were available in the laboratory, having been previously prepared by other group members by literature methods.[2,3] *o*-$C_6H_4(AsMe_2)_2$ was prepared according to the literature.[4]

Good laboratory practise was followed at all times, including the use of appropriate personal protective equipment, and fume cupboards while handling volatile or hazardous substances. Organo-phosphorus and -arsenic compounds are toxic and can be pyrophoric, and were handled with care in small quantities, being treated with aqueous sodium hypochlorite prior to disposal. Residues containing lead and tin were treated as hazardous waste and collected in separate clearly labelled containers for disposal. Organic residues were separated into those containing chlorinated and unchlorinated solvents and sent for incineration. Non-toxic aqueous residues were washed down the sink in dilute form.

IR spectra were recorded as Nujol mulls between CsI plates using a Perkin Elmer Spectrum 100 spectrometer over the range 4000-200 cm^{-1}. NMR spectra were recorded using a Bruker AVII400 or AVIIIHD400 spectrometer. ^{1}H and $^{13}C\{^{1}H\}$ spectra were referenced to the residual solvent reference, ^{19}F to external $CFCl_3$, $^{31}P\{^{1}H\}$ to 85% H_3PO_4, ^{11}B to $[BF_3(OEt_2)]$, ^{27}Al to $[Al(H_2O)_6]^{3+}$, ^{29}Si to $SiMe_4$, $^{119}Sn\{^{1}H\}$ to $SnMe_4$ and ^{207}Pb to $PbMe_4$. For the $^{119}Sn\{^{1}H\}$ NMR spectra recorded $Cr(acac)_3$ was used as a relaxation agent.

Appendix 1

ESI mass spectra were obtained from solutions in CH_3CN using a VG Biotech Platform. Microanalytical measurements were performed by London Metropolitan University.

Single crystal X-ray data were collected using a Rigaku AFC12 goniometer equipped with an enhanced sensitivity (HG) Saturn724+ detector mounted at the window of an FR-E+ SuperBright molybdenum (λ = 0.71073 Å) rotating anode generator with VHF or HF Varimax optics (70 or 100 µm focus), with the crystal held at 100 K (N_2 cryostream). Structure solution and refinements were performed with either SHELX(S/L)97 or SHELX(S/L)2013,[5] with H atoms bonded to C placed in calculated positions using default C–H distances. Where additional restraints were required, details are provided in the cif file for each structure.

References for Appendix 1

1. W. Levason, R. Patel and G. Reid, *J. Organomet. Chem.*, 2003, **688**, 280-282.

2. E. P. Kyba, S. T. Liu and R. L. Harris, *Organometallics*, 1983, **2**, 1877-1879.

3. H. C. E. McFarlane and W. McFarlane, *Polyhedron*, 1983, **2**, 303-304.

4. R. D. Feltham, A. Kasenally and R. S. Nyholm, *J. Organomet. Chem.*, 1967, **7**, 285-288.

5. G. Sheldrick, *Acta Crystallogr. Sect. A: Found. Crystallogr.*, 2008, **64**, 112-122.